#

FACULTÉ DES ÉTUDES SUPÉRIEURES ET POSTOCTORALES

uOttawa

L'Université canadienne
Canada's university

FACULTY OF GRADUATE AND POSDOCTORAL STUDIES

Suad Mohamed Abuzariba

AUTEUR DE LA THÈSE / AUTHOR OF THESIS

Ph.D. (Physics)

GRADE / DEGREE

Department of Physics

FACULTÉ, ÉCOLE, DÉPARTEMENT / FACULTY, SCHOOL, DEPARTMENT

Theoretical Calculation of System Performance of Fiber Optic Network with Chromatic Dispersion, Polarization Mode Dispersion, Polarization Dependent Loss, and Amplifier Spontaneous Emission Noise

TITRE DE LA THÈSE / TITLE OF THESIS

Liang Chen

DIRECTEUR (DIRECTRICE) DE LA THÈSE / THESIS SUPERVISOR

CO-DIRECTEUR (CO-DIRECTRICE) DE LA THÈSE / THESIS CO-SUPERVISOR

Bruce Campbell

James Harden

Peter Piercy

Scott Yann
Queen's University

Gary W. Slater

Le Doyen de la Faculté des études supérieures et postdoctorales / Dean of the Faculty of Graduate and Postdoctoral Studies

Theoretical Calculation of System Performance of Fiber Optic Network with Chromatic Dispersion, Polarization Mode Dispersion, Polarization Dependent Loss, and Amplifier Spontaneous Emission Noise

by

Suad Mohamed Abuzariba

Thesis submitted to the Faculty of Graduate and Postdoctoral Studies in partial fulfillment of the requirements for the Degree of

Doctor of Philosophy

Ottawa-Carleton Institute for Physics

University of Ottawa

Ottawa, Canada

Your file Votre référence
ISBN: 978-0-494-69120-5
Our file Notre référence
ISBN: 978-0-494-69120-5

To my parents, my brothers, my sisters, my husband, my children;
Hwra, Mohamed, and Moaied

Abstract

This thesis includes a theoretical study of the performance of an optical network system with linear impairments: chromatic dispersion (CD), polarization mode dispersion (PMD), polarization dependent loss (PDL), and amplified spontaneous emission (ASE) noise. Both the Q-factor and bit error rate (BER) were used as performance parameters in this study.

First, an analytical optical eye diagram evaluation for a system of highly mode coupled PMD/PDL fiber and lumped sections (up to fifteen sections) have been presented in this study. Based on this evaluation we found that with PDL considered as well as PMD, the Q-factor of the output becomes higher than that of a Maxwellian fiber having the same total root mean-squared PMD and PDL values, when the mean-square PDL element of the lumped sections makes up the major portion of the total mean-square of the whole system. Whereas without considering PDL, the Q-factor becomes higher as the mean-square PMD element of the Maxwellian fiber takes the major portion of the total mean-square PMD element of the whole system. Also the worst case for the Q-factor occurred when the lumped sections were in the middle between two equivalent Maxwellian fibers, rether than if the lumped sections were followed by Maxwellian fiber or the Maxwellian fiber is followed by the lumped sections. We also note that two equivalent Maxwellian fibers connected in series will not give the same Q-factor as a Maxwellian fiber equivalent calculated by concatenation rules unless they have the same values of PMD, PDL, and polarization direction correlation elements.

Second, considering ASE-noise besides CD, PMD, and PDL, improved values of bit error rate (BER) were gotten using the moment generation function for the optical system in cases of ON-OFF modulation format and DPSK modulation format. We found that, even when considering the noise only without the signal, the probability density function of the output current was dependent on the output state of polarization.

Supervisor Dr. Liang Chen

Statement of Originality

This work contains no material which has been accepted for the award of any other degree or diploma in any University or other tertiary institution and, to the best of my knowledge and belief, contains no material previously published or written by another person, except where due reference has been made in the text.

I give consent to this copy of my thesis, when deposited in the University Library, being available for loan and photocopying.

SIGNED:..

DATE:...

Acknowledgements

First of all, thanks God for your help and support all the time.

I would like to thank my supervisor, Dr. Liang Chen, for his guidance with this research. Also, I have to thank him for his encouragement and support to me in all the years that we spend in the work of this thesis.

I would like to thank all the people in my country, Libya, about this opportunity to study in Canada. Also, I would like to thank all the people who encouraged me in Ottawa University.

I would like to thank all members in our fiber optics group, in particular Dr. Saeed Hadjifaradji, Dr. Zhongxi Zhang, Dr. Ziyi Zhang and Dr. Xiaoyi Bao, for their help and kindness during the years of my work with them .

Finally, I would like to thank my husband, Altaher Mohamed Khadoura , my children; Hwra, Mohamed, and Moaied for their understanding and patience with me throughout all the years of my work in this thesis.

Contents

List of Acronyms

ASE	Amplified Spontaneous Emission
BER	Bit Error Rate
CD	Chromatic Dispersion
CW	Continuous Wave
DGD	Differential Group Delay
GVD	Group Velocity Dispersion
DOP	Degree of Polarization
DSF	Dispersion Shifted Fibers
DPSK	Differential Phase Shift Keying
EDFA	Erbium-Doped Fiber Amplifier
ER	Extinction Ratio
FUT	Fiber Under Test
i.i.d	independent and identically distributed
IM/DD	Intensity Modulation with Direct Detection
JME	Jones Matrix Eigenanalysis
LAN	Local Area Network
LHP	Linear Horizontal Polarization
LCP	Left Circular Polarization
LVP	Linear Vertical Polarization
MAN	Metropolitan Area Networks
MGF	Moment Generation Function
NEP	Noise Equivalent Power
NRZ	Non Return-to-zero

Chapter 1

Introduction

As it is a tradition to start a Ph D thesis with an introduction to the subject under study, I'll start with a small introduction about this thesis. This introduction is essential to get a clear idea about the background of the thesis subject, i.e. the system performance of an optical fiber network, and review information related to this subject.

In the first section I will give an idea about the discovering of fibers that are used in communication systems, followed by a small section that describes the *advantages* of using optical fibers in communication systems. The unwanted errors that result from the use of fibers in network communication are presented in the third section. The fourth section shows the *objectives of this project.* In the last section of this chapter, I present the *organization of the following chapters* in this thesis.

1.1 Optical fibers

Optical fibers are extensively used in optical communications since they provide transmission over long distances at high data rates with less loss. A fiber is used to carry light along their length with the use of the total internal refraction effect. In fact, the optical fiber is a cylindrical dielectric waveguide which transmits the light along its axis.

The main structure of a fiber consists of a core surrounded by cladding layer of lower refractive index, so that light is kept in the core of the fiber.

There are two main types of fibers; fibers that have large diameters and support many transverse propagating modes are called *multi-mode fibers*, while those which have smaller diameters and a single mode are called single-mode fibers. In network communication where the signal travels over long distance, it is preferred to use the single mode fiber type. A single-mode fiber is designed to support only one mode of propagation of light; the principal advantage of letting light propagate in only one mode is that inter-modal dispersion can be avoided. Inter-modal dispersion happens as a result of the relative delays between light propagation in the various modes in a multi-mode fiber. In a single-mode fiber, as there is only one mode available for light propagation (theoretically), inter-modal dispersion is nonexistent. In reality, however, there are two modes of propagation of light even in a single-mode fiber. A single mode fiber, thus virtually acts as a two channel medium with the input data pulses being split and differentially delayed [1]. The attenuations of these two modes are identical (normally).

The story of using optic fibers in communications has a deep root that started in the early 1840s, when *Daniel Colladon* and *Jacques Babinet,* in Paris, demonstrated the guiding of light by refraction which is the principle that makes fiber optics possible. Then in 1854 the British physicist *John Tyndall* demonstrated that light signals could be bent. After passing with all of the scientists's effort in more than a century, a theoretical description of using single mode fibers in communications was published in 1961 by *Elias Snitzer*. In that description the fiber had a light loss of one decibel per meter, which is inadequate for the communication devices that need a light loss of no more than 20 dB/km. Nevertheless, using optical fibers for communication was not proposed until 1963, when the Japanese scientist Jun-ichi Nishizawa at Tohoku University proposed it. This invitation was the key to open a wide door in the communications field.

On the other hand, the high attenuation that accompanied the optic fibers in communication, at that time, was an important issue. Although fibers available during the 1960s had an attenuation of around 1000 dB/km, this obstacle was soon overcome by researchers led by Donald Keck at Corning when they fabricated the first low-loss optical fiber with attenuation around 20dB/km in the wavelength region around 0.63 μm [2]. In 1965, *Charles K. Kao* and *A. Hockham* of the British company *Standard Telephones and Cables* (STC) discovered that this attenuation can be reduced below 20 dB/km; the threshold for making fiber optics a viable technology. Moreover, in 1970, a team of scientists, *Robert Maurer*, *Donald Keck*, and *Peter Schultz* succeeded in developing a glass fiber that carried a pattern of light waves that could be decoded a thousand miles away. With the development of fiber modulation over the years, this attenuation was reduced more and more.

As it is well known, fibers are usually made from plastic, glass or a combination of both, but those that are made from glass have lower attenuation. Currently a variety of fibers are used in different industries depending on the applications. In fact fiber-optic technology has become an iconic word in many branches.

1.2 The advantages of using fibers in communication

The large space that optical fibers have taken today in several fields has come as a result of a wide collection of advantages they have, each depending on the field of use. In the field of communications, using optical fibers has several advantages such as:

- Size and weight: an optical fiber has a diameter that ranges between 10 μm and 50 μm which gives it the advantage of occupying the negligible space that it occupies. Furthermore, optical fibers are very light in weight, and hence they are effectively working in many devices.

- Flexibility: fiber cables are easy to bend or twist, which makes them easy to handle, install, store, and transport.
- Low cost and reliability: optical fibers are available in abundance because they are cheap; optical fibers are made from silicon glass. Hence, its quality is not affected by external radiation.
- Enormous bandwidth: optical fibers have enormous transmission bandwidths and high data transmission rate since the information carrying capacity of a transmission system is directly proportional to the carrier frequency of the transmitted signals and the optical carrier frequency is in the range of 10^{14} Hz.
- Low loss: with the development of ultra low loss fibers and the erbium doped silica fibers that are used as optical amplifiers, it is possible to make low loss communication fibers for long distance with loss as low as 0.002 dB/km.
- Immunity to cross talk: optical fibers are free from any electromagnetic interference or radio frequency interference because they are working as dielectric wave guides. Moreover, even when many fibers are cabled together the cross talk is negligible since optical interference between different fibers is practically impossible.
- Digital signals: optical fibers are ideally suited for carrying digital information, which is especially useful in computer networks.

- Low power: because signals in optical fibers degrade less, we need lower power transmitters than those needed in the case of copper wires (high voltage electrical transmitters)
- Information security: unlike the case of the transmitted signal in copper cables, the transmitted signal through optical fibers cannot be drawn from a fiber without tampering with it.
- All these advantages give optical fiber systems the leading position in modern communication systems.

1.3 The impairments of optical fiber communication systems

Even with all of the advantages of fiber optic systems, there are some impairments that are associated with use of the optical fiber in network and communication systems. Therefore, it is an important issue to study those impairments carefully. Because of that, there have been extensive studies to reduce the effect of these impairments in optic fiber networks, each focusing on one or more impairments. Because of these impairments there were limitations in the performance of optic fiber networks. These limitations can be described as follows: the fundamental limitations of a fiber optic communication system include fiber loss, chromatic dispersion and some nonlinear effects when the bit rate is relatively low (2.5 Gbits/second or lower) [3]. With the development of high bit rates (≥ 10 Gbits/second) and more complex fiber optic communication systems, polarization mode dispersion (PMD) and polarization dependent loss (PDL) become additional obstacles in optic fiber communication systems [4-6]. PMD is a random effect resulting from intrinsic (geometrical birefringence and intrinsic stress) and extrinsic (lateral stress, bending and twisting) sources and it introduces pulse broadening that can be up to 20ps in installed fibers. On the other hand, PDL causes power fluctuation and it can be up to 0.4 dB in fiber components [7-9]. Moreover, the interaction of PMD and PDL can cause further system impairments [6, 9]. In fact, due to the stochastic perturbations of environmental factors, such as temperature and vibration, PMD and PDL can be considered as random effects. Hence, their effect in optical systems has to be studied statistically. In this manner we can describe this effect as follows.

1- PMD is expressed in terms of principal states of polarization (PSP's) and differential group delay (DGD), where DGD is the difference of time delays when a lightwave is transmitted in the two orthogonal PSP's. Both PSP and DGD are wavelength and time dependent. The average of DGD over wavelength or time is PMD [4, 10].
2- The statistical distribution of DGD is Maxwellian without PDL, and it is a combination of Gaussian and Maxwellian with high PDL [11, 12].
3- Due to the interaction of PMD and PDL there are some anomalous phenomena, such as pulse narrowing with finite DGD and pulse broadening with zero DGD [13].
4- The system impact of PMD has been studied both in analog and digital systems. For analog systems it has been shown that pulse broadening due to PMD follows a Rayleigh distribution [14]. For digital systems the impact of PMD has been studied in terms of system outage probability [5] and the statistical distributions of eye-opening [7] and Q-factor [15].

1.4 Objectives of this project

The main objective of this project is to develop a good performance evaluation for optical fiber systems by developing a theoretical model for measuring the Q-factor (Part I) and calculating the bit error rate (Part II) for the output current, including almost all of the impairments inherent in optical systems, including chromatic dispersion, polarization mode dispersion, polarization dependent loss, and amplified spontaneous emission (ASE) noise.

1.5 The thesis organization

The rest of the thesis is organized as follows:

Chapter 2 presents the theoretical background of the major fiber characteristics that affect the pulse evolution in an optical fiber, including the necessary introduction to the types of lightwave systems in section (2.1). Section (2.2) presents a discription of the propagation of light in optical fiber, followed by section (2.3) , which gives some analytical description of wave plate theory, and polarization in Jones and Stokes spaces. Section (2.4) describes the polarization impairments in optical systems. The last section (2.5) shows some of the performance parameters in optical communication systems.

The main work in this thesis comes in two parts:

Part I : In the first part of this thesis we use the Q-factor as a performance parameter.

This part includes Chapter 3 and Chapter 4:

Chapter 3: considers the **chromatic dispersion**, **polarization mode dispersion**, and **polarization dependent loss or gain** in our highly mode coupled model.

Chapter 4: presents an analyitical model to evaluate the eye diagram for an optical system of a highly mode coupled PMD/PDL fiber with lumped sections.

Part II : In the second part, we use the bit error rate as a performance parameter in our calculations. This part contains Chapter 5 and Chapter 6:

Chapter 5 considers another fiber impairment to our calculation, namely the **Amplified Spontaneous Emission Noise.** This chapter demonstrates the effect of noise in our model. By using the saddle point method, we present in this chapter a clear method that give the probability of error in optical systems.

Chapter 6 : investigates for the first time (to our knowledge) how three ASE noises impact in bit error rate calculations for an optical system dealing with partially polarized noise in this chapter.

Chapter 7 concludes the dissertation, summarizes the achievements of the research and gives recommendations for future work.

Chapter 2

Theoretical Background

For a better understanding of high speed optical fiber network systems, it is necessary to start with background about some related theoretical concepts.

2.1 Types of lightwave systems

Fiber optic systems act as information highways; the information flows through the fiber and then is distributed and delivered to the customers via access networks. In fact, fiber-optic communication systems are lightwave systems that employ optical fibers as a light guiding medium.

The main function of lightwave systems is to transport information at a specified bit rate and bit error rate (BER) over a specified distance. So the length of the lightwave systems can be classified in two categories: short-haul and long-haul. In short-haul links there are no repeaters or amplifiers and typically distances up to many tens of kilometres. This type is widely used in metropolitan area networks (MANs) or local area networks (LANs). On the other hand, long-haul links contain repeaters to compensate for loss and/or dispersion, and may cover up to several thousand kilometres in length. They are widely used in large-scale terrestrial networks such as wide area networks (WANs) and undersea intercontinental networks. Table (2.1) summarizes the differences between the short-haul and long-haul systems.

Difference	***Short-haul systems***	***Long-haul systems***
Repeaters	No repeaters or amplifiers	Contains repeaters and/or amplifiers
Length	~10 Km	~1000 km
Applications	MANs, LANs	WANs, undersea intercontinental networks

Table (2.1) Comparison between short-haul and long-haul systems

2.2 Propagation of light in the optical fiber

In the field of fiber optics it is well known that it is preferred to use monochromatic light, such as from a laser. However, even a laser radiation is not totally monochromatic, but it is the best light source now. The polarization of monochromatic light represents the oscillation direction of the electric field and there are several ways to represent the polarization of the light. The most famous ones use Stokes vectors (in Stokes space) and the Jones vectors (in Jones space).

The change of the polarization of light on transmission through a fiber can be described as the rotation of its Stokes vector $\hat{s}$, a 3-D vector of unit length indicating the polarization of the light with components which are the Stokes parameters. This vector corresponds to the 2-D complex Jones ket vector $|s>$. The 3-D space of Stokes vectors and the 2-D space of Jones vectors are different representations that we can use to describe the propagation of light in a fiber. To connect these two spaces, we use the Pauli matrices $\sigma_1, \sigma_2, \sigma_3$ (In Stokes space it is a Pauli spin vector $\vec{\sigma} = (\sigma_1, \sigma_2, \sigma_3)$)

[16]. The input light passes through the fiber to emerge as the output as shown in figure (2.1) .

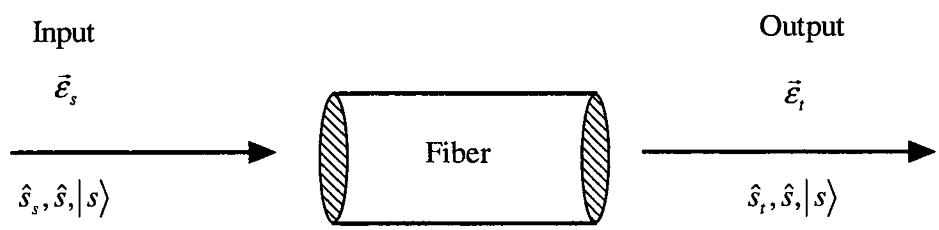

Fig 2.1 Block diagram of optic fiber system

The Fourier transformation of the electric field vector of the input and output light are $\vec{E}_s = e|s\rangle$ and $\vec{E}_t = e|t\rangle$, respectively. The phase and polarization information are included in $|s>$ and $|t>$, whereas e indicates the magnitude of the electric field.

2.3 Polarization impairments in optical communication systems

2.3.1 Polarization mode dispersion

It is well known now that PMD is one of the major limiting factors for high-speed optical communication systems, and because of that it is an important issue to study, especially with today's high bit rate. The adverse effects of PMD on system performance were identified in the early 1990s [17]. Since that time a lot of research has focused on studying this phenomenon. In this section we present some details about polarization mode dispersion, and the necessary principles related to it.

2.3.1.1 Causes of PMD

The main cause of PMD is the asymmetry of the optic fiber. Asymmetry in the core of the fiber simply means that the core of the fiber is not perfectly round. The core might be oval or out-of-round as in Figure (2.2); this may be inherent in the fiber manufacturing process, or may be a result of mechanical stress on the fiber.

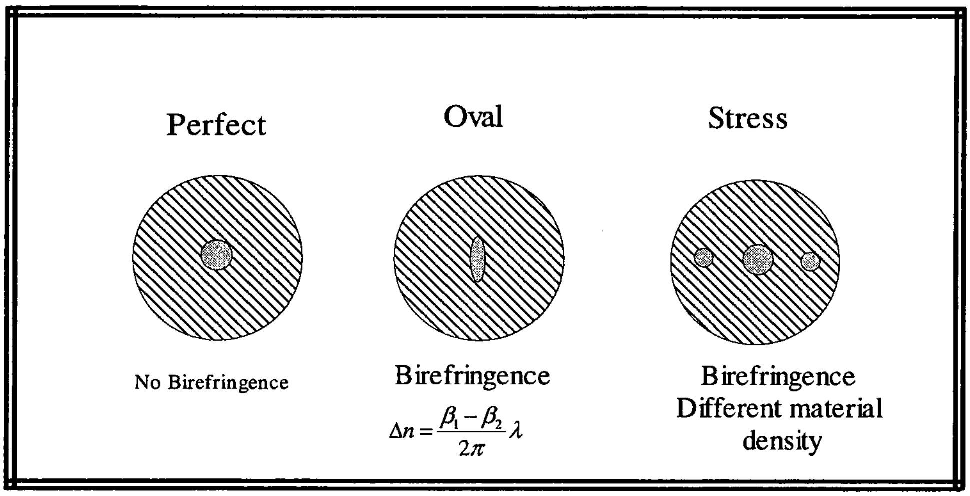

Fig. 2.2 The Cross-section of the optical fiber

2.3.1.2 Birefringence

Ideal single mode fibers have perfectly circularly symmetric cross sections; hence the two polarization modes are degenerate and propagate with the same velocity. However, in real fibers such degeneracy is broken since the fibers are not perfectly circular and can also be subjected to local stresses. Consequently, the propagating light is split into two local polarization modes that travel with different velocities and results in the rotation of polarization orientation with the distance. The difference in propagation times between the two orthogonal polarization modes at a given wavelength results in pulse spreading.

2.3.1.3 Phase velocity and group velocity

Optical transmission media are characterized by two optical velocities, phase velocity v_p and group velocity v_g. Both of them play a role in PMD. A superposition of plane waves can describe the propagation of light in a homogeneous medium. After traveling a distance z, the electric field at z is related to the incident field by

$$E(z,t) = E(0,t)\exp\left(i\omega_0\left(t - \frac{z}{v_p}\right)\right) \tag{2.1}$$

This form describes the electric field as a plane wave at central frequency ω_0, propagating at phase velocity $v_p = |\omega_0/k(\omega_0)|$, modulated by the input signal's envelope $E(0,t)$, traveling at the group velocity $v_g = (dk/d\omega|_{\omega_0})^{-1}$ with higher orders revealing chromatic dispersion and its slope. A phase (group) index of refraction is associated with the phase (group) velocity.

2.3.1.4 Principal states of polarization

To the first order, PMD is the group-velocity difference between two orthogonal states of polarization; these orthogonal states are the principal states of polarization (PSP) [18, 19]. When the principal state of polarization is excited at the fiber input, impulses will propagate undistorted and the signal will stay completely polarized because the output polarization remains constant to first order as a function of optical frequency. On the other hand, if the signal polarization is a mixture of the PSP's, impulse broadening occurs in the time domain, and the signal becomes depolarized in the frequency domain. The input state of polarization (SOP) can be expressed as the vector sum of two components, each component being aligned with one of the PSPs.

Kogelnik et al [20] describes the PSP in the frequency domain as following. For a specific length of the fiber, there is a pair of input polarization states at every frequency. This pair of states is the two PSPs. In other words, a PSP is that input polarization state for which the output state of polarization is independent of frequency over a small frequency range. With this definition, PMD can be characterized as a vector represented as

$$\vec{\tau} = \Delta\tau \, \hat{P} \tag{2.2}$$

where $\Delta\tau$ is the length of PMD vector (DGD), and $\hat{P}$ is the direction of PMD vector and it is along the axis that joins the two output PSP points in Stokes space.

A single-mode fiber can be thought to have a set of two orthogonal principal states of polarization (PSPs) which have certain properties. A light pulse aligned with one of the fiber's two input PSPs will emerge out of the fiber end as a single pulse, unchanged in shape. Along the corresponding output PSP of the fiber, the emerging pulse will be polarized. On the other hand, if the pulse's state of polarization (SOP) is aligned anywhere between the two input PSPs (but not aligned along either of them), the pulse will be split into two orthogonal components. Using this concept for PSP, we can use a concatenation of randomly oriented short sections of birefringent fiber (as we will see later) to describe any long single-mode fiber. In each section both the degree of birefringence and the orientation of the principal axes remain constant, but they change randomly from section to section. Each fiber section can be treated as a phase plate using a Jones matrix. Then the propagation of each frequency component associated with an optical pulse through the entire fiber is governed by a composite Jones matrix by multiplying individual Jones matrices for each fiber section.

2.3.1.5 The mathematical expressions of the PMD vector

The PMD vector $\vec{\tau}$ is a Stokes vector pointing in the direction of the slow principal state of polarization (PSP) with a length equal to the DGD. There are several ways to describe the PMD vector mathematically, such as the Jones Matrix eigenvector analysis [3], σ-expansion [9], time domain moments [10], and Muller matrix method [21].These expressions correspond to four different yet closely related views of PMD. On the other hand, these expressions are the basis for different experimental approaches.

The rotation of the output Stokes vector on the Poincare sphere as ω changes is governed by the law of infinitesimal rotation as [16]

$$\frac{\partial \hat{s}}{\partial \omega} = \vec{\tau} \times \hat{s} \, . \tag{2.3}$$

The combination of the infinitesimal rotation laws for PMD with the birefringence gives the dynamical PMD equation [16]:

$$\frac{\partial \hat{\tau}}{\partial z} = \frac{\partial \vec{\beta}}{\partial \omega} + \vec{\beta} \times \vec{\tau} \, , \tag{2.4}$$

where $\vec{\beta}$ is the birefringence vector.

This equation describes the evolution of the PMD vector with distance.

In general, the analytical treatment of PMD is quite complex because of its statistical nature. Therefore, statistical predictions are needed to account its effects [22, 23].

2.3.1.6 Second order PMD

Second order PMD is the change of the DGD (first order PMD) with changes in wavelength [24]. When the PMD vector has a nonnegligible dependence on frequency, higher order distortions take place [25]. Moreover, higher order PMD induces depolarization and polarization-dependent chromatic dispersion [26].

In modern lightwave systems, that have a bit rate which climbs from 10 to 40 Gb/s and higher, there were several studies of the high order PMD, especially at the second order [25, 26, 27]. Hence, it is important to take into account of impairments caused by the fiber's polarization mode dispersion including higher orders [28]. As an example, the second-order effect becomes more important than the first-order effect when the chirp factor (phase-amplitude coupling factor) is greater than one [29]. (A chirped pulse means that the frequency of the pulse is changing with time, and the chirp factor of the pulse is proportional to the rate of change of the pulse frequency with time.)

Mathematically, the PMD vector can be expanded as a Taylor series with ω as the independent variable as

$$\vec{\tau}\,(\omega) = \vec{\tau}\,(\omega_0) + \vec{\tau}_\omega(\omega - \omega_0) + \left(\frac{1}{2}\right)\frac{d^2}{d\omega^2}(\vec{\tau}_\omega)(\omega - \omega_0)^2 + \cdots. \tag{2.5}$$

The second order term in the expansion corresponds to second order PMD ($\vec{\tau}_\omega = \frac{d}{d\omega}(\vec{\tau})$). The physical significance of second-order PMD is that it causes a polarization-dependent pulse broadening or compression (termed polarization dependent chromatic dispersion or PCD) and the rotation of the PSPs with frequency.

Eyal and others [30] have proposed a description of PMD based on an exponential expansion of the Jones matrix of the transmission medium. With this description different orders of PMD are treated separately as different subsystems and the overall behaviour of the transmission medium is obtained from serially concatenating these systems. In the old fibers PMD had larger values than values in modern fibers; see table (2.2) [31].

Fiber Type	***MeanDGD Coefficient*** $\left(\frac{\langle\Delta\tau\rangle}{L}\right)$	***Average DGD for L=625km***
Modern Fibers (Low PMD)	$\leq 0.1ps/\sqrt{L}$	2.5 ps
Old Fibers(High PMD)	$\sim 2ps/\sqrt{L}$	50 ps

Table (2.2) Polarization Mode Dispersion in Old and Modern Fibers

2.3.1.7 PMD measurement techniques

As a final point about PMD, I believe that we have mention to the available ways to measure PMD. To measure PMD there are various measurement techniques. Table (2.3) summarizes some of the important methods (and some of their characteristics) to measure PMD. (Full details are in Ref. [18].)

Type	***Method***	***Measures***	***Light Source***	***Analyzer***	***Range***
Time Domain Mea.	Differential Pulse Delay	DGD	Short (Unchirped) Laser Pulses	High-Speed Oscilloscope	$\geq 10\,ps$
Time Domain Mea.	Modulation Response	DGD	Intensity-Modulated (Unchirped) Laser	RF-Spectrum Analyzer	$\geq 20\,ps$
Time Domain Mea.	Interferometric	DGD	Broad-Band CW LED (or Lamp)	Michelson Interferometer	$\leq 100\,ps$
Frequency Domain Mea.	Fixed Analyzer	DGD	Narrow-Band Tunable CW Laser	Polarizer and Power Meter	$0.1ps - 1ns$
Frequency Domain Mea.	Poincare Sphere	DGD+PSP	Narrow-Band Tunable CW Laser	Complete Polarimeter	$1fs - 1ns$
Frequency Domain Mea.	Jones Matrix Analysis	DGD+PSP	Narrow-Band Tunable CW Laser	Complete Polarimeter	$1fs - 1ns$

Table (2.3) Measuring Polarization Mode Dispersion in Optical Fibers

2.3.2 Polarization dependent loss and gain

Another polarization sensitive phenomenon that arises because the optical fibers and optical components absorb power in different amounts along the orthogonal axes is called polarization dependent loss (PDL). PDL is a varying insertion loss arising from the dependence of a component's transmission coefficient on the state of polarization [32-34].

2.3.2.1 Definition of the PDL

Polarization dependent loss is defined as the maximum change in the power transmitted by an optical component as the input state of polarization is varied over all possible polarization states. On the decibel scale PDL is given as

$$PDL_{dB} = 10\log\left(\frac{P_{max}}{P_{min}}\right) \tag{2.6}$$

Since the state of polarization of the transmitted light is randomly changing in time, PDL and PDG may cause the system performance to vary in a random manner as a function of time. On the other hand, PDL induces additional waveform distortions by interaction with PMD. This effect is small in real systems [35] but it is still present [36].

2.3.2.2 Sources of the PDL

The major sources for polarization dependent loss are:

1- The unequal spectral absorption of the orthogonal polarization components (Dichroism). 2- Fiber bending. 3- Angled optical interfaces. 4- Oblique reflections.

In fact, polarization dependent loss was recognized as a critical issue because various inline optical components (such as isolators, couplers, filters, and switches) may have nonnegligible PDL values (> 0.2 dB). The total value of PDL for a series of concatenated elements is usually different from the sum of each single PDL-element contribution. That is because the resulting total PDL depends on the relative orientations of the PDL axis at each connection [37].

2.3.2.3 *Combined PDL and PMD*

Gisin and Huttner [9] were the first ones to consider the combined effect of PMD and PDL in their seminal work. They showed that the combination of PMD and PDL will lead to a complex principal state vector. The autocorrelation function of such a complex principal state vector has been reported [38].

Due to the interaction of PMD and PDL the amplitude of PMD, its statistics, the two PSPs, and so on are different from those of null PDL [9, 12]. Furthermore, several studies have shown that PDL can induce some anomalous phenomena in pulse transmission, such as pulse narrowing with finite differential group delay (DGD) [13] and pulse broadening with zero DGD [39].

With assuming negligible values of PDL, the two PSPs are mutually orthogonal [40].On the other hand, with considering PDL the two PSPs are no longer orthogonal in general [41]. Ref. [42] presented some example calculations of PMD and PDL for various input pulse widths. Due to the effect of higher order PMD and PDL [43], the effective PDL and the effective PMD for a pulse increased with the input pulse width. This happens if both PMD and PDL are present in the system, but without PMD, the PDL vector of the fiber is frequency independent [8]. This means that PDL for a pulse is bandwidth independent [44]. Furthermore, in the presence of PMD, the PDL vector is frequency dependent (higher order PDL) except when the PMD and PDL vectors are parallel or antiparallel.

When PDL is not present, the PSPs for a pulse without chirp are coincident with the SOPs. Hence, a minimum pulse broadening will occur. When considering a system with

PDL, the distortion is not a minimum when the pulse is launched along either of the two PSPs. With a complete knowledge of the input and output state of polarization for three independent polarizations, Heffner [45] gave a correct DGD value for a system having PDL/G. A more simple method, using the Poincare sphere, was proposed by Chen [42] to measure the complex principal states of the polarization vector for a system with PDL/G. The probability density function of PMD without considering PDL is Maxwellian [9, 10], but when strong PDL fluctuations are taken in to consideration, it deviates from the Maxwell probability density function [12].

Because of the frequency dependence of the PDL and PMD vectors (the PMD vector has the orientation of the PSP and length equal to the DGD.) the polarization states for a pulse that maximize/minimize the power transmission (maximize/minimize the time delay) cannot be identical for each frequency component in the pulse. Consequently, the frequency components in the pulse cannot all reach their maximum/minimum power transmission (maximum/minimum time delay) for a given state of polarization. As a result, the PDL and PMD values for a pulse are generally less than those for a single frequency.

2.3.3 Loss and dispersion

For low bit rate fiber optic communication systems (2.5 Gbits/second and below) and short transmission distance, the main impairments are fiber loss and fiber chromatic dispersion.

2.3.3.1 Fiber loss

Fiber loss is usually expressed in units of dB as

$$\alpha = -10\ log_{10}\left[\frac{P_{out}}{P_{in}}\right], \tag{2.7}$$

where P_{out} is the optical power at the fiber output end when the optical power P_{in} is launched in to the fiber. Sometimes fiber loss is expressed by the loss per kilometre. Due to the fiber loss, the optical signal is attenuated and the signal to noise ratio (SNR) at the receiver is decreased, and as a result the BER of the whole system is increased. Presently the fiber loss is compensated by using optical amplifiers, such as erbium-doped fiber amplifiers (EDFAs).

2.3.3.2 Dispersion

When an optical pulse propagates in an optical fiber, different frequency components travel with different velocities. The centre of the pulse travels with a speed called the group velocity $v_g = d\omega/d\beta$ where ω is the frequency and β here is the propagation constant. The time delay due to the group velocity is the group delay $\tau_g = L/v_g$. The change of the group delay with frequency is the dispersion.

2.3.3.3 Types of dispersion

1) Material dispersion: the index of refraction of the medium changes with wavelength. Material dispersion is intrinsic to the molecular structure of the material used to fabricate the fiber. In fact, material dispersion is the dominant factor in chromatic dispersion for conventional single-mode optical fibers. It occurs due to the response of the bound electrons of the dielectric medium, which oscillate with different amplitudes depending on the frequency of the incident electromagnetic wave. Therefore, it causes a wavelength dependent refractive index $n(\omega)$.

2) Waveguide dispersion: the index change across a waveguide means that different wavelengths have different delays. Waveguide dispersion is related to the geometry of the optical fiber, such that the confinement of the mode in an optical fiber causes the propagation constant to be dependent on the frequency ω. Generally, the waveguide dispersion makes a relatively small contribution to the total dispersion in comparison to the material dispersion. The waveguide dispersion can be changed by the fiber profile design and it may have a positive or negative value; see figure (2.3).

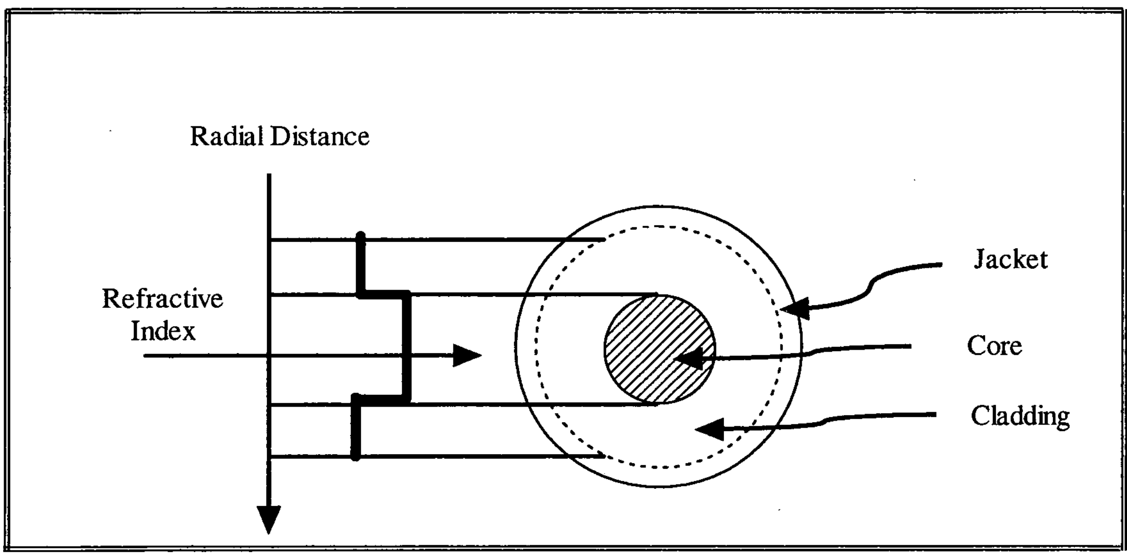

Fig 2.3 The cross section and refractive index for optical fiber

3) Modal dispersion: different modes propagate at different group velocities.

4) Polarization mode dispersion: it is a form of modal dispersion where two different polarizations of light in a waveguide, which normally travel at the same speed, travel at different speeds due to random imperfections and asymmetries, causing random spreading of the optical pulses.

Due to the fact that the global chromatic dispersion of a single-mode fiber is a combined effect of both material dispersion and waveguide dispersion, it is possible to tailor, under some conditions, the zero-dispersion wavelength of a single-mode fiber by balancing the material dispersion against the waveguide dispersion.

2.3.3.4 *Measurement techniques for chromatic dispersion*

Over the past thirty years, there were many techniques developed to measure the chromatic dispersion of single-mode fiber. Each method had a particular fiber range and operating conditions in which the measurements would yield good results. Without going into details for these techniques, we present a summary of some methods in table (2.4).

The dispersion changes with wavelength of any type of fiber in a transmission window can be described by Taylor expansion around the center wavelength λ_0 as

$$D = D + S\,(\lambda - \lambda_0) + C\,(\lambda - \lambda_0)^2 + \ldots \qquad (2.8)$$

where $S = dD/d\lambda$ is the dispersion slope and $C = (1/2)\, d^2D/d\lambda^2$ is the dispersion curvature. With a good approximation [45], the first three terms are enough. For most transmission fibers, the dispersion curvature is small and can be neglected. However, when more accurate dispersion compensation is needed it is necessary to consider the dispersion curvature of the dispersion slope compensation fiber.

Technique	***Advantages& Disadvantages***	***Resolution** (ps)*	***Sample Length***
Time of flight	Indirect method, tunable laser needed, Fast electronics required, long sample fiber length	50-100 ps	*2* 1km
Phase-shift method	Indirect method: modulated phase-shift Direct method: differential phase-shift Utilize frequency modulation	20 ps	~0.5-1 km
Mode-field Diameter	Temporal detection not required Determine waveguide, dispersion only Material dispersion		
Nonlinear analysis	λ_D must be known precisely to see nonlinear effect		
Beam Propagation Method	No experimental setup required Did not account for geometry fluctuation		
White-light interferometer	High resolution Indirect: central wavelength method Direct: turning point analysis Nonlinear fit method	0.1-0.8 ps	0.5-1 m

Table (2.4) Some techniques to measure chromatic dispersion

Practically, this can be accomplished by adding a second compensation fiber to compensate the dispersion curvature. This type of dispersion compensation fiber is called a *dispersion curvature compensation fiber*.

In long haul systems, there are three kinds of fibers that are commonly used. These are standard single mode fibers (SMF), dispersion shifted fibers (DSF) and nonzero dispersion shifted fibers (NZDSF).

These fibers have different dispersion and dispersion slope values in the 1550-nm window. The dispersion values, dispersion slope values and the dispersion/dispersion slope ratio of the different types of the fibers at 1550nm are listed in table (2.5) [46]. Standard single mode fibers with a dispersion of around 17ps/nm/km at 1550 nm limits the transmission distance to less than 100km for a system with 10Gbit/s bit rate or higher [45].

$\boldsymbol{Fiber\ Type}$	$\boldsymbol{Dispersion}$ $(\boldsymbol{ps/nm \cdot km})$	$\boldsymbol{Dispersion\ Slope}$ $(\boldsymbol{ps/nm^2 \cdot km})$	$\boldsymbol{\frac{Dispersion}{Dispersion\ Slope}}$ $(\boldsymbol{nm})$
Standard SMF	17	0.058	298
NZDSF Type 1	4.2	0.085	50
NZDSF Type 2	4.5	0.045	100
NZDSF Type 3	8	0.057	140

Table (2.5) Different transmission fiber types

2.3.3.5 *Group Velocity Dispersion*

When the light travels in a single mode fiber which has a length L, a specific spectral component at frequency ω would arrive at the end of the fiber after a time delay $T = \frac{L}{v_g}$, where v_g is the group velocity, defined as $v_g = (d\beta/d\omega)^{-1}$ [47]. The frequency dependence of the group velocity leads to pulse broadening because different spectral components of the pulse disperse during propagation and do not arrive simultaneously at the output. The extent of the pulse broadening is given by

$$\Delta T = \frac{dT}{d\omega}\Delta\omega = \frac{d}{d\omega}\left(\frac{L}{v_g}\right)\Delta\omega = L\frac{d^2\beta}{d\omega^2}\Delta\omega = L\beta_2\Delta\omega \qquad (2.9)$$

The parameter $\beta_2 = \frac{d^2\beta}{d\omega^2}$ is the group velocity dispersion (GVD) parameter; it determines how much an optical pulse would broaden on propagation inside the fiber. The GVD parameter is a function of the wavelength. The frequency spread $\Delta\omega$ may also be determined by the wavelength range $\Delta\lambda$ emitted by the optical source. On the other hand, the extent of the pulse broadening can be written using $\omega = 2\pi c/\lambda$ and $\Delta\omega = \left(-\frac{2\pi c}{\lambda^2}\right)\Delta\lambda$ as:

$$\Delta T = \frac{d}{d\lambda}\left(\frac{L}{v_g}\right)\Delta\lambda = DL\,\Delta\lambda, \qquad (2.10)$$

where $D = \frac{d}{d\lambda}\left(\frac{1}{v_g}\right) = -\frac{2\pi c}{\lambda^2}\beta_2$ is the dispersion parameter and it is expressed in units of ps/(km.nm). A fiber will have a zero-dispersion when $\lambda = \lambda_D$ or $\beta_2 = 0$, where λ_D is the zero-dispersion wavelength. Vanishing of β_2 ($\beta_2 = 0$) doesn't mean that the total dispersion is equal to zero, since the third and higher order terms are still present in the fiber at λ_D. In fact, as wave propagates through the fiber at λ_D, the third order dispersion parameter β_3 is dominant. For ultra-short optical pulse, the pulse will be distorted by the third order dispersion and other higher order dispersion parameters.

Pulses experience broadening even when the first order dispersion is zero. This is because of the higher-order dispersive effects, which are governed by the dispersion slope [1]. In practise, D cannot be zero at all wavelengths which are contained within the pulse spectrum centered at zero-wavelength. Hence, the wavelength dependence of D plays a role in the pulse broadening. The dispersion slope, sometimes called the differential-dispersion parameter, can be written as

$$S = (\frac{2\pi c}{\lambda^2})^2\beta_2 + (\frac{4\pi c}{\lambda^3})\beta_3 \tag{2.11}$$

where $\beta_3 = \frac{d\beta_2}{d\omega} = d^3\beta/d\omega^3$ is the third order dispersion parameter.The numerical value of the dispersion slope has an important role in the design of the modern WDM (wavelength division multiplexing) systems. As a result of the positive value of the dispersion slope ($S > 0$) for most fibers, different channels have slightly different GVD values. Therefore, it is difficult to compensate the dispersion for all channels simultaneously. Either small or negative dispersion slope has to be produced to solve this matter. Reduced slope fibers (small S) and reverse-dispersion fibers have been developed practically [48] and now are used in many applications [49, 50].

2.3.3.6 *Dispersion regimes*

There are two different dispersion regimes in fibers, normal dispersion regime and anomalous dispersion regime. A fiber is said to exhibit normal dispersion when $\lambda <$

λ_D or $\beta_2 > 0$, where λ_D is the zero-dispersion wavelength. In the normal dispersion regime, longer wavelength components in the pulse travel faster than shorter wavelength components, resulting in different frequency components arriving the receiver at different times. Similarly, a fiber said to be in the anomalous dispersion regime when $\lambda > \lambda_D$ or $\beta_2 < 0$, the opposite case to normal dispersion.

There are several techniques to measure the chromatic dispersion of optical fibers. Each method has a particular range and operating conditions in which the measurements would yield good results.

2.3.3.7 PMD and chromatic dispersion

The amount of distortion that the pulse suffers depends on the combined effects of PMD, chromatic dispersion, and the chirp. The effect of PMD is usually much less than the chromatic dispersion in ordinary single mode fibers, nevertheless it becomes significantly irritating for high speed networks transmitting bandwidths of the order of Gbs and above.

Unlike chromatic dispersion, techniques have not yet matured to eradicate the effect of PMD by modifying the design of the optical fiber. However its precise measurement is the key to a successful design of an optical network and its future expansion. A comparison between CD and PMD is presented in table (2.6).

2.4 The Performance of optical systems

2.4.1 Probability of error:

There are several ways of measuring the rate of error occurrences in a digital data stream. The most common one is the bit error rate (BER).

Chromatic Dispersion	Polarization Mode Desperation
Rather stable	Very stable in components
Linear effect making compensation relatively easy	Linear effect that is time varying in fiber links making compensation difficult
Independent on the launched polarization state	Dependent on the launched polarization state.

Table (2.6) Comparison between CD and PMD

To compute the bit error rate at the receiver we have to know the probability distribution of the signal at the output. At the receiver the decision is made as to whether a 0 or 1 is sent. The probability that the equalizer output current is less than I_{th} when a logical 1 pulse is sent can be written as

$$P_1(I_{th}) = \int_0^{I_{th}} p(y|1)dy \tag{2.12.a}$$

where $p(y|1)$ is the probability density function when a logical 1 is sent.

The probability that the output current exceeds I_{th} when a logical 0 is transmitted can be written as

$$P_0(I_{th}) = \int_{I_{th}}^{\infty} p(y|0)dy. \tag{2.12.b}$$

where $p(y|0)$ is the probability density function when a logical 0 is transmitted. Then probability of error for a sequence of logical 0's and 1's is

$$P_e = aP_1(I_{th}) + bP_0(I_{th}) \tag{2.13}$$

The weighting factors a and b are determined by the a priori distribution of the data.

2.4.2 Bit error rate

Achieving a desired bit-error rate (BER) with a given outage probability, after the signal is transmitted through an optical system, is a fundamental problem in the design of the optical fiber transmission systems. The measure of the performance is usually bit-error-rate (BER). The bit error rate can be written as

$$BER = \frac{Error\ Bits}{Total\ Number\ of\ Bits} \tag{2.14}$$

Since BER depends on probability, this number represents the actual BER of the link only if the number of transmitted bits tends to infinity.

With a strong signal and an unperturbed signal path, this number is very small as to be insignificant. It becomes significant when we wish to maintain a sufficient signal-to-noise ratio in the presence of imperfect transmission through the parts of the transmission systems such as the amplifiers, filters, mixers, etc. Any in-depth analyses of the processes that affect BER require significant mathematical analysis.

The design of optical communication systems relies on the estimation of performance figure of merits such as the BER and a number of derived quantities. The most commonly used are the receiver sensitivity (the average received power resulting in a given BER), the power penalty (the difference between the sensitivity at the output of the system) or the error free transmission distance. In order to simulate the behaviour of optical links or sub-systems, it is therefore essential to be able to compute the BER in an effective and reliable way.

Shake in 2002 [51] has mentioned several approaches that make it possible to detect various impairments, including both digital and analog techniques such as bit error rate estimation [52], optical power measurement , optical SNR evaluation with spectrum measurement [53], Q-factor monitoring [54], and pseudo BER estimation using two decision circuits [55].

In order to ensure accurate and reliable transmitted data, persistency and consistency of the data detector or receiver need to be clearly studied. The measurement of bit error rate (BER) is a step toward the development of a reliable and error-free data receiver.

2.4.2.1 Computation of the BER in Digital Systems

There are a number of techniques to compute the bit error rate in digital systems, such as:

1- Monte Carlo: this method basically relies on error counting over a large number of simulation runs. A rule of thumb is that the number of bits used in the simulation should be of the order of $(10/P_e)$, where P_e is the error probability [56] (typical values of which are of order of 10^{-9}). This method is not suitable for practical implementation due to its excessive requirements on computation time.

2- Importance sampling: this method relies on the fact that only a very small fraction of the samples is required for evaluation of BER using the Monte Carlo method are actually responsible for errors. By artificially increasing the number of errors in an invertible way, it is possible to decrease the variance of the Monte Carlo estimator, and therefore to reduce the number of simulation runs necessary for an estimation of BER within a certain interval [57]. The technique relies on the choice of a proper biased distribution suitable for a specific problem. In a special class of biased distributions based on large deviations theory was applied to the problem of the simulation of optical communication systems [57].

3- Extreme value theory: it is based on the statistical phenomenon that the extreme samples taken from groups of samples from a population are governed by a distribution which is identical in form irrespective of the distribution of the underlying population, so long as the latter belongs to a broad class. Since it is the extreme values of the waveform process at the decision-device input that causes errors, the extreme-value distribution is in principle the only information necessary to compute the bit error rate [56].

4- The tail extrapolation technique: this technique assumes that the tails of the probability density function (pdf) of the decision variable can be described by a generalised exponential function from which the BER can be calculated [58]. Fitting Gaussian distribution to a noisy waveform at the input of the decision circuit is a special case of this more general method.

5- The Quasi-analytical approach: with this approach the propagation of the deterministic signal is separated from the noise generation processes, such as when the effects of noise captured by an appropriately defined equivalent noise source at the receiver input. The sampled noise-free signal is input to the decision circuit and the pdf from an equivalent noise source is used to compute the BER analytically. This method is commonly used in a number of simulation tools where the pdf of the equivalent noise source is often assumed to be Gaussian [59].

6- Moment generating functions method: With this method the BER can be calculated by using the derivation of moment generating function of the decision variable and then by computing its inverse Laplace transform of it one can obtain the bit error rate [60].

2.4.3 Q-Factor:

When the system BER is too low to be measured within a reasonable amount of time; it is useful to adopt the Q-factor measurement as indirect technique to measure the BER.

Q-factor is a function of the means and the standard deviations of the received electric currents in the marks and in the spaces. It's a dimensionless parameter widely used to measure the performance of the optical lightwave systems [59, 60, 62]. In simulation codes, Q-factor can be calculated based on the split-step method [64]. With this method we can write Q-factor as

$$Q = \frac{\mu_1 - \mu_0}{\sigma_1 + \sigma_0} \tag{2.15}$$

where μ_1 and μ_0 are the mean values of the decision variable I_k, obtained by sampling the current $I(t)$ at the electrical filter output at the instant t_k, for the bit "1" and "0", respectively. σ_1 and σ_0 are the corresponding standard deviations for μ_1 and μ_0.

Q-factor can be used to give an approximate value for the bit-error rate under the assumption that the electric currents in the marks and in the spaces at the receiver are both Gaussian distributed [63]. Even though the actual distributions of the marks and spaces are not Gaussian, considering the distribution of the marks and spaces provide a good estimate of the bit-error rate (BER) in some cases [61]. On the other hand, when the bit-error rate can be directly measured in the receiver (BER>10^{-13}), the Q factor can be estimated from the bit-error rate. The Q-factor is analytically related to the BER on the Gaussian assumption due to the equation [64]

$$BER = \left(\frac{1}{2}\right) erfc\left(\frac{Q}{\sqrt{2}}\right), \tag{2.16}$$

where $erfc$ is the complementary error function defined as

$$erfc(x) = \frac{2}{\sqrt{\pi}} \int_x^{\infty} \exp(-y^2)\, dy\,. \tag{2.17}$$

When the optical signal is affected by either optical linear effects such as dispersion, or optical nonlinear effects such as crosstalk, and its histogram is distorted, the probability density function of the transmitted marks and spaces is no longer a Gaussian distribution. For that situation equation (2.15) can not be used to estimate the signal's BER. However, the statistical properties of the signal can be regarded as the superposition of two sets of Gaussian random processes [65]. In this case, the BER can be given as the sum of the probabilities that these Gaussian processes are above or below the decision threshold respectively.

As a final point, it's important to say that the design and performance evaluation of the optical fiber communication systems relies just as much on the accuracy and efficiency of receiver models as it does on accuracy and efficient modeling of the transmission line.

Chapter 3

Polarization Effects in Optical Fiber Communications

3.1 Introduction

The role of polarization effects in telecommunication systems can be detrimental as it can cause pulse broadening and impair system performance. In the past decades extensive studies of polarization effects in single mode fiber have been done. For examples see Ref.s [4, 12, 15, 22, 27].

3.1.1 The origin of polarization effects in single mode fibers

The origin of polarization effects in single mode fibers is related to the asymmetry in either the fiber geometry or the stress distribution in the fibers. In practice, it is very difficult to make fibers with perfect circular symmetry so that the two orthogonal HE_{11} [66] modes have the same propagation constant. In fact, the distortion of the geometry of the fiber core leads directly to different propagation constants or phase velocities in the two polarization modes. On the other hand, the fiber is formed with different chemical composition with distinct thermal expansion coefficients at different radial positions in the fiber. The distortion in geometry can cause the stress field in the core to become asymmetric as the fiber is drawn and cooled down from a high temperature. Through the stress-optic effect, the asymmetric stress is translated into an anisotropic refractive index change across the fiber. Moreover, after the fiber is made, there are more external factors that may affect the polarization properties of the single mode fibers such as bending, twisting, or applying lateral load to the fibers when the fibers are deployed for actual use.

The birefringence is defined as the difference of the effective refractive indices in the two polarization modes

$$B = \Delta n_{eff} = n_{eff}^{x} - n_{eff}^{y} \tag{3.1}$$

The fundamental polarization property of a fiber is characterized by birefringence B. The birefringence affects the evolution of fields propagating in the fiber, which results in a periodic evolution of the state of polarization along the fiber. This leads to the difference of the propagation constants between the two local polarization modes $\Delta\beta$ ($\Delta\beta = (\omega \Delta n_{eff})/c$). The characteristic length or period of the polarization evolution is usually called beat length. The beat length L_B is directly related to the difference of the propagation constants as $L_B = \frac{2\pi}{\Delta\beta} = \lambda/B$.

In telecommunication systems, light is often transmitted in the pulse form. In this case we can describe the pulse broadening by the local difference of the group velocity. Therefore, the concept of group birefringence and group beat length are used instead of the phase birefringence and phase beat length. The group birefringence is defined as:

$$\Delta n_g = B - \lambda \frac{d B}{d \lambda} \tag{3.2}$$

(In conventional fibers including transmission fibers and speciality fibers such as PMFs, the difference between the phase and the group birefringence is often negligible [67].)

3.1.2 Polarization evalution in birefringent fibers

It is well known that making fibers with low polarization mode dispersion is a critical issue [68].To understand the polarization evolution in birefringent fibers we need a detailed mathematical description. The Jones matrix formalism [4, 44] can be used to describe various effects in polarization evolutions. It describes the full details of the polarization evolution. In fact, the usual formalism to analyze polarization effects in optical fibers is the Jones formalism.

Maintaining the state of polarization in single mode fibers can be achieved by making fibers with very high birefringence or very low birefringence. In a fiber with very low birefringence, the polarization state is very sensitive to external perturbation. A slight perturbation, such as bending or pressing the fiber, will induce sufficient birefringence to alter the state of the polarization. In practice, fibers with very high birefringence (on order of 10^{-4}) are typically utilized. Moreover, the linear input state of polarization is typically aligned with one of the birefringence axes of the polarization maintaining fiber to achieve a polarization maintaining operation.

3.2 Fundamental mathematical tools

In our work we have used some fundamental tools to evaluate the performance of the optical fiber system in presence of chromatic dispersion and polarization effects: polarization mode dispersion and polarization dependent loss/gain. Hence, we need to recall some properties of these tools.

3.2.1 Pauli spin matrices and spin vector

Spin vector and Pauli spin matrices are used widely in the main parts in this thesis. Because of that, we review their properties here. The analysis of lightwave transmission systems is dealing with a complex 2x2 matrices when we used the matrix analysis. One of the convenient ways to treat these matrices is to use the spin vector notation. The spin vector notation consists of treating the three spin matrices of Jones space as the three components of a vector in Stokes space. The spin matrices have the properties:

1- They are Hermitian $(\sigma_i = \sigma_i^{\dagger})$,

2- They are Unitary $(\sigma_i{}^{-1} = \sigma_i^{\dagger})$,

3- They have zero trace $(Tr\,(\sigma_i) = 0)$,

4- They obey the multiplication rules $(\sigma_i^2 = I\,;\ \sigma_i\sigma_j = -\sigma_j\sigma_i = i\sigma_k)$, where $(\,i,j,k\,)$ any cyclic permutation.

3.2.2 State of polarization of a lightwave on the Poincare sphere

The electric field of a light wave propagates in the z-direction and has the components E_x and E_y in x and y directions, respectively. The state of polarization of a lightwave on the Poincare sphere can be represented with the vector $\vec{s}$, where their components $(s_x\,, s_y\,, s_z)$ are related to electric field's components [22].

By using Jones space, polarization states are described by two dimensional complex column vector, the so-called ket vector $|s\rangle = \binom{e_x}{e_y}$. The corresponding conjugate row vector is a row vector called bra and it is defined as $\langle s| = (e_x^* \quad e_y^*)$. For any complex multiplier q the states of polarization (SOP), $|s\rangle$ and $q|s\rangle$ are same. The corresponding Stokes vector $\hat{s} \equiv (s_x, s_y, s_z)$ is defined by $\hat{s} \equiv \langle s|\vec{\sigma}|s\rangle/\langle s|s\rangle$, where $\vec{\sigma}$ is the Pauli matrix vector.

3.2.3 PMD vector

The PMD vector $\vec{\tau}(z,\omega)$ is a three component polarization vector in Stokes space. Due to the external mechanical stresses and environmental conditions the PMD vector varies in random fashion with fiber length, and the optical frequency. Each of the three components of the PMD vector is a superposition of many small random variables which, according to the central limit theorem, would give them a Gaussian distribution. Moreover, if the PMD vector is isotropic, then the three components would have identical Gaussian probability distribution functions. In some situations, the fiber length is constant, then only the drift and frequency variation of the PMD vector are of interest. The magnitude of the PMD vector equal to the differential group delay time between the fast and slow principal states of polarization, i.e.,$\Delta\tau = |\vec{\tau}|$. In the case of negligible polarization dependent loss PDL, the PMD vector $\vec{\tau}(z,\omega)$ is related the output polarization Stokes vector $\vec{S}$ (at a constant input polarization to the fiber) via eq. (2.13). This equation forms the basis for most of the known statistical properties of PMD, and it provides a very elegant concatenation rule for the PMD vector of a sequence of birefringent elements. The PMD vector

$$\vec{\tau} = \Delta\tau\,\hat{s} \tag{3.3}$$

defines the polarization of the slow PSP via the unit Stokes vector $\hat{s}$ and the differential group delay $\Delta\tau$ of pulses launched with the two PSPs. Recall equation (2.2), which gives the relation between the input and output Jones vectors $|s>$, $|t>$, respectively as:

$$|t> = T\,|s> \tag{3.4}$$

We can write the frequency dependent part of the Jones matrix that contained in the fiber's transmission matrix T as $U(\omega)$, which is related to the PMD vector in equation (3.4) using the relation [16]:

$$\left({}^{1}/_{2}\right)(\vec{\tau}\cdot\vec{\sigma}) = i\,U^{\dagger}\,U_{\omega} \tag{3.5}$$

where $\vec{\sigma}$ is the Pauli spin vector.

3.2.4 The statistics of polarization dependent loss

Using single mode fibers in telecommunications produces an attenuation which depends on the polarization of the propagating light. This attenuation is extremely small for standard telecom fibers [8]. On the other hand, for combination of several optical elements, such as in optical systems, the global polarization dependent loss has an effective value which can affect the performance of the system. In general, the global polarization dependent loss can not be determined by the sum of the individual values of the polarization dependent loss of each element.

Polarization dependent loss (PDL) is defined using the maximum and minimum transmissions T_{Max}, T_{Min}, respectively [8] as $\Gamma = \dfrac{T_{Max} - T_{Min}}{T_{Max} + T_{Min}}$. With N elements, the maximum transmission is $T_{Max1\ldots N} = T_{Max1}\,T_{Max2}\ldots T_{MaxN}$, and the minimum transmission is $T_{Min1\ldots N} = T_{Min1}\,T_{Min2}\ldots T_{MinN}$. For two passive elements

$$PDL_1 = 10\log[\frac{I_{Max_1}}{I_{Min_1}}], \tag{3.6.a}$$

$$PDL_2 = 10\log[\frac{I_{Max2}}{I_{Min_2}}], \tag{3.6.b}$$

where $I_{Max1,2}$ and $I_{Min1,2}$ are the maximum and the minimum intensities for the first and second PDL sections, respectively. If the horizontal polarization axes of both elements are aligned with one another, then the polarization dependent loss of the two combined elements can be added (or subtracted) as

$$PDL_1 + PDL_2 = 10\log[\frac{I_{Max_1} \cdot I_{Max2}}{I_{Min1} \cdot I_{Min2}}]. \tag{3.7}$$

Practical optical systems may contain N polarization elements. In this case it is impossible to align their axes. In reality, the first PDL element will partially polarize the light and the next one will attenuate the light. The degree of this attenuation depends on the relative orientation of the two PDL elements. Moreover, due to the effect of the connecting fibers, the intrinsic PDL of the elements will fluctuate with the time. Consequently, statistical methods have to be used in order to obtain the global PDL.

3.2.5 The interplay between PDL and PMD

The interplay between PDL and PMD is often present and it causes more impairment that is because the combined presence of PMD and PDL may introduce fluctuations larger than those estimated by the mean square rules. Moreover, the coupling between PMD and PDL is randomly distributed along the link and only a statistical description of the total accumulated PDL can be given.

There were several publications which have shown theoretical analyzes that PDL can enhance the pulse broadening that caused by PMD [6,74,75].

Another important result, based on the study of the combination of PDL and PMD, that is the differential group delay, without considering PDL, is Maxwellian distributed, and the two principal states of polarization are orthogonal. With taking PDL in the consideration, the interaction between PMD and PDL makes the DGD distribution deviate from Maxwellian and the two principal states of polarization are not orthogonal any more. Moreover, it has been shown that, for optical systems, the presence of PDL might reduce the efficiency of some PMD compensators [76].

3.2.6 Chromatic dispersion

Chromatic dispersion is one of the major sources of transmission degradation in high speed optical communication systems. With neglecting the higher order CD affect in a dispersive fiber (single mode fiber), the low-pass transfer function of the fiber has the form

$$H_{CD}(f) = e^{-i2\pi^2\beta_2 f^2 L} \tag{3.8}$$

with $\beta_2 = -\lambda^2 D(\lambda)/(2\pi c)$. Here $D(\lambda)$ is the fiber CD parameter at wavelength λ, L the fiber length, and f the frequency deviation with respect to the carrier frequency.

3.2.7 Modeling a single-mode fiber:

Gisin and Huttner [9] presented a nice description for a standard single-mode telecom fiber. We will use this model as a start point in our work. Considering a concatenation of optical fibers, each of them is supporting two polarization modes. The birefringence β_j is equal to the differential group delay (DGD) between the two modes. The PDL of the j[th] trunk can be expressed (in dB) as $10\log(e^{2\alpha_j})$, where $e^{2\alpha_j} = I_{max}/I_{min}$. For N trunks, the complex Jones vector is

$$\vec{\mathrm{E}}_{out} = \left[\exp\left(-\alpha_0 - \sum_{j=1}^{N}\frac{\alpha_j}{2}\right)\right] T_N(\omega)\vec{\mathrm{E}}_{in}\,, \tag{3.9}$$

where α_0 is the polarization independent overall loss, $\exp\left(-\alpha_0 - \sum_{j=1}^{N}\frac{\alpha_j}{2}\right)$describes the global attenuation,and

$$T_N(\omega) = \exp\left[\left(-i\vec{\beta}_N\omega + \vec{\alpha}_N\right)\cdot\frac{\vec{\sigma}}{2}\right]\ldots\exp\left[\left(-i\vec{\beta}_2\omega + \vec{\alpha}_2\right)\cdot\frac{\vec{\sigma}}{2}\right]\exp\left[\left(-i\vec{\beta}_1\omega + \vec{\alpha}_1\right)\cdot\frac{\vec{\sigma}}{2}\right], \tag{3.10}$$

here $\vec{\sigma} \equiv (\sigma_x, \sigma_y, \sigma_z)$ is the Pauli matrix vector whose three components are the Pauli matrices which defined as:

$$\sigma_x = \begin{pmatrix} 0 & 1 \\ 1 & 0 \end{pmatrix}, \quad \sigma_y = \begin{pmatrix} 0 & -i \\ i & 0 \end{pmatrix}, \quad \sigma_z = \begin{pmatrix} 1 & 0 \\ 0 & -1 \end{pmatrix}. \tag{3.11}$$

The Pauli matrices are used widely in many mathematical and physical applications; they have useful proprieties, a good review of the properties of Pauli matrices can be found in ref. (16).

3.2.8 The waveplate model:

It is well accepted that the PMD in a fiber transmission link can be modeled as a concatenation of many birefringence sections with random birefringence axes. This model has been known as a waveplate model. This model contains all PMD orders. Hence, it is called an all-order PMD model. An all-order model is a concatenation of many birefringence sections $U_i(\omega)$ with random orientations, Figure (3.1). The magnitude of the birefringence of each section may be equal or not equal to each others.

Since the autocorrelation function of the PMD vector is a periodic function of frequency, it is important to make sure that the period of the PMD autocorrelation function is much larger than the signal bandwidth. The relation between the total DGD and the DGD for each section is given as [69]: $\langle\tau^2\rangle = \sum_{i=1}^{N}\langle\Delta\tau_i^2\rangle$. Furthermore, there are two types of the waveplate models:

1- The conventional waveplate model:

In his model, the fiber is treated as a concatenation of N polarization maintaining fiber segments and every segment has DGD and PDL values uniformly distributed within certain ranges. The maximum DGD and PDL of each segment are β_{max} , and α_{max} , respectively.

The maximum DGD and PDL values generated by this model are $N \cdot \beta_{max}$ and $N \cdot \alpha_{max}$, respectively. With a large enough number of birefringence sections (large than 15 [67]), this model yields a distribution for the differential group delay (DGD) close to a Maxwellian function [70].

The disadvantage of this model is that it produces zero DGD or PDL probability density when the DGD or PDL is larger than $N \cdot \beta_{max}$ or $N \cdot \alpha_{max}$. This would introduce errors in modeling of the PMD and PDL-induced system degradation because high BER usually occurs at large DGD and PDL.

2- The new waveplate model:

In order to overcome the limitation of the conventional waveplate model, a new waveplate model has been introduced by Lu and others [76]. With this new waveplate model, the DGD and PDL in each fiber segment do not have an upper limit. The new waveplate model rapidly converges towards a Maxwellian DGD distribution even at DGD probability densities as low as 10^{-35} (N=15).

3.2.9 System of highly mode coupled PMD/PDL fiber:

PMD has been treated analytically by assuming that the fiber consists of many sections, each having a small value of PMD, and each is coupled randomly to the

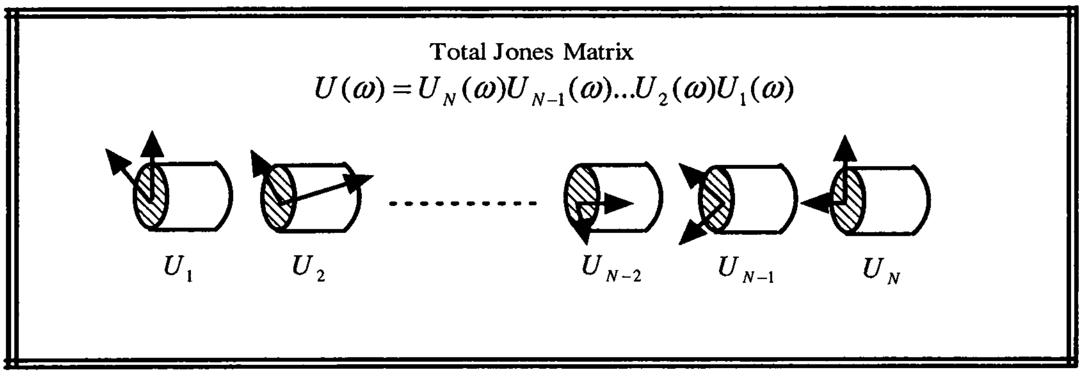

Fig. 3.1The Waveplate Model

adjacent sections. This statistical treatment was shown to lead to a Maxwellian probability density function [4, 10].

The differential group delay is assumed to follow a Maxwellian distribution since this distribution is a very good approximation to the exact distribution. However, the number of birefringent elements in a link is usually unknown, and the Maxwellian distribution is only exact for an infinite number of concatenated birefringent elements.

In standard optical transmission fibers, the DGD is a random variable with a Maxwellian probability density function (PDF) [1, 26, 70]. However, system components like isolators, couplers, rotators, etc, have birefringence that is usually deterministic, which means that the PMD vector of the component is more or less constant with wavelength and does not drift with time. The PDF of the DGD of such an element is a delta function. Hence we expect a combination of random and deterministic PMD throughout the link. Furthermore, PMD emulators consisting of a finite number of concatenated birefringent elements will usually deviate from a Maxwellian in having a maximum attainable DGD [73] (mathematically, the PDF of the DGD is identically zero above a certain maximum value).

3.3 System model

The system under the study is shown in figure (3.2) in its simple description. In fact, we will focus, here, on part of the optical system, that summarizes the idea of considering some lumped sections, which denoted the optical devices in the real situation, beside the whole fiber as a high mode coupling PMD and PDL (or as it is called Maxwellian fiber).

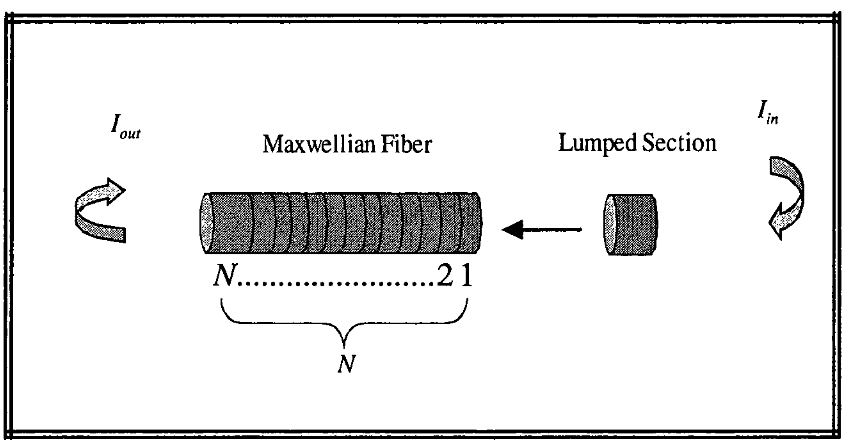

Figure (3.2) System modeling

3.4 The analytical model

The output light intensity as a function of time can be written as

$$I(t) = \vec{E}^*_{out}(t) \cdot \vec{E}_{out}(t) , \tag{3.12}$$

the output electric field itself is related to the input electric field with the relation:

$$\vec{E}_{out}(\omega) = A\, T(\omega)\vec{E}_{in}(\omega) \tag{3.13}$$

parameter A , as well as $T(\omega)$, in the last equation depends on the system under the study.

3.4.1 Q-factor of the output intensity

To calculate the Q-factor of the output intensity we need to find the mean intensity at the maximum and minimum points, we will call them $\langle I(t)\rangle_{max}$, $\langle I(t)\rangle_{min}$, respectively. Furthermore, we need to calculate the standard deviation at the maximum and minimum points, we will call them $\sigma(t)_{max}$, and $\sigma(t)_{min}$, respectively. Then we can use the well known definition of Q-factor, which is given as

$$Q = \frac{\langle I(t)\rangle_{max} - \langle I(t)\rangle_{min}}{\sigma(t)_{max} + \sigma(t)_{min}}. \tag{3.14}$$

3.4.2 The output intensity

With the help of the standard wave plate model, we can consider the fiber in our system as containing N sections and then we take the limit at the end [45].In this case we can rewrite the output electric field as

$$\vec{E}_{out}(\omega) = A_N(e^{i\varphi_{CD}(\omega)})T_N(\omega)\vec{E}_{in}(\omega). \tag{3.15}$$

The Jones matrix $T_N(\omega)$ contains the information about the PMD and PDL in the system, while $e^{i\varphi_{CD}(\omega)}$ is related to the chromatic dispersion (CD). On the other hand, A_N is related to overall polarization-independent attenuation α_0, and the polarization dependent loss/gain (PDL/G) α_j.Since we are following Ref. [41] in this chapter and the next one, we preferred to use the same notation in that reference for both of these chapters. The parameter A explicitly written as $A_N = \exp[-\alpha_0 - \sum_{j=1}^{N}|\alpha_j|/2]$. While the explicit form of the $T_N(\omega)$ is the transform matrix propagation $T_N(\omega) = e^{-i\frac{\vec{\beta}_1\cdot\vec{\sigma}}{2}} e^{\frac{\vec{\alpha}_1\cdot\vec{\sigma}}{2}} e^{-i\frac{\vec{\beta}_2\cdot\vec{\sigma}}{2}} e^{\frac{\vec{\alpha}_2\cdot\vec{\sigma}}{2}} \dots e^{-i\frac{\vec{\beta}_N\cdot\vec{\sigma}}{2}} e^{\frac{\vec{\alpha}_N\cdot\vec{\sigma}}{2}}$, where $\vec{\sigma}$ is the standard Pauli matrices, $\vec{\beta}_j = \beta_j\hat{\beta}_j$.represents the j^{th} PMD wave plate that has DGD β_j and the fast-axis polarization is expressed by the unit vector $\hat{\beta}_j$ in the Stokes space. Similarly, $\vec{\alpha}_j = \alpha_j\hat{\alpha}_j$ represents the j^{th} PDL/G wave plate with the PDL value expressed in decibels by $20\,|\alpha_j|log_{10}\,e$ and the maximum transmission is expressed by the unit vector $\hat{\alpha}_j$ in the Stokes space. In Jones space we can write the input electric field as

$$\vec{E}_{in}(\omega) = f_{in}(\omega)\begin{bmatrix} x \\ y \end{bmatrix}, \tag{3.16}$$

Here $f_{in}(\omega)$is the Fourier transform of the input pulse sequence, $\begin{bmatrix} x \\ y \end{bmatrix}$ is a unit vector in Jones space. Hence the output intensity can be written as

$$I(t) = \left(\frac{|A_N|^2}{2\pi}\right)\int_{-\infty}^{\infty} d\omega \int_{-\infty}^{\infty} d\acute{\omega} \left\{e^{i[\omega_{CD}(\acute{\omega})-\omega_{CD}(\omega)]}\right\}\left\{[x^* \quad y^*]\, T_N^{\dagger}(\acute{\omega})T_N(\omega)\begin{bmatrix} x \\ y \end{bmatrix}\right\}$$

$$\times \left\{e^{i(\omega-\acute{\omega})t} f_{in}^{*}(\acute{\omega}) f_{in}(\omega)\right\}. \tag{3.17}$$

In the last equation the term $T_N^{\dagger}(\acute{\omega})T_N(\omega)$ has the form

$$T_N^{\dagger}(\acute{\omega})T_N(\omega) = \Gamma_{0,N}(\acute{\omega},\omega)I + \vec{\Gamma}_N(\acute{\omega},\omega)\cdot\vec{\sigma}\,, \tag{3.18}$$

and the term $[x^* \quad y^*]\, T_N^{\dagger}(\acute{\omega})T_N(\omega)\begin{bmatrix} x \\ y \end{bmatrix}$ has the form

$$[x^* \quad y^*]\, T_N^{\dagger}(\acute{\omega})T_N(\omega)\begin{bmatrix} x \\ y \end{bmatrix} = \Gamma_{0,N}(\acute{\omega},\omega)I + \vec{\Gamma}_N(\acute{\omega},\omega)\cdot\hat{m}\,, \tag{3.19}$$

where I is a 2×2 unity matrix, $\hat{m}$ is a unit Stokes vector representing the input state of polarization and $\hat{m} = [x^* \quad y^*]\,\vec{\sigma}\begin{bmatrix} x \\ y \end{bmatrix}$.

At this point let us consider just one added lumped section L, in this case our previous equations still apply by switching the notation of N to L.

$$I(t) = \left(\frac{|A_L|^2}{2\pi}\right)\int_{-\infty}^{\infty} d\omega \int_{-\infty}^{\infty} d\acute{\omega}\,\{e^{i[\omega_{CD}(\omega)-\omega_{CD}(\acute{\omega})]}\}\{[x^* \quad y^*]\, T_L^{\dagger}(\acute{\omega})T_L(\omega)\begin{bmatrix} x \\ y \end{bmatrix}\}$$

$$\times\{e^{i(\omega-\acute{\omega})t} f_{in}^*(\acute{\omega})f_{in}(\omega)\}. \tag{3.20}$$

Moreover, for a system contains both the high mode coupling and one lumped section, the output intensity is

$$I(t) = \left(\frac{|A_{N+L}|^2}{2\pi}\right)\int_{-\infty}^{\infty} d\omega \int_{-\infty}^{\infty} d\acute{\omega}\,\{e^{i[\omega_{CD}(\acute{\omega})-\omega_{CD}(\omega)]}\}\{[x^* \quad y^*]\, T_{N+L}^{\dagger}(\acute{\omega})T_{N+L}(\omega)\begin{bmatrix} x \\ y \end{bmatrix}\}$$

$$\times\{e^{i(\acute{\omega}-\omega)t} f_{in}^*(\acute{\omega})f_{in}(\omega)\}. \tag{3.21}$$

3.4.3 The statistical average of the intensity:

To calculate the output light intensity averaged over the input state of polarization $\hat{m}$ as well as PMD and PDL/G, we will use the method first introduced by Karlsson and Brentel [74]. Using the last equation, the averaged intensity can be written as

$$\langle I(t)\rangle = \left(\frac{|A_{N+L}|^2}{2\pi}\right)\int_{-\infty}^{\infty} d\omega \int_{-\infty}^{\infty} d\acute{\omega}\, \{e^{i[\omega_{CD}(\omega)-\omega_{CD}(\acute{\omega})]}\}\{\langle \Gamma_{0,N+L}(\acute{\omega},\omega) I + \vec{\Gamma}_{N+L}(\acute{\omega},\omega)\cdot \hat{m}\rangle\}$$

$$\times \{e^{i(\acute{\omega}-\omega)t} f_{in}^{*}(\acute{\omega}) f_{in}(\omega)\}. \qquad (3.22)$$

where

$$\Gamma_{0,N+L}(\acute{\omega},\omega) =$$

$$\left(\cosh\alpha_N \cos(\beta_N\Delta\omega)\,\Gamma_{0,N-1} + i\cosh\alpha_N\, sin(\beta_N\Delta\omega)(\hat{\beta}_N\cdot\vec{\Gamma}_{N-1}) + sinh\alpha_N\, cos(\beta_N\bar{\omega})(\hat{\alpha}_N\cdot\vec{\Gamma}_{N-1}) + sinh\alpha_N\, sin(\beta_N\bar{\omega})[\hat{\alpha}_N\cdot(\vec{\Gamma}_{N-1}\times\vec{\beta}_N)] + (\hat{\alpha}_N\cdot\hat{\beta}_N)\{i\, sinh\alpha_N\, sin(\beta_N\Delta\omega)\Gamma_{0,N-1} + (\hat{\beta}_N\cdot\vec{\Gamma}_{N-1})\, sinh\alpha_N[cos(\beta_N\Delta\omega) - cos(\beta_N\bar{\omega})]\}\right)\left(\cosh\alpha_l \cos(\beta_l\Delta\omega)\,\Gamma_{0,l-1} + i\cosh\alpha_l\, sin(\beta_l\Delta\omega)(\hat{\beta}_l\cdot\vec{\Gamma}_{l-1}) + sinh\alpha_l\, cos(\beta_l\bar{\omega})(\hat{\alpha}_l\cdot\vec{\Gamma}_{l-1}) + sinh\alpha_l\, sin(\beta_l\bar{\omega})[\hat{\alpha}_l\cdot(\vec{\Gamma}_{l-1}\times\vec{\beta}_l)] + (\hat{\alpha}_l\cdot\hat{\beta}_l)\{i\, sinh\alpha_l\, sin(\beta_l\Delta\omega)\Gamma_{0,l-1} + (\hat{\beta}_l\cdot\vec{\Gamma}_{l-1})\, sinh\alpha_l[cos(\beta_l\Delta\omega) - cos(\beta_l\bar{\omega})]\}\right), \qquad (3.23.a)$$

$$\vec{\Gamma}_{N+L}(\acute{\omega},\omega) = \Big(\hat{\beta}_N\{I\, sin(\beta_N\Delta\omega)\Gamma_{0,N-1} + [cos(\beta_N\Delta\omega) - cos(\beta_N\bar{\omega})(\hat{\beta}_N\cdot\vec{\Gamma}_{N-1})]\} + cos(\beta_N\bar{\omega})(\vec{\Gamma}_{N-1}) + sin(\beta_N\bar{\omega})(\vec{\Gamma}_{N-1}\times\hat{\beta}_N) + \hat{\alpha}_N(sinh\alpha_N\, cos(\beta_N\Delta\omega)\Gamma_{0,N-1} + i\, sinh\alpha_N\, sin(\beta_N\Delta\omega)(\hat{\beta}_N\cdot\vec{\Gamma}_{N-1}) + (cosh\alpha_N - 1)\{i\,(\hat{\alpha}_N\cdot\hat{\beta}_N) sin(\beta_N\Delta\omega)\Gamma_{0,N-1} + (\hat{\alpha}_N\cdot\hat{\beta}_N)[cos(\beta_N\Delta\omega) - cos(\beta_N\bar{\omega})](\hat{\beta}_N\cdot\vec{\Gamma}_{N-1}) + cos(\beta_N\bar{\omega})(\hat{\alpha}_N\cdot\vec{\Gamma}_{N-1}) + sin(\beta_N\bar{\omega})[\hat{\alpha}_N\cdot(\vec{\Gamma}_{N-1}\times\vec{\beta}_N)]\})\Big) \times \Big(\hat{\beta}_l\{I\, sin(\beta_l\Delta\omega)\Gamma_{0,l-1} + [cos(\beta_l\Delta\omega) - cos(\beta_l\bar{\omega})(\hat{\beta}_l\cdot\vec{\Gamma}_{l-1})]\} + cos(\beta_l\bar{\omega})(\vec{\Gamma}_{l-1}) + sin(\beta_l\bar{\omega})(\vec{\Gamma}_{l-1}\times\hat{\beta}_l) + \hat{\alpha}_l(sinh\alpha_l\, cos(\beta_l\Delta\omega)\Gamma_{0,l-1} + i\, sinh\alpha_l\, sin(\beta_l\Delta\omega)(\hat{\beta}_l\cdot\vec{\Gamma}_{l-1}) + (cosh\alpha_l - 1)\{i\,(\hat{\alpha}_l\cdot\hat{\beta}_l) sin(\beta_l\Delta\omega)\Gamma_{0,l-1} + (\hat{\alpha}_l\cdot\hat{\beta}_l)[cos(\beta_l\Delta\omega) - cos(\beta_l\bar{\omega})](\hat{\beta}_l\cdot\vec{\Gamma}_{l-1}) + cos(\beta_l\bar{\omega})(\hat{\alpha}_l\cdot\vec{\Gamma}_{l-1}) + sin(\beta_l\bar{\omega})[\hat{\alpha}_l\cdot(\vec{\Gamma}_{l-1}\times\vec{\beta}_l)]\})\Big)$$

(3.23.b) where $\Delta\omega = (\omega - \acute{\omega})/2$ and $\bar{\omega} = (\omega + \acute{\omega})/2$.

With the help of the mathematical properties of averaging over a random unit vector $\hat{n}$ for given constant vectors $\vec{A}$ and $\vec{B}$; $\langle\hat{n}\cdot\vec{A}\rangle = \langle\hat{n}\cdot\vec{B}\rangle = 0$, $\langle(\hat{n}\cdot\vec{A})(\hat{n}\cdot\vec{B})\rangle = \left(\frac{1}{3}\right)(\vec{A}\cdot\vec{B})$, and $\langle(\hat{\alpha}_j\cdot\vec{A})(\hat{\alpha}_j\cdot\vec{B})\rangle = \left(\frac{1}{3}\right)\langle\vec{A}\cdot\vec{B}\rangle$, with the use of all these assistants, we can calculate the averaged intensity of the output light to get:

$$\langle I(t)\rangle = \left(\frac{|A_{N+L}|^2}{2\pi}\right)\int_{-\infty}^{\infty} d\omega \int_{-\infty}^{\infty} d\acute{\omega}\left\{e^{i[\omega_{CD}(\omega)-\omega_{CD}(\acute{\omega})]}\right\}\langle\Gamma_{0,N+L}(\acute{\omega},\omega)\rangle\{e^{i(\acute{\omega}-\omega)t} f_{in}^{*}(\acute{\omega})f_{in}(\omega)\}, \tag{3.24}$$

here $\langle\Gamma_{0,0}(\acute{\omega},\omega)\rangle = 1$. The last step is to take the limit such that when $N\rightarrow\infty$, both α_N,β_N vanish ($\alpha_N\rightarrow 0, and\ \beta_N\rightarrow 0$), while $N\alpha^2 = \langle\eta^2\rangle$ and $N\beta^2 = \langle\Delta\tau^2\rangle$ are kept constant. This gives

$$\lim_{N\rightarrow\infty}\langle\Gamma_{0,N+L}(\acute{\omega},\omega)\rangle = \{\cosh\alpha_L\ \cos(\beta_L\Delta\omega) + i\langle\hat{\alpha}_L\cdot\hat{\beta}_L\rangle\sinh\alpha_L\ \sin(\beta_L\Delta\omega)\}$$

$$\times\exp\{\left(\tfrac{1}{2}\right)\langle\eta^2\rangle - \left(\tfrac{1}{8}\right)\langle\Delta\tau^2\rangle(\Delta\omega)^2 + i\langle\hat{\alpha}_L\cdot\hat{\beta}_L\rangle\sqrt{\langle\eta^2\rangle\langle\Delta\tau^2\rangle}(\Delta\omega)\} \tag{3.25}$$

3.8.4 The variation of the light intensity

The variation of output light intensity due to PMD and PDL/G $\langle[I(t)]^2\rangle$ can be calculated using the equation (3.21) as

$$\langle[I(t)]^2\rangle$$

$$= \left(\frac{|A_{N+L}|^4}{2\pi}\right)\int_{-\infty}^{\infty} d\omega_1 \int_{-\infty}^{\infty} d\acute{\omega}_1 \int_{-\infty}^{\infty} d\omega_2 \int_{-\infty}^{\infty} d\acute{\omega}_2 \left\{e^{i[\omega_{CD}(\omega_1)-\omega_{CD}(\acute{\omega}_1)]}e^{i[\omega_{CD}(\omega_2)-\omega_{CD}(\acute{\omega}_2)]}\right\}$$

$$\times\langle\left[\Gamma_{0,N+L}(\acute{\omega}_1,\omega_1) + \vec{\Gamma}_{N+L}(\acute{\omega}_1,\omega_1)\cdot\hat{m}\right]\left[\Gamma_{0,N+L}(\acute{\omega}_2,\omega_2) + \vec{\Gamma}_{N+L}(\acute{\omega}_2,\omega_2)\cdot\hat{m}\right]\rangle$$

$$\times\{e^{i(\acute{\omega}_1-\omega_1)t}\, e^{i(\acute{\omega}_2-\omega_2)t} f_{in}^{*}(\acute{\omega}_1)f_{in}(\omega_1)\, f_{in}^{*}(\acute{\omega}_2)f_{in}(\omega_2)\} \tag{3.26}$$

In this equation we will use the average over a random unit vector $\hat{m}$, that defined as $\langle(\hat{m} \cdot \vec{\Gamma}_1)(\hat{m} \cdot \vec{\Gamma}_2)\rangle = \left(\frac{1}{3}\right)\left(\vec{\Gamma}_1 \cdot \vec{\Gamma}_2\right)$, with this assistant we get that

$$\langle[I(t)]^2\rangle$$

$$= \left(\frac{|A_{N+L}|^4}{2\pi}\right)\int_{-\infty}^{\infty} d\omega_1 \int_{-\infty}^{\infty} d\acute{\omega}_1 \int_{-\infty}^{\infty} d\omega_2 \int_{-\infty}^{\infty} d\acute{\omega}_2 \left\{e^{i[\omega_{CD}(\omega_1)-\omega_{CD}(\acute{\omega}_1)]} e^{i[\omega_{CD}(\omega_2)-\omega_{CD}(\acute{\omega}_2)]}\right\}$$

$$\times \left\{\langle\Gamma_{0,N+L}(\acute{\omega}_1,\omega_1)\Gamma_{0,N+L}(\acute{\omega}_2,\omega_2)\rangle + (1/3)\langle\vec{\Gamma}_{N+L}(\acute{\omega}_1,\omega_1)\cdot\vec{\Gamma}_{N+L}(\acute{\omega}_2,\omega_2)\rangle\right\}$$

$$\times \{e^{i(\omega_1-\acute{\omega}_1)t}\, e^{i(\omega_2-\acute{\omega}_2)t} f_{in}^*(\acute{\omega}_1) f_{in}(\omega_1)\, f_{in}^*(\acute{\omega}_2) f_{in}(\omega_2)\} \tag{3.27}$$

The second order correlation functions can be calculated as following

$$\begin{bmatrix}\langle\Gamma_{0,N+L}(\omega_1,\acute{\omega}_1)\Gamma_{0,N+L}(\omega_2,\acute{\omega}_2)\rangle \\ \langle\vec{\Gamma}_{N+L}(\omega_1,\acute{\omega}_1)\cdot\vec{\Gamma}_{N+L}(\omega_2,\acute{\omega}_2)\rangle\end{bmatrix} = \begin{bmatrix}L_{11} & L_{12}\\ L_{21} & L_{22}\end{bmatrix}\begin{bmatrix}M_{11} & M_{12}\\ M_{21} & M_{22}\end{bmatrix}\begin{bmatrix}\langle\Gamma_{0,N-1}(\omega_1,\acute{\omega}_1)\Gamma_{0,N-1}(\omega_2,\acute{\omega}_2)\rangle \\ \langle\vec{\Gamma}_{N-1}(\omega_1,\acute{\omega}_1)\cdot\vec{\Gamma}_{N-1}(\omega_2,\acute{\omega}_2)\rangle\end{bmatrix}$$

$$= \begin{bmatrix}L_{11} & L_{12}\\ L_{21} & L_{22}\end{bmatrix}\begin{bmatrix}M_{11} & M_{12}\\ M_{21} & M_{22}\end{bmatrix}^N \begin{bmatrix}1\\0\end{bmatrix} \tag{3.28}$$

With the use of the notations $\Delta\omega_1 = \omega_1 - \acute{\omega}_1$, $\Delta\omega_2 = \omega_2 - \acute{\omega}_2$, $\overline{\omega_1} = \omega_1 + \acute{\omega}_1$, and $\overline{\omega_2} = \omega_2 + \acute{\omega}_2$, the explicit form of the elements $L_{11}, L_{12}, L_{21}, L_{22}, M_{11}, M_{12}, M_{21}$, and M_{22} are given in the Appendix B. Then we take the continuum limit, and with using the approximation of ignoring all orders higher than the second order of α_N and β_N.

3.9 The computational method

In order to obtain Q-factor using the analytical model above, a matlab code was used to calculate the values of Q-factor. The main code is provided in the Appendix B.

3.10 Results and Discussion

3.10.1 Points to be considered in the results

The results that presented here were taken with some considered points, which need to be explained to get a clear view about our model, those points are:

3.10.1.1The input pulse shape

The input pulse, that is considered in our results was a Gaussian pulse (usually created by a Mach-Zehnder interferometer modulator). The shape of such pulse is given as $f_{in}(t) = A\exp[-t^2(1+iC)/(2D^2T^2)]$, where C is the chirp factor, D is the duty cycle of the pulses, T the pulse width. Our results, here, were taken with pulse width $= 25ps$, and duty cycle $D < 1$ for return to zero pulses. Also, we consider a pulse sequence of ... $00\ 11\ 00$ ... as input sequence.

3.10.1.2 CD, PMD, and PDL values

The chromatic dispersion CD value is $2ps/nm$ and its dispersion slope $S = 0.01\,ps/nm^2$ for a carrier wavelength at $1550\,nm$. Moreover, we used the function $\phi_{CD} = \frac{b_2(\omega-\omega_0)^2}{2} + \frac{b_3(\omega-\omega_0)^3}{6}$ to describe the chromatic dispersion, here ω_0 is the carrier frequency, and $b_2 = d^2b/d\omega^2$ and $b_3 = d^3b/d\omega^3$ are related to the slope S by $S = \frac{\omega_0{}^4 b_3}{(2\pi c)^2} + \frac{2\omega_0{}^3 b_2}{(2\pi c)^2}$, b is the propagation constant. The values of PMD for lumped sections were taken as average $\Delta\tau$, i.e. $\langle\Delta\tau\rangle$, where as for the Maxwellian fiber a Maxwellian distribution has been considered as $\langle \Delta\tau^2 \rangle = 3\pi \langle \Delta\tau \rangle^2/8$. Also, the PDL values for Maxwellian fiber were considered as a Maxwellian distribution given as $\langle \eta^2 \rangle = 3\pi \langle \eta \rangle^2/8$ Moreover, we corvert the decibel values for PDL to dimensionless units by using the relation $\langle \eta \rangle = \langle \eta \rangle_{dB} / (20 \log_e 10)$.

3.10.1.3 PMD and PDL polarization directional correlation

The local PMD and PDL polarization directional correlation $\langle \hat{\alpha} \cdot \hat{\beta} \rangle$ can be measured with the autocorrelation of the complex principal state of polarization (PSP) vectors. This means that $-1 \leq \langle \hat{\alpha} \cdot \hat{\beta} \rangle \leq 1$, the strong correlation between PMD and PDL polarization direction corresponding to the case when $\langle \hat{\alpha} \cdot \hat{\beta} \rangle = \pm 1$. On the other hand the complete random correlation between the PMD and PDL polarization direction corresponds to the case $\langle \hat{\alpha} \cdot \hat{\beta} \rangle = 0$, this situation could be realized in ultra-long-haul links where many components are interleaved. In our results, from this chapter, we considered the case when the PMD and PDL polarization directional correlation is neither strong nor random. Specifically we consider the case when $\langle \hat{\alpha} \cdot \hat{\beta} \rangle = 0.15$ [75] as a case in between the strong and the random correlation between the PMD and PDL polarization direction. This situation was considered for both the lumped section and the Maxwellian fiber.

3.9.2 The main results:

3.10.2.1 The position of the lumped sections

To see if there is any effect of the position of the lumped section in the whole system, we did consider different cases; lumped sections followed by Maxwellian fiber, Maxwellian fiber followed by lumped sections, and lumped sections in between two equivalent Maxwellian fibers.

Figure (3.3) presents the input and output for these three situations, with a conclusion that the system with lumped sections followed by Maxwellian fiber, and the system with Maxwellian fiber followed by lumped sections give same average current output to each other, while the situation is different when we consider a system of lumped sections in between two equivalent Maxwellian fibers that is because of the relative orientation between PMD and PDL vectors, (PMD value was 2.5ps, and PDL value was 0.1 dB in all cases for the Maxwellian fiber. For the lumped sections, PMD= $15 \times 0.1 = 1.5\, ps$ and PDL= $15 \times 0.1\, dB$).

A more clear view is presented in figure (3.4) for the three situations. This figure presented Q-factor as a function of the total squared PMD (the total squared PMD for the whole system is the sum PMD squared for the Maxwellian fiber and PMD squared for the lumped system) for a system of fifteen lumped sections in the three situations with PDL equal to $0.5\, dB$ for the Maxwellain fiber and $15 \times 0.1\, dB$ for the lumped sections. The circle curve is for a system with equivalent Maxwellian fiber only, it is clear that Q-factor is overestimated (after 10 ps^2 for the whole system, which is the considered values in real systems) by viewing Maxwellian distribution for the whole system instead of considering it as lumped sections with Maxwellian. This show even a highly coupled PMD and PDL fiber linked with a lumped section is not equivalent to another highly coupled PMD/PDL fiber.

3.10.2.2 Constant value of PMD or PDL

For constant values of PMD, we studied the effect of changing the PDL values in several examples of the systems using our model. Figure (3.5.a) shows the case when all five sections have same values of PMD that is given as $\Delta\tau_{lum} = \sum_{j=1}^{5} \Delta\tau_j$ and same value of PDL, that is given as $\eta_{lum} = \sum_{j=1}^{5} \eta_j$, whereas, figure (3.5.b) presents the case when the five lumped sections having different values of PMD and PDL. The PMD values for the lumped sections are given as $\Delta\tau_{lum} = \sum_{j=1}^{5} j\Delta\tau_j$, and the PDL values given as $\eta_{lum} = \sum_{j=1}^{5} j\eta_j$. From these two sub-figures we can see that it is important to consider the detailed make-up of the lumped sections.

3.10.2.3 The PMD and PDL portions between Maxwellian fiber and lumped sections

The total PMD in the system is given by the equation $\langle\Delta\tau^2\rangle_{total} = \delta\langle\Delta\tau^2\rangle_{Max} + (1-\delta)\langle\Delta\tau^2\rangle_{lum}$, where δ is a parameter describes the portion that is taken by the Maxwellian fiber from the total PMD value in the whole system. Similarly, the total PDL in the whole system can be given as $\langle\eta^2\rangle_{total} = \varepsilon\langle\eta^2\rangle_{Max} + (1-\varepsilon)\langle\eta^2\rangle_{lum}$, ε is a parameter that describes the portion of PDL that is taken by the Maxwellian fiber from the total PDL in the whole system. Figure (3.6) presents a sample of an eye diagram for a system of three Maxwellian fibers contained lumped sections in between them. The Q-factor of this system as a function the parameters δ, and ε are given in figure (3.7). It is clear from this figure that these parameters play an important role in the Q-factor of the output. This means that the distribution of the total PMD and PDL values has a major effect on the output performance of the system.

3.10.3 Some side effects

To work with high accuracy, we tried to get converged values of Q-factor that related to number of points, duty cycle, and chirp value. We discuss them is the following.

3.10.3.1 Number of points

By number of points, we mean the points that are calculated in each period when we draw the curves of the output Q-factor. Figure (3.8) present Q-factor as a function of the inverse the number of points that is considered in one period for a system of three Maxwellian fibers connected with two lumped section in between them, the total PMD value is 2.8 ps, and total PDL values is 0.5dB. The Q-factor was calculated for this system (as example) at number of points $n = 11, 16, 32, 64, 128$. The converged result was obtained at $n = 64$. Hence we considered 64 points in each period for our calculations.

3.10.3.2 Duty cycle

The duty cycle means the ratio of the time interval where light is not zero within an existing pulse to bit period. Figure (3.9) presents Q-factor against the duty cycle of system of three Maxwellian fibers connected with two lumped sections in between them, the total PMD value is 2.8ps, and total PDL values is 0.5dB. The best Q-factor value was found at duty cycle $D = 0.24 - 0.25$.

3.10.3.3 Chirp value

We consider a Gaussian pulse shape created by Mach-Zehnder interferometer modulator, and it is well known that such a modulator is not chirp free. Hence, we calculated the Q-factor for several values of the chirp C.

Figure (3.10) shows that Q-factor decreases with increasing the chirp value (as expected).This figure is for a system of Maxwellian fiber followed by fifteen lumped sections. The PMD and PDL values are: PMD(M)=2.5ps, PMD(L)=15×0.1ps, PDL(M)=0.5dB,and PDL(L)=15× 0.01dB

3.11 Conclusion

-With considering PDL in a system consists from Maxwellian fiber and lumped sections, the Q-factor of the output will decrease which means that the output signal has more broadening. This is because of the interaction between PMD and PDL. As an example figure (3.11) present the effect of introducing PDL to the system

-For constant PDL, when the polarization mode dispersion of the Maxwellian fiber is of the same order or smaller than the polarization mode desperation of the lumped part, the outage probability will be overestimated by the use of an equivalent Maxwellian distribution.

-For constant PMD, Q-factor of the system consists from Maxwellian fiber and lumped sections will decrease uniformly as the ratio between the polarization dependent loss of the Maxwellian part and the lumped sections is increased.

-Putting lumped sections in the middle between two Maxwellian fibers makes Q-factor of the output intensity less than the situation if they were putting at the beginning or at the end of Maxwellian fiber. We have studied: Maxwellian fiber followed by lumped sections, lumped sections followed by Maxwellian fiber, lumped section in between two Maxwellian fibers.

The Q-factor of the output intensity is the same in the two first cases, but it become less if the lumped sections are sandwiched in between two Maxwellian fibers.

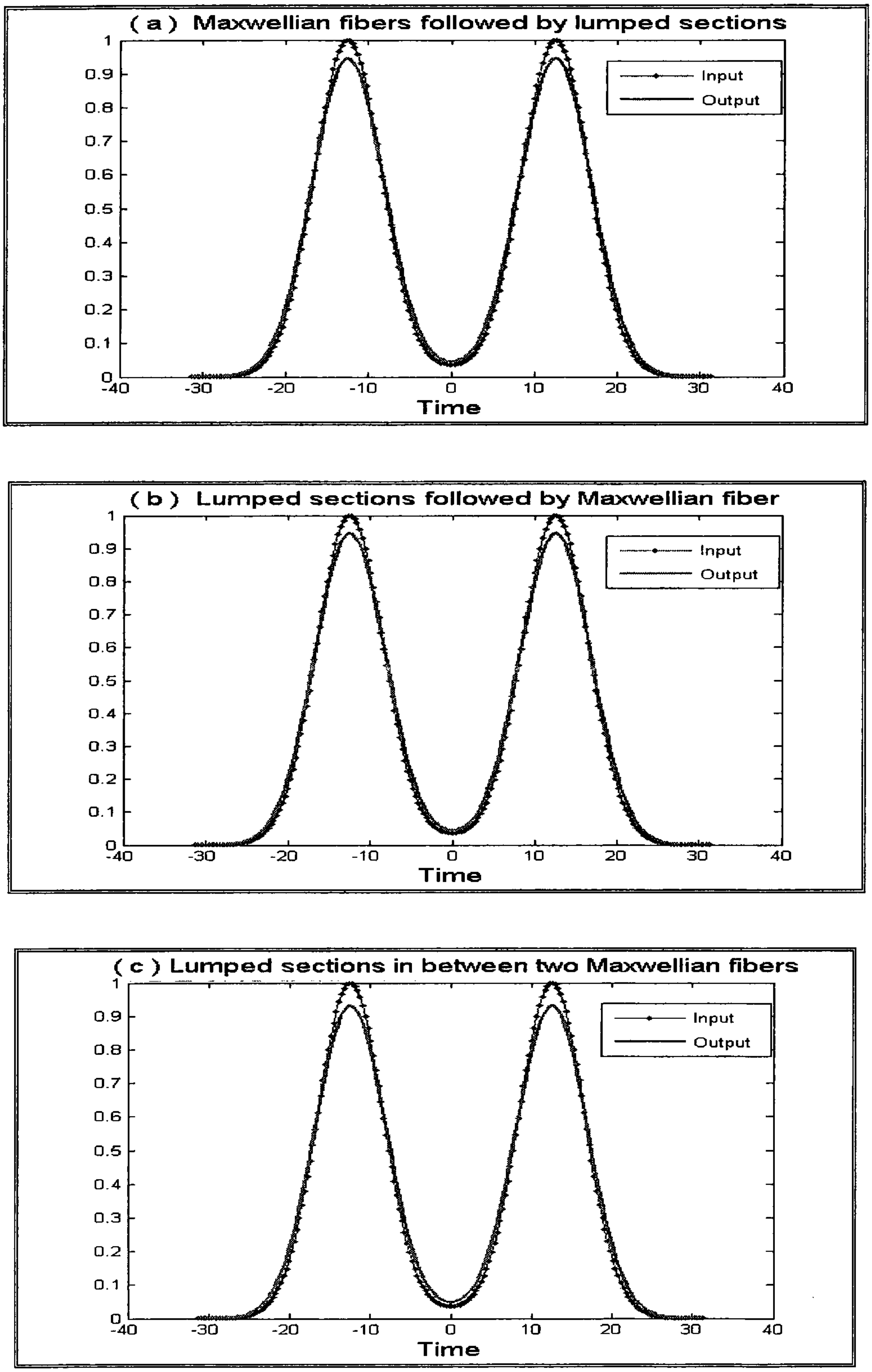

Figure (3.3) Input and average output current as a function of time

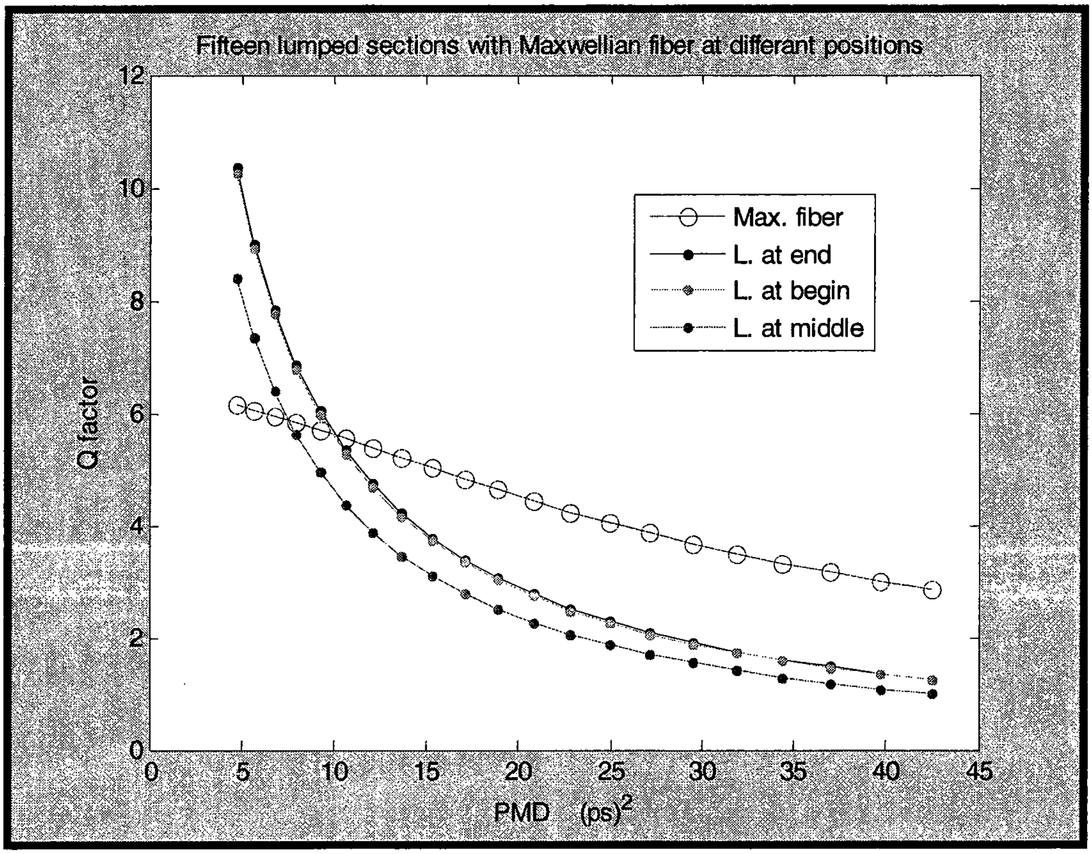

Figure (3.4) Q-factor against PMD for a system of Maxwellian fiber only and Maxwellian fiber+ fifteen lumped sections, (PDL (M)=0.5 dB, PDL(L)=15*0.1 dB)

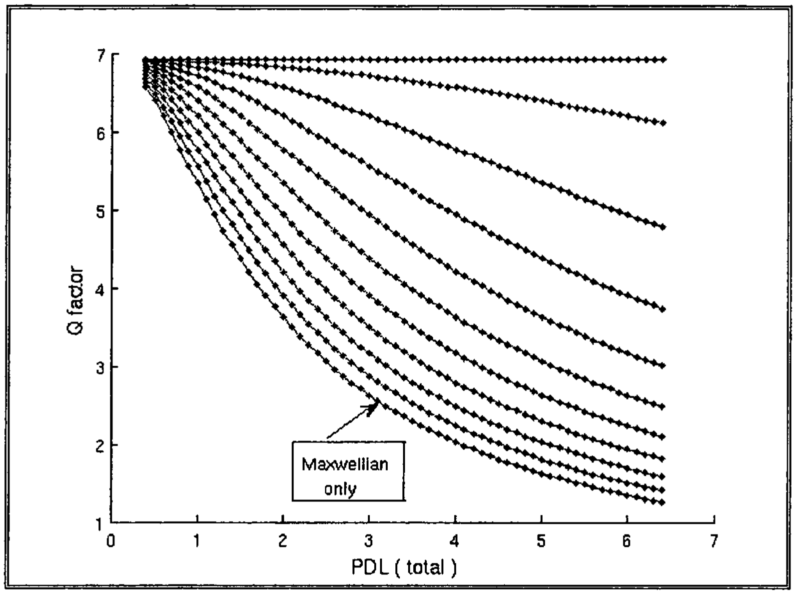

(a)

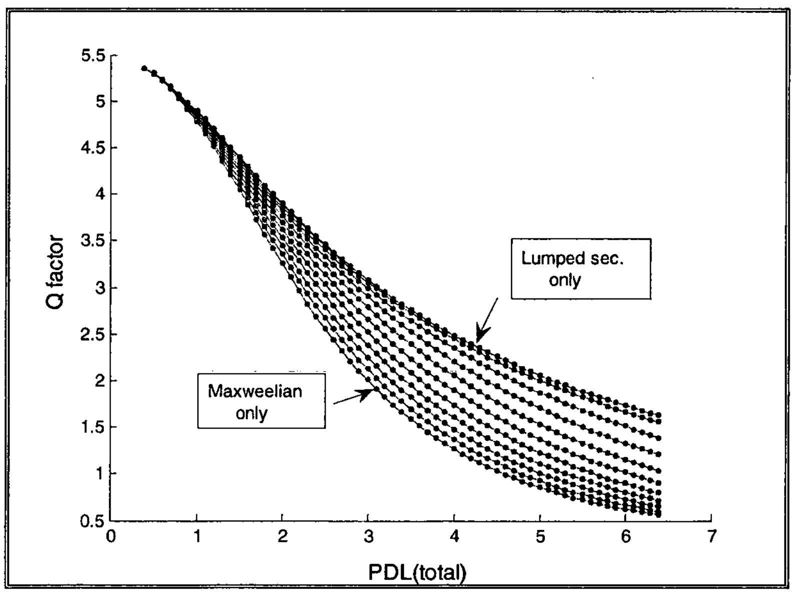

(b)

Figure (3.5) Q_factor as a function of the total PDL (dB) for a system contained Maxwellian fiber followed by five lumped section (a)The Lumped sections has the same values of PMD and PDL (b) The Lumped sections has different values of PMD and PDL

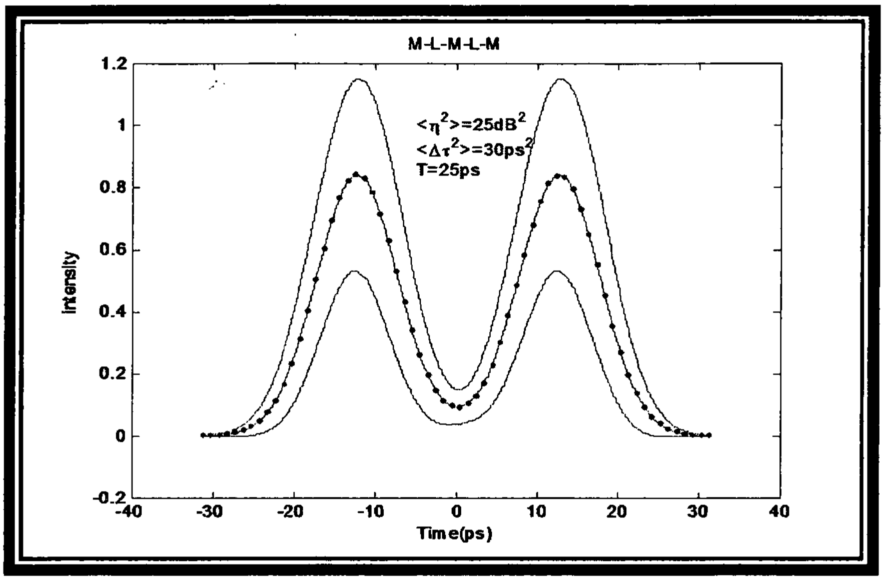

(a)

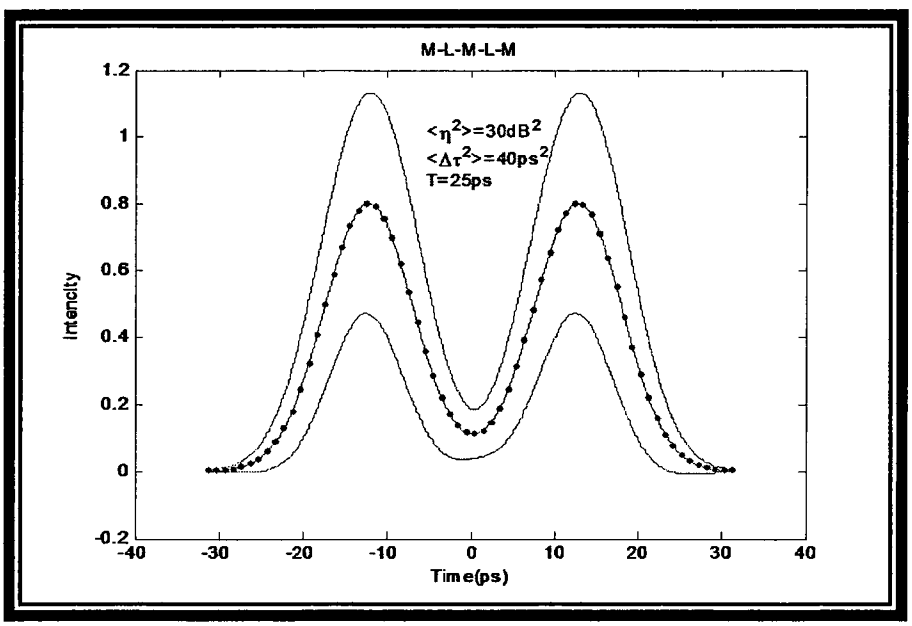

(b)

Figure (3.6) Sample of eye diagram for a system of three Maxwellian fibers contains lumped sections in between them (a) $<\Delta\tau^2>_{total}=30ps^2$, $<\eta^2>_{total}=25dB^2$,(b) $<\Delta\tau^2>_{total}=40ps^2$, $<\eta^2>_{total}=30dB^2$

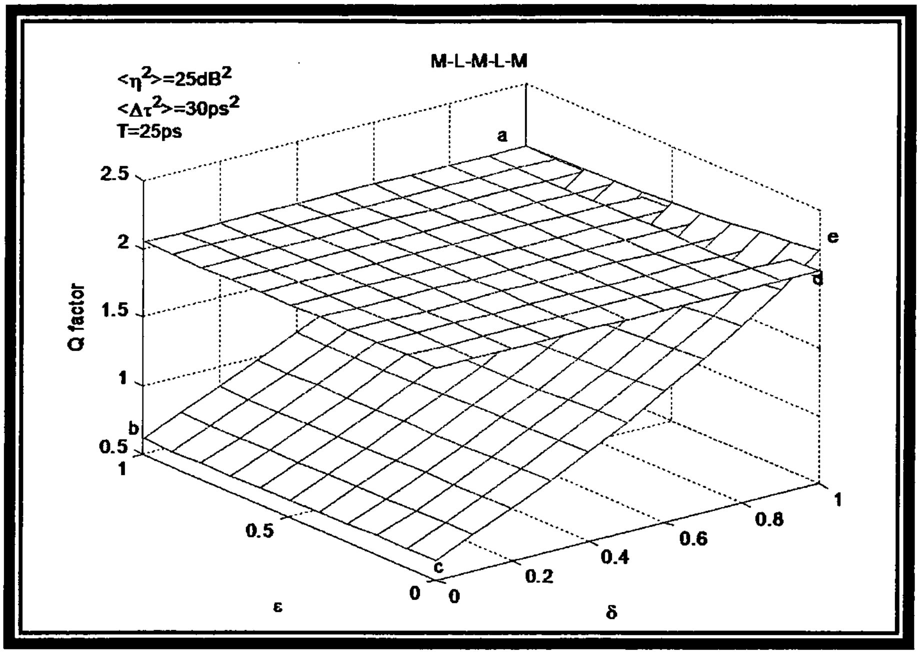

(a)

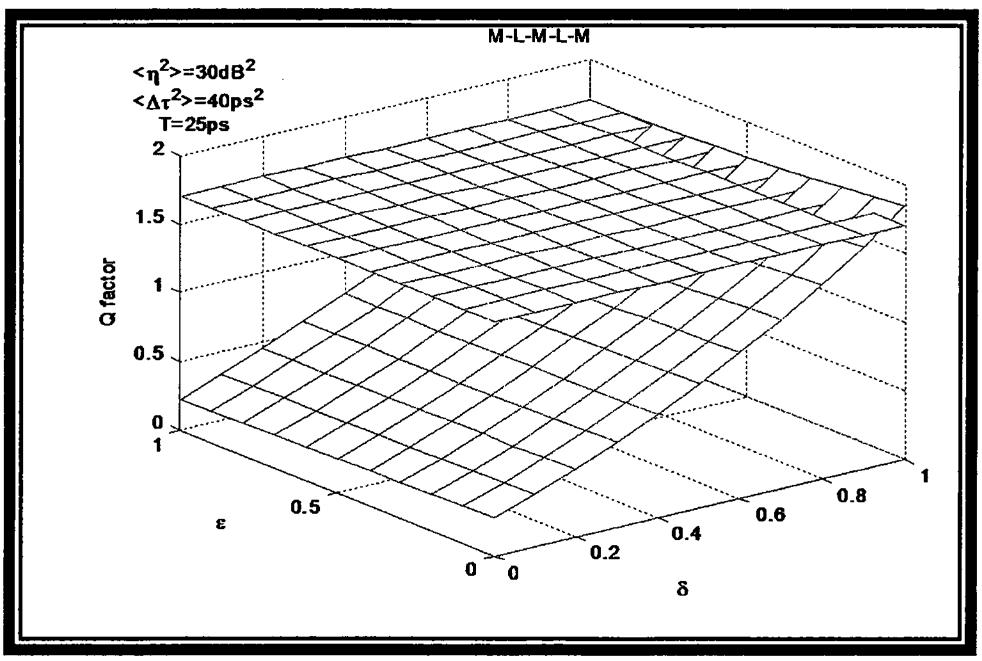

(b)

Figure (3.7) the effect of the partition parameters on Q-factor for a system of three Maxwellian fibers contained lumped sections in between them (a) . (b)

The Accuracy of the calculations

1

Number of points

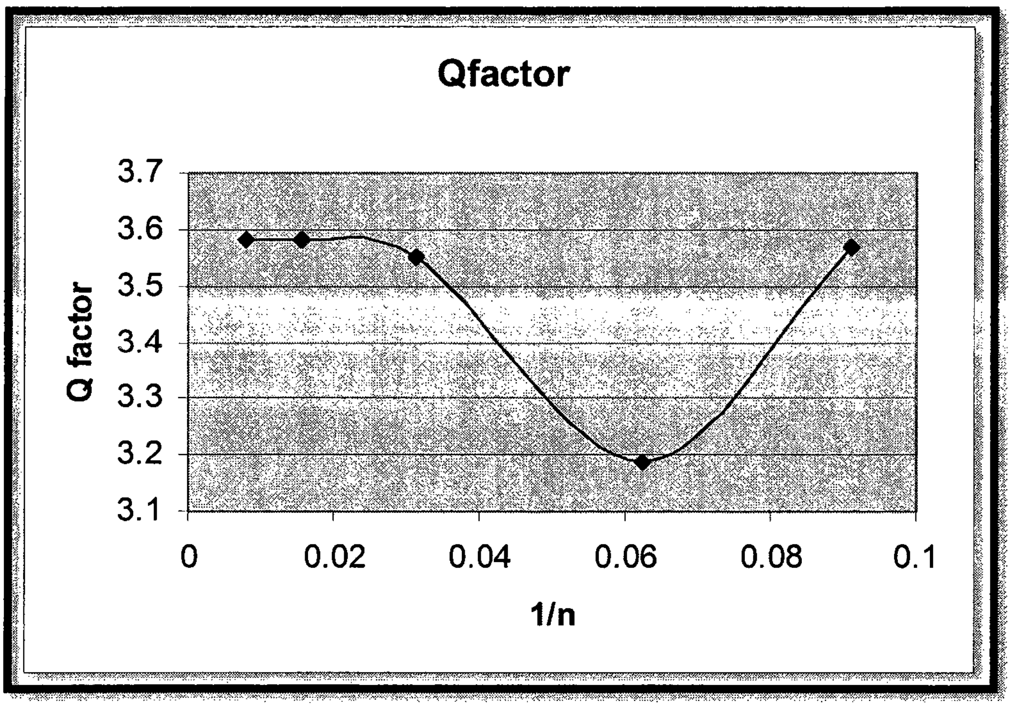

Figure (3.8) Q-factor as a function of the number of points for a system of three Maxwellian fibers contains a lumped sections in between them, total PMD=2.8ps, total PDL=0.5dB

2

Duty Cycle

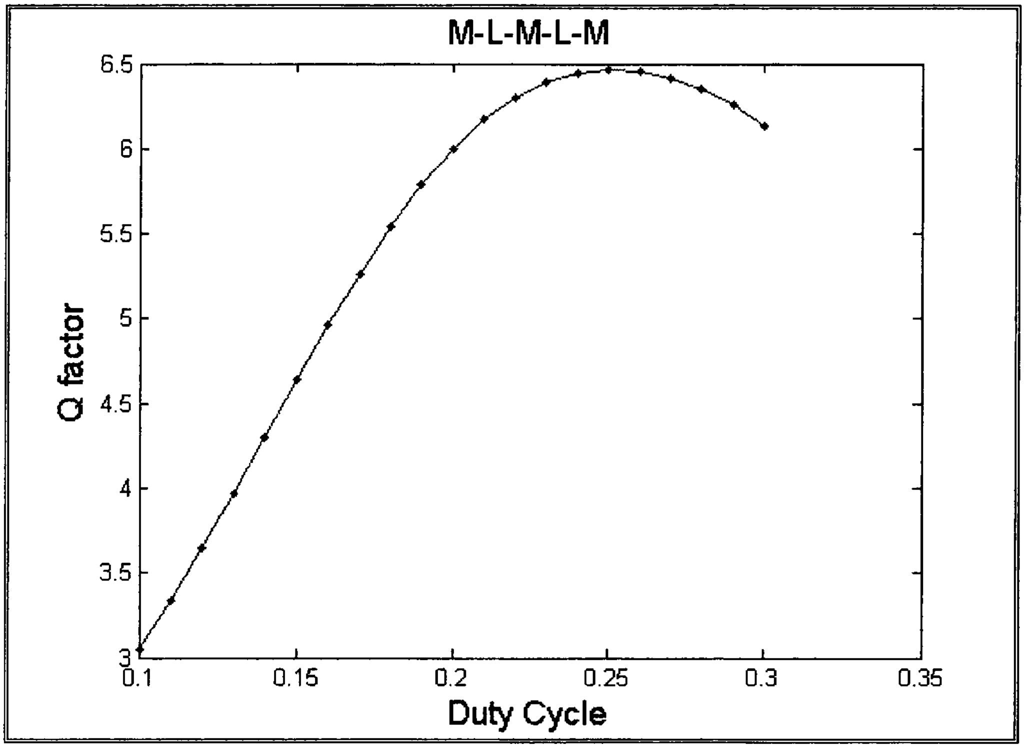

Figure (3.9) Q-factor as a function of the duty cycle for a system of Three Maxwellian fibers containing lumped sections in between them; the total PMD is 2.8 ps, the total PDL is 0.5dB.

3

Chirp Values

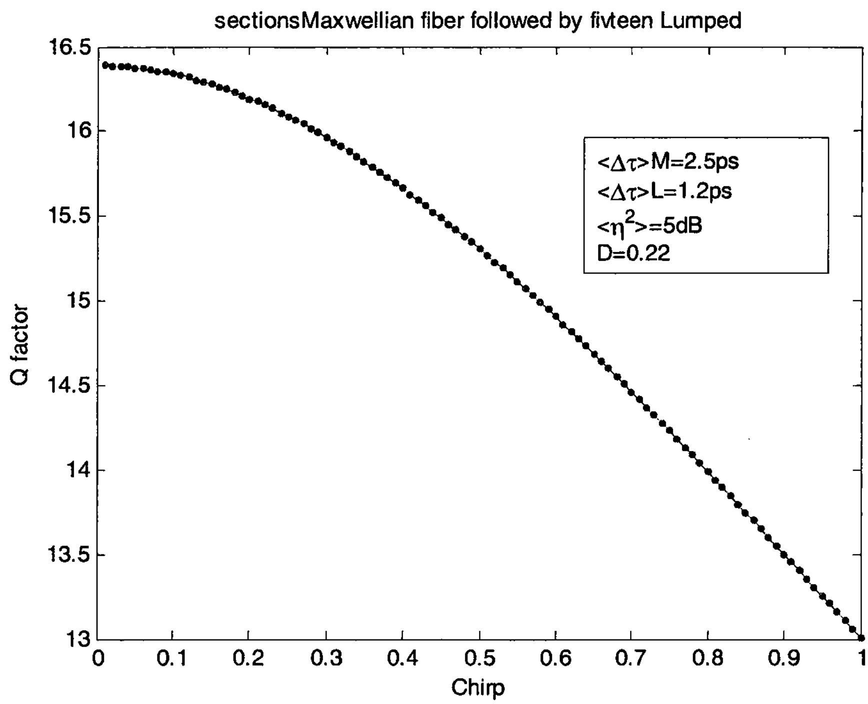

Figure (3.10) Q-factor as a function of chirp value for a system of Maxwellian fiber followed by fifteen lumped sections, PMD(M)=2.5ps, PMD(L)=15× 0.1ps, PDL(M)=0.5dB,and PDL(L)=15× 0.01dB

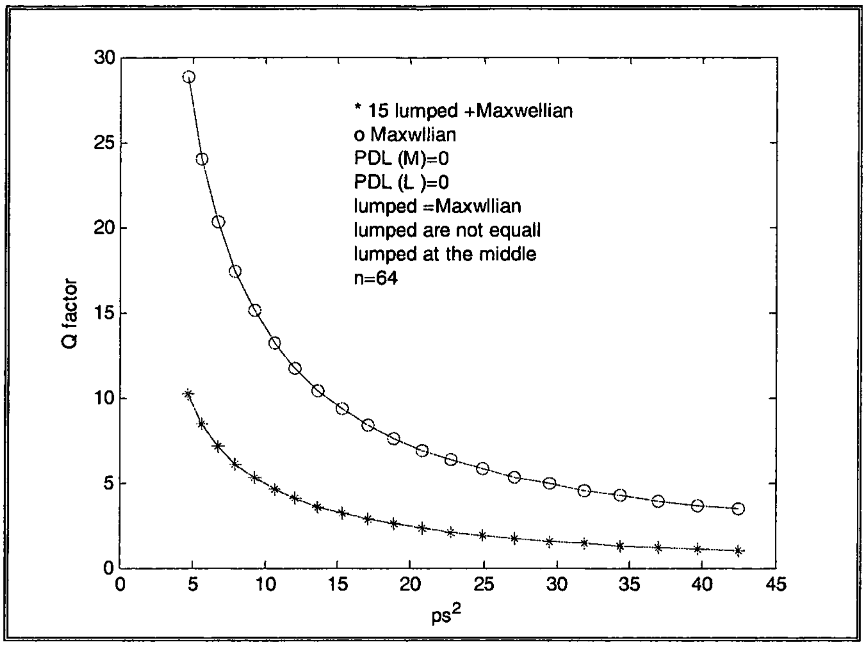

(a)

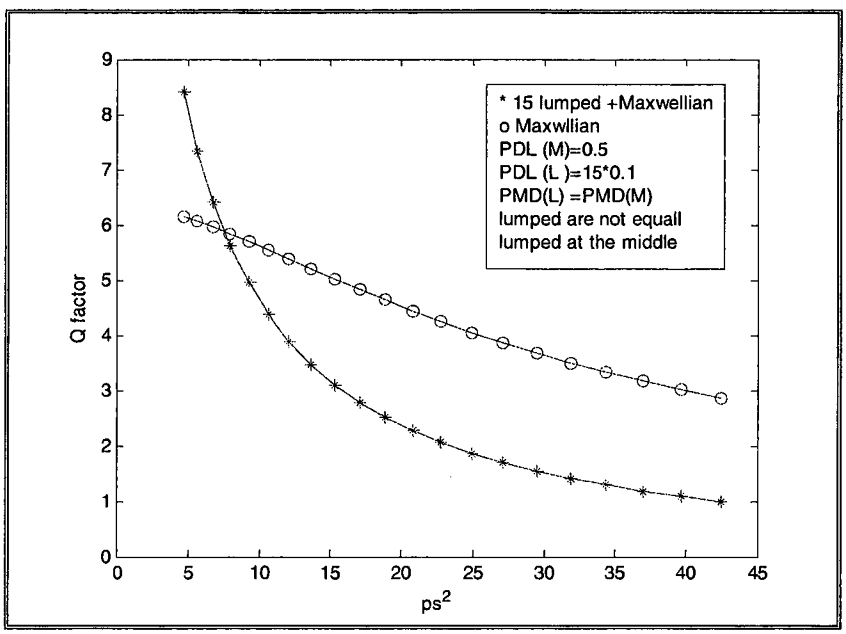

(b)

Figure (3.11) Effect of PDL on Q_factor (a) PDL=0 (b) PDL≠0, in both cases PMD equally distributed between the lumped sections and Maxwellian fiber.

Chapter 4

Analytic Optical Eye Diagram Evaluation for a System of Highly Mode Coupled PMD/PDL Fiber and Lumped Sections

This chapter has been published in the proceedings of the Photonic North Conference (2006). In this chapter, we give an analytical expression to evaluate the optical eye diagram due to polarization-mode dispersion (PMD), polarization-dependent loss (PDL), and chromatic dispersion (CD) for a system of highly mode coupled fiber with lumped sections at any given optical pulse sequence. We found that by considering PDL and the polarization direction correlation between PMD and PDL, a system with highly mode coupled fiber with lumped sections can have either higher or lower Q-factor than a highly mode coupled system with same root mean square PDL/PMD values. Also we noticed that a system of two highly mode coupled fibers connected together is not equivalent to a system of highly mode coupled fiber when fluctuations are considered.

4.1 Introduction

Polarization effects are one of the important impairments in optical fiber communication systems, especially when these systems operate beyond 10 Gb/s/channel [4,12]. Polarization mode dispersion (PMD), as one of polarization effects, is recognized by many researchers as one of the significant factors that limits the long-haul links [4, 5, 12, 15, 31, 40, 41]. Polarization dependent loss or gain (PDLG) is another important polarization effect that needs to be considered with PMD as the network complexity increases. The combined effect of PMD and PDL was considered for the first time by Gisin and Huttner [9] when they have shown that the combination of PMD and PDL will lead to a complex principal state vector. Therefore, it is not sufficient to analyze PMD and PDL separately [76], for example with effective zero differential group delay (DGD), PMD and PDL interaction still induced pulse spreading [39]. As it is well-known for a highly mode coupled PMD system, its DGD obeys Maxwellian statistical distribution [22], so we will call the fiber with Maxwellian statistical distribution of DGD as Maxwellian PMD fiber, as well as the fiber with a Maxwellian distribution for both PMD and PDL as Maxwellian PMD and PDL fiber. On the other hand, communication networks are complex , they include highly mode coupled PMD, PDL, and lumped sections like couplers, isolators, filters, multiplexers, demultiplexers, combiner/splitters, variable optical attenuators (VOAs), Erbium doped optical amplifiers (EDFA) and optical add/drop multiplexing switches (OADMS).

There were few theoretical works which had studied the communication systems with these lumped sections. One of these works was the work of C. Antonelli and A. Mecozzi [77], they gave an analytical expression for the probability density function of the differential group delay for a concatenation of PMD fiber and an arbitrary number of lumped elements. However they didn't consider PDL in their work. Since the combined effect of PMD and PDL leads to more accurate understanding of the fiber communication system, we extended the work of Antonelli and Mecozzi to include both PMD and PDL. In this work, we are following the previous work in Ref.[42], with an extension to a system consists of Maxwellian PMD and PDL fibers and lumped sections.

4.2 The concept of principal states of polarization

The properties of PMD can be described and understood with the concept of principal states of polarization (PSPs). In our work it was one of the parameters which we have to set, the local correlation $\langle \hat{\alpha}_j \cdot \hat{\beta}_j \rangle$ between the PMD unit vector $\hat{\beta}_j$ and the PDL unit vector $\hat{\alpha}_j$. Hence, its important for us to get a clear idea about the autocorrelation function related to the subject.

Writing the complex PSP vector explicitly in its real and imaginary parts as:

$$\vec{W}_N(\omega) = \vec{\Omega}_N(\omega) + i\,\vec{\Lambda}_N(\omega), \tag{4.1}$$

The autocorrelation functions are $\langle \vec{\Omega}_N(\omega) \cdot \vec{\Omega}_N(\omega) \rangle$,$\langle \vec{\Omega}_N(\omega) \cdot \vec{\Lambda}_N(\omega) \rangle$, and $\langle \vec{\Lambda}_N(\omega) \cdot \vec{\Lambda}_N(\omega) \rangle$, where $\langle \cdots \rangle$ is the average over statistical fluctuations of the PMD and PDL element. These autocorrelation functions have been investigated by Chen and others [37]. On the other hand, the local correlation $\langle \hat{\alpha}_j \cdot \hat{\beta}_j \rangle$ between the PMD unit vector $\hat{\beta}_j$ and the PDL unit vector $\hat{\alpha}_j$ could be neither zero [1] nor ± 1 [38].

Here it's convenient to recall some mathematical properties for averaging over a random unit vector $\hat{n}$

$$\langle \hat{n} \cdot \vec{A} \rangle \equiv 0 = \langle \hat{n} \cdot \vec{B} \rangle \ , \tag{4.2.a}$$

$$\langle (\hat{n} \cdot \vec{A})(\hat{n} \cdot \vec{B}) \rangle = \left(\tfrac{1}{3}\right)(\vec{A} \cdot \vec{B}). \tag{4.2.b}$$

Furthermore, considering the local correlation between $\hat{\alpha}_j$ and $\hat{\beta}_j$, we also have:

$$\langle (\hat{\alpha}_j \cdot \vec{A})(\hat{\beta}_j \cdot \vec{B}) \rangle = \left(\tfrac{1}{3}\right)\langle \hat{\alpha}_j \cdot \hat{\beta}_j \rangle (\vec{A} \cdot \vec{B}). \tag{4.3}$$

Here the generic expression $\langle \hat{\alpha}_j \cdot \hat{\beta}_j \rangle$ is used to represent the local PMD and PDL directional correlation.

Using the strategy that is introduced by Karlsson and Brentel [74], Chen and others [42] were able to get the continuum limit for the whole fiber $(N \to \infty)$. The continuum limit is taken in such a way that $N \to \infty$, $\alpha \to 0$, $\beta \to 0$ while keeping $N\alpha^2 = \langle \eta^2 \rangle$, $N\beta^2 = \langle \Delta\tau^2 \rangle$ constants. Because of the frequency dependence of the PDL and DGD vectors, the polarization states for a pulse that maximize/minimize the power transmission (maximize/minimize the time delay) cannot be identical for each frequency component in the pulse. Consequently, the frequency components in the pulse cannot all reach their maximum/minimum power transmission (maximum/minimum time delay) for a given state of polarization. As a result, the PDL and PMD values for a pulse are generally less than those for a single frequency.

4.3 The analytical model

Our model consists of Maxwellian PMD and PDL fibers connected with lumped sections. By Maxwellian PMD and PDL fiber we mean the continuum limit of highly mode coupled PMD, PDL fibers. This is achieved by considering a series of N PMD element $\vec{\beta}_j$ each followed by a PDLG element $\vec{\alpha}_j$. Then at the end we take a continuum limit in such a way that $N \to \infty, \alpha \to 0$, and $\beta \to 0$ while $N\alpha^2 = \langle \eta^2 \rangle$ and $N\beta^2 = \langle \Delta\tau^2 \rangle$ are kept constant. For the lumped sections each PMD element $\vec{\beta}_l$ is followed by a PDLG element $\vec{\alpha}_l$. Our goal is to treat the statistics of PMD and PDLG analytically such that the statistical average of the time-dependent output light intensity as well as its variation can be evaluated exactly for a given input pulse sequence. Thus one can accurately evaluate the optical eye diagram resulting from all the polarization impairments in the system. Using the standard wave plate model, we can write the output electric field $\vec{E}_{out}(\omega)$ related to the input electric field $\vec{E}_{in}(\omega)$ for a system that consists of highly mode coupled (Maxwellian) fibers M_1, M_2 and lumped sections L_1, L_2... with Jones matrix as

$$\vec{E}_{out}(\omega) = A_{N_1+N_2+L} \exp[i\varphi_{CD}(\omega)] T_{N_1+N_2+L}(\omega) \vec{E}_{in}(\omega) \tag{4.4}$$

where $A_{N_1+N_2+L} = \exp(-\alpha_0 - \sum_{K=1}^{n} |\alpha_{Lk}|/2 - \sum_{j=1}^{N_1} |\alpha_j|/2 - \sum_{i=1}^{N_2} |\alpha_i|/2)$, α_0 describes the overall polarization-independent attenuation, $\varphi_{CD}(\omega)$ stands for the CD of the system. $T_{N_1+N_2+L}(\omega)$ is a 2×2 transformation matrix . It is related to the transformation matrix of the Maxwellian fiber $T_N(\omega)$ as

$$T_{N_1}(\omega) = \exp(-i\omega\vec{\beta}_1 \cdot \vec{\sigma}/2)\exp(\vec{\alpha}_1 \cdot \vec{\sigma}/2)....\exp(-i\omega\vec{\beta}_{N_1} \cdot \vec{\sigma}/2)\exp(\vec{\alpha}_{N_1} \cdot \vec{\sigma}/2), \tag{4.5.a}$$

and the lumped sections $\vec{T}_L(\omega)$. Where

$$T_L(\omega) = \exp(-i\omega\vec{\beta}_{l1} \cdot \vec{\sigma}/2)\exp(\vec{\alpha}_{l1} \cdot \vec{\sigma}/2)....\exp(-i\omega\vec{\beta}_{\ln} \cdot \vec{\sigma}/2)\exp(\vec{\alpha}_{\ln} \cdot \vec{\sigma}/2). \tag{4.5.b}$$

Here, $\vec{\beta}_j = \beta_j \hat{\beta}_j$ represents the j^{th} PMD wave plate that has differential group delay (DGD), β_j and the fast-axis polarization is expressed by the unit vector $\hat{\beta}_j$ in the Stokes space, $\vec{\alpha}_j = \alpha_j \hat{\alpha}_j$ stands for the j^{th} PDLG wave plate with the value expressed in decibels by $20|\alpha_j|\log_{10} e$, and unit vector $\hat{\alpha}_j$ in the Stokes space, Where $\vec{\sigma}$ is the standard Pauli matrices. $T_{N_1,N_2+L}(\omega)$ can be defined as $T_{N_1,N_2+L}(\omega) = T_{N_1,N_2}(\omega)T_L(\omega)$ for the case of lumped sections followed by Maxwellian PMD and PDL fiber, $T_{N_1,N_2+L}(\omega) = T_L(\omega)T_{N_1,N_2}(\omega)$ for the case of Maxwellian fiber followed by lumped sections, and $T_{N+L}(\omega) = T_{N_1}(\omega)T_L(\omega)T_{N_2}(\omega)$ in case of lumped sections in between two Maxwellian fibers. The input light electric field is written as

$$\vec{E}_{in}(\omega) = f_{in}(\omega)\begin{bmatrix} x \\ y \end{bmatrix} \tag{4.6}$$

The column matrix $\begin{bmatrix} x \\ y \end{bmatrix}$ is a unit vector in the Jones space representing the input state of polarization and $f_{in}(\omega)$ is the Fourier transform of the input pulse sequence determined by the modulation format $E_{in}(t)$:

$$f_{in}(\omega) = \frac{1}{\sqrt{2\pi}}\int_{-\infty}^{\infty}\exp(i\omega t)E_{in}(t)dt. \tag{4.7}$$

Therefore, the output light intensity can be written as (neglecting an obvious constant)

$$I(t) = \vec{E}^*_{out}(t)\cdot\vec{E}_{out}(t)$$

$$= \frac{|A_{N+L}|^2}{2\pi}\int_{-\infty}^{\infty}d\omega\int_{-\infty}^{\infty}d\omega'\exp\{i[\varphi_{CD}(\omega') - \varphi_{CD}(\omega)]\}$$

$$\times\begin{bmatrix} x^* & y^* \end{bmatrix}T^*_{N_1+N_2+L}(\omega)T_{N_1+N_2+L}(\omega')\begin{bmatrix} x \\ y \end{bmatrix}\exp[i(\omega-\omega')t]f^*_{in}(\omega)f_{in}(\omega'). \tag{4.8}$$

Using the transmission matrix $T_{N_1+N_2+L}(\omega)$ for our system, we can write

$$T^*_{N_1+N_2+L}(\omega)T_{N_1+N_2+L}(\omega') = \Gamma_{0,N_1+N_2+L}(\omega,\omega')\mathrm{I} + \vec{\Gamma}_{N_1+N_2+L}(\omega,\omega')\cdot\vec{\sigma}, \tag{4.9}$$

where I is a 2×2 unity matrix. Therefore, the intensity is

$$I(t) = \frac{\left|A_{N_1+N_2+L}\right|^2}{2\pi}\int_{-\infty}^{\infty}d\omega\int_{-\infty}^{\infty}d\omega' \exp\{i[\varphi_{CD}(\omega') - \varphi_{CD}(\omega)]\}[\Gamma_{0,N_1+N_2+L}(\omega,\omega') + \vec{\Gamma}_{N_1+N_2+L}(\omega,\omega')\cdot\hat{m}]$$

$$\times\exp[i(\omega-\omega')t]f^*_{in}(\omega)f_{in}(\omega'), \tag{4.10}$$

where $\hat{m} = \begin{bmatrix} x^* & y^* \end{bmatrix}\vec{\sigma}\begin{bmatrix} x \\ y \end{bmatrix}$ is a unit vector representing the input state of polarization in Stokes space. Then we can derive the following relations:

The statistical average of the intensity can be written as

$$< I(t) >= \frac{\left|A_{N_1+N_2+L}\right|^2}{2\pi}\int_{-\infty}^{\infty}d\omega\int_{-\infty}^{\infty}d\omega' \exp\{i[\varphi_{CD}(\omega') - \varphi_{CD}(\omega)]\} < \Gamma_{0,N_1+N_2+L}(\omega,\omega') + \vec{\Gamma}_{N_1+N_2+L}(\omega,\omega')\cdot\hat{m} >$$

$$\times\exp[i(\omega-\omega')t]f^*_{in}(\omega)f_{in}(\omega'). \tag{4.11}$$

Using the properties for averaging over a random unit vector $\hat{n}$ for given constant vectors $\vec{A}$ and $\vec{B}$ [41] as in eq.s (4.2.a), (4.2.b).

Introducing the local correlation between $\hat{\alpha}_j$ and $\hat{\beta}_j$, where $<(\hat{\alpha}\cdot\hat{\beta})>=\sum_{i=1}^{N}\hat{\alpha}_j\cdot\hat{\beta}_j/N$ is a generic expression representing the local PMD and PDLG polarization directional correlation [93].After averaging the input state of polarization $\vec{m}$, we get

$$\langle I(t)\rangle = \frac{\left|A_{N_1+N_2+L}\right|^2}{2\pi}\int_{-\infty}^{\infty} d\omega \int_{-\infty}^{\infty} d\omega' \exp\{i[\varphi_{CD}(\omega') - \varphi_{CD}(\omega)]\} < \Gamma_{0,N_1+N_2+L} >$$

$$\times \exp[i(\omega-\omega')t] f_{in}^{*}(\omega) f_{in}(\omega') \tag{4.12}$$

The variation of the light intensity due to PMD and PDLG is

$$< [I(t)]^2 >= \frac{\left|A_{N_1+N_2+L}\right|^4}{4\pi^2}\int_{-\infty}^{\infty} d\omega_1 \int_{-\infty}^{\infty} d\omega_1' \int_{-\infty}^{\infty} d\omega_2 \int d\omega_2' \exp\{i[\varphi_{CD}(\omega_1') - \varphi_{CD}(\omega_1) + \varphi_{CD}(\omega_2') - \varphi_{CD}(\omega_2)]\}$$
$$\times \exp[i(\omega_1 - \omega_1' + \omega_2 - \omega_2')t]([< \Gamma_{0,N_1+N_2+l}(\omega_1,\omega_1')\Gamma_{0,N_1+N_2+l}(\omega_2,\omega_2') >$$

$$+\frac{1}{3} < \vec{\Gamma}_{N_1+N_2+l}(\omega_1,\omega_1') \cdot \vec{\Gamma}_{N_1+N_2+l}(\omega_2,\omega_2') >]) f_{in}^{*}(\omega_1) f_{in}(\omega_1') f_{im}^{*}(\omega_2) f_{in}(\omega_2'). \tag{4.13}$$

To go to the continuum limit for the Maxwillian fiber, we adopt the strategy first introduced by Karlsson and Brentel [74], which was used by several researchers [42, 77]. Using the recursion relationship with definition, $\Delta\omega_i = (\omega_i - \omega_i')/2$ and $\varpi_i = (\omega_i + \omega_i')/2$ for $i \in \{1,2\}$, we get

$$< \Gamma_{0,N+L}(\omega,\omega') >= [\cosh\alpha_L \cos(\beta_L \Delta\omega) + i < \hat{\alpha}_L \cdot \hat{\beta}_L > \sinh\alpha_L \sin(\beta_L \Delta\omega)]$$

$$\times < \Gamma_{0,N+L-1}(\omega,\omega') >, \tag{4.14}$$

where $< \Gamma_{0,N}(\omega,\omega') >$ was given in Ref.[42].

Now we will see the effect of the position of the lumped sections on the output intensity, we consider three cases:

(a)Maxwellian fiber followed by lumped sections, (b) lumped sections followed by Maxwellian fiber, and (c) the lumped sections is between two fibers. From eq. (4.8) we can see that $\langle I(t)\rangle$ in the three cases are the same. But the difference between these three cases come from the $\langle I^2(t)\rangle$.

The second order correlation function is given by

$$\begin{bmatrix} <\Gamma_0(\omega_1,\omega_1')\Gamma_0(\omega_2,\omega_2')> \\ <\vec{\Gamma}(\omega_1,\omega_1')\cdot\vec{\Gamma}(\omega_2,\omega_2')> \end{bmatrix} = \begin{bmatrix} M_{11} & M_{12} \\ M_{21} & M_{22} \end{bmatrix} \begin{bmatrix} L_{11} & L_{12} \\ L_{21} & L_{22} \end{bmatrix} \begin{bmatrix} 1 \\ 0 \end{bmatrix} \tag{4.15.a}$$

for the case (a),

$$\begin{bmatrix} <\Gamma_0(\omega_1,\omega_1')\Gamma_0(\omega_2,\omega_2')> \\ <\vec{\Gamma}(\omega_1,\omega_1')\cdot\vec{\Gamma}(\omega_2,\omega_2')> \end{bmatrix} = \begin{bmatrix} L_{11} & L_{12} \\ L_{21} & L_{22} \end{bmatrix} \begin{bmatrix} M_{11} & M_{12} \\ M_{21} & M_{22} \end{bmatrix} \begin{bmatrix} 1 \\ 0 \end{bmatrix} \tag{4.15.b}$$

for the case (b), and

$$\begin{bmatrix} <\Gamma_0(\omega_1,\omega_1')\Gamma_0(\omega_2,\omega_2')> \\ <\vec{\Gamma}(\omega_1,\omega_1')\cdot\vec{\Gamma}(\omega_2,\omega_2')> \end{bmatrix} = \begin{bmatrix} M_{11} & M_{12} \\ M_{21} & M_{22} \end{bmatrix} \begin{bmatrix} L_{11} & L_{12} \\ L_{21} & L_{22} \end{bmatrix} \begin{bmatrix} M_{11} & M_{12} \\ M_{21} & M_{22} \end{bmatrix} \begin{bmatrix} 1 \\ 0 \end{bmatrix} \tag{4.15.c}$$

for the case (c).

where M matrix denotes the effect describing Maxwellian PMD and PDL fiber, and L matrix describes the lumped section, and it depends on the number of the lumped sections k, and $k = 1,\ldots,n$. We assume that the lumped sections are connected together. So we can write

$$\begin{bmatrix} L_{11} & L_{12} \\ L_{21} & L_{22} \end{bmatrix} = \begin{bmatrix} L_{11}(n) & L_{12}(n) \\ L_{21}(n) & L_{22}(n) \end{bmatrix} \cdots\cdots\cdots \begin{bmatrix} L_{11}(1) & L_{12}(1) \\ L_{21}(1) & L_{22}(1) \end{bmatrix} \tag{4.16}$$

with $L(1)$ matrix denotes the first lumped section, and $L(n)$ denotes the n[th] lumped section. The elements of L and M matrixes are given in the Appendix (A).

As can be seen the different location of the lumped sections doesn't affect $\langle I(t)\rangle$. However it does affect $\langle I^2(t)\rangle$. Therefore it affects the Q-factor.

From the above calculation, it is not obvious if two Maxwellian fibers linked together would be equivalent to a new Maxwellian fiber. Consider two Maxwellian fibers M_1 and M_2 connected in serial fashion. Assume they have $\langle\Delta\tau_I^2\rangle$ and $\langle\Delta\tau_{II}^2\rangle$ as a mean-square pristine DGD, $\langle\eta_I^2\rangle$ and $\langle\eta_{II}^2\rangle$ for pristine PDL element, and $\langle\hat{\alpha}_I\cdot\hat{\beta}_I\rangle$, $\langle\hat{\alpha}_{II}\cdot\hat{\beta}_{II}\rangle$ for the polarization direction correlation respectively, we can write from the average current $\langle I(t)\rangle$ expression

$$<\Gamma_{0,N}(\omega,\omega')>=\exp[\frac{1}{2}(<\eta_I{}^2>+<\eta_{II}{}^2>)-\frac{1}{8}(<\Delta\tau_I{}^2>+<\Delta\tau_{II}{}^2>)(\omega-\omega')^2$$

$$+\frac{1}{2}i(<\hat{\alpha}_I\cdot\hat{\beta}_I>\sqrt{<\eta_I{}^2><\Delta\tau_I{}^2>}+<\hat{\alpha}_{II}\cdot\hat{\beta}_{II}>\sqrt{<\eta_{II}{}^2><\Delta\tau_{II}{}^2>})(\omega-\omega')] \tag{4.17}$$

To view it as one equivalent Maxwellian fiber we require the following concatenation rules: $<\Delta\tau_{III}>^2=<\Delta\tau_I>^2+<\Delta\tau_{II}>^2$, $<\eta_{III}>^2=<\eta_I>^2+<\eta_{II}>^2$, and

$$\langle\hat{\alpha}_{III}\cdot\hat{\beta}_{III}\rangle=\frac{\langle\hat{\alpha}_I\cdot\hat{\beta}_I\rangle\sqrt{\langle\Delta\tau_I^2\rangle\langle\eta_I^2\rangle}+\langle\hat{\alpha}_{II}\cdot\hat{\beta}_{II}\rangle\sqrt{\langle\Delta\tau_{II}^2\rangle\langle\eta_{II}^2\rangle}}{\sqrt{(\langle\Delta\tau_I^2\rangle+\langle\Delta\tau_{II}^2\rangle)(\langle\eta_I^2\rangle+\langle\eta_{II}^2\rangle)}}$$

We have

$$< \Gamma_{0,N}(\omega,\omega') >= \exp[\frac{1}{2} < \eta_{III}{}^2 > -\frac{1}{8} < \Delta\tau_{III}{}^2 > (\omega-\omega')^2$$

$$+\frac{1}{2} i < \hat{\alpha}_{III} \cdot \hat{\beta}_{III} > \sqrt{< \eta_{III}{}^2 >< \Delta\tau_{III}{}^2 >}(\omega-\omega')] \quad (4.18)$$

However this concatenation rule formed by demanding the same average current wouldn't give the same equivalent current variation $\langle I^2(t) \rangle$ in general.

4.4 Results and discussion

To study the effect of the interaction between PMD and PDLG on the eye diagram for our system, we will look at the effect of introducing PDL in the system. For a Gaussian input pulse created by Mach-Zehnder interferometer modulator, its shape can be written as

$f(t) = A\exp\left[-\frac{t^2(1+iC)}{2D^2T^2}\right]$ where C is the chirp factor and D denotes the duty cycle of the pulses for $D<1$. To get an optimum performance on the optical eye diagram we used the duty cycle (the ratio of the time interval where light is not zero within an existing pulse to the bit period) D=0.24, for a pulse of sequence of ...001100... for a pulse width $T = 25 ps$. Also we choose $CD = 0.1 ps/nm$, and its dispersion slope $S = -3.3\times10^{-3} ps/nm^2$ for a carrier wavelength of $1530nm$ where $\varphi_{CD}(\omega) = b_2(\omega-\omega_0)^2/2 + b_3(\omega-\omega_0)^3/6$, where ω_0 is the carrier frequency and $b_2 (= d^2b/d\omega^2)$, $b_3 (= d^3b/d\omega^3)$ are related to CD and S by a CD of $-\omega_0^2 b_2/(2\pi c)$ and $S = \omega_0^4 b_3/(2\pi c)^2 + 2\omega_0^3 b_2/(2\pi c)^2$. Here b refers to the propagation constant in fiber and c is the speed of light. For the Maxwellian fiber we used Maxwellian distribution to find $<\Delta\tau^2>$ and $<\eta^2>$, i.e., $<\Delta\tau^2>_{Maxwil.} = 3\pi <\Delta\tau>^2{}_{Maxwil}/8$ and $<\eta^2>_{Maxwil} = 3\pi <\eta>^2{}_{Maxwil}/8$. For a different values of DGD for the lumped sections we choose the same values as those which was used in Ref. [77] ,they were related by the relation $\Delta\tau_l = l\Delta\tau_0$. For PDLG element we used the same relation which was $\eta_l = l\eta_0$. Moreover, we use $<\eta> = <\eta>_{dB}/(20\log e)$ to convert decibels to the dimensionless unit.

Note that, the local PMD and PDLG polarization directional correlation is $<\hat{\alpha}\cdot\hat{\beta}>$, and its value varies from -1 to +1 [42]. When $<\hat{\alpha}\cdot\hat{\beta}>=\pm 1$, it corresponds to the strong correlation between PMD and PDLG polarization directions, i.e., the local fast axis is always parallel or antiparallel to the local maximum attenuation axis. This could be potentially realized when the fiber links are made of only single-mode fibers. On the other hand $<\hat{\alpha}\cdot\hat{\beta}>=0$ corresponds to the complete random correlation between the PMD and PDLG polarization direction, which could be realized in ultra-long-haul links where many components are interleaved. In our calculations we choose $<\hat{\alpha}\cdot\hat{\beta}>_{Maxwil.}=<\hat{\alpha}\cdot\hat{\beta}>_{lump.}=0.15$ which seemed to be a typical value for field fiber [42].

Figure (4.2) shows the effect of varying of (a) $<\Delta\tau>^2_{total}$ considering $<\eta>^2_{total}$ to be constant, (b) $<\eta>^2_{total}$ at constant value of $<\Delta\tau>^2_{total}$ on the Q-factor of the output intensity for a system of Maxwellian fiber followed by fifteen lumped sections. The Q factor is calculated from [3]

$$Q=\frac{<I(t)>_{\max}-<I(t)>_{\min}}{\sigma(t)_{\max}+\sigma(t)_{\min}} \tag{4.19}$$

where $<I(t)>_{\max(\min)}$ refers to the mean intensity at maximum (minimum) point, $\sigma(t)_{\max(\min)}$ refers to the standard deviation at the maximum (minimum) point, and $\sigma(t)=\{<[I(t)]^2>-<I(t)>^2\}^{\frac{1}{2}}$.In experiment, usually the total mean-square DGD of the whole system is taken as a Maxwellian, which is easy to measure, but in realty it is not exactly Maxwellian. It contains a portion for the lumped sections. So it was taken as $<\Delta\tau^2>_{total}=\delta<\Delta\tau^2>_{Maxwil.}+(1-\delta)<\Delta\tau^2>_{lump.}$, and the total mean-square of PDL element was $<\eta^2>_{total}=\varepsilon<\eta^2>_{Maxwil..}+(1-\varepsilon)<\eta^2>_{lump.}$, where δ,ε are constants varying from 0 (lumped sections) to 1 (Maxwellian fiber). In figure (4.2.a) the middle curve corresponds to the case of equally distributing the mean-square DGD between the Maxwellian fiber and the lumped sections. The upper curve corresponds to case of $\delta=1$, and the lower curve corresponds to $\delta=0$.The value of $<\eta>^2_{total}$ was taken such that $<\eta>_{Maxwel.}=1dB$ and $<\eta^2>_{lump.}=\sum_{m=1}^{15}m^2<\eta_0^2>$, $<\eta_0>=0.1dB$. One can conclude from the figure that Q-factor is overestimated if we were to use a Maxwellian distribution for the whole system composed by Maxwellian and lumped fiber sections. In figure (4.2.b) the total mean-square DGD was taken as $<\Delta\tau>_{Maxwel}=2.5ps$, and $<\Delta\tau^2>_{lump.}=\sum_{m=1}^{15} m^2 <\Delta\tau_0^2>$, $<\Delta\tau_0>=0.1ps$. It appeared from the figure that we would underestimate in Q-factor by considering the PDL of the whole system as Maxwellian distribution of the same value with the total mean-square PDL of the system. It is clear from those two cases in Fig. (4.2), that there will be situations that one could be either overestimate or underestimate system's Q-factor if one treated the system as Maxwellian only when in fact the link is involving lumped PMD and PDL sections.

Figure (4.3) shows the effect of changing δ,ε from 0 to1, for the system in figure (4.2), on the Q-factor of the output intensity. In figure (4.3.a) $<\eta>^2_{total}=0dB$, it is clear that the Q-factor increases as δ increases from 0 (lumped sections) to 1 (Maxwellian fiber),and it is stable for increasing ε from 0 to 1 since $<\eta>^2_{total}=0dB^2$. On the other hand, in figure (4.3.b) when $<\eta>^2_{total}=10dB^2$ ($<\eta>_{Maxwel.}=2.9dB$ or $<\eta>_{Lump.}=3.16dB$) for increasing ε from 0 to 1 Q-factor decreases i.e. Q-factor increases as the lumped sections take on the major portion of total PDL. With the interaction of PMD and PDL (figure (4.3.b)) there is a new region (ade) appeared in addition to the original one (abcd) in figure (4.3.a) when $<\eta>^2_{total}=0dB$.In the original region (abcd) we would overestimate the Q-factor by considering the DGD of the whole system as Maxwellian distribution. With considering somewhat unphysical value of PDL $<\eta>^2_{total}=100dB$ ($<\eta>_{Maxwel.}=9.2dB$ or $<\eta>_{Lump.}=10dB$) in figure (4.3.c), it appeared that we even have bigger (ade) region. In (ade) region we would underestimate the Q-factor by considering Maxwellian distribution for the whole system.

From other point of view, we want to see the effect of the position of the lumped sections, in the whole system, on the Q-factor. For a system of Maxwellian fiber with 5 lumped sections we studied the three cases: (a) lumped sections followed by Maxwellian fiber, (b) Maxwellian fiber followed by lumped sections, (c) lumped sections in between two equal Maxwellian fibers. By equal we mean that the two Maxwellian fibers have the same DGD, and PDL elements, and their summation equal to PMD, PDL elements for the Maxwellian fiber in case (a) and case (b). Figure (4.4) shows that effect when $<\Delta\tau>^2_{total}=30ps^2$, $<\eta>^2_{total}=16dB$ ($<\eta>_{Maxwel.}=3.69dB$ or $<\eta>_{Lump.}=4dB$), $D=0.24, C=0.1$, $<\hat{\alpha}\cdot\hat{\beta}>_{Maxwel.}=<\hat{\alpha}\cdot\hat{\beta}>_{lumped}=0.15$. From figure (4.4) we can conclude that the worst situation for the lumped sections is when they are in between the Maxwellian fibers, and if they are followed by Maxwellian fiber or Maxwellian fiber was followed by them gives the same Q-factor for the output intensity.

As a side note we found that for a system of two Maxwellian fibers connected together their Q-factor is not the same ,in general, to a third equivalent Maxwellian fiber. When the two Maxwellian fibers M_I, M_{II}, defined in the appendix A have $<\Delta\tau_I>,<\Delta\tau_{II}>$ for PMD, and $<\eta_I>,<\eta_{II}>$ for PDL elements, respectively, and $\langle\hat{\alpha}_I\cdot\hat{\beta}_I\rangle$, $\langle\hat{\alpha}_{II}\cdot\hat{\beta}_{II}\rangle$ for the polarization direction correlation respectively.

The third Maxwellian fiber M_{III} has $<\Delta\tau_{III}>,<\eta_{III}>$ for PMD and PDL elements respectively, Where $<\Delta\tau_{III}{}^2>=<\Delta\tau_I^2>+<\Delta\tau_{II}^2>$, $<\eta_{III}^2>=<\eta_I^2>+<\eta_{II}^2>$ and $\langle\hat{\alpha}_{III}\cdot\hat{\beta}_{III}\rangle=\dfrac{\langle\hat{\alpha}_I\cdot\hat{\beta}_I\rangle\sqrt{\langle\Delta\tau_I^2\rangle\langle\eta_I^2\rangle}+\langle\hat{\alpha}_{II}\cdot\hat{\beta}_{II}\rangle\sqrt{\langle\Delta\tau_{II}^2\rangle\langle\eta_{II}^2\rangle}}{\sqrt{(\langle\Delta\tau_I^2\rangle+\langle\Delta\tau_{II}^2\rangle)(\langle\eta_I^2\rangle+\langle\eta_{II}^2\rangle)}}$ for the polarization direction correlation. The average output intensity is the same in both cases. However their variations are not. Figure (4.5) shows the output intensity and its variation in both cases as a function of the time when C=0.1 and D=0.24.This result might be explained by the non commuting nature of PMD and PDL interaction, especially when PMD and PDL directional correlation is considered leading to non linear PMD and PDL interaction.

4.5 Conclusion

Using the parameters DGD$\langle\Delta\tau^2\rangle$, PDLG$\langle\eta^2\rangle$, CD, and PMD PDLG polarization direction correlation $\langle\hat{\alpha}\cdot\hat{\beta}\rangle$ we have obtained an analytical expression to evaluate the optical eye diagram for a system contains of Maxwellian fibers and lumped sections. We found that, considering PDL as well as PMD, the Q-factor of the output becomes higher than that of the Maxwellian fiber having the same total root mean square PMD and PDL values , when the mean-square PDL element of the lumped sections takes the major portion from the total mean-square of the whole system. Whereas without considering PDL, Q-factor becomes higher as the mean-square PMD element of the Maxwellian fiber takes the major portion of the total mean-square PMD element of the whole system. Also the worst case for the Q-factor occurred when the lumped sections were in the middle between two equal equivalent Maxwellian fibers rather than the case lumped sections were followed by Maxwellian fiber or the Maxwellian fiber was followed by the lumped sections. We also note that two equivalent Maxwellian fibers connected in series will not give the same Q-factor as a Maxwellian fiber equivalent by concatenation rule unless they have the same values of PMD, PDL, and polarization direction correlation elements.

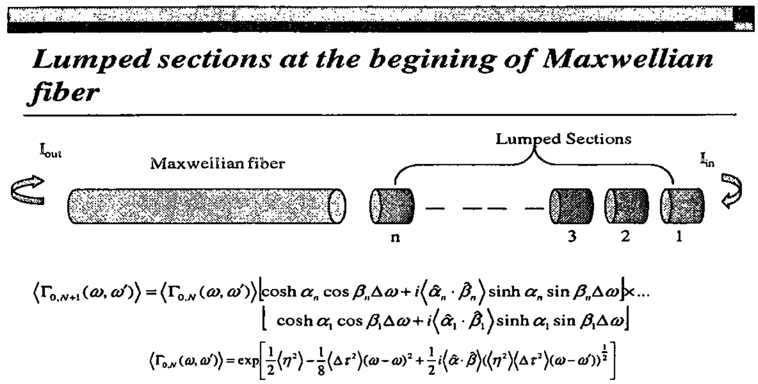

(a)

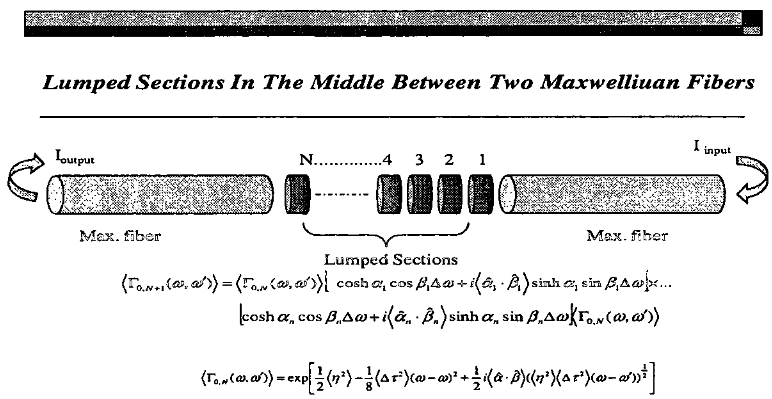

(b)

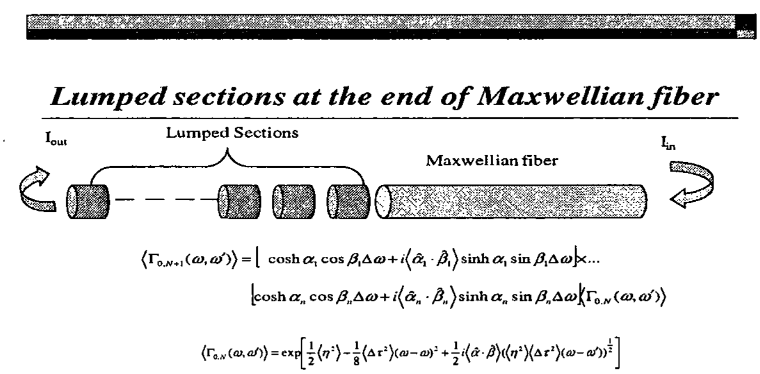

(c)

Figure (4.1) A system consists of (a) two lumped sections followed by Maxwellian fiber (b) two lumped sections separated by Maxwellian fiber and all of these in between two Maxwellian fibers.(c) Maxwellian fiber followed by lumped sections

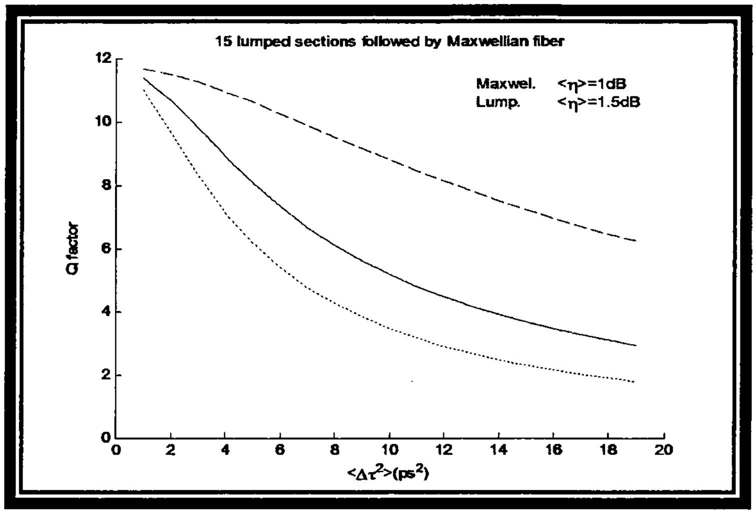

(a)

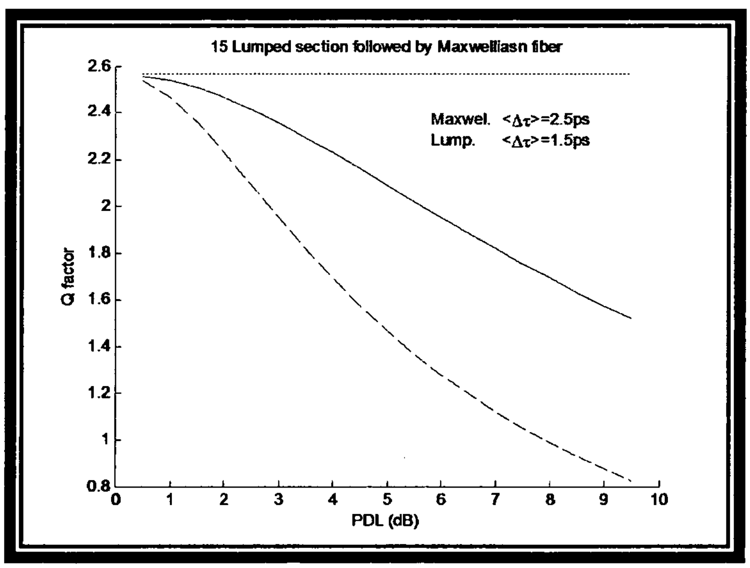

(b)

Figure (4.2) Q-factor of the output intensity varies with the mean-square of (a) total DGD, (b) total PDL for a system of Maxwellian fiber followed by fifteen lumped sections. When $\delta, \varepsilon = 0$ (the short dashed curves i.e. lumped sections only), $\delta, \varepsilon = 0.5$ (The solid curves), and $\delta, \varepsilon = 1$ (the long dashed curves i.e. the Maxwellian fiber only).

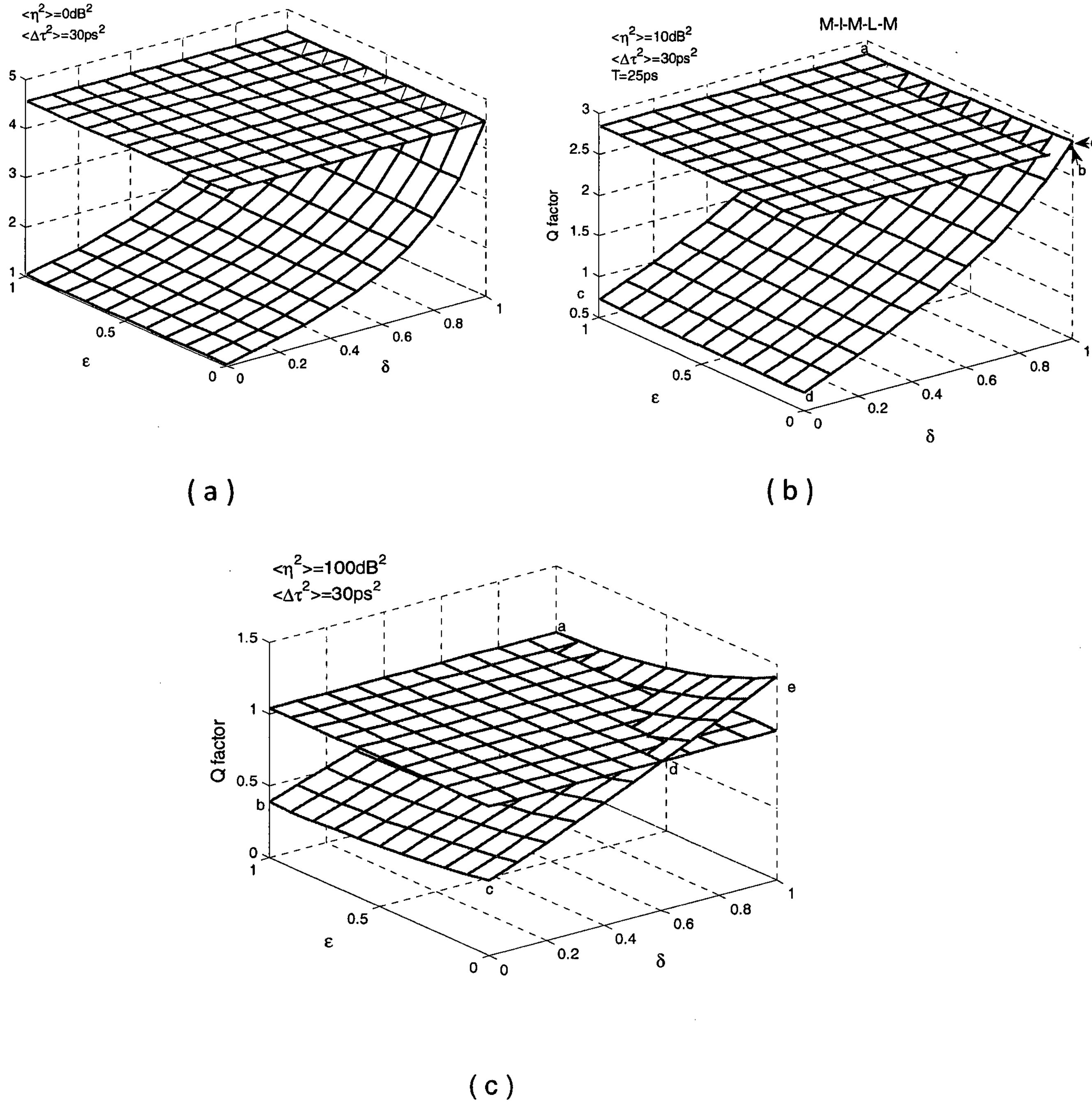

Figure (4.3). The effect of the partition parameters δ, ε on the Q-factor for system of Maxwellian fiber followed by 5 lumped sections. $<\Delta\tau>^2_{total}=30ps^2$, C=0.1, D=0.24 for (a) $PDL=0dB$, (b), and (c) $PDL\neq 0dB$.

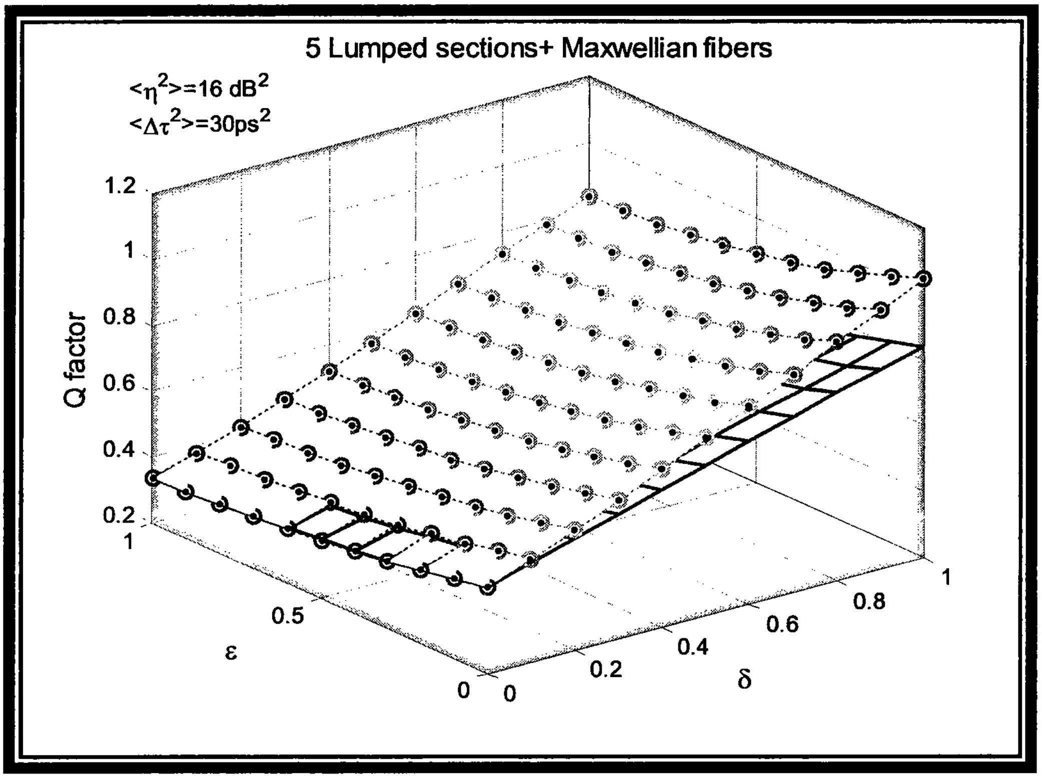

Figure (4.4) Q-factor for a system of 5 lumped sections followed by Maxwellian fiber (open circled line mesh), Maxwellian fiber followed by 5 lumped sections (dotted line mesh), and 5 lumped sections in between two equivalent Maxwellian fibers (solid line mesh).

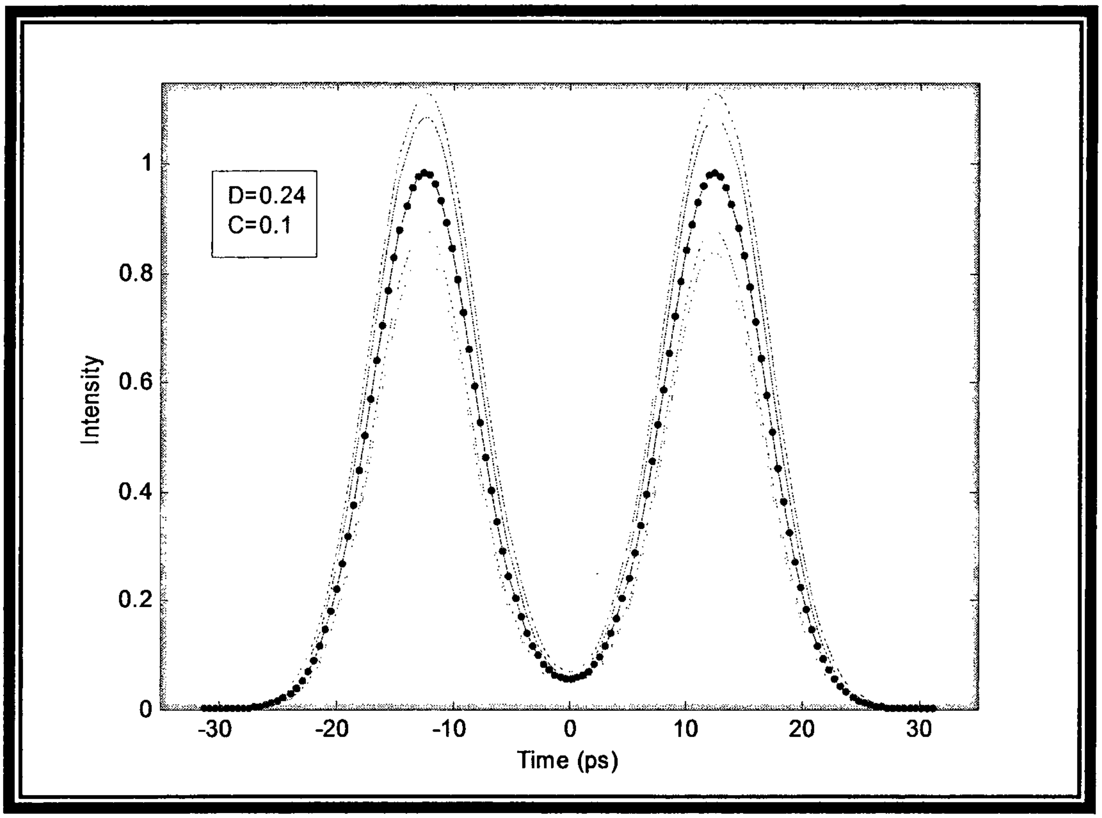

Figure (4.5) Optical eye diagram for wavelength 1530 nm,D=0.24, C=0.1. The dotted-solid curve is the output intensity$< I(t) >$ varies as a function of the time, the dashed and the dashed-dotted curves are $< I(t) > +\sigma$ and $< I(t) > -\sigma$, respectively, in the case of one fiber with $< \Delta\tau_{III} >= \sqrt{2}ps$, $< \eta_{III} >= \sqrt{2}dB$ and $\langle \hat{\alpha}_{III} \cdot \hat{\beta}_{III} \rangle = 0.15$. The solid and dotted curves are the $< I(t) > +\sigma$ and $< I(t) > -\sigma$,respectively. In the case of two Maxwellian fibers M_1 $(< \Delta\tau_I >= 1ps, < \eta_I >= 1dB, \langle \hat{\alpha}_I \cdot \hat{\beta}_I \rangle = 0.15$, and $M_2 (< \Delta\tau_{II} >= 1ps, < \eta_{II} >= 1dB, \langle \hat{\alpha}_{II} \cdot \hat{\beta}_{II} \rangle = 0.15.)$ are connected together

Chapter 5

Bit Error Rate Calculation for Optical System with CD, PMD, PDL, and ASE Noise

This chapter presents one of the primary contributions of this dissertation; a mathematical model to evaluate the bit error rate for the optical transmission systems is presented. This chapter is organized as: section 5.1 is an introduction to the performance of the optical communication systems. Section 5.2 gives an overview to some important concepts in our calculation in this chapter such as amplified spontaneous emission (ASE) noise, probability of error, and moment generation function. In section 5.3 we will explain our system modeling under the study. The analytical treatment of the system is presented in section 5.4. Our results and their discussion are presented in section 5.5.

5.1 Introduction

To evaluate the performance of a linear optical communication system, one conceptually simple way is the Monte-Carlo method. However, this method is computationally inefficient when dealing with rare but physically important events, e.g., the BER in an all-optical transmission channel, where the error probability is usually less than 10^{-9} . To improve the simulation efficiency one needs advanced simulation techniques.

Due to the effective way of using moment generation function (MGF) to evaluate the bit error rate [78, 79], it has attracted a lot of attention in recent years. Providing a complete description for the signal and noise processes encountered in an optical system, the MGF can be used to evaluate BER, Q-factor, and SNR for many cases with various PMD and PDL effects and using different modulations, as we will discusse in this chapter.

5.2 Overview

In this chapter we introduce impairment to our calculation that is the noise. In fact we consider only the amplified spontaneous emission noise and we didn't consider the transmitter noise or the receiver noise.

5.2.1 *Amplified spontaneous emission as another impairment in the optical systems*

Detection of signal is typically affected by attenuation and dispersion. Furthermore, with the use of amplifiers, there is an additional impairment because of noise that may appear in the receiver due to the presence of amplified spontaneous emission (ASE). In practice, using amplifiers helps to improve the signal propagation span. That is because the increase in the signal amplitude will help overcome noise generated in the receiver's front end. However, the optical background noise, which accompanies the desired optical signal, will also be amplified along with the signal. Consequently, the optical signal-to-noise ratio (OSNR) will tend to degrade as it passes through the transmission system.

Optical signal to noise ratio (OSNR) is the measure of the ratio of signal power to noise power in an optical channel. Hence, OSNR is important because it suggests a degree of impairment when the optical signal is carried by an optical transmission system that includes optical amplifiers [80].

The dominant noise source, usually, is the thermal noise. By using high gain, low noise optical amplifier we can increase the signal level incident on a detector. Hence, the thermal noise is rendered insignificant. Therefore, the amplifier noise contributions dominate, and their effect can be minimized by using an additional optical filter. In such preamplifier receivers, high sensitivities have been obtained [81, 82].

The development of preamplifier receivers requires an investigation of the noise sources; there were several studies in this subject.

5.2.2 *The origin of amplified spontaneous emission noise*

Due to the low propagation loss of optical fibers, data signals can travel many kilometres before amplification is needed. Nevertheless, when the distance between transmitter and receiver approaches and goes beyond 100km, amplifiers are necessary.

Optical amplifiers have replaced the rather involved process of the fiber optic repeater station. It created a revolution in long distance optical communication systems. In fact, simplicity and reliability of the repeater compartment are especially important when the optical fiber cable is used as a submarine cable. Since its invention in 1986, the Erbium-doped fiber amplifier (EDFA) has made tremendous progress. In these days, it is well known that using EDFA as optical preamplifiers improves the receiver sensitivity of the detection systems. Due to the importance of optical amplifiers there have been many papers analyzing such systems [83].

Optical amplifiers employ the mechanism of stimulated emission to amplify the incident optical power. The main ingredients of such amplifiers include a gain medium, which exhibits photon emission in the wavelength range of interest, and a pumping mechanism (optical or electrical) which is used to create population inversion and increase the number of excited state electrons. Some of the high speed fiber communication systems have used optical amplifiers which are fabricated with semiconductor materials; figure (5.1) presents that.

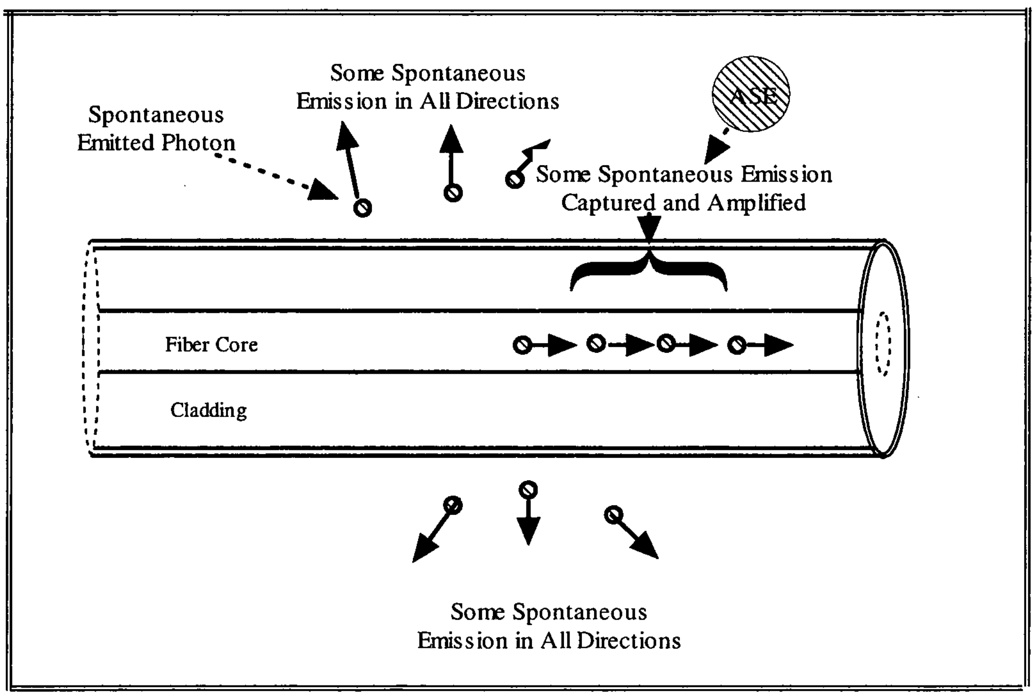

Figure 5.1 Generation of the ASE noise

Recently, fiber amplifiers employ rare-earth ions, such as erbium, neodymium, and ytterbium, as the gain medium to realize fiber amplifiers operating at different wavelengths covering the visible to the infrared region. Because of the ability of operating at 1.55μm (the wavelength region in which fiber loss is minimum), a particular interest was given to Erbium-doped fiber amplifiers (EDFAs). Furthermore, EDFAs provides a broadband, relatively flat, gain spectrum which makes it possible to use multiple wavelengths. Each wavelength acts as an autonomous lightpath and can carry different forms of voice, video, and data traffic. On the other hand, with the ability of producing extremely high optical gain levels, EDFAs can be used with large spacing between consecutive optical amplifier repeaters in the long-haul transmission system. Moreover, due to the large bandwidth and slow gain dynamics of amplification, the amplifier is virtually transparent to the data rate or format. Hence the installed system may be upgraded without changing the intermediate repeater equipment.

Erbium-doped fiber amplifiers (EDFA): Erbium-doped fiber amplifiers are optical fibers of which the cores are doped with the rare-earth element Erbium. By exciting the Erbium ions to higher energy levels, one can achieve amplification of signals at wavelengths interesting for optical communication (~ 1550 nm). In this case, the energy levels are not very sharp, which leads to a relatively large gain bandwidth.

By sending a beam of light in to the fiber (the pump process), we can excite the $Er^{3+} - ions$. With operating the pump at wavelength 980nm, Er^{3+} will rise from the ground state L_1 to higher state L_3, as illustrated in figure (5.2). However, the ions will rapidly decay to energy level L_2 (the lifetime in L_3 is ~ $1\mu s$) . On the other hand, operating the pump at 1480 nm excites the ions to level L_2 directly. Then a relaxation to level L_1 will happen (relaxation from L_2 to L_1 will occur after ~ 10ms) . This relaxation will produce photons in the wavelength band 1520-1570nm [84]. This is called spontaneous emission. Spontaneous emission will experience amplification as it propagates through the fiber. This is termed amplified spontaneous emission (ASE).

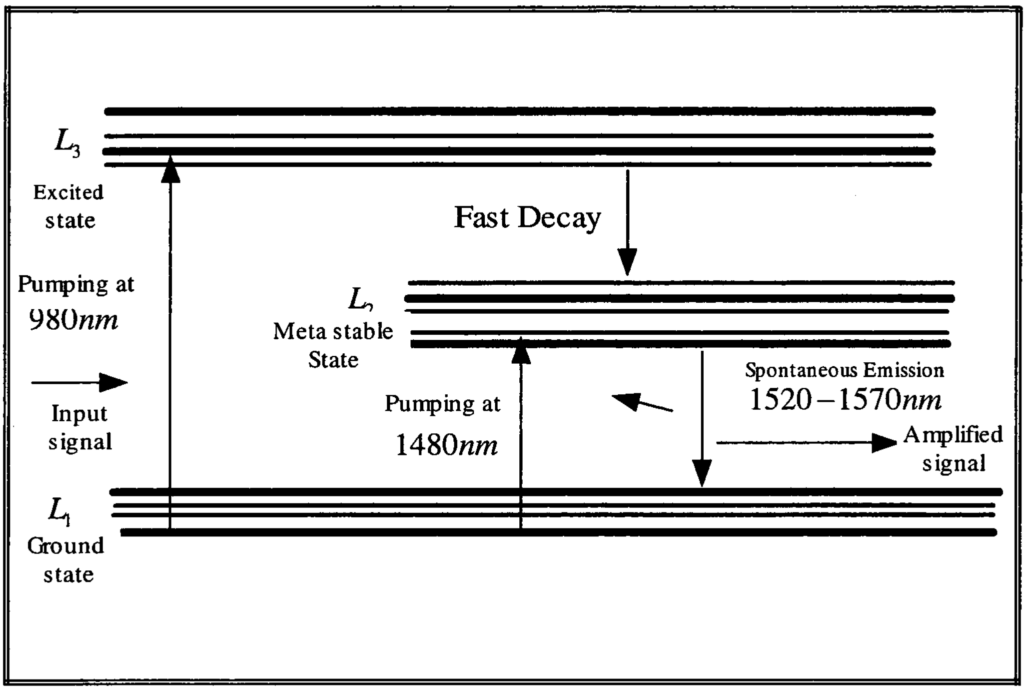

Figure (5.2) Energy levels of Erbium ions in EDFA

One important point to reduce the amplified spontaneous emission (ASE) power at the detector is the bandpass filter always had to be taken much broader than the bandwidth of the data signal [85]. Moreover, optical filtering has some major effects; it can close the eye diagram by introducing intersymbol interference (ISI) [86], and it affects the signal-amplified spontaneous emission (ASE) beat noise by distorting the signal and by filtering ASE noise [87], Kuznetsov [88] studied the both effects.

5.2.3 Probability of error

Achieving a desired bit-error rate (BER) with a given outage probability, after the signal is transmitted through an optical system, is a fundamental problem in the design of the optical fiber transmission systems. BER can also be defined (in some range of applications) in terms of the probability of error (POE) as $POE = \left(\frac{1}{2}\right) \mathrm{erf}\left(\sqrt{\frac{E_b}{N_0}}\right)$ [87] where erf is the error function, E_b is the energy in one bit and N_0 is the noise power spectral density (noise power in a 1Hz bandwidth). The error function is different for each of various modulation methods. The energy per bit E_b can be determined by dividing the carrier power by the bit rate. As an energy measure it has the unit of Joules. N_0 is in power (Joules per second) per Hz , this identified that E_b/N_0 is a dimensionless numerical ratio.

Consider that $x(t)$ to take two possible values $x_0(t)$ and $x_1(t)$. At time $t = t_0$, we have $x_0 = x_0(t_0)$ and $x_1 = x_1(t_0)$. Conditional probability for symbol x_0 and x_1 can be represented by $P_{y|x_0}(y)$ and $P_{y|x_1}(y)$, respectively. If the probability for both symbols is equal then $P(x_0) = P(x_1) = 1/2$ .The probability of error and it can be calculated as

$$P_e = \int_T^{\infty} P_{y|x_0}(y)P(x_0)\ dy + \int_{-\infty}^{T} P_{y|x_1}(y)P(x_1)\ dy \qquad (5.1)$$

One way to lower the spectral noise density is to reduce the bandwidth, but the bandwidth which required for transmitting the desired bit rate is limited. Also, we can increase the energy per bit by using higher power transmission, but interference with other systems can limit that option. A lower bit rate can increase the energy per bit, but that may creates loss in the capacity. Ultimately, optimizing E_b/N_0 is a balancing act among these factors.

Another factor is PDL. In fact the accumulated PDL caused by various optical components can result in partially polarized ASE noise before the receiver. Lima and others [89] have studied this for on-off shift keying format, with considering both PMD and PDL, to evaluate the bit error rate (BER). On the other hand, Zhang and others [90] have used DPSK (and OOK) modulation format for the same purpose (considering the influences of the filter and pulse shaping)

5.2.4 Moment generation function

Bit error rates for optical systems are in the range 10^{-9}–10^{-15} typically. In this range, the usual Gaussian fitting Q-factor approximation does not work well. Instead using the characteristic function, or equivalently the moment-generating function solved the problem here; moment-generating function can be used to obtain BER values as small as $\sim 10^{-20}$ in specific cases. As example, Forestieri [91] had reached values of 10^{-18} for the BER at signal-to-noise ratio amount $\sim 19\,dB$ using a computationally efficient approach to accurately evaluate BER via MGF. Zhang and others [90] have reached a value of 10^{-25} at signal to noise ratio $\sim 18\,dB$ (for DPSK modulation format) by extending Forestieri's method to include PMD and PDL effects.

The moment generation function (MGF) or equivalently the characteristic function method was originally proposed in the 1990's to evaluate the BERs of some simplified direct-detection lightwave communication systems [60, 91]. Decomposing electrically filtered noise as uncorrelated components [91] successfully gave an accurate MGF and therefore the BER of a one dimensional (1D) model with CD, arbitrary signal pulse shape and pre-and post-detection filtering. Later research showed that this MGF method could be extended to cases consisting of various linear effects (ASE noise, CD, PMD, and PDL) and using different modulation formats (OOK, DPSK, and optical duobinary) [90, 92, 93].

5.3 The system modeling

In our modeling system, figure (5.3.a) for OOK and figure (5.3.b) for DPSK, the optical signal $\vec{s}_{in}(t)$ is launched into the fiber system with two lumped chromatic dispersion $(CD_1 \, and \, CD_2)$, lumped PMD $(PMD_1 \, and \, PMD_2)$, and lumped PDL $(PDL_1 \, and \, PDL_2)$ sections in the linear regime. Then it is amplified by a flat gain amplifier G. This amplifier added amplified spontaneous emission (ASE) noise. The normalized ASE noise is considered as additive white Gaussian noise $\vec{n}_{in}(t)$ with a two-sided power spectral density $N_0 = n_{sp} \frac{G-1}{G} h\nu$, where $n_{sp} \geq 1$ is the spontaneous-emission or population inversion parameter and $h\nu$ is the photon energy. We consider that $G \gg 1$ so that $N_0 = n_{sp} \, h\nu$ [91]. ASE noise from the flat gain amplifier G is partially polarized due to the PDL [89] and then the signal is optically filtered. The optical filter is followed by a photodetector. Finally the detected current is electrically filtered by the postdetection filter and sampled at the time t_k.

5.4 The analytical treatment

5.4.1 Characteristic function of the detected current

The instantaneous current at the decision circuit can be written as

$$y(t,\tilde{t}) = \{< \vec{E}_{out}(t,\tilde{t})|\vec{E}_{out}(t) > + < \vec{E}_{out}(t)|\vec{E}_{out}(t,\tilde{t}) >\}/2, \tag{5.2}$$

$\tilde{t} = 0 \quad (OOK)$, $\tilde{t} = T_b \quad (DPSK)$.

Using Fourier transform $E(t) = \frac{1}{\sqrt{2\pi}} \int d\omega \, e^{-i\omega t} \, E(\omega)$, the instantaneous current is

$$y(t,\tilde{t}) = \frac{1}{2\pi} \int d\omega \int d\acute{\omega} \, e^{i(\acute{\omega}-\omega)t} \left[e^{i\acute{\omega}\tilde{t}} + e^{-i\omega\tilde{t}}\right] H_r\,(\acute{\omega}-\omega)\, H_o^*\,(\acute{\omega})\, H_o(\omega)$$

$$\times < \vec{E}_{out}(\acute{\omega})|\vec{E}_{out}(\omega) > \tag{5.3}$$

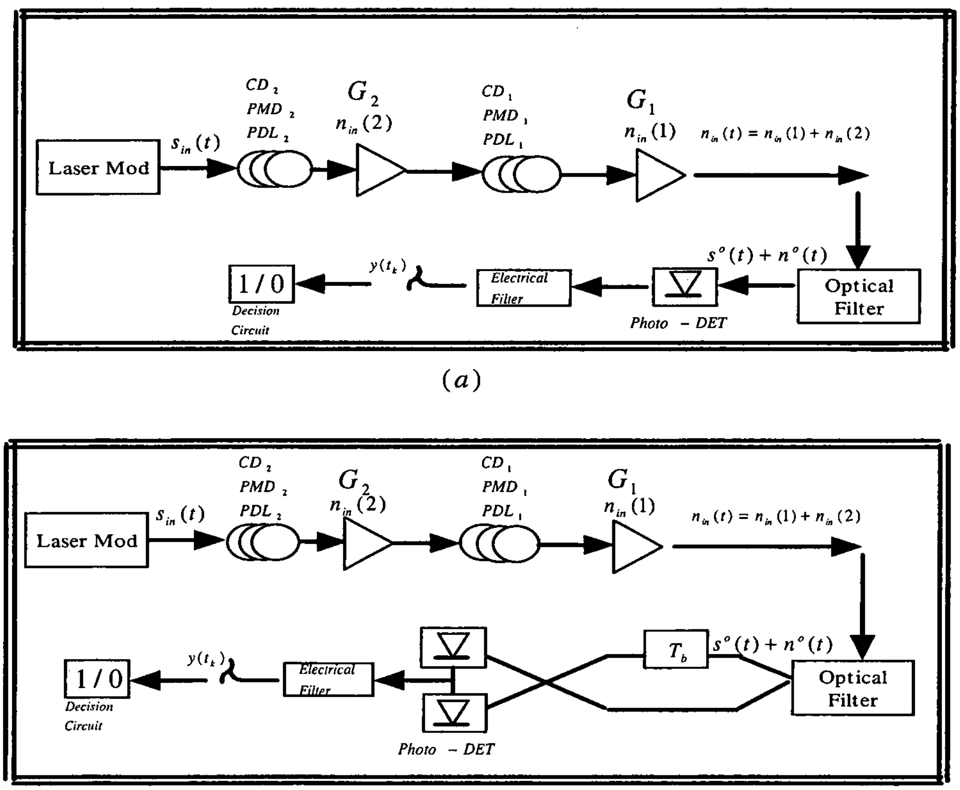

(b)

Fig (5.3) Equivalent low-pass system model for
(a) OOK, (b) DPSK

In this chapter we are dealing with two sections of PMD, two sections of PDL and two noises, so the output field has the form

$$\left|\vec{E}_{out}(\omega)\right> = e^{i\left(\Psi_{L1}^{CD}(\omega)+\Psi_{L2}^{CD}(\omega)\right)}\, T(\vec{\alpha}_2)T(\vec{\tau}_2,\omega)T(\vec{\alpha}_1)T(\vec{\tau}_1,\omega)\left|\vec{E}_{in}(\omega)\right> +$$

$$e^{i\left(\Psi_{L2}^{CD}(\omega)\right)}\, T(\vec{\alpha}_2)T(\vec{\tau}_2,\omega)\left|\vec{e}_1^{\,(n)}(\omega)\right> + \left|\vec{e}_2^{\,(n)}(\omega)\right> \tag{5.4}$$

where $\vec{e}_1^{\,(n)}$ and $\vec{e}_2^{\,(n)}$ represent ASE noise optical fields.

The PMD Jones matrix has the form $T(\vec{\tau}_j,\omega) = \exp(-i(\frac{1}{2})\omega\, \vec{\tau}_j \cdot \vec{\sigma})$, PDL Jones matrix is $T(\vec{\alpha}_j) = \exp(-\alpha_j/2)\exp(\vec{\alpha}_j \cdot \vec{\sigma})/2$ and the chromatic dispersion up to the 3^{rd} order is $\Psi_j^{CD} = L_j\,[(\frac{1}{2})\beta_2\omega^2 + (\frac{1}{6})\beta_3\omega^3]$, j denoted to the number of the section($j = 1,2$). For simplicity we will rewrite equation (5.4) as following

$$\left|\vec{E}_{out}(\omega)\right> = S_1 + S_2 + S_3\,, \tag{5.5}$$

$$S_1 = e^{i\left(\Psi_{L1}^{CD}(\omega)+\Psi_{L2}^{CD}(\omega)\right)}\, T(\vec{\alpha}_2)T(\vec{\tau}_2,\omega)T(\vec{\alpha}_1)T(\vec{\tau}_1,\omega)\left|\vec{E}_{in}(\omega)\right>\,, \tag{5.6.a}$$

$$S_2 = e^{i\left(\Psi_{L2}^{CD}(\omega)\right)}\, T(\vec{\alpha}_2)T(\vec{\tau}_2,\omega)\left|\vec{e}_1^{\,(n)}(\omega)\right>, \tag{5.6.b}$$

$$and\ \ S_3 = \left|\vec{e}_2^{\,(n)}(\omega)\right>. \tag{5.6.c}$$

For the critical expression $<\vec{E}_{out}(\acute{\omega})\left|\vec{E}_{out}(\omega)\right>$ we have nine distinct terms as

$$<\vec{E}_{out}(\acute{\omega})\left|\vec{E}_{out}(\omega)\right> = S_1^*S_1 + S_2^*S_2 + S_3^*S_3 + S_1^*S_2 + S_2^*S_1 + S_1^*S_3 + S_3^*S_1 + S_2^*S_3 + S_3^*S_2 \tag{5.7}$$

The explicit forms of these nine terms are giving in the appendix C.

In order to proceed with the noise fields averaging, we introduce the following short hand notation $f(\acute{\omega},\omega,t,\tilde{t}) = \left(\frac{1}{2\pi}\right) e^{i(\omega \acute{-} \omega)t} \left[e^{i\acute{\omega}\tilde{t}} + e^{-i\omega\tilde{t}} \right] H_r(\acute{\omega}-\omega)\, H_o^*(\acute{\omega})\, H_o(\omega)$. Also, we introduce a super noise field vector (depending on the noise fields dimensions)

$$\left|\vec{N}(\omega)\right> = \begin{bmatrix} \left|\vec{e}_1{}^{(n)}(\omega)\right> \\ \left|\vec{e}_2{}^{(n)}(\omega)\right> \end{bmatrix}. \tag{5.8}$$

Furthermore, by discarding the noise expressions in the last eight terms of $<\vec{E}_{out}(\acute{\omega})\left|\vec{E}_{out}(\omega)\right>$ we can introduce a ket-vector

$$\left|\vec{b}(\acute{\omega})\right> = \begin{bmatrix} \int d\omega\, f(\acute{\omega},\omega,t,\tilde{t}) S_2^* S_1 \\ \int d\omega\, f(\acute{\omega},\omega,t,\tilde{t}) S_3^* S_1 \end{bmatrix}. \tag{5.9.a}$$

On the other hand we will combine the terms $S_1^* S_2$ and $S_1^* S_3$ to introduce the bra-vector

$$<\vec{b}(\omega)\Big| = \left[\int d\omega\, f(\acute{\omega},\omega,t,\tilde{t}) S_1^* S_2 \quad \int d\omega\, f(\acute{\omega},\omega,t,\tilde{t}) S_1^* S_3\right]. \tag{5.9.b}$$

Finally, we introduce the square block matrix Q containing the terms $S_2^* S_2, S_3^* S_3, S_2^* S_3,$ $and\ S_3^* S_2$ as

$$Q = \begin{bmatrix} \int d\omega\, f(\acute{\omega},\omega,t,\tilde{t}) S_2^* S_2 & \int d\omega\, f(\acute{\omega},\omega,t,\tilde{t}) S_2^* S_3 \\ \int d\omega\, f(\acute{\omega},\omega,t,\tilde{t}) S_3^* S_2 & \int d\omega\, f(\acute{\omega},\omega,t,\tilde{t}) S_3^* S_3 \end{bmatrix} \tag{5.10}$$

With the new vectors; the ket-vector $\left|\vec{N}(\omega)\right>$, the bra-vector $<\vec{b}(\omega)\Big|$, the ket-vector $\left|\vec{b}(\acute{\omega})\right>$ and the square matrix Q, we can rewrite the instantaneous detecting current at the decision circuit as

$$y(t,\tilde{t}) = <\vec{N}\left|Q\right|\vec{N}> + <\vec{b}\left|\vec{N}\right> + <\vec{N}\left|\vec{b}\right> + \int d\acute{\omega} \int d\omega\, f(\acute{\omega},\omega,t,\tilde{t}) S_1^* S_1\,. \tag{5.11}$$

In fact, this equation is just another view to equation (5.2). Mathematically, $y(t,\tilde{t})$ is a physical variable which is a function of complex Gaussian variable, in this case we can get the moment generation function as following: for a physical variable ξ which is defined in a quadratic form as $\xi = c + \lambda w^* w + b^* w + b w^*$ and $w = x + iy$ is a complex Gaussian variable. Then $\xi = c + \lambda(x^2 + y^2) + 2xRe(b) + 2y\, Im(b)$ and its characteristic function is

$$\langle e^{is\xi}\rangle = \int_{-\infty}^{\infty} dx\, \rho_G(x) \int_{-\infty}^{\infty} dy\, \rho_G(y)\, e^{is\xi} = \frac{1}{1-\sigma^2\lambda is}\, e^{[isc - \frac{\sigma^2|\tilde{b}|^2 s^2}{1-\sigma^2\lambda is}]}. \tag{5.12}$$

5.4.2 Probability density function of the modeling system:

Using inverse Fourier transform, from the characteristic function we can get the probability density function as

$$\rho(\xi) = \left(\frac{1}{2\pi}\right)\int_{-\infty}^{\infty} ds\, e^{-is\xi} \quad < e^{is\xi} >$$

$$= \left(\frac{1}{2\pi}\right)\int_{-\infty}^{\infty} ds\, e^{-is(\xi-c)}\, \frac{1}{1-\sigma^2\lambda is}\, e^{[-\frac{\sigma^2|\tilde{b}|^2 s^2}{1-\sigma^2\lambda is}]}. \tag{5.13}$$

For M complex random independent and identical distributed (i.i.d.) Gaussian variable we have $\xi = c + \sum_{j=1}^{M}[diag(\lambda_j) w_j^* w_j + b_j^* w_j + w_j^* b_j]$. The moment generation function is

$$\Psi_{t_k}(t) = \prod_{j=i}^{M} \frac{1}{1-\sigma^2\lambda_j is}\, e^{[-\frac{\sigma^2|\tilde{b_j}|^2 s^2}{1-\sigma^2\lambda_j is}]} \tag{5.14}$$

where t_k is the sampling time, and the probability density function is

$$\rho(\xi) = (\frac{1}{2\pi}) \int_{-\infty}^{\infty} ds\, e^{-is(\xi-c)} \prod_{j=i}^{M} \frac{1}{1-\sigma^2\lambda_j is} \quad e^{[-\frac{\sigma^2|\widetilde{b_j}|^2 s^2}{1-\sigma^2\lambda_j is}]} \tag{5.15}$$

Now if compare ξ with our current y we find that

$$c = y_{ss} = \int d\acute{\omega} \int d\omega\, f(\acute{\omega}, \omega, t, \tilde{t}) S_1^* S_{1,}, \tag{5.16}$$

$$\xi - c = I_n = \sum_{j=1}^{M} diag(\lambda_j) w_j^* w_j + b_j^* w_j + w_j^* b_j$$

$$= < \vec{N}|Q|\vec{N} > + < \vec{b}|\vec{N} > + < \vec{N}|\vec{b} > \tag{5.17}$$

With the known λ_j and by replacing $is \rightarrow \tilde{s}$ and using the inverse Laplace transform we have

$$\rho(y_{ss} + I_n) = (\frac{1}{2i\pi}) \int_{u_0-i\infty}^{u_0+i\infty} d\tilde{s}\, e^{-\tilde{s}(I_n)} \prod_{j=i}^{M} \frac{1}{1-\sigma^2\lambda_j\tilde{s}} \quad e^{[-\frac{\sigma^2|\widetilde{b_j}|^2\tilde{s}^2}{1-\sigma^2\lambda_j\tilde{s}}]}, \tag{5.18}$$

$$\frac{1}{\sigma^2 \max\ \{|\lambda_j^-|\}} < u_0 < \frac{1}{\sigma^2 \max\ \{\lambda_j^+\}}.$$

Here λ_j^+, λ_j^-stands for the positive and negative λ_j , respectively.Therefore, to evaluate the probability density function as a function of the whole detecting current ($y = y_{ss} + I_n$) we need to get the values of the integration as a function of the part related to noise (I_n) ;the noise-noise beating and the signal-noise beating.

5.4.3 Probability of error occurrence:

For moment generation function given in equation (5.14), we can rewrite the probability density function as

$$\rho_{y_{th}}\ (\varsigma) = \left(\frac{1}{2i\pi}\right)\int_{u_0-i\infty}^{u_0+i\infty} d\tilde{s}\ \Psi_{t_k}(\tilde{s}) e^{-\tilde{s}(\varsigma)}, \tag{5.19}$$

$$\frac{1}{\sigma^2 \max\ \{|\lambda_j^-|\}} < u_0 < \frac{1}{\sigma^2 \max\ \{\lambda_j^+\}}.$$

The left hand tail probability:

$$P\{y_{ss} < y_{th}\} = \int_{-\infty}^{y_{th}} \rho_{y_{th}}\ (\varsigma)\, d\varsigma\ = \int_{-\infty}^{\infty} \rho_{y_{th}}\ (\varsigma) u(y_{th} - \varsigma)\, d\varsigma \tag{5.20}$$

where y_{th} is the detection threshold, and $u(x)$ is a unit step function. Using the inverse Laplace transform we get

$$P\{y_{ss} < y_{th}\} = \left(\frac{1}{2i\pi}\right)\int_{u_0-i\infty}^{u_0+i\infty} \Psi_{t_k}(\tilde{s})\ \left(\int_{-\infty}^{\infty} u(y_{th} - \varsigma)\ \ e^{-\tilde{s}(\varsigma)} d\varsigma\ \right) d\tilde{s}$$

$$P\{y_{ss} < y_{th}\} = \left(-\frac{1}{2i\pi}\right)\int_{u_0-i\infty}^{u_0+i\infty} \frac{\Psi_{t_k}(\tilde{s})}{\tilde{s}} e^{-\tilde{s} y_{th}} d\tilde{s}\ , \tag{5.21}$$

$$\frac{1}{\sigma^2 \max\ \ |\lambda_j^-|} < u_0 < 0$$

where the restriction on the u_0 range is necessary for the convergence of the inner integral in the last two equations.

The right-hand tail probability:

The right-hand tail probability can be evaluated in a similar manner

$$P\{y_{ss} > y_{th}\} = \int_{y_{th}}^{\infty} \rho_{y_{th}}\ (\varsigma)\, d\varsigma\ = \int_{-\infty}^{\infty} \rho_{y_{th}}\ (\varsigma) u(\varsigma - y_{th})\, d\varsigma \tag{5.22}$$

$$P\{y_{ss} > y_{th}\} = \left(\frac{1}{2i\pi}\right)\int_{u_0-i\infty}^{u_0+i\infty} \Psi_{t_k}(\tilde{s})\ \left(\int_{-\infty}^{\infty} u(\varsigma - y_{th})\ \ e^{-\tilde{s}(\varsigma)} d\varsigma\ \right) d\tilde{s}$$

$$P\{y_{ss} > y_{th}\} = \left(-\frac{1}{2i\pi}\right)\int_{u_0-i\infty}^{u_0+i\infty} \frac{\Psi_{t_k}(\tilde{s})}{\tilde{s}} e^{-\tilde{s}y_{th}} d\tilde{s}\ , \qquad 0 < u_0 < \frac{1}{\sigma^2 \max\{\lambda_j{}^+\}} \tag{5.23}$$

5.4.4 The saddle point approximation:

Since the line integral of an analytic function and the integration path are independent, we can rewrite both the left-hand tail and the right-hand tail as

$$P\{y_{ss} < y_{th}\} = \left(-\frac{1}{2i\pi}\right)\int_{c_-} \frac{\Psi_{t_k}(\tilde{s})}{\tilde{s}} e^{-\tilde{s}y_{th}} d\tilde{s}\ , \tag{5.24.a}$$

$$P\{y_{ss} > y_{th}\} = \left(\frac{1}{2i\pi}\right)\int_{c_+} \frac{\Psi_{t_k}(\tilde{s})}{\tilde{s}} e^{-\tilde{s}y_{th}} d\tilde{s}\ . \tag{5.24.b}$$

The integration contours $c_\pm$ are conveniently chosen to closely approximate the paths of steepest descent passing through the saddle points $u_0^\pm$ of the integrands on the real x-axis.

Let us take a look to the integrands in the last two equations; we can write $\frac{\Psi_{t_k}(\tilde{s})}{\tilde{s}} e^{-\tilde{s}y_{th}} = e^{\Phi_{t_k}(\tilde{s})}$, taking the logarithmic function of the both sides gives

$$\Phi_{t_k}(\tilde{s}) = \log\left(\Psi_{t_k}(\tilde{s})\right) - \log(\tilde{s}) - \tilde{s}y_{th} \tag{5.25}$$

Substitute the value of $\Psi_{t_k}(t)$ from equation (5.14) gives

$$\Phi'_{t_k}(\tilde{s}) = \sum_{j=1}^{M}\{\left[\frac{\sigma^2|\widetilde{b_j}|^2\tilde{s}^2}{1-\sigma^2\lambda_j\tilde{s}}\right] - \log\ [1-\sigma^2\lambda_j\tilde{s}]\} - \log(\tilde{s}) - \tilde{s}y_{th} \tag{5.26.a}$$

differentiate this equation with respect to $\tilde{s}$ gives

$$\Phi''_{t_k}(\tilde{s}) = \sum_{j=1}^{M}\{\left[\frac{2\sigma^2|\widetilde{b_j}|^2\tilde{s}\ \ (1-\sigma^2\lambda_j\tilde{s}/2)}{(1-\sigma^2\lambda_j\tilde{s})^2}\right] + \frac{\sigma^2\lambda_j}{[1-\sigma^2\lambda_j\tilde{s}]}\} - \frac{1}{\tilde{s}} - y_{th} \tag{5.26.b}$$

The roots of this equation are the saddle points u_0^- and u_0^+ . These two roots (saddle points) can be found by using a numerical method.

Using Newton's method we can get the saddle points, details are in the appendix D

5.4.5 The paths of steepest descent $c_\pm$

The paths of steepest descent $c_\pm$ are well approximated by parabolas of the form:

$$\tilde{s} = u_0^\pm + \left(\tfrac{1}{2}\right)kv^2 + iv, \tag{5.27}$$

$$k = \frac{\Phi'''_{t_k}\left(u_0^\pm\right)}{3\Phi''_{t_k}\left(u_0^\pm\right)}$$

where $\Phi'''_{t_k}\left(u_0^\pm\right)$ is the third derivative of $\Phi \quad_{t_k}\left(u_0^\pm\right)$, it has the form:

$$\Phi'''_{t_k}(\tilde{s}) = \sum_{i=1}^{M}\{\sum_{j=1}^{M}\{\frac{(6\,(\sigma^2)^2|\widetilde{b_j}|^2\lambda_j)}{\left[1-\sigma^2\lambda_j\tilde{s}\right]^2} + \frac{2(\sigma^2\lambda_j)^3}{\left[1-\sigma^2\lambda_j\tilde{s}\right]^3} - \frac{(24\sigma^2|\widetilde{b_j}|^2)(2\sigma^2\lambda_j)^2[1-\sigma^2\lambda_j\tilde{s}/2]}{[1-\sigma^2\lambda_j\tilde{s}]^4}\}\} - \frac{2}{(\tilde{s}^3)} \tag{5.28}$$

5.4.6 Evaluation of the integrals by using the parabola contours:

In order to evaluate the probabilities given in equations (5.24.a.), (5.24.b), we rewrite those two equations as

$$P\{y_{ss} < y_{th}\} = \left(\frac{1}{\pi}\right)\int_0^\infty Re\{\,e^{\Phi_{t_k}(u_0^+ + (\frac{1}{2})kv^2+iv)}(1-ikv)\}, \tag{5.29.a}$$

$$P\{y_{ss} > y_{th}\} = \left(-\frac{1}{\pi}\right)\int_0^\infty Re\left\{\,e^{\Phi_{t_k}(u_0^- + (\frac{1}{2})kv^2+iv)}(1-ikv)\right\}. \tag{5.29.b}$$

These two integrations are evaluated by the trapezoidal rule to get

$$P\{y_{ss} > y_{th}\} \cong \left(\frac{\Delta\gamma}{\pi}\right)[\left(\tfrac{1}{2}\right)f(0) + \sum_{n=1}^{\infty} f(n\Delta\gamma)] \tag{5.30.a}$$

for the Zero bit, and for the One bit we have

$$P\{y_{ss} < y_{th}\} \cong \left(-\frac{\Delta\gamma}{\pi}\right)[(\tfrac{1}{2})f(0) + \textstyle\sum_{n=1}^{\infty} f(n\Delta\gamma)] \tag{5.30.b}$$

where $f(\gamma) = Re\{e^{\Phi_{t_k}(u_0^- + (\frac{1}{2})kv^2 + iv)}(1 - ikv)\}$ and the initial step size is $\Delta\gamma = \frac{1}{\sqrt{2\Phi''_{t_k}(u_0^{\pm})}}$.

The sum of $f(n\Delta\gamma)$ can be stopped when $f(n\Delta\gamma)$ becomes negligible and halving the step size until the result is stabilized in desired accuracy.

5.4.7 The final bit error rate:

The bit error rate can be obtained using the form [90, 91]

$$BER_{y_{th}}(t_k) = \left(\frac{\pm 1}{2\pi i}\right)\int_{c_\pm} \frac{\Psi_{t_k}(s)}{s}\, e^{-s y_{th}} ds \tag{5.31}$$

where $+$ and c_+ correspond for $y_{ss} < y_{th}$, while $-$ and c_- for $y_{ss} > y_{th}$. Averaging BERs over all bits in the De Bruijn sequence gives

$$BER = \textstyle\sum_{k=0}^{N-1} BER_{th}(t_k)/N, \tag{5.32}$$

and $t_k = t_0 + kT_b$.

5.5 The computational method

In order to obtain the final bit error rate a matlab code was used to calculate the values of the bit error rate. The main code is provided in the appendix E.

5.6 Results and discussions:

In this section, we first give some details about the system we consider, then we present some of the results we had achieved.

5.6.1 Points to be considered in our code

1- The intersymbol interference

To include the intersymbol interference, we used a 32-bit sequence (16-Zeros and 16-Ones) as in figure (5.4). Hence, the probability of error in Zeros bits is $P_0 = \frac{\sum_{k=0}^{15} P_0\,(t_k)}{16}$. Similarly, the probability of error in Ones bits is $P_1 = \frac{\sum_{k=0}^{15} P_1\,(t_k)}{16}$.The total probability of error (assuming bits One and Zero are sent with equal probability) is $BER = \frac{P_0+P_1}{2}$. When the system input has a on-off keying (OOK) modulation format, the sequence $\{a_n\}$ has taken 2^5-bit de Bruijn sequence [90, 91, 94, 95], i.e., 0000 0111 0111 1100 1011 0101 0011 0001. Repetition of this sequence yields all possible configurations of a 5-bit string from 00000 to 11111 [90, 91]. For the system with a balanced DPSK receiver shown in Figure (5.4.b), $a_i = (\in \{e^{i0}, e^{i\pi}\})$ is determined by requiring the received codes at sampling instants $t_k\ (t_k = t_0 + kT_b, k = 0, \dots, N-1)$, normalized as "0" or "1" with no signal distortion, form a de Bruijn sequence.

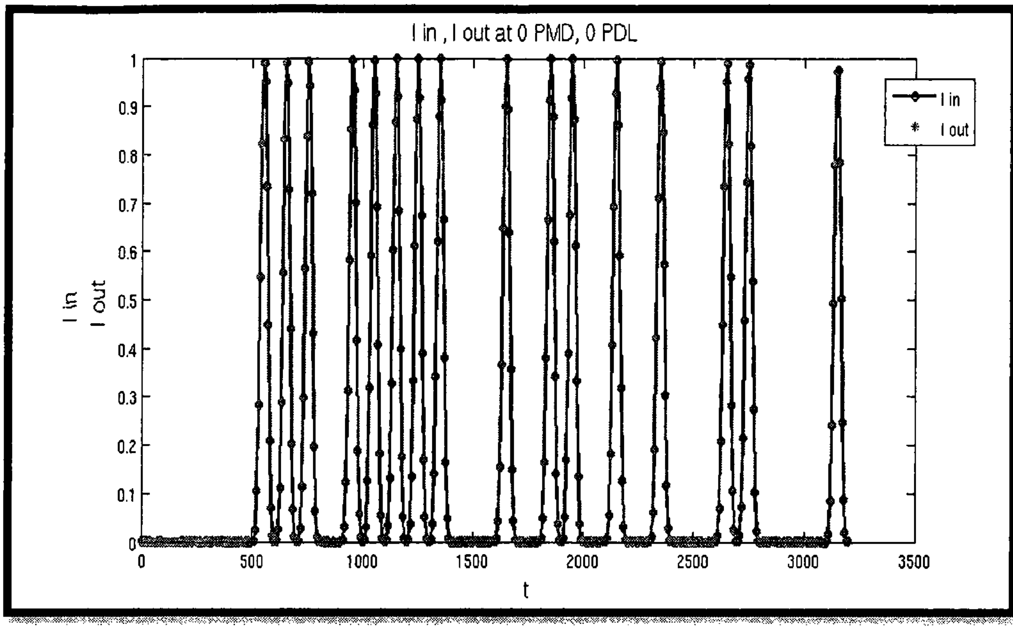

(a)

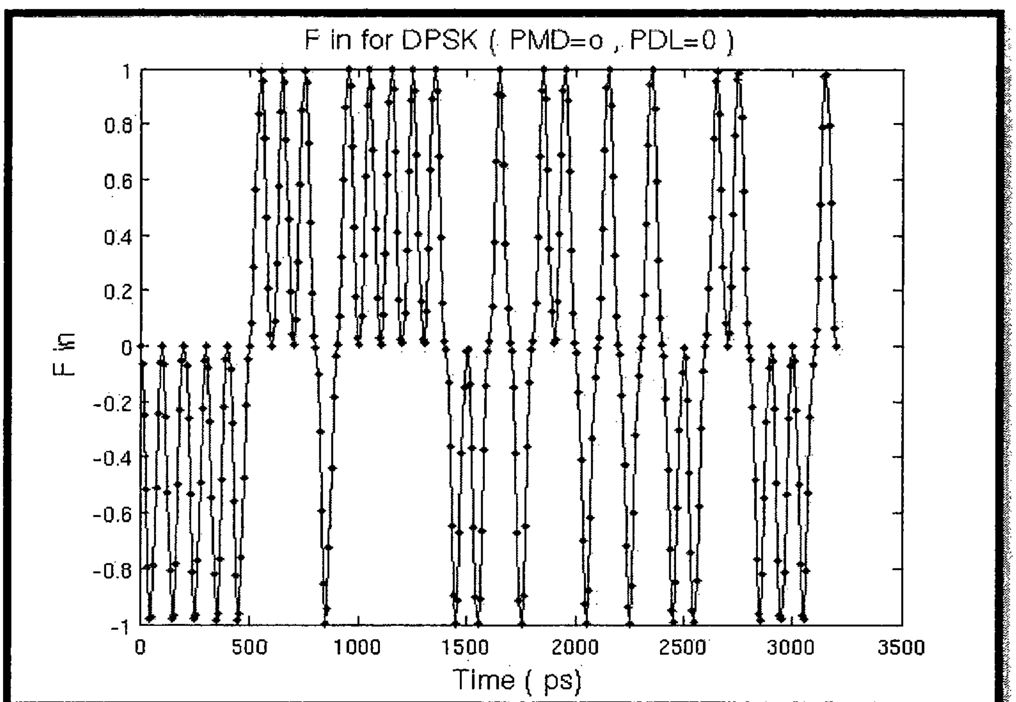

(b)

Figure (5.4) (a) Input, output intensity versus time for OOK (b) Input electric field versus the time for DPSK. In both cases PMD=PDL=0

2- The input signal

Different signal pulse shapes mean different spectral bandwidth, while different modulations can result in different correlations between adjacent signal bits and thus leads to different signal spectral distributions. The first-order PMD (i.e., DGD) causes the difference in arrival times of the two orthogonal modes of optical signal and leads to pulse broadening in time domain. Thus the RZ signal should be more tolerant to the PMD-induced intersymbol interference (ISI) than the NRZ signal, because the PMD effect on the RZ signal can be viewed as the increment of its duty cycle.

RZ-DPSK modulation format gives 3dB improvement in the receiver sensitivity due to the balanced detection scheme, which gives an increase in the system margin (reduced input power or increase the transmission length of the fiber). Furthermore, RZ-DPSK has lower peak power and constant pulse amplitude which reduces the effect of fiber nonlinearity. Therefore, we used RZ-DPSK as input signal.

The amplitude of the input signal $\vec{s}_{in}(t)$ can be assumed to be a periodic repetition of signal $d(t) = \sum_{i=0}^{N-1} a_i p(t - iT_b)$ with period NT_b, $|\vec{s}_{in}(t)| = s_{in}(t) = \sum_{n=-\infty}^{\infty} d(t - nNT_b)$. Here $p(t)$ determines the elementary input pulse shape and a_i determines the logic value of the i^{th} bit. When N is large enough $s(t)$ is a pseudorandom signal. In this case we can use a mathematical tractability with physical properties close to the real situations.

This amplitude is $s(t) = \sum_{n=-\infty}^{\infty} d(t - nNT_b) \equiv \sum_{l=-\infty}^{\infty} s_l\, e^{2i\pi lt/(NT_b)}$,where $s_l = \frac{P(f_l)}{NT_b} A_l$, $A_l = \sum_{m=0}^{N-1} a_m\ e^{-2i\pi ml/N}$, with $P(f_l) = \int_0^{T_b} dt\ p(t)\, e^{-2i\pi f_l t}$, $f_l =$

l/NT_b .In the low-pass configuration, $p(t)$ is the elementary input pulse shape. We consider a raised cosine as input pulse. The raised cosine pulse [90] is given as $p(t) = \sqrt{2E_b/T_b} \cos\left[\frac{\pi}{2} cos^2\left(\frac{\pi t}{T_b}\right)\right]$, where E_b is the optical energy per transmitted bit. Due to its periodicity, the input signal $\vec{s}_{in}(t)$ can be expanded in Fourier series as $\vec{s}_{in}(t) = s_{in}(t)|\vec{p}_s >= \sum_{l=-\infty}^{\infty}(s_{in})_l e^{-i(\frac{2\pi lt}{NT_b})} |\vec{p}_s >$. For simplicity, we assumed that all Fourier components of input signal are polarized in the same direction represented by a constant unit vector $|\vec{p}_s >= [x, y]^T$ in 2D Jones space.

3- The description of the noise expansion

When the overall impulse response of the pre- and postdetection filters at the receiver has finite time duration T_0, then the value of the sample $y(t_k)$ is solely determined by the values that the input waveform of the optical filter takes on in the time interval $(t_k - T_0, t_k)$.

Real filters, practically, have finite impulse responses. However, theoretical filters may not have finite duration impulse responses. Therefore, from practical point of view, with the overall impulse response duration T_0 we could replace their input waveform with another one which coincides only in the time interval $(t_k - T_0, t_k)$. This leaves the value of the sample $y(t_k)$ unchanged.

The above discussion means that an exact description of the input noise wave in the aforementioned time interval has a sufficient statistics. Hence, we can write a Karhunen-Loéve [90, 91] expansion for $\vec{n}_{in}(t)$ in the interval $t_k - T_0 < t < t_k$ only.

The noise $\vec{n}_{in}(t)$ is an additive white Gaussian noise (AWGN) which allows us to choose any orthonormal base for the expansion [90, 91]. For a Fourier base $\{\varphi_m(t) = \left(\frac{1}{\sqrt{T_0}}\right) e^{2i\pi m(t-t_k+T_0)/T_0}\}_{m=-\infty}^{\infty}$ the relevant noise process is $n(t) = \sum_{m=-\infty}^{\infty}(N_{in})_m\, \varphi_m(t),\ \ t_k - T_0 < t < \ t_k$. Here the expansion coefficients $(N_{in})_m$ are treated as complex independent and identically distributed (i.i.d) random variables (r.v.) with Gaussian PDFs of zero mean and variance $\sigma^2 = N_0/(2T_0)$ [90, 91]. The value of T_0 depends upon the optical and postdetection filters.

4- The optical and electrical filters

The optical filter we have used in our code was assumed to be Fabry-Perot. The low-pass transfer function of the Fabry-Perot optical function is [92] $H_o = \frac{1}{1+\frac{2if}{B_o}}$, where B_o is the 3-dB bandwidth (full-width at half-maximum) of the optical filter.

A fifth-order Bessel type was used as a low-pass electrical filter in the code, its transfer function is [92] $H_e(f) = 945/(iF^5 + 15F^4 - i105F^3 - 420F^2 + i945F + 945)$, where $F = 2.43f/B_e$ and B_e is the bandwidth of the electrical filter.

Both B_0 and B_e are defined in terms of the bit rate $R,$ which is the reciprocal of the bit duration T_b $(R = 1/T_b)$.

5- Aligned the signal and the noise in the same direction

By introducing a polarizer before or after the optical filter, the signal and the noise can be aligned in the same direction. Figure (5.5.a) and Figure (5.5.b) describe our system in OOK and DPSK cases. These two figures are equivalent to those in figures (5.3) with an additional polarizer located before (or after) the optical filter. In this case we can rewrite the vector forms of the input signal and noise as

$\vec{s}_{in}(t) = \sum_{l=-\infty}^{\infty}[s_{in}(t)]_l = \sum_l (S_{in})_l \, e^{-i2\pi lt/NT_b}$, $\vec{n}_{in}(t) = \sum_{m=-\infty}^{\infty}[n_{in}(t)]_m = \sum_m (N_{in})_m \, e^{-i2\pi m(t-t_k+T_0)/T_0}$, respectively. Here in both $[s_{in}(t)]_l \equiv (S_{in})_l \, e^{-i2\pi lt/NT_b}$ and $[n_{in}(t)]_m \equiv (N_{in})_m \, e^{-i2\pi m(t-t_k+T_0)/T_0}$, due to the optical filter response $h_0(t)$ [or $H_0(f)$], only those components with frequencies within the filter bandwidth B_0 need to be considered. According to this, we can introduce Dirac bra-ket notations for the input signal as

$$|s_{in}(t_k)> = \left[(S_{in})_{-L} \, e^{\frac{i2\pi Lt_k}{NT_b}} \quad , \dots , (S_{in})_L \, e^{\frac{-i2\pi Lt_k}{NT_b}} \quad \right]^T,$$

$$< s_{in}(t_k)| = \left[(S_{in})_{-L}^* \, e^{\frac{-i2\pi Lt_k}{NT_b}} \quad , \dots , (S_{in})_L^* \, e^{\frac{i2\pi Lt_k}{NT_b}} \quad \right]$$

, Where L is defined as $L = \eta \, N \, B_0 \, T_b$, η is a dimensionless parameter must be determined iteratively. Similarly, the Dirac bra-ket notations for the input noise are

$$|n_{in}(t_k)> = |N_{in}> = [(N_{in})_{-M} \quad , \dots , (N_{in})_M \quad]^T,$$

$$< n_{in}(t_k)| =< N_{in}| = \left[(N_{in})_{-M}^* \quad , \dots , (N_{in})_M^* \quad \right] ,$$

M has the definition $M = \mu \, B_0 \, T_b$, μ a dimensionless parameter can be determined iteratively.

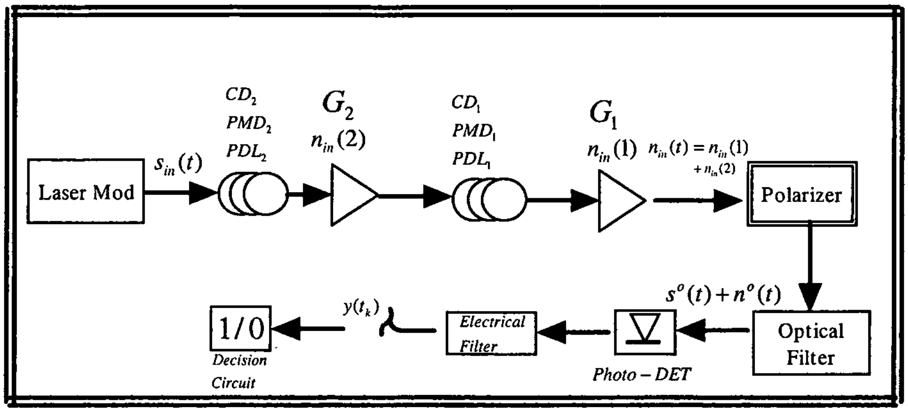

(a)

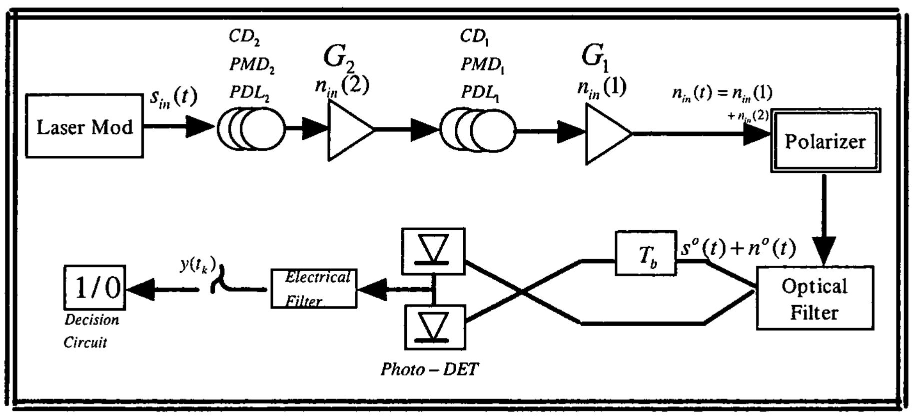

(b)

Fig (5.5) Signal and noise aligned in the same direction
(a) OOK, (b) DPSK

6- The CD index ξ

The CD index ξ defined as $\xi = 10^{-4}D(\lambda)LR^2$ [92] in the unit of $10^4(Gb/s)^2\,ps/nm$, where R is the bit rate in Gb/s, L the fiber length which was considered, and D is the fiber CD parameter (at $\lambda = 1.55\mu m$, $D(\lambda) = \frac{17ps}{nm}/km$). Some of the considered values are given in table (5.1).

$L\ (km)$	0	29.4	58.8	88.24	117.7	147
ξ	0	5	10	15	20	25

Table (5.1) some values of the fiber length and related CD indexes.

5.6.1 The main results

5.6.2.1 CD, PMD, PDL, and ASE noise impacts on optical systems:

1-Pure CD:

The effects of CD on optical performance are closely related with how signal spectrum is distributed near the carrier frequency, since the signal is distorted by CD according to $H_{CD}(f) = e^{-i2\pi^2\beta_2 f^2 L}$. To increase the CD limited transmission, the phase effect in the modulation can be used. The optical and electrical filters are used to limit the spectral bandwidths of the signal and ASE noise.

As a start point for our work to get the best values of BER, we compared our system with the work in Ref. 90. Figure (5.6) present our results (figure (5.6. a)), and the work that have done in Ref. 90 (figure (5.6. b)). It is clear that there is an excellent agreement between our work and the work in Ref. [90] for OOK modulation format. For DPSK modulation format, also there where an excellent agreement between our work and Ref [90] up to SNR=18, since Ref. [90] has considered the SNR up to 18 and we considered this value up to 20.

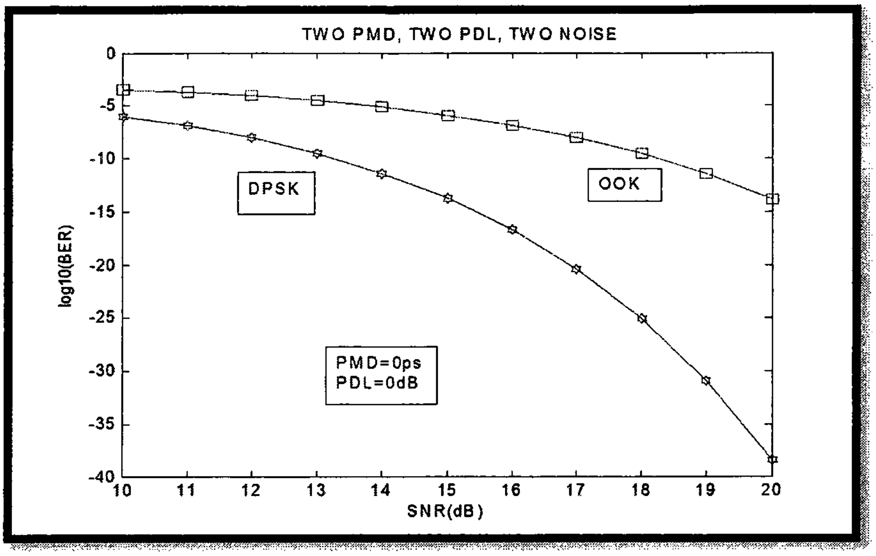

(a)

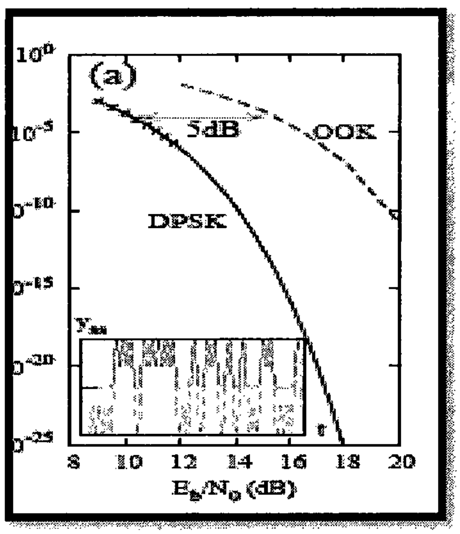

(b)

Figuer (5.6) (a) Log BER versus — ( ) in our work, (b) BER versus — [90] . Both (a) and (b) has — — for OOK and — — for DPSK. The system has no PMD, PDL ( ) in both (a) and (b).

To see how CD can affect our model performance, we consider its effect on the BER. Therefore, the bit error rate as a function of CD index was considered at specified signal to noise ratio (SNR). The CD index (as we mentioned before) is defined as $\xi = 10^{-4}D(\lambda)LR^2$ in the unit of $10^4\ (Gb/s)^2\ ps/nm$, where $R = 1/T_b$ is the bit rate in Gb/s. We considered a $10\ Gb/s$ as the bit rate and $\lambda = 1550\ nm$ which yields$D(\lambda) \approx 17\ ps\ nm/km$. Alternatively, the CD impact can be studied by considering a value of SNR. Here the required SNR is defined to be E_b/N_0, with N_0 the two-sided power spectral density of ASE noise [90-92] and E_b is the optical energy per transmitted bit. Figure (5.7) shows the effect of CD index ξ on $\log(BER)$ at $SNR = 18$ for OOK (a) and DPSK (b) in a pure CD effect ($PMD = PDL = 0$). In both cases, as expected, increasing the CD index induced a higher BER. Comparing curves in Fig (5.7.a) and (5.7.b), one can see that the BER for OOK is always higher than its values in DPSK. This is due the fact that, in the case of DPSK, any two adjacent signal bits are correlated with each other, which leads to more concentrated signal spectra than OOK case. Usually, for DPSK the two adjacent bits are correlated in the receiver part. The bandwidth of the optical and electrical filters for both OOK and DPSK case are given in the table (5.2) [92] .

Modulation format type	***OOK***	***DPSK***
$B_o\ T_b$	1.8	2.2
$B_e\ T_b$	0.65	0.65

Table (5.2) the optimum values of $B_o\ T_b$,and $B_e\ T_b$ for OOK and DPSK

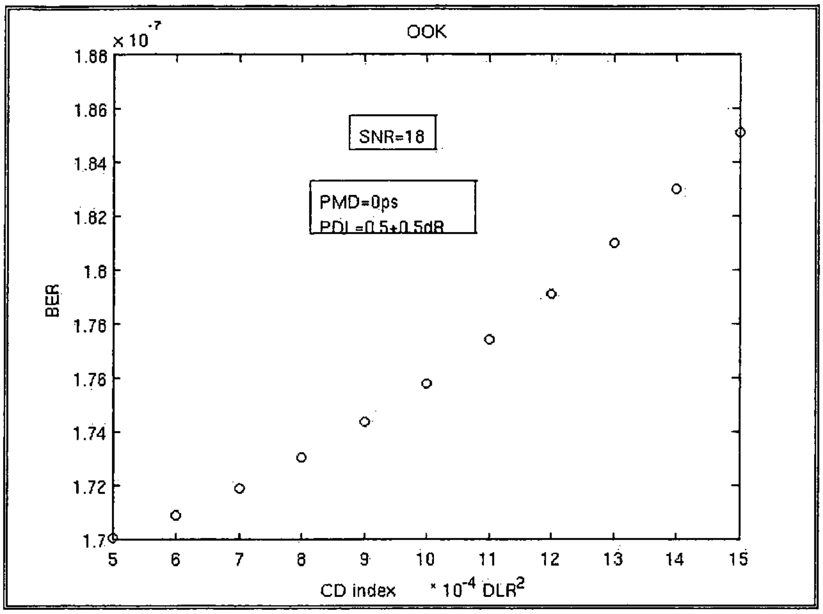

(a)

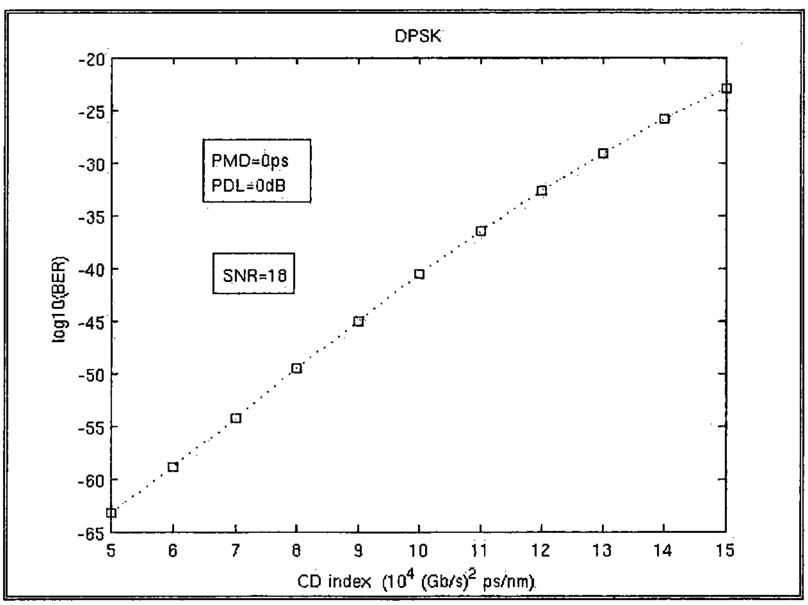

(b)

Figure (5.7) Log (BER) versus CD index for (a) OOK, (b) DPSK

PMD=PDL=0

2-Pure noise impact on BER

Noise as another impairment in our optical system, gives some penalty to the output system. Figure (5.8.a) shows that considering noise only as the only impairment in optical system produces a very low BER (which is true in reality). Furthermore, as it is well known increasing SNR gives better BER.

3-CD and noise impact on BER

With considering both CD and ASE noise in our calculation as in figure (5.8.b), a higher BER values will show up.

4-CD, noise, and PDL impact on BER

We had considered PDL beside the first two impairments (CD and the noise) to get, as expected, an increase in the bit error rate. Figure (5.8.c) present this with PDL=0.5dB for each sections, and CD=20 equally distributed between the two sections. The total noise, also, considered to be equally distributed between the two sections.

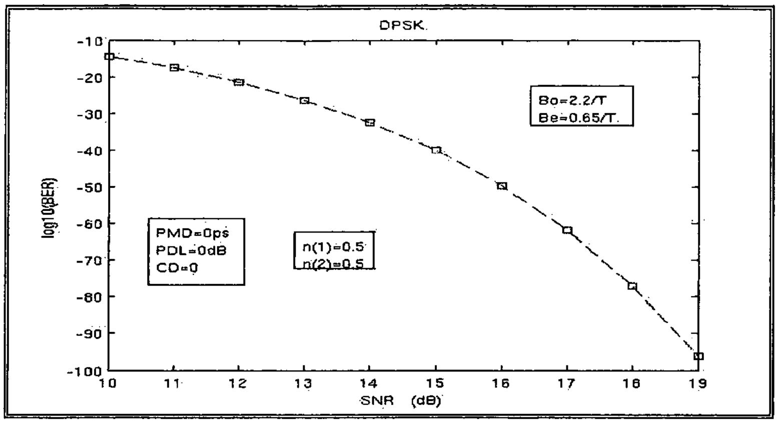

(a)

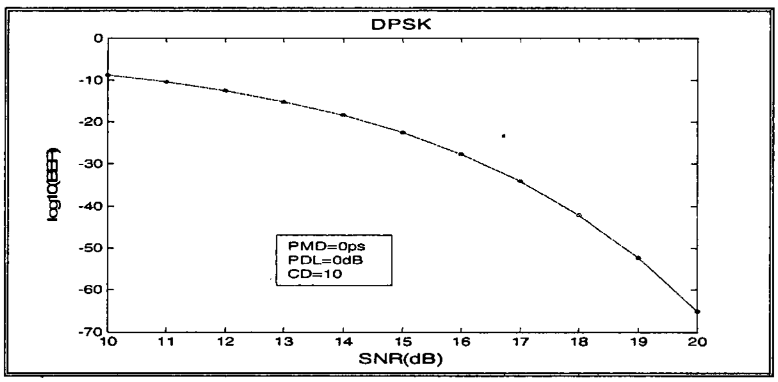

(b)

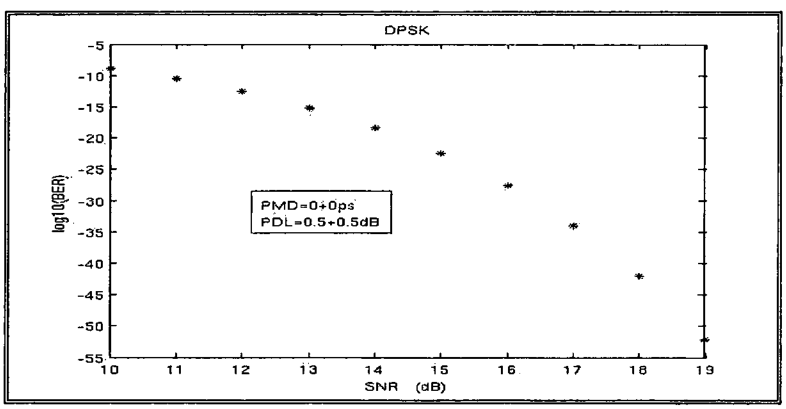

(c)

Fig (5.8) Log(BER) versus SNR for DPSK ($B_o = \frac{2.2}{T_b}, B_e = \frac{0.65}{T_b}$).(a)Two equal ASE noises are considered ($\alpha = \tau = CD = 0$) (b) Two equal ASE noises and CD indexes are considered ($\alpha = \tau = 0, CD_1 = CD_2 = 1$ (c) Two equal noises, CD indexes and PDL values($\tau = 0, CD_1 = CD_2 = 10, \alpha_1 = \alpha_2 = 0.5dB$

5.6.2.2 Effect of CD's spatial distribution

1- Without considering PMD and PDL:

Even if it is not the real situation to consider these cases, but it is useful to see the effect of inversing the higher value of CD between the two sections without considering any other effects. Figure (5.9.a) presents this case, and it shows that a small improvement happen when the first section has the small CD value (5) than the second one who has the big CD value (10). With inversing the two values, the first section takes 10 as CD value and the second section takes 5 as CD value, a higher BER values will arise. Perhaps, this improvement in the BER of the output when the signal faced first a small CD value then it passes through the amplifier G_1 and the third stage is the lager CD value, whereas when the signal faced the larger CD first as the first stage then the amplifier followed by the small CD value will present a higher BER of the output.

2- With considering PMD and PDL:

With considering PMD and PDL we are getting closer to the real system. Figure (5.9.b) shows that there was no noticeable difference on the output (same log BER) if we exchange the lower and higher CD values between the two sections, with the same PMD and PDL values. This result is in agreement with the work in Ref. [90].

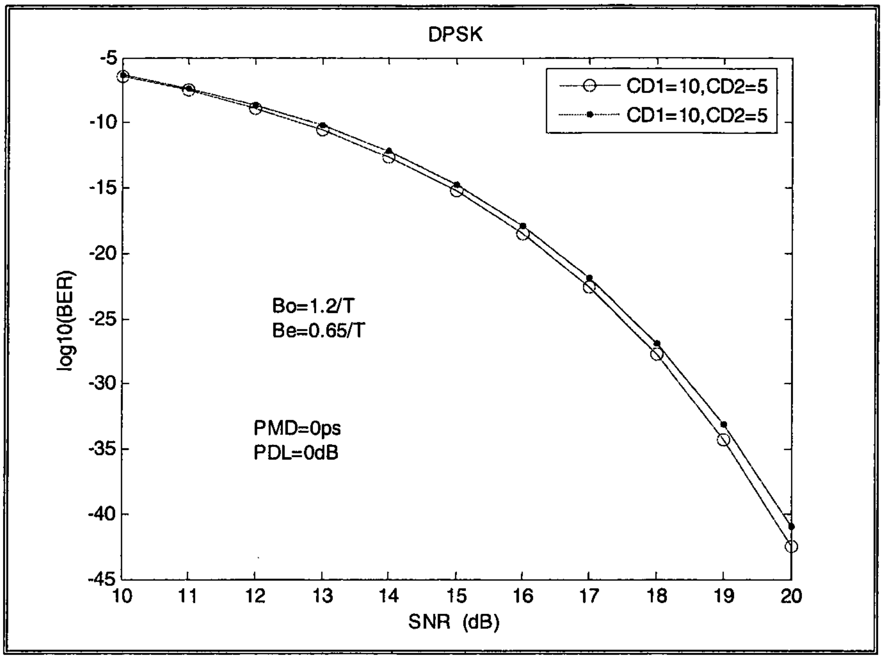

(a)

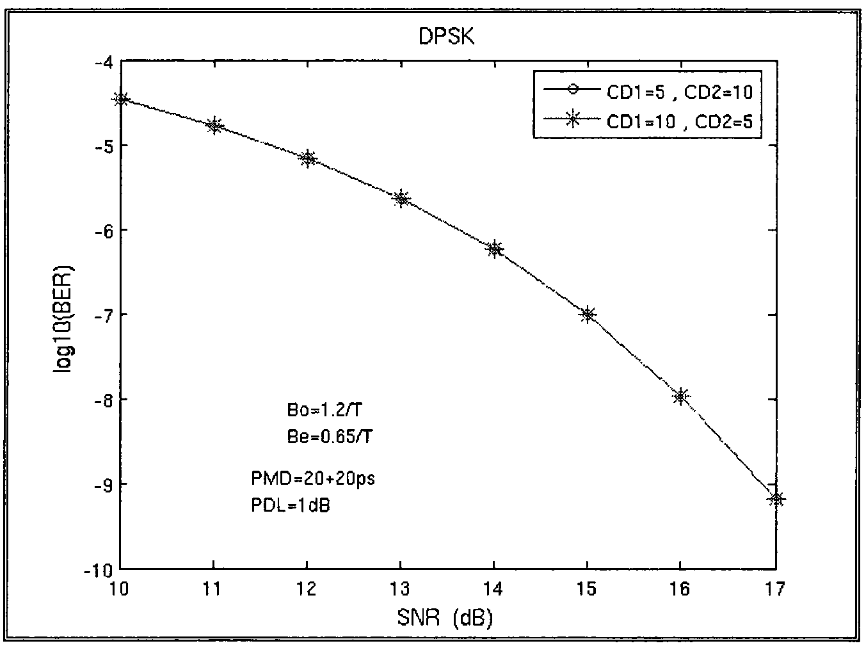

(b)

Figure (5.9) The effect of CD index on BER (a) without PMD & PDL

(b) with PMD & PDL

5.6.3 *The optimum values of the bandwidth of the optical and electrical filters*

a) The optical filter

We used Fabry-Perot (FP) type as optical filter in our calculation. To get an optimum value of the bandwidth of this optical filter we plot log BER as a function of SNR for several values of the optical filter bandwidth, and we found that the best output BER can be gotten when $B_o T = 1.2$, as shown in figure (5.10.a).PMD has a values of 20ps in each section, PDL has 0.5dB in each section, and CD=17 in each section.

b) The electrical filter

The electrical filter which we had used was the fifth order Bessel type, as we had done with the optical filter; we did with the electrical filter to get a best output. The best BER is found at $B_e T = 0.65$. Also, here, PMD has a values of 20ps in each section, PDL has 0.5dB in each section, and CD=17 in each section. This is presented in figure (5.10.b).

5.6.4 *All the impairments together*

Now we will consider all the impairments together; PMD, PDL, CD, and noise. Considering CD, PMD, PDL and the ASE noise make a difference on the output even for small PMD values. Figure (5.11) shows that even increasing the values of PMD by small amount result a rise to the values of BER. The PDL values were 0.25dB in each section, CD=17 in each section and the ASE noise are equally distributed in both sections.

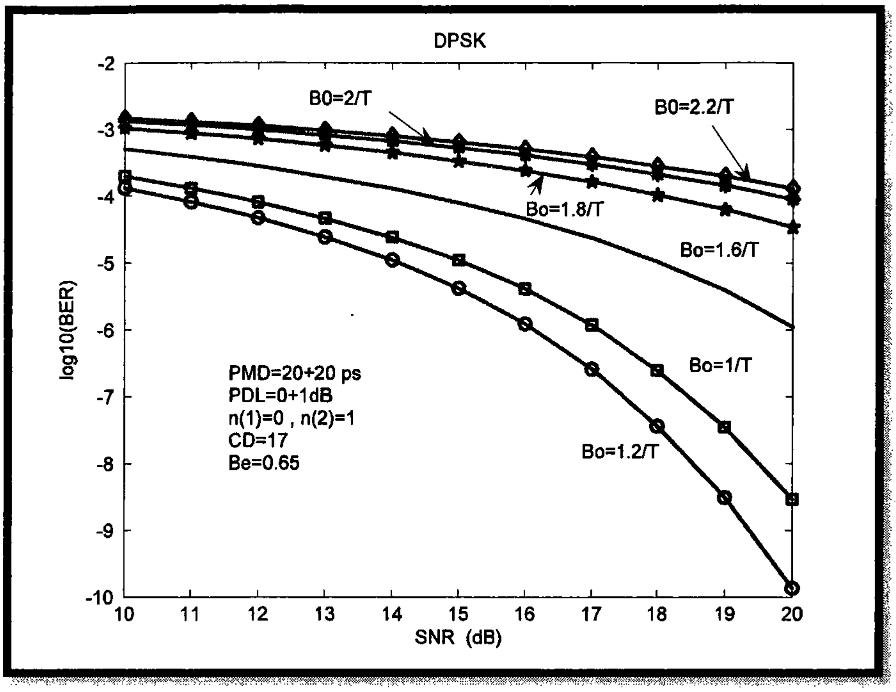

(a)

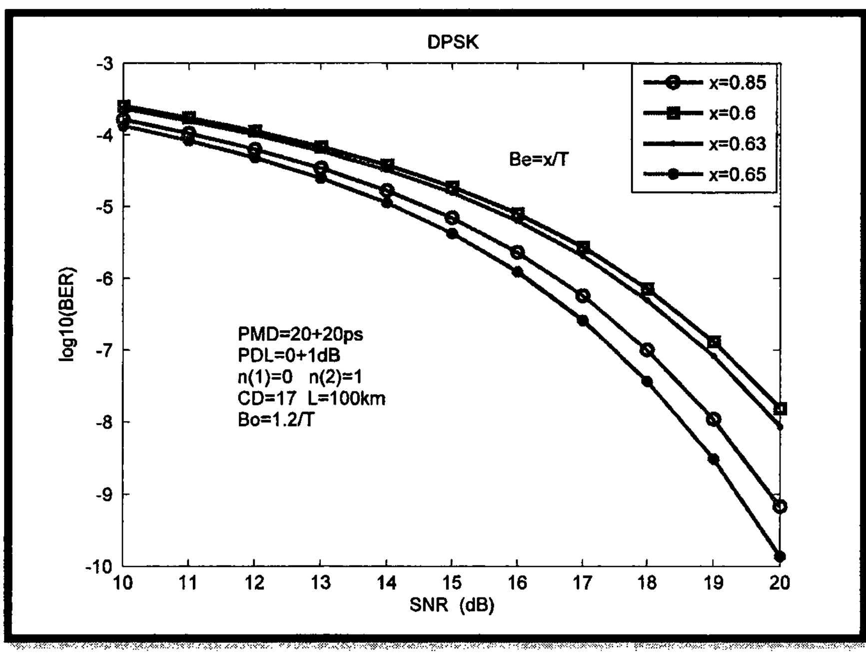

(b)

Figure (5.10) Log (BER) versus SNR for several values of

(a) The optical filter (b) The electrical filter.

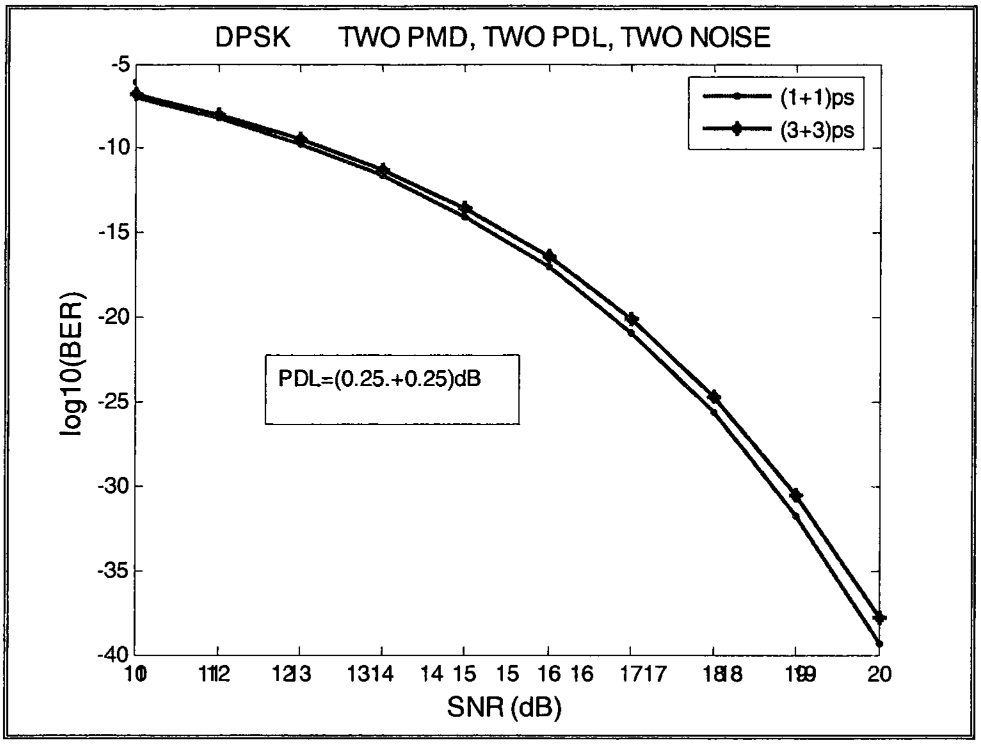

Fig (5.11) Log(BER) as a function of SNR With PMD, PDL, CD and noise

5.6.5 Improvement for DPSK decoding receiver :

In the real operating systems, the time delay between the two arms in the DPSK decoding receiver is not exactly one bit period, for this reason we consider this delay as a portion of one bit period. Figure (5.12) present this case, and it is clear from this figure that better values of the BER can be gotten when we consider this situation. For my information, it's the first time to consider this factor (the delay between the two arms in the receiver in DPSK case) which gives a big improvement to the BER for DPSK system.

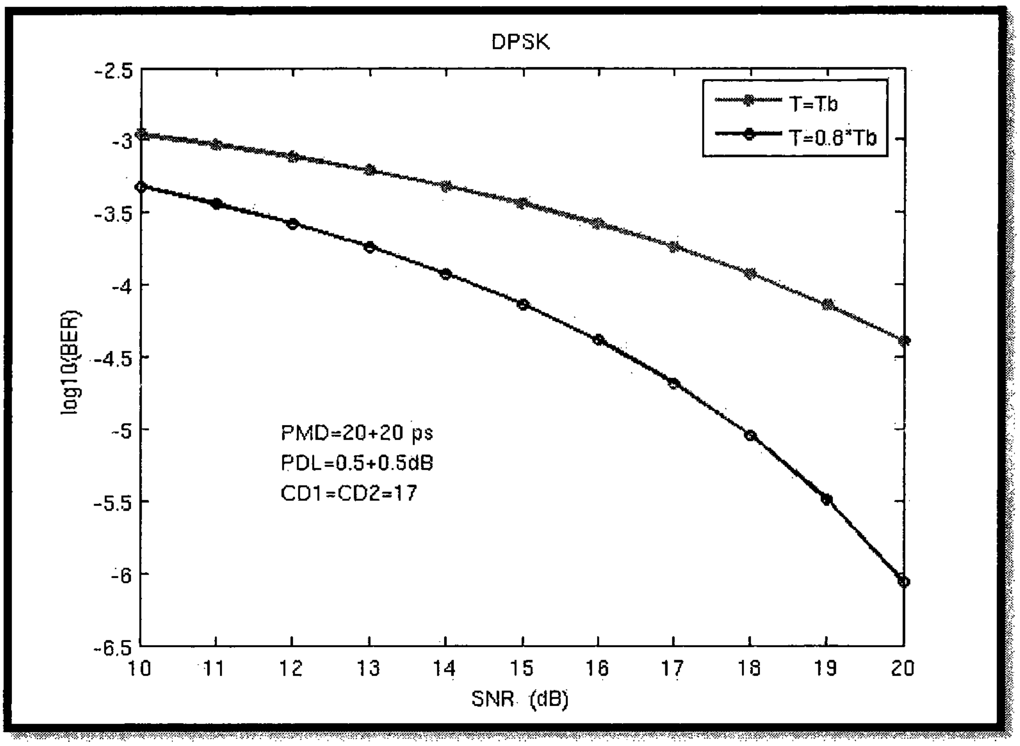

Figure (5.12) The effect of the bit duration on BER with considering PMD, PDL, CD and noise

Chapter 6

Partially Polarized Noise

In this chapter we will work on the noise characteristics; we will focus on the study of an optical system with three noise sources while ignoring the signal. This chapter is organized as follows. Section 6.1 gives an introduction to our subject, in Section 6.2 we present the theoretical description of the problem. Our results and a physical discussion are presented in Section 6.3.

6.1 Introduction

Optical transmission systems suffer from various limiting factors, especially when increasing bit rates are considered. The dispersion limit decreases with the square of the bit rate. At 2.5 Gb/s, optical signals can travel well beyond 1000 km on standard single-mode fiber before the signal degrades significantly, while for 40Gb/s signals the same effect will occur after only 2-4km [96].The transmission distance of any fiber-optic communication system is limited by fiber loss and dispersion.

The rapid progress of the technology of the amplifiers has made possible long-haul transmission, in which the unavoidable attenuation of the lossy fiber segments is compensated by the action of in-line amplifiers without electronic regeneration. For long-haul lightwave systems, this limitation is overcome using optical amplifiers. Nevertheless, using optical amplifiers also contributes to performance degradation [97].

With the increasing importance of the optical communications, getting a clear signal at the receiver became an important issue. It was an essential goal to get better signals.

Hence, several approaches have been used to study the optical system performance. In the transmission stage, optical signal inevitably suffers from impairments. Noise and distortion-based physical effects are the major categories in the impairments which lead to system performance degradation. The noise may include amplifier spontaneous emission ASE, receiver noise, laser noise... etc.

The primary sources of distortion are due to fiber components, chromatic dispersion (CD), polarization mode dispersion (PMD), polarization dependent loss (PDL), and non-linearties. Particularly, during the propagation of the optical wave along the fiber, the birefringence properties of optical fiber systems change its state of polarization.

A tremendous efforts has been made to study PMD, PDL and their combined effects [6,98-102]. Focusing on the first category, for optical preamplifier direct detection systems, the signal-independent amplified spontaneous emission self-beat noise (ASE-ASE) constitutes the dominant noise source [103]. The signal is accompanied by the amplified spontaneous emission (ASE) noise generated in the amplifier. The noise is partitioned into two polarization modes. The first mode has the same polarization as the signal, and the second mode has the orthogonal polarization. In the absence of PDL there is an equal amount of noise in the two modes, the noise is unpolarized. However, PDL modifies the amount of noise in the two modes, so that the noise becomes partially polarized. The two noise modes are coupled through polarization-mode dispersion (PMD) and through polarization changes induced by PDL [104].On the other hand, the evaluation of the state of polarization (SOP) is an important issue for the optical communications [105, 106].

The statistical evolution of ASE in fibers is of practical importance, since knowledge of the output statistics of the ASE is, for example, necessary to accurately estimate bit error rate (BER) in fiber links. To achieve accurate estimates of the BER the polarization state of the ASE must also be known [107]. For the first time to our knowledge, in this work we found that, even without considering the signal itself, the output state of polarization from the ASE noises is polarization dependent. We found that the probabilty density function of the ASE-ASE beating is clearly affected by changing the output state of polarization.

6.2 Theoretical description

1- ASE Noise

The primary source of additive noise in optically amplified systems is due to the amplified spontaneous emissions (ASE) produced by the optical amplifiers used as intermediate repeaters and as preamplifiers at the receiver end. The ASE noise mixes with the signal and produces beat noise components at the square-law receiver. The ASE noise is very broadband (~40 nm) and needs to be carefully analyzed to evaluate its degrading effect on system performance.

To represent the ASE noise we can't use Fourier series directly since the ASE noise is random and nonperiodic, in this case we have to find an orthonormal series where the coefficients are independent, but identically distributed random variables. This form of a series, termed the Karhunen-Loeve expansion [91], it is really an extension of the more general Fourier series, but with the basis functions defined so as to satisfy the uncorrelated coefficients condition.

Hence the objective is to find the orthonormal basis set. Following Ref. [91], if we consider the fact that in practics all filters have finite impulse responses, and then we can replace their input waveform with another one which coincides only in the time interval $(t_k - T_0, t_k)$, where T_0 is the impulse response of the pre- and post-detection filters at the receiver. So in this interval we can choose any orthonormal base for the expansion $\omega(t)$ where $t_k - T_0 < t < t_k$, taking into account that $\omega(t)$ is Additive White Gaussian noise (AWGN) [95, 96]. Using Fourier base we can write $\omega(t)$ as

$$\omega(t) = \sum_{m=-M}^{M} n_m \, e^{2i\pi m(t-t_k+T_0)/T_0} \qquad , t_k - T_0 < t < t_k \tag{6.1}$$

$$n_M = \omega_M H_0(\tfrac{M}{T_0}), \qquad M = \eta \, B_0 T_0 \tag{6.2}$$

where ω_M are complex i.i.d. Gaussian r.v. with zero mean and in-phase and quadrature components of variance $\sigma^2 = N_0/2T_0$, $H_0(f)$ is transfer function of the optical filter, η is a dimensionless parameter , B_0 is the noise equivalent bandwidth of optical filter. Here we assumed that the overall duration of the impulse response of the optical bandwidth B_0 and electrical bandwidth B_e filters is $T_0 = \mu(\frac{1}{B_o} + \frac{1}{B_e})$. The dimensionless fitting parameter μ must be determined iteratively [91].

2. The system modeling

   To see the polarization effect on the performance of the optical systems, we will consider its effect on ASE noise itself even without the signal. For this purpose, as we will see, we ignore the signal part in our work.

Figure (6.1) shows the considered part of an optical system. We will consider this part as our system under the study.

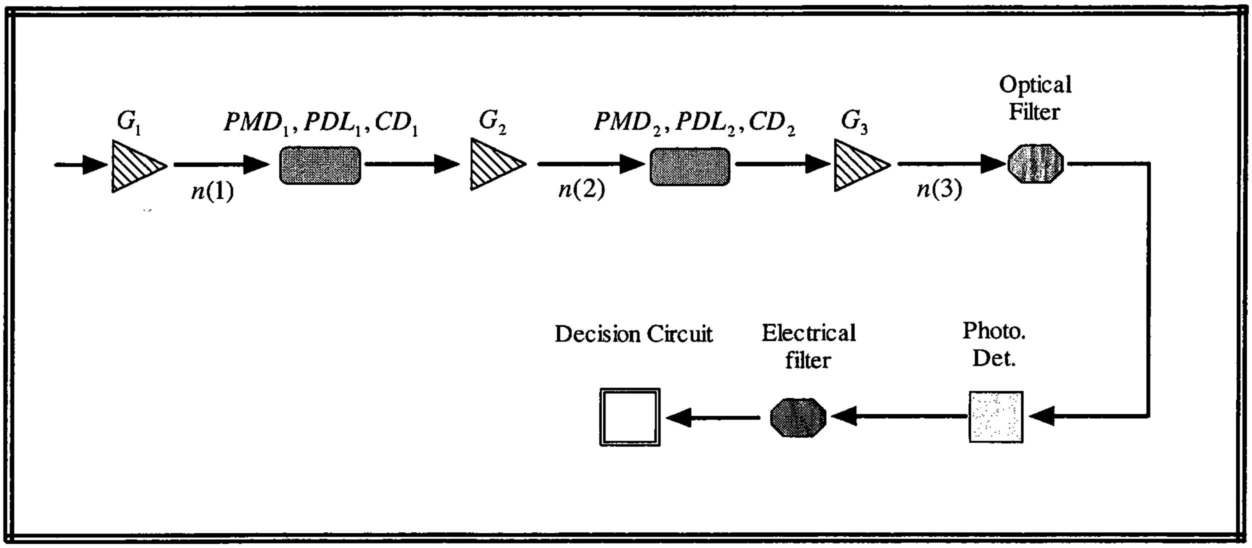

Figure (6.1) System Modeling

The model system started with an amplifier G_1 introduced ASE noise $n(1)$, followed by a lumped PMD_1, PDL_1, CD_1 . Another amplifier G_2 introduced another ASE noise $n(2)$, this one is also followed by the second lumped $PMD_2, PDL_2,$ CD_2 . The last amplifier G_3 gives the third ASE noise $n(3)$. The ASE noises are considered as additive Gaussian noises with two-sided power spectral density $N_0 = n_{sp}\frac{G-1}{G}h\nu$, where $n_{sp} \geq 1$ is the spontaneous-emission or population-inversion parameter and $h\nu$ is the photon energy. We assume that $G \gg 1$ so that $N_0 \approx n_{sp}h\nu$. An optical filter, photo-detector, and electrical filter add after that to the complete system. At the end a decision circuit is presented to sample the current at the time t_k . At the decision circuit, the instantaneous current can be written as

$$I(t) = \{\langle \vec{E}_{out}(t) | \vec{E}_{out}(t) \rangle + \langle \vec{E}_{out}(t) | \vec{E}_{out}(t) \rangle\}/2 \qquad \text{(OOK)} \qquad (6.3.a)$$

$$I(t) = \{\langle \vec{E}_{out}(t+T_b) | \vec{E}_{out}(t) \rangle + \langle \vec{E}_{out}(t) | \vec{E}_{out}(t+T_b) \rangle\}/2 \qquad \text{(DPSK)} \qquad (6.3.b)$$

In more clear equation:

$$I(t,\tilde{t}) =$$

$$\frac{1}{2\pi} \int d\omega \int d\acute{\omega}\, e^{i(\acute{\omega}-\omega)t} \left[e^{i\acute{\omega}\tilde{t}} + e^{-i\acute{\omega}\tilde{t}}\right] H_E(\acute{\omega}-\omega) H_o^*(\acute{\omega}) H_o(\omega) \langle \vec{E}_{out}(\acute{\omega}) | \vec{E}_{out}(\omega) \rangle \qquad (6.4)$$

Here H_E is the transfer function of the low-pass electrical filter. In our study we used a fifth-order Bessel type, i.e.$H_E(f) = \frac{945}{iF^5+15F^4-i105F^3-420F^2+i945F+945}$ with $= 2.43f/B_r$, B_r is the 3-dB cut-off frequency [74]. The transfers function of the low-pass optical filter is H_o. In this work the optical filter is a Fabry-Perot (FP) filter, its transfer function is given under the Lorentzian approximation as [108] $H_o(f) = 1/(1+2if/B_o)$ where B_o is the 3-dB bandwidth (full-width at half-maximum) of the optical filter. In general, eq.(6.4) can be written as

$$I(t,\tilde{t}) = y_{SS} + (y_{SN} + y_{NS}) + y_{NN} \qquad (6.5)$$

Where y_{SS} stands for the signal-signal beating, y_{NN} is noise-noise beating and ($y_{SN} + y_{NS}$) represents the noise-signal beating. The details are in the appendix A. For the noise-noise beating $y_{NN} = \langle \vec{N} | \vec{N} \rangle$, we can study its polarization dependence by projection to a specific output state $|\vec{\varepsilon}\rangle\langle\vec{\varepsilon}|$ and rewrite as $y_{NN} = \langle \vec{N} | \vec{\varepsilon} \rangle \langle \vec{\varepsilon} | \vec{N} \rangle$, where $\vec{\varepsilon}$ is the analysing output state of polarization unit vector in Stokes space and $|\vec{\varepsilon}\rangle\langle\vec{\varepsilon}| = \frac{1}{2}(I + \vec{\varepsilon}\cdot\vec{\sigma})$ [16], $\vec{\sigma}$ is Pauli spin matrices vector, then

$$y_{NN}^{\varepsilon} = \frac{1}{2}\{\langle\vec{N}|\vec{N}\rangle + \vec{\varepsilon}\cdot\langle\vec{N}|\vec{\sigma}|\vec{N}\rangle\} \tag{6.6}$$

In eq. (6.6) the noise-noise beating has two terms, the first one is related to unpolarized noise and the second one is related to the polarized noise. In our system the noise vector can be written as :

$$|\vec{N}\rangle = T_1|\vec{n}(1)\rangle + T_2|\vec{n}(2)\rangle + |\vec{n}(3)\rangle \tag{6.7}$$

where

$$T_r = \exp\left(-i\Psi_{\mathrm{L_r}}^{\mathrm{CD}}\right) T_{PDL_r}(\alpha_r) T_{PMD_r}(\tau_r, \omega); \qquad r = 1,2 \tag{6.8}$$

where $\exp\left(-i\Psi_{\mathrm{L_r}}^{\mathrm{CD}}\right)$ is the transfer function of the chromatic dispersion given by [90] as

$$\Psi_{\mathrm{L_r}}^{\mathrm{CD}}(\mathrm{f}) = 2\pi^2\, \beta_2 \mathrm{f}^2 \mathrm{L_r}, \tag{6.9}$$

$T_{PDL_r}(\alpha_r)T_{PMD_r}(\tau_r, \omega)$ is the transmission Jones matrix [9, 16, 35, 95] given as

$$T_{PDL_r}(\alpha_r) = \tfrac{1}{2}(1+e^{-\alpha_r}) + \tfrac{1}{2}(1-e^{-\alpha_r})(\vec{\alpha}_r\cdot\vec{\sigma}), \tag{6.10}$$

$$T_{PMD_r}(\tau_r, \omega) = \cos\left(\frac{\tau_r\omega}{2}\right) - i\sin\left(\frac{\tau_r\omega}{2}\right)(\vec{\tau}_r\cdot\vec{\sigma}) \tag{6.11}$$

Using eqs. ((6.8), (6.9)) we can rewrite the instantaneous detection current as

$$I(t,\tilde{t}) = c + \langle\vec{N}|\vec{b}\rangle + \langle\vec{b}|\vec{N}\rangle + \langle\vec{N}|Q|\vec{N}\rangle \tag{6.12}$$

The square matrix Q is Hermitian, and we can diagonalize it with unitary transformation U, such that $U^{\dagger}QU = diag\ [\lambda_j]$.

The moment generation function of I [91] is

$$\langle e^{isI}\rangle = \frac{1}{1-2\langle\Delta^2\rangle\lambda is}\exp\left[isc-\frac{2\langle\Delta^2\rangle|\tilde{b}|^2 s^2}{1-2\langle\Delta^2\rangle\lambda is}\right] \quad (6.13)$$

where $\langle\Delta^2\rangle$ is the variance of the noise distribution. The probability density function of I is

$$\rho(I) = \frac{1}{2\pi}\int_{-\infty}^{\infty} ds\, e^{-is(I-c)}\prod_{j=1}^{M} \frac{1}{1-2\langle\Delta^2\rangle\lambda is}\exp\left[-\frac{-2\langle\Delta^2\rangle|\tilde{b}|^2 s^2}{1-2\langle\Delta^2\rangle\lambda is}\right] \quad (6.14)$$

As we mentioned before, we will consider the noise only (ignore the signal), in this case $|b_j| = c = 0$. The probability density function now becomes

$$\rho(I) = \frac{1}{2\pi}\int_{-\infty}^{\infty} ds\, e^{-is(I)}\prod_{j=1}^{M} \frac{1}{1-2\langle\Delta^2\rangle\lambda_j is} \quad (6.15)$$

here the poles are at $s_j = -\frac{i}{2\langle\Delta^2\rangle\lambda_j}$.

Using the residue theorem, the probability density function can be written as

$$\rho(I_n) = i\sum_j e^{-is_j(I)} \prod_{q\neq j}^{M} \frac{-\frac{1}{2\langle\Delta^2\rangle i\lambda_j}}{1-2\langle\Delta^2\rangle\lambda_q is_j} \quad (6.16)$$

s_j is in the lower complex plane $\lambda_j > 0$.

Using the definition of λ_j the probability density function of I is

$$\rho(I_n) = \sum_j\left(\prod_{q\neq j}^{M} \frac{X}{\lambda_j-\lambda_q}\right) \quad e^{-IX/\lambda_j} \quad ; \qquad X = \frac{1}{2\langle\Delta^2\rangle} \quad (6.17)$$

6.3 Results and discussions

Since return to zero (RZ) modulation format has an improved sensitivity than nonreturn to zero (NRZ) modulation format [103,109], in this chapter, we used RZ modulation format in all of our results. Also, our values of PMD and PDL are close to those in the real systems.

6.3.1 Several cases of output state of polarization

In this subsection we will try to see if there is any change in the probability density function itself when we change the output state of polarization. If so, we will try also to investigate the range of the change in it. Figures (6.2) presents the probability density function of the output noise current as a function of the output current for system contains a three noises (equally distributed ; i.e., $n(1)=n(2)=n(3)=(1/3)n_{total}$) and two sections of fiber, that is have two PMD, PDL, CD sections, in-between the ASE noise sources. The total PMD value is 40ps (20ps in each section), total PDL value is 1dB (0.5dB in each section), and total CD index value is 20 (10 for each section). In both figures (6.2.a), and (6.2.b), we present the six output state of polarizations; linear horizontal polarization (LHP), linear vertical polarization (LVP), linear +45° Polarization (L+45° P), linear -45° polarization (L-45° P), right circular polarization (RCP), and left circular polarization (LCP). Figure (6.2.a) presents the case when we used OOK modulation format as detection system for our output noise current, while figure (6.2.b) presents our output noise current with DPSK modulation format. It is clear that in both cases the analysing output state of polarization creates change in the probability density function of the output current, which will affect the bit error rate of the system.

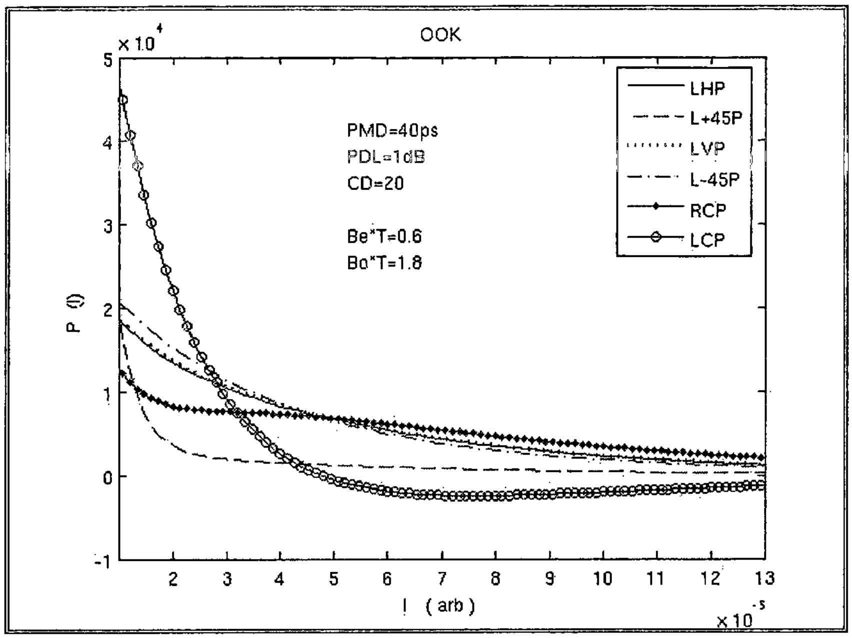

(a)

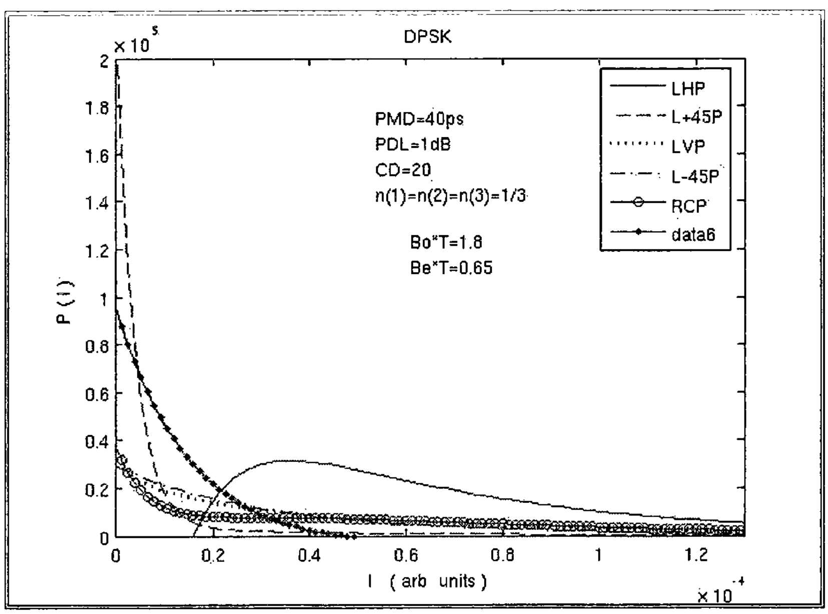

(b)

Figure (6.2) The output current probability density function against the output current at a given polarization for (a) OOK system with (b) DPSK system with. For both case the value of, PMD is 40ps, PDL =1 dB, CD=20

6.3.2 The impact of the optical filter

In the previous subsection, we had gotten an important result saying that the analysing output state of polarization can significantly affect the probability density function of the noise output current, in this subsection, for the same system that we had considered in the previous section we will try to see if that effect has the same behaviour if we consider different values of the bandwidth of the optical filter. Figure (6.3), and figure (6.4), present the probability density function of the noise output current against the output current , for the six cases of the output state of polarization LHP, LVP, L+45° P, L-45° P, RCP, and LCP, when we consider several values of the bandwidth of the optical filter ($B_o\, T = 2.2\,,1.8,\ and\ 1.4$) . As before the total PMD value is 40ps (20ps in each section), total PDL value is 1dB (0.5dB in each section), and total CD index value is 20 (10 for each section). The six figures that presented in figure (6.3), and figure (6.4), show the six output state of polarization, each figure presents one case. All the results in figure (6.3) belonged to OOK modulation format, while figure (6.4) belonged to DPSK modulation format. In all figures, the optical filter's bandwidth has the same values ($B_o\, T = 2.2\,,1.8, and\ 1.4$). Those figures show that the choice of the optical filter's bandwidth, also will affect the bit error rate via the probability density function of the output current. Moreover, the parameter η we had considered in our calculation as a dimensionless parameter [90, 91] depending on the optical filter shape. when $\eta = 1$ then $M = B_o T_0$ and this gives $H_o \left(\frac{M}{T_0}\right) = H_o\,(B_o\,)$,i.e. the transfer function of the optical filter at the 3-dB bandwidth (full-width at half-maximum) of the optical filter. Hence, for a better accuracy we need to increase the values of η even higher than one $(\eta \geq 1)$ so that we are sure that all the frequency components in the spectrum are included, but not so large than one since that is not useful to get better accuracy . As an example figure (6.5) present our previous system with the same values of PMD, PDL, and CD for OOK modulation format. Those figures show that this parameter has effect with all states of polarization that we had considered.

6.3.3 The ASE noise distribution in optical system

Now we will turn to see the ASE noise more closely. For the same system that we considered in this chapter, and also with the same values of PMD, PDL, and CD index values; our goal in this subsection is to see if there is any effect of the strength distribution of the noises. For this propose, figure (6.6) are working with OOK modulation format and with optical filter that has a bandwidth of $B_oT = 1.8$ while the electrical filter's bandwidth takes the value that satisfied the relation $B_eT = 0.65$. As before, in figure (6.6) we consider the six cases of the output state of polarization; LHP, LVP, L+45°P, L-45°P, RCP, and LCP. In all cases we ignored the first noise in the system $n(1)$ first and then we did the same thing for the third noise $n(3)$, in both cases we evaluated the probability density function of the output. As it is shown in figure (6.6), the probability density function in the two situations are different, that is because partially polarized noise is due to the PDL distribution, and the first noise is followed (in our system under the study) with PDL element, whereas the third one is not.

6.4 Conclusion

We quantitatively showed that PDL in optical systems can make unpolarized optical ASE noises to become partially polarized. This indicated that overall system performance must be polarization dependent when PDL exists.

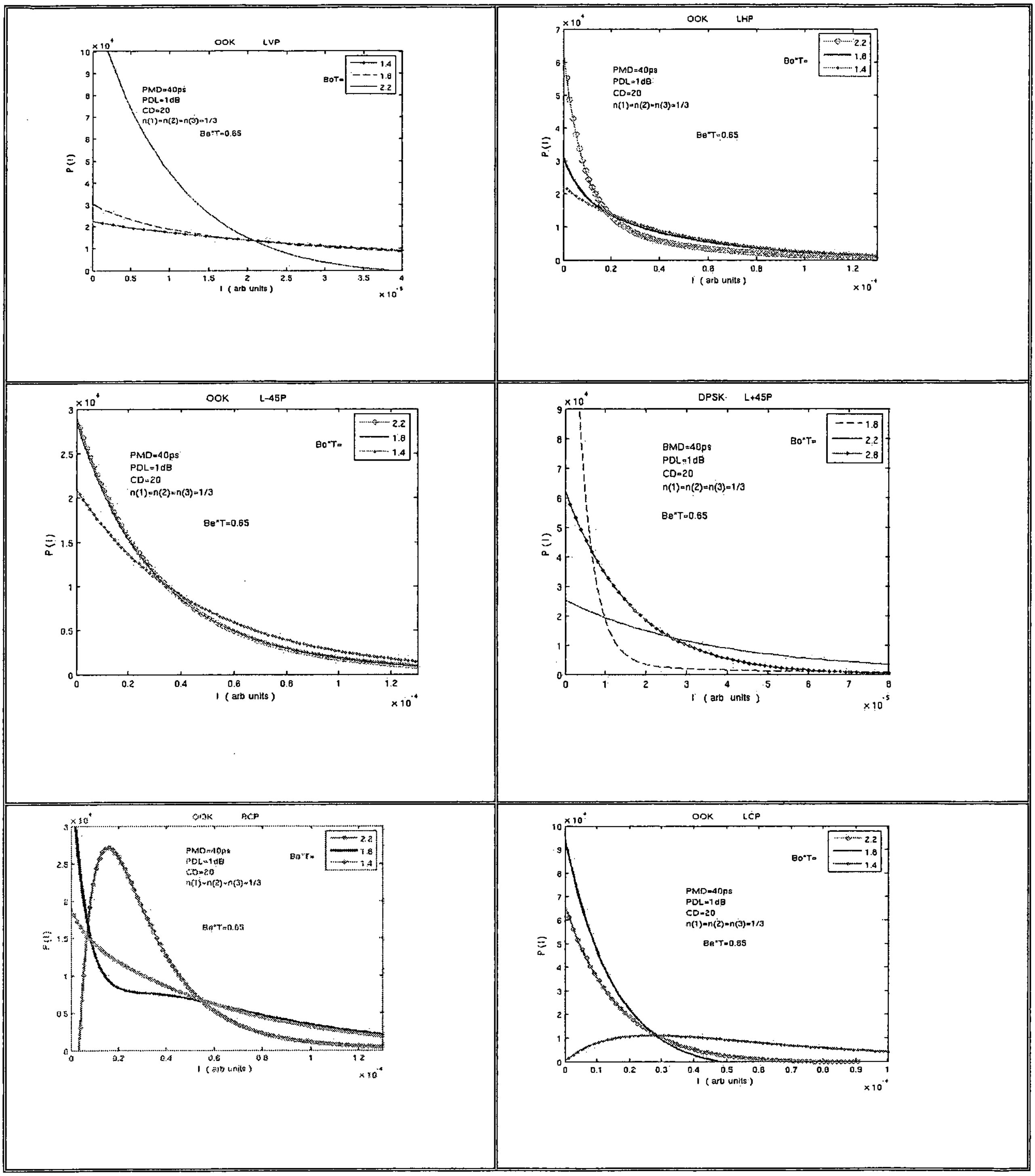

Figure (6.3) The probability density function of the output current against the output current for OOK system at different values oB_of ($B_o\,T = 2.2\,,1.8, 1.4$).PMD=40ps, PDL=1dB, CD=20, for each output state of polarization.

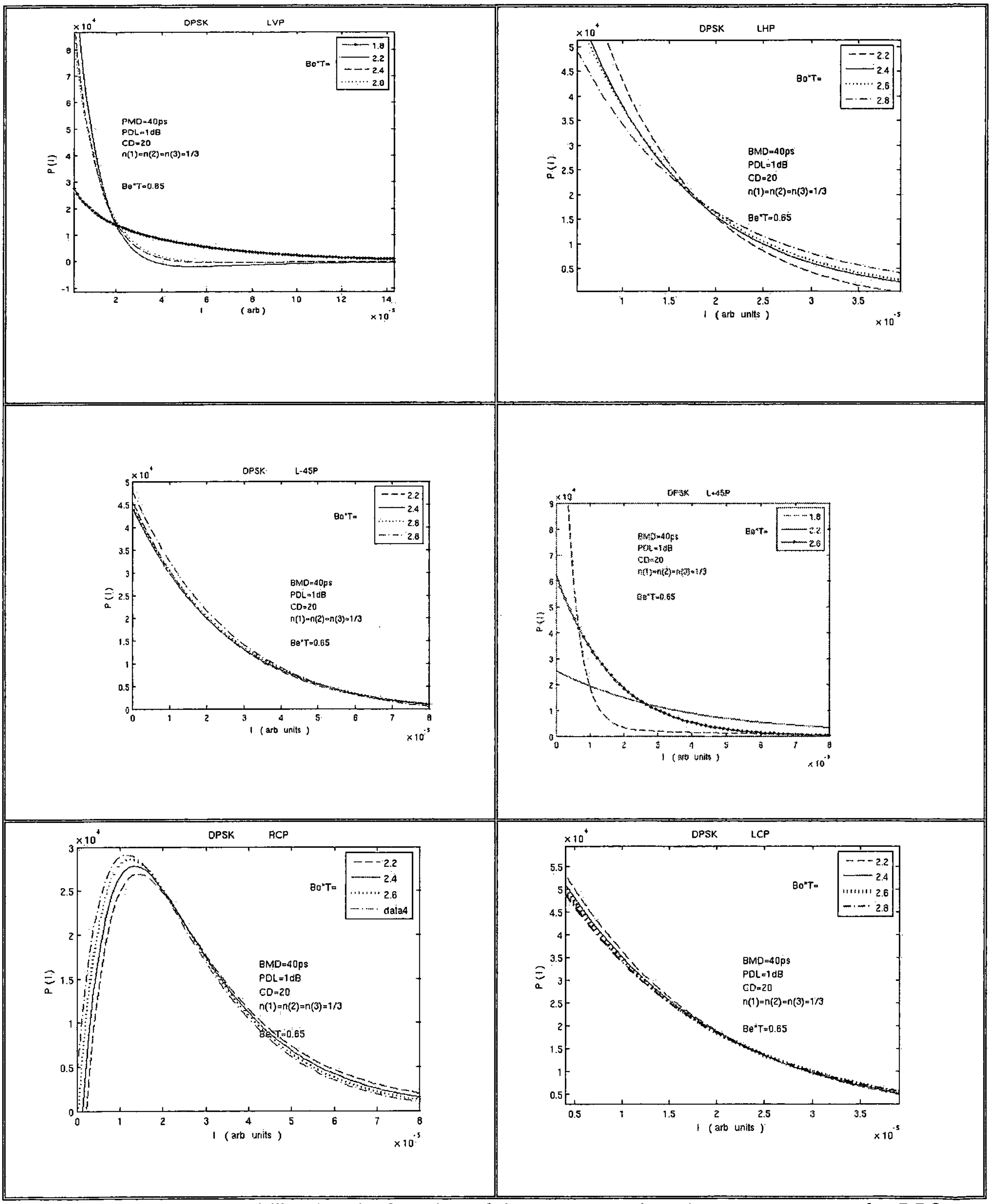

Figure (6.4) The probability density function of the output against the output current for DPSK system at different values of B_o ($B_o\,T = 2.2, 2.4, 2.6, 2.8$).PMD=40ps, PDL=1dB, CD=20, for each output state of polarization.

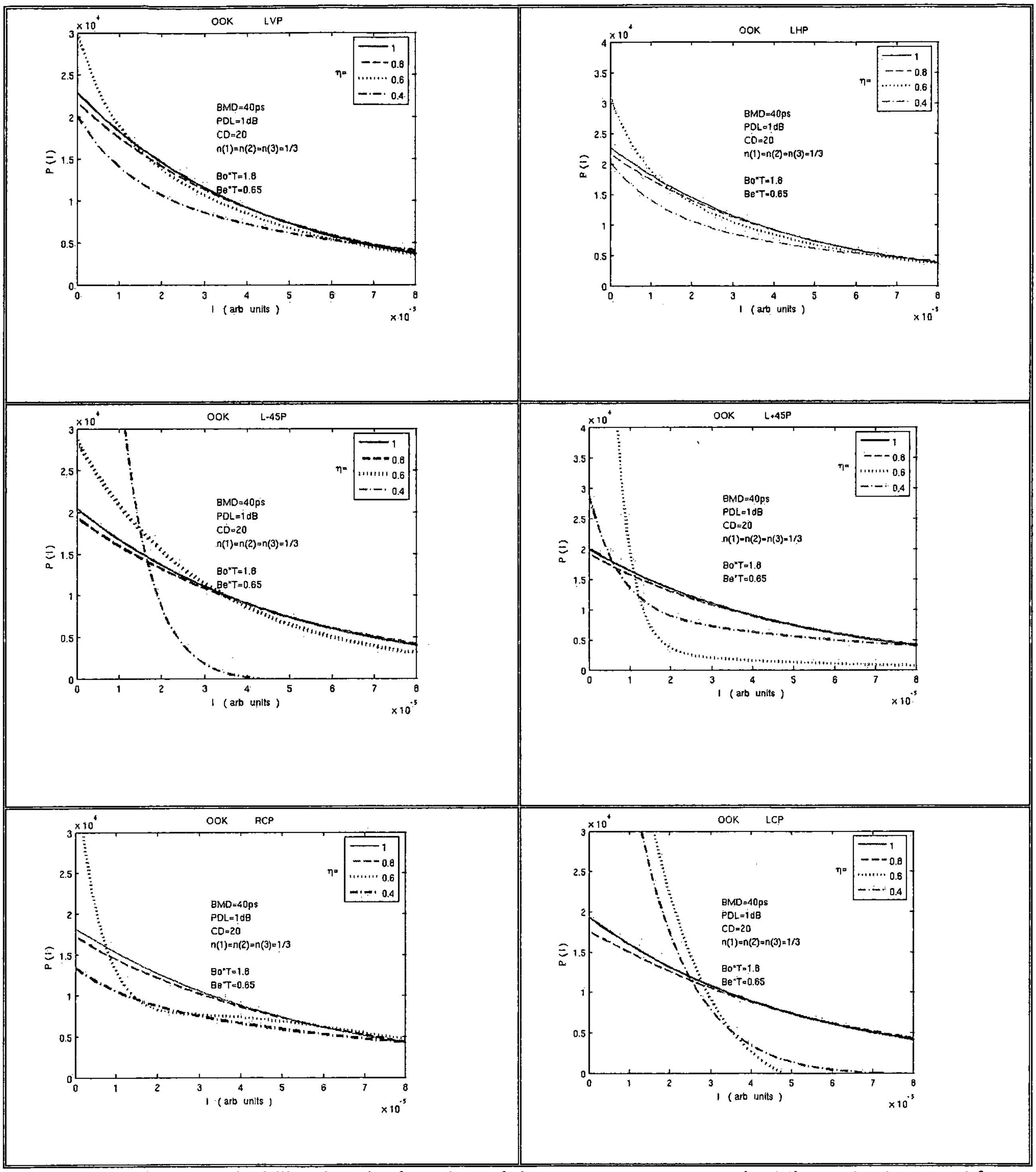

Figure (6.5)The probability density function of the output current against the output current for OOK system at different values of η.PMD=40ps, PDL=1dB, CD=20. This is for each output state of polarization

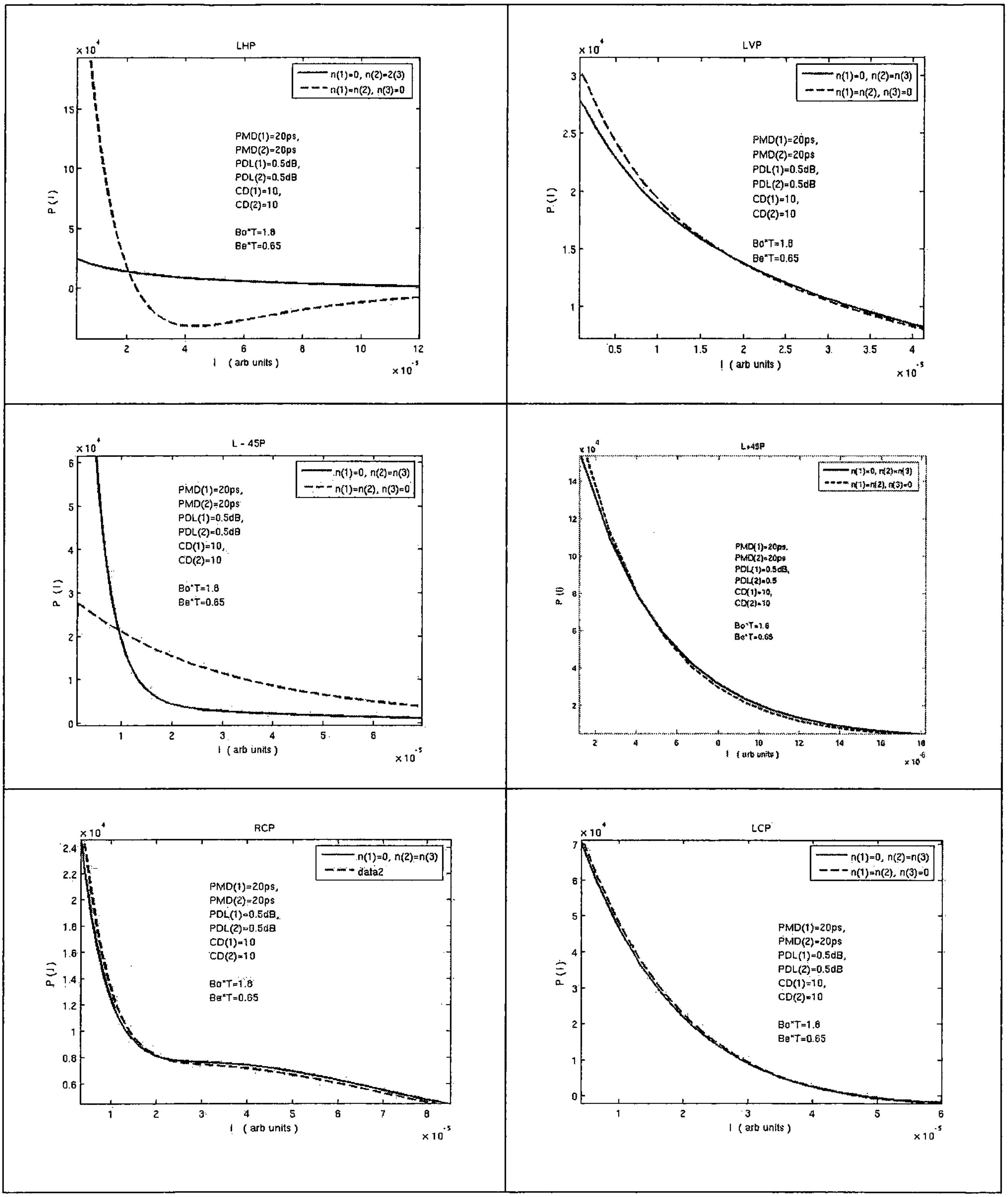

Figure (6.6) The probability density function of the output current against the output current in the cases of finishing the first noise and finishing the last noise ($B_o T = 1.8, B_e T = 0.65$).PMD=40ps, PDL=1dB, CD=20, for each output state of polarization.

Chapter 7

Conclusion

An analytical expression to evaluate the optical eye diagram for a system consists of Maxwellian fibers and lumped sections had been presented in the first part of this thesis. With considering the **chromatic dispersion** (CD), **polarization mode dispersion** (PMD), and **polarization dependent loss** (PDL), we used (in the first three chapters) Q-factor as a performance parameter. We found that with considering PDL as well as PMD, the Q-factor of the output becomes higher than that of the Maxwellian fiber having the same total root mean- square PMD and PDL values , when the mean-square PDL element of the lumped sections takes the major portion from the total mean-square of the whole system. Whereas without considering PDL, Q-factor becomes higher as the mean-square PMD element of the Maxwellian fiber takes the major portion of the total mean-square PMD element of the whole system. Also the worst case (in the considered cases) for the Q-factor occurred when the lumped sections is in between two equal equivalent Maxwellian fibers than if the lumped section are followed by Maxwellian fiber or the Maxwellian fiber is followed by the lumped sections. We also note that two equivalent Maxwellian fibers connected in series will not give the same Q-factor as a single Maxwellian fiber equivalent by concatenation rule unless they have the same values of PMD, PDL, and polarization direction correlation elements.

Bit error rate was used ,in the second part of this thesis, as a performance parameter for optical systems that contained the impairments **chromatic dispersion** (CD), **polarization mode dispersion** (PMD), **polarization dependent loss** (PDL), and the **amplified spontaneous emission** (ASE) **noise** simultaneously using both Off-On Keying (OOK) modulation format, and differential phase-shift keying (DPSK) modulation format. We evaluated the error probability in lightwave systems, we had gotten an excellent values for bit error rates for both OOK ($10^{-14}\, at\, SNR\, 20$), and DPSK

(10^{-25} $at\ SNR$ 20) by using the moment generation function method. It is found that moment generation function is the most efficient method to predict the bit error rate, with considering almost all the impairment (except the nonlinear impairments) in the optical fiber systems.

An analytical evaluation of the bit error probability of a preamplifier direct detection system has been presented. Moreover, by comparing the bit error rate of different polarization systems, the effect of partially polarized noise on the optical system is studied.

With the help of Dirac bra-ket notations, the probability density function for an optical system with three unpolarized ASE noises had been studied (for the first time to our knowledge) using different values of optical and electrical filter's bandwidths.

Future Work

Future work may study the same impairments in optical fiber communication systems; chromatic dispersion, polarization mode dispersion, polarization dependent loss, and the noise that we had studied beside the last impairment, which are the nonlinear effects in optical systems.

Appendix (A)

The elements of the L matrix in chapter 4 are given as:

$$L_{11}(n) = \cosh^2 \alpha_n \cos(\beta_n \Delta\omega_1)\cos(\beta_n \Delta\omega_2) \ + \frac{i}{2} < \hat{\alpha}_n \cdot \hat{\beta}_n > \sinh 2\alpha_n \sin[\beta_n (\Delta\omega_1 + \Delta\omega_2)]$$

$$- < (\hat{\alpha}_n \cdot \hat{\beta}_n)^2 > \sinh^2 \alpha_n \sin(\beta_n \Delta\omega_1)\sin(\beta_n \Delta\omega_2),$$

$$L_{12}(n) = \frac{1}{3}(\sinh^2 \alpha_n[\cos(\beta_n \Delta\omega_1)\cos(\beta_n \Delta\omega_2) + \sin(\beta_n \varpi_1)\sin(\beta_n \varpi_2)]$$

$$+\frac{i}{2} < \hat{\alpha}_n \cdot \hat{\beta}_n > \sinh 2\alpha_n \{\sin[\beta_n(\Delta\omega_1 + \Delta\omega_2)] + \sin(\beta_n \Delta\omega_1)[\cos(\beta_n \Delta\omega_2) - \cos(\beta_n \varpi_2)]$$

$$+\sin(\beta_n \Delta\omega_2)[\cos(\beta_n \Delta\omega_1) - \cos(\beta_n \Delta\varpi_1)]\} + < (\hat{\alpha}_n \cdot \hat{\beta}_n)^2 > \sinh^2 \alpha_n \{\cos(\beta_n \Delta\omega_1)[\cos(\beta_n \Delta\omega_2) - \cos(\beta_n \varpi_2)]$$

$$+\cos(\beta_n \Delta\omega_2)[\cos(\beta_n \Delta\omega_1) - \cos(\beta_n \varpi_1) - \sin(\beta_n \varpi_1)\sin(\beta_n \varpi_1)\}),$$

$$L_{21}(n) = \sinh^2 \alpha_n \cos(\beta_n \Delta\omega_1)\cos(\beta_n \Delta\omega_2) - \sin(\beta_n \Delta\omega_1)\sin(\beta_n \Delta\omega_2)$$

$$+ < \hat{\alpha}_n \cdot \hat{\beta}_n > \{i \sinh \alpha_n \cosh \alpha_n \sin[\beta_n (\Delta\omega_1 + \Delta\omega_2)] - \sinh^2 \alpha_n \sin(\beta_n \Delta\omega_1)\sin(\beta_n \varpi_2)\},$$

$$L_{22}(n) = \frac{1}{3}(2\cos[\beta_n(\varpi_1 - \varpi_2)] + \cos(\beta_n \Delta\omega_1)\cos(\beta_n \Delta\omega_2)$$

$$+\sinh^2 \alpha_n \{\cos[\beta_n(\varpi_1 \ + \varpi_2)] - \sin(\beta_n \Delta\omega_1)\sin(\beta_n \Delta\omega_2)\}$$

$$+\frac{i}{2} < \hat{\alpha}_n \cdot \hat{\beta}_n > \sinh 2\alpha_n \sin[\beta_n (\Delta\omega_1 + \Delta\omega_2)]$$

$$+ < (\hat{\alpha}_n \cdot \hat{\beta}_n)^2 > \sinh^2 \alpha_n \{\cos(\beta_n \Delta\omega_1)\cos(\beta_n \Delta\omega_2) - \cos[\beta_n(\varpi \ - \varpi_2)]\}).$$

The M matrix has the elements

$$M_{11}=e^{g}[\cosh(f^{2}+\frac{h^{2}}{3})^{1/2}+\frac{f}{(f^{2}+\frac{h^{2}}{3})^{1/2}}\sinh(f^{2}+\frac{h^{2}}{3})^{1/2}], \tag{16-a}$$

$$M_{12}=e^{g}[\frac{h}{3(f^{2}+\frac{h^{2}}{3})^{1/2}}\sinh(f^{2}+\frac{h^{2}}{3})^{1/2}], \tag{16-b}$$

$$M_{21}=e^{g}[\frac{h}{(f^{2}+\frac{h^{2}}{3})^{1/2}}\sinh(f^{2}+\frac{h^{2}}{3})^{1/2}], \tag{16-c}$$

$$M_{22}=e^{g}[\cosh(f^{2}+\frac{h^{2}}{3})^{1/2}-\frac{f}{(f^{2}+\frac{h^{2}}{3})^{1/2}}\sinh(f^{2}+\frac{h^{2}}{3})^{1/2}], \tag{16-d}$$

where

$$f=\frac{1}{3}\langle\eta^{2}\rangle-\frac{1}{6}\langle\Delta\tau^{2}\rangle[(\Delta\omega_{1})^{2}+(\Delta\omega_{2})^{2}-(\varpi_{1}-\varpi_{2})^{2}]$$
$$+\frac{1}{3}i\langle\hat{\alpha}\cdot\hat{\beta}\rangle(\langle\eta^{2}\rangle\langle\Delta\tau^{2}\rangle)^{\frac{1}{2}}(\Delta\omega_{1}+\Delta\omega_{2}),$$

$$g=\frac{2}{3}\langle\eta^{2}\rangle-\frac{1}{3}\langle\Delta\tau^{2}\rangle[(\Delta\omega_{1})^{2}+(\Delta\omega_{2})^{2}+\frac{1}{2}(\varpi_{1}-\varpi_{2})^{2}]$$
$$+\frac{2}{3}i\langle\hat{\alpha}\cdot\hat{\beta}\rangle(\langle\eta^{2}\rangle\langle\Delta\tau^{2}\rangle)^{\frac{1}{2}}(\Delta\omega_{1}+\Delta\omega_{2}),$$

$$h=\langle\eta^{2}\rangle-\langle\Delta\tau^{2}\rangle\Delta\omega_{1}\Delta\omega_{2}+i\langle\hat{\alpha}\cdot\hat{\beta}\rangle(\langle\eta^{2}\rangle\langle\Delta\tau^{2}\rangle)^{\frac{1}{2}}(\Delta\omega_{1}+\Delta\omega_{2}).$$

Appendix (B)

```
%%%% EVALUATION OF EYE DIAGRAM USING Fast Fourier Transform

                    % Ten lumped sections with Maxwellian fiber

clear;

format long;

tic;

%rand('state',sum(100*clock));

%%%%%%%%%%%%%%%%%     Input data

D=0.24;      %Duty cycle= in [0,1]

D2=D*D;

rho=0.15;     %local corr. of <\alpha.\beta> ( Maxwellian fiber)

rho_1=0.15;   %local corr. of <\alpha.\beta> ( Lumped section 1)

rho_2=0.15;   %local corr. of <\alpha.\beta> ( Lumped section 2)

rho_3=0.15;   %local corr. of <\alpha.\beta> ( Lumped section 3)

rho_4=0.15;   %local corr. of <\alpha.\beta> ( Lumped section 4)

rho_5=0.15;   %local corr. of <\alpha.\beta> ( Lumped section 5)

rho_6=0.15;   %local corr. of <\alpha.\beta> ( Lumped section 6)

rho_7=0.15;   %local corr. of <\alpha.\beta> ( Lumped section 7)

rho_8=0.15;   %local corr. of <\alpha.\beta> ( Lumped section 8)

rho_9=0.15;   %local corr. of <\alpha.\beta> ( Lumped section 9)

rho_10=0.15;  %local corr. of <\alpha.\beta> ( Lumped section 10)

%%%%%%%%%%%%

ch=0.1;           %Chirp value

cLV=3*10^8;         %light velocity

cc=2*pi*cLV*10^-3;   %nm/ps
```

```
lambda_0=1530;       %Carrier wavelength
omega_0=cc/lambda_0;  %Carrier frequency
Disp=0.1;            %Chromatic disperssion (ps/nm) @ Carrier wavelength=1530 nm
bet2=-cc*Disp/(omega_0*omega_0);
Disp_Slope=-3.3e-3;  %Disperssion slope
bet3=(Disp_Slope+2*omega_0*Disp/cc)/(omega_0*omega_0/cc)^2;
%%%%%%%%%%%%%%      %Pulse shape parameters:
A=1; %amplitude of the pulse
T=25;%100; % Pulse width
A2=A*A;
T2=T*T;
chp=1+i*ch;
sq_chp=sqrt(chp);
chm=1-i*ch;
sq_chm=sqrt(chm);
ch2=ch*ch;
chpm=1+ch2;
chmm=1-ch2;
%%%%%%%%%%%%%%%%       PDL values
pdl_dB=1;    %PDL  (Maxwellian fiber)
ta_dB1=0.1 ;  %PDL  (Lumped sec. 1)
ta_dB2=0.1;   %PDL  (Lumped sec. 2)
ta_dB3=0.1;   %PDL  (Lumped sec. 3)
ta_dB4=0.1;   %PDL  (Lumped sec. 4)
ta_dB5=0.1;   %PDL  (Lumped sec. 5)
ta_dB6=0.1;   %PDL  (Lumped sec. 6)
ta_dB7=0.1;   %PDL  (Lumped sec. 7)
ta_dB8=0.1;   %PDL  (Lumped sec. 8)
ta_dB9=0.1;   %PDL  (Lumped sec. 9)
```

```
ta_dB10=0.1;  %PDL  (Lumped sec. 10)
dum11=3*pi/8;
temp11=1/(20*log10(exp(1)));
eta_ave=pdl_dB*temp11;          %PDL (Maxwellian fiber)
eta2_ave=dum11*eta_ave*eta_ave; %<\eta^2> (Maxwellian fiber)
ta_1=ta_dB1*temp11;   %PDL in dB (Lumped sec. 1)
ta_2=ta_dB2*temp11;   %PDL in dB (Lumped sec. 2)
ta_3=ta_dB3*temp11;   %PDL in dB (Lumped sec. 3)
ta_4=ta_dB4*temp11;   %PDL in dB (Lumped sec. 4)
ta_5=ta_dB5*temp11;   %PDL in dB (Lumped sec. 5)
ta_6=ta_dB6*temp11;   %PDL in dB (Lumped sec. 6)
ta_7=ta_dB7*temp11;   %PDL in dB (Lumped sec. 7)
ta_8=ta_dB8*temp11;   %PDL in dB (Lumped sec. 8)
ta_9=ta_dB9*temp11;   %PDL in dB (Lumped sec. 9)
ta_10=ta_dB10*temp11; %PDL in dB (Lumped sec. 10)
A_n4=exp(-eta2_ave-ta_1^2-ta_2^2-ta_3^2-ta_4^2-...
   ta_5^2-ta_6^2-ta_7^2-ta_8^2-ta_9^2-ta_10^2);
A_n2=sqrt(A_n4);
A_n=sqrt(A_n2);
tem1=T2*(1-ch2)/4;
cT=ch*T;
D2T2=D2*T2;
p4=4*pi*pi;
 %%%%%%%%%%%%%%%%%%%%%%    PMD (ps)
start_ntau=1; %starting the loop; and one means ntau=0
for ntau=start_ntau:31;%floor(sqrt(Dtau_tot/dum11)*10)
  ntau
  Delta_tau=(ntau-1)/10;
Delta_tau_M2=dum11*Delta_tau*Delta_tau; %<Delta Tau^2> in ps^2
```

```
suu=Delta_tau_M2;%Delta_tau_lu2=Delta_tau_M2;
x=sqrt(suu/10);
su_1=x;        % PMD in Lum. 1
su_2=x;        % PMD in Lum. 2
su_3=x;        % PMD in Lum. 3
su_4=x;        % PMD in Lum. 4
su_5=x;        % PMD in Lum. 5
su_6=x;        % PMD in Lum. 6
su_7=x;        % PMD in Lum. 7
su_8=x;        % PMD in Lum. 8
su_9=x;        % PMD in Lum. 9
su_10=x;       % PMD in Lum. 10
%%%%%%%%%%%%%%%%
srt=rho*sqrt(eta2_ave*Delta_tau_M2);
ex1=exp(eta2_ave/2);
ex12=exp(2*eta2_ave/3);
n=64;          %Number of the points
tt_max=1*T+6.25; %Time axes in ps
%%%%%%%%%%%%%%%%%%%%%%%%%%%%%%%%%%%%%%%%%
                                 % FFT
limit_time=tt_max;
t=linspace(-limit_time,limit_time,n);
fm=exp(-(t+T/2).*(t+T/2)/(2*D2T2)*(1+i*ch));%Gaussian pulse shape
fp=exp(-(t-T/2).*(t-T/2)/(2*D2T2)*(1+i*ch));
ftt=A*(fm+fp);
fwp=fft(ftt);
fw=conj(fwp)/n;%
[B1,B2]=meshgrid(fwp,fw);
z=B1.*B2;
```

```
Ts=(t(2)-t(1));
Ws=2*pi/Ts;
ww=Ws*(-n/2:(n/2)-1)/n;
[wp,w]=meshgrid(ww);
CD_w=exp(-i*(bet2*w.*w/2+bet3*w.^3/6));
CD_wp=exp(i*(bet2*wp.*wp/2+bet3*wp.^3/6));
CD=CD_w.*CD_wp;
wmwp=w-wp;
Gamma_0n1=exp(-Delta_tau_M2*(w-wp).^2/8)*ex1.*exp(i*(w-wp)*srt/2);
II_1=cosh(ta_1)*cos(su_1*wmwp)+i*(rho_1)*sinh(ta_1)*sin(su_1*wmwp);
II_2=cosh(ta_2)*cos(su_2*wmwp)+i*(rho_2)*sinh(ta_2)*sin(su_2*wmwp);
II_3=cosh(ta_3)*cos(su_3*wmwp)+i*(rho_3)*sinh(ta_3)*sin(su_3*wmwp);
II_4=cosh(ta_4)*cos(su_4*wmwp)+i*(rho_4)*sinh(ta_4)*sin(su_4*wmwp);
II_5=cosh(ta_5)*cos(su_5*wmwp)+i*(rho_5)*sinh(ta_5)*sin(su_5*wmwp);
II_6=cosh(ta_6)*cos(su_6*wmwp)+i*(rho_6)*sinh(ta_6)*sin(su_6*wmwp);
II_7=cosh(ta_7)*cos(su_7*wmwp)+i*(rho_7)*sinh(ta_7)*sin(su_7*wmwp);
II_8=cosh(ta_8)*cos(su_8*wmwp)+i*(rho_8)*sinh(ta_8)*sin(su_8*wmwp);
II_9=cosh(ta_9)*cos(su_9*wmwp)+i*(rho_9)*sinh(ta_9)*sin(su_9*wmwp);
II_10=cosh(ta_10)*cos(su_10*wmwp)+i*(rho_10)*sinh(ta_10)*sin(su_10*wmwp);
Gamma_0=Gamma_0n1;
II=II_1.*II_2.*II_3.*II_4.*II_5.*II_6.*II_7.*II_8.*...
   II_9.*II_10;
gg=CD.*Gamma_0.*II;%exp(i*(w1-w2));
g_sh=fftshift(gg);%.*cstt;%.*
g=g_sh;
zg=z.*g;
%%%%%%%%%%%%%%%%%%%%%%%%%%%%%%%%%%%%%%%%%%%%%%%%%%%%%%%%%%%%%%%%%%%%%%
                                % Intensity
I = z;
```

```
Ig=zg;%ones(n,n);
for p = 1:2:length(size(z))
I = fft(I,[],p);
I = ifft(I,[],p+1);
Ig= fft(Ig,[],p);
Ig= ifft(Ig,[],p+1);
end
I_i=real(diag(I));
I_o=A_n2*real(diag(Ig));
%figure;plot(t,I_i,'.-',t,I_o,'-o')
I_in=I_i;
I_out=I_o;
clear Gamma_0;
%%%%%%%%%%%%%%%%%%%%%%%%%%%%%%%%%%%%%%%%%%%%%%%%%%%%%%%%%%%%%
                                          % Variance
g_var=g; clear g;
CD_sh=fftshift(CD);
q1=(w-wp);
q1_sh=fftshift(q1);
q3=w+wp;
q3_sh=fftshift(q3);
clear m;
for k=1:n
k;
for m=1:n
t1=(q1.^2+q1_sh(m,k)^2)/4;
t2=((q3-q3_sh(m,k)).^2)/4;
t3=srt*(q1+q1_sh(m,k))/2;
t4=q1*q1_sh(m,k)/4;
```

```
hp=2*eta2_ave/3-Delta_tau_M2*(t1+t2/2)/3+2*i*t3/3;
f=eta2_ave/3-Delta_tau_M2*(t1-t2)/6+i*t3/3;
d=eta2_ave-Delta_tau_M2*t4+i*t3;
g=sqrt(f.*f+d.*d/3);
ex3=exp(hp);
if abs(g)<10^(-9)
  sh=1;
else
  sh=sinh(g)./g;
end
%Lumped section No.1
su1_1=su_1*q3;
su1_sh_1=su_1*q3_sh(m,k);
su2_1=su_1*q1;
su2_sh_1=su_1*q1_sh(m,k);
su3_1=su_1*(q1+q1_sh(m,k));
su4_1=su_1*(q3-q3_sh(m,k));
Hw1_1=cos(su2_1).*cos(su2_sh_1);
Hw2_1=sin(su3_1);
Hw3_1=sin(su2_1).*sin(su2_sh_1);
Hw4_1=sin(su1_1).*sin(su1_sh_1);
Hw5_1=cos(su2_1)-cos(su1_1);
Hw6_1=cos(su2_sh_1)-cos(su1_sh_1);
chta_1=cosh(ta_1);
shta_1=sinh(ta_1);
ch2ta_1=cosh(2*ta_1);
sh2ta_1=sinh(2*ta_1);
F11=chta_1.*chta_1.*Hw1_1+...
+(i/2)*sh2ta_1.*Hw2_1*rho_1-...
```

```
shta_1.*shta_1*Hw3_1*rho_1*rho_1;
F12=shta_1.*shta_1*(Hw1_1+Hw4_1)/3-chta_1.*chta_1*Hw3_1/3+...
(i/2)*rho_1*sh2ta_1*(Hw2_1+sin(su2_1)*Hw6_1+...
sin(su2_sh_1).*Hw5_1)/3+...
rho_1*rho_1*shta_1.*shta_1*(cos(su2_1)*Hw6_1+...
cos(su2_sh_1).*Hw5_1-Hw4_1)/3;
F21=shta_1.*shta_1*Hw1_1-Hw3_1+rho_1*(i*shta_1*chta_1*Hw2_1-...
shta_1.*shta_1*Hw3_1);
F22= (2/3)*cos(su4_1)+Hw1_1/3+...
shta_1.*shta_1*(cos(su4_1)-Hw3_1)/3+...
(i/2)*rho_1*sh2ta_1*Hw2_1/3+...
rho_1*rho_1*shta_1.*shta_1*(Hw1_1-cos(su4_1))/3;
%Lumped section No.2
su1_2=su_2*q3;
su1_sh_2=su_2*q3_sh(m,k);
su2_2=su_2*q1;
su2_sh_2=su_2*q1_sh(m,k);
su3_2=su_2*(q1+q1_sh(m,k));
su4_2=su_2*(q3-q3_sh(m,k));
Hw1_2=cos(su2_2).*cos(su2_sh_2);
Hw2_2=sin(su3_2);
Hw3_2=sin(su2_2).*sin(su2_sh_2);
Hw4_2=sin(su1_2).*sin(su1_sh_2);
Hw5_2=cos(su2_2)-cos(su1_2);
Hw6_2=cos(su2_sh_2)-cos(su1_sh_2);
chta_2=cosh(ta_2);
shta_2=sinh(ta_2);
ch2ta_2=cosh(2*ta_2);
sh2ta_2=sinh(2*ta_2);
```

```
S11=chta_2.*chta_2.*Hw1_2+...
+(i/2)*sh2ta_2.*Hw2_2*rho_2-...
shta_2.*shta_2*Hw3_2*rho_2*rho_2;
S12=shta_2.*shta_2*(Hw1_2+Hw4_2)/3-chta_2.*chta_2*Hw3_2/3+...
(i/2)*rho_2*sh2ta_2*(Hw2_2+sin(su2_2)*Hw6_2+...
sin(su2_sh_2).*Hw5_2)/3+...
rho_2*rho_2*shta_2.*shta_2*(cos(su2_2)*Hw6_2+...
cos(su2_sh_2).*Hw5_2-Hw4_2)/3;
S21=shta_2.*shta_2*Hw1_2-Hw3_2+rho_2*(i*shta_2*chta_2*Hw2_2-...
shta_2.*shta_2*Hw3_2);
S22=(2/3)*cos(su4_2)+Hw1_2/3+...
shta_2.*shta_2*(cos(su4_2)-Hw3_2)/3+...
(i/2)*rho_2*sh2ta_2*Hw2_2/3+...
rho_2*rho_2*shta_2.*shta_2*(Hw1_2-cos(su4_2))/3;
%Lumped section No.3
su1_3=su_3*q3;
su1_sh_3=su_3*q3_sh(m,k);
su2_3=su_3*q1;
su2_sh_3=su_3*q1_sh(m,k);
su3_3=su_3*(q1+q1_sh(m,k));
su4_3=su_3*(q3-q3_sh(m,k));
Hw1_3=cos(su2_3).*cos(su2_sh_3);
Hw2_3=sin(su3_3);
Hw3_3=sin(su2_3).*sin(su2_sh_3);
Hw4_3=sin(su1_3).*sin(su1_sh_3);
Hw5_3=cos(su2_3)-cos(su1_3);
Hw6_3=cos(su2_sh_3)-cos(su1_sh_3);
chta_3=cosh(ta_3);
shta_3=sinh(ta_3);
```

```
ch2ta_3=cosh(2*ta_3);
sh2ta_3=sinh(2*ta_3);
T11=chta_3.*chta_3.*Hw1_3+...
+(i/2)*sh2ta_3.*Hw2_3*rho_3-...
shta_3.*shta_3*Hw3_3*rho_3*rho_3;
T12=shta_3.*shta_3*(Hw1_3+Hw4_3)/3-chta_3.*chta_3*Hw3_3/3+...
(i/2)*rho_3*sh2ta_3*(Hw2_3+sin(su2_3)*Hw6_3+...
sin(su2_sh_3).*Hw5_3)/3+...
rho_3*rho_3*shta_3.*shta_3*(cos(su2_3)*Hw6_3+...
cos(su2_sh_2).*Hw5_3-Hw4_3)/3;
T21=shta_3.*shta_3*Hw1_3-Hw3_3+rho_3*(i*shta_3*chta_3*Hw2_3-...
shta_3.*shta_3*Hw3_3);
T22= (2/3)*cos(su4_3)+Hw1_3/3+...
shta_3.*shta_3*(cos(su4_3)-Hw3_3)/3+...
(i/2)*rho_3*sh2ta_3*Hw2_3/3+...
rho_3*rho_3*shta_3.*shta_3*(Hw1_3-cos(su4_3))/3;
%Lumped section No.4
su1_4=su_4*q3;
su1_sh_4=su_4*q3_sh(m,k);
su2_4=su_4*q1;
su2_sh_4=su_4*q1_sh(m,k);
su3_4=su_4*(q1+q1_sh(m,k));
su4_4=su_4*(q3-q3_sh(m,k));
Hw1_4=cos(su2_4).*cos(su2_sh_4);
Hw2_4=sin(su3_4);
Hw3_4=sin(su2_4).*sin(su2_sh_4);
Hw4_4=sin(su1_4).*sin(su1_sh_4);
Hw5_4=cos(su2_4)-cos(su1_4);
Hw6_4=cos(su2_sh_4)-cos(su1_sh_4);
```

```
chta_4=cosh(ta_4);
shta_4=sinh(ta_4);
ch2ta_4=cosh(2*ta_4);
sh2ta_4=sinh(2*ta_4);
O11=chta_4.*chta_4.*Hw1_4+...
+(i/2)*sh2ta_4.*Hw2_4*rho_4-...
shta_4.*shta_4*Hw3_4*rho_4*rho_4;
O12=shta_4.*shta_4*(Hw1_4+Hw4_4)/3-chta_4.*chta_4*Hw3_4/3+...
(i/2)*rho_4*sh2ta_4*(Hw2_4+sin(su2_4)*Hw6_4+...
sin(su2_sh_4).*Hw5_4)/3+...
rho_4*rho_4*shta_4.*shta_4*(cos(su2_4)*Hw6_4+...
cos(su2_sh_4).*Hw5_4-Hw4_4)/3;
O21=shta_4.*shta_4*Hw1_4-Hw3_4+rho_4*(i*shta_4*chta_4*Hw2_4-...
shta_4.*shta_4*Hw3_4);
O22= (2/3)*cos(su4_4)+Hw1_4/3+...
shta_4.*shta_4*(cos(su4_4)-Hw3_4)/3+...
(i/2)*rho_4*sh2ta_4*Hw2_4/3+...
rho_4*rho_4*shta_4.*shta_4*(Hw1_4-cos(su4_4))/3;
%Lumped section No.5
su1_5=su_5*q3;
su1_sh_5=su_5*q3_sh(m,k);
su2_5=su_5*q1;
su2_sh_5=su_5*q1_sh(m,k);
su3_5=su_5*(q1+q1_sh(m,k));
su4_5=su_5*(q3-q3_sh(m,k));
Hw1_5=cos(su2_5).*cos(su2_sh_5);
Hw2_5=sin(su3_5);
Hw3_5=sin(su2_5).*sin(su2_sh_5);
Hw4_5=sin(su1_5).*sin(su1_sh_5);
```

```
Hw5_5=cos(su2_5)-cos(su1_5);
Hw6_5=cos(su2_sh_5)-cos(su1_sh_5);
chta_5=cosh(ta_5);
shta_5=sinh(ta_5);
ch2ta_5=cosh(2*ta_5);
sh2ta_5=sinh(2*ta_5);
V11=chta_5.*chta_5.*Hw1_5+...
+(i/2)*sh2ta_5.*Hw2_5*rho_5-...
shta_5.*shta_5*Hw3_5*rho_5*rho_5;
V12=shta_5.*shta_5*(Hw1_5+Hw4_5)/3-chta_5.*chta_5*Hw3_5/3+...
(i/2)*rho_5*sh2ta_5*(Hw2_5+sin(su2_5)*Hw6_5+...
sin(su2_sh_5).*Hw5_5)/3+...
rho_5*rho_5*shta_5.*shta_5*(cos(su2_5)*Hw6_5+...
cos(su2_sh_5).*Hw5_5-Hw4_5)/3;
V21=shta_5.*shta_5*Hw1_5-Hw3_5+rho_5*(i*shta_5*chta_5*Hw2_5-...
shta_5.*shta_5*Hw3_5);
V22= (2/3)*cos(su4_5)+Hw1_5/3+...
shta_5.*shta_5*(cos(su4_5)-Hw3_5)/3+...
(i/2)*rho_5*sh2ta_5*Hw2_5/3+...
rho_5*rho_5*shta_5.*shta_5*(Hw1_5-cos(su4_5))/3;
%Lumped section No.6
su1_6=su_6*q3;
su1_sh_6=su_6*q3_sh(m,k);
su2_6=su_6*q1;
su2_sh_6=su_6*q1_sh(m,k);
su3_6=su_6*(q1+q1_sh(m,k));
su4_6=su_6*(q3-q3_sh(m,k));
Hw1_6=cos(su2_6).*cos(su2_sh_6);
Hw2_6=sin(su3_6);
```

```
Hw3_6=sin(su2_6).*sin(su2_sh_6);
Hw4_6=sin(su1_6).*sin(su1_sh_6);
Hw5_6=cos(su2_6)-cos(su1_6);
Hw6_6=cos(su2_sh_6)-cos(su1_sh_6);
chta_6=cosh(ta_6);
shta_6=sinh(ta_6);
ch2ta_6=cosh(2*ta_6);
sh2ta_6=sinh(2*ta_6);
X11=chta_6.*chta_6.*Hw1_6+...
+(i/2)*sh2ta_6.*Hw2_6*rho_6-...
shta_6.*shta_6*Hw3_6*rho_6*rho_6;
X12=shta_6.*shta_6*(Hw1_6+Hw4_6)/3-chta_6.*chta_6*Hw3_6/3+...
(i/2)*rho_6*sh2ta_6*(Hw2_6+sin(su2_6)*Hw6_6+...
sin(su2_sh_6).*Hw5_6)/3+...
rho_6*rho_6*shta_6.*shta_6*(cos(su2_6)*Hw6_6+...
cos(su2_sh_6).*Hw5_6-Hw4_6)/3;
X21=shta_6.*shta_6*Hw1_6-Hw3_6+rho_6*(i*shta_6*chta_6*Hw2_6-...
shta_6.*shta_6*Hw3_6);
X22= (2/3)*cos(su4_6)+Hw1_6/3+...
shta_6.*shta_6*(cos(su4_6)-Hw3_6)/3+...
(i/2)*rho_6*sh2ta_6*Hw2_6/3+...
rho_6*rho_6*shta_6.*shta_6*(Hw1_6-cos(su4_6))/3;
%Lumped section No.7
su1_7=su_7*q3;
su1_sh_7=su_7*q3_sh(m,k);
su2_7=su_7*q1;
su2_sh_7=su_7*q1_sh(m,k);
su3_7=su_7*(q1+q1_sh(m,k));
su4_7=su_7*(q3-q3_sh(m,k));
```

```
Hw1_7=cos(su2_7).*cos(su2_sh_7);
Hw2_7=sin(su3_7);
Hw3_7=sin(su2_7).*sin(su2_sh_7);
Hw4_7=sin(su1_7).*sin(su1_sh_7);
Hw5_7=cos(su2_7)-cos(su1_7);
Hw6_7=cos(su2_sh_7)-cos(su1_sh_7);
chta_7=cosh(ta_7);
shta_7=sinh(ta_7);
ch2ta_7=cosh(2*ta_7);
sh2ta_7=sinh(2*ta_7);
N11=chta_7.*chta_7.*Hw1_7+...
+(i/2)*sh2ta_7.*Hw2_7*rho_7-...
shta_7.*shta_7*Hw3_7*rho_7*rho_7;
N12=shta_7.*shta_7*(Hw1_7+Hw4_7)/3-chta_7.*chta_7*Hw3_7/3+...
(i/2)*rho_7*sh2ta_7*(Hw2_7+sin(su2_7)*Hw6_7+...
sin(su2_sh_7).*Hw5_7)/3+...
rho_7*rho_7*shta_7.*shta_7*(cos(su2_7)*Hw6_7+...
cos(su2_sh_7).*Hw5_7-Hw4_7)/3;
N21=shta_7.*shta_7*Hw1_7-Hw3_7+rho_7*(i*shta_7*chta_7*Hw2_7-...
shta_7.*shta_7*Hw3_7);
N22= (2/3)*cos(su4_7)+Hw1_7/3+...
shta_7.*shta_7*(cos(su4_7)-Hw3_7)/3+...
(i/2)*rho_7*sh2ta_7*Hw2_7/3+...
rho_7*rho_7*shta_7.*shta_7*(Hw1_7-cos(su4_7))/3;
%Lumped section No.8
su1_8=su_8*q3;
su1_sh_8=su_8*q3_sh(m,k);
su2_8=su_8*q1;
su2_sh_8=su_8*q1_sh(m,k);
```

```
su3_8=su_8*(q1+q1_sh(m,k));
su4_8=su_8*(q3-q3_sh(m,k));
Hw1_8=cos(su2_8).*cos(su2_sh_8);
Hw2_8=sin(su3_8);
Hw3_8=sin(su2_8).*sin(su2_sh_8);
Hw4_8=sin(su1_8).*sin(su1_sh_8);
Hw5_8=cos(su2_8)-cos(su1_8);
Hw6_8=cos(su2_sh_8)-cos(su1_sh_8);
chta_8=cosh(ta_8);
shta_8=sinh(ta_8);
ch2ta_8=cosh(2*ta_8);
sh2ta_8=sinh(2*ta_8);
E11=chta_8.*chta_8.*Hw1_8+...
+(i/2)*sh2ta_8.*Hw2_8*rho_8-...
shta_8.*shta_8*Hw3_8*rho_8*rho_8;
E12=shta_8.*shta_8*(Hw1_8+Hw4_8)/3-chta_8.*chta_8*Hw3_8/3+...
(i/2)*rho_8*sh2ta_8*(Hw2_8+sin(su2_8)*Hw6_8+...
sin(su2_sh_8).*Hw5_8)/3+...
rho_8*rho_8*shta_8.*shta_8*(cos(su2_8)*Hw6_8+...
cos(su2_sh_8).*Hw5_8-Hw4_8)/3;
E21=shta_8.*shta_8*Hw1_8-Hw3_8+rho_8*(i*shta_8*chta_8*Hw2_8-...
shta_8.*shta_8*Hw3_8);
E22= (2/3)*cos(su4_8)+Hw1_8/3+...
shta_8.*shta_8*(cos(su4_8)-Hw3_8)/3+...
(i/2)*rho_8*sh2ta_8*Hw2_8/3+...
rho_8*rho_8*shta_8.*shta_8*(Hw1_8-cos(su4_8))/3;
%Lumped section No.9
su1_9=su_9*q3;
su1_sh_9=su_9*q3_sh(m,k);
```

```
su2_9=su_9*q1;
su2_sh_9=su_9*q1_sh(m,k);
su3_9=su_9*(q1+q1_sh(m,k));
su4_9=su_9*(q3-q3_sh(m,k));
Hw1_9=cos(su2_9).*cos(su2_sh_9);
Hw2_9=sin(su3_9);
Hw3_9=sin(su2_9).*sin(su2_sh_9);
Hw4_9=sin(su1_9).*sin(su1_sh_9);
Hw5_9=cos(su2_9)-cos(su1_9);
Hw6_9=cos(su2_sh_9)-cos(su1_sh_9);
chta_9=cosh(ta_9);
shta_9=sinh(ta_9);
ch2ta_9=cosh(2*ta_9);
sh2ta_9=sinh(2*ta_9);
G11=chta_9.*chta_9.*Hw1_9+...
+(i/2)*sh2ta_9.*Hw2_9*rho_9-...
shta_9.*shta_9*Hw3_9*rho_9*rho_9;
G12=shta_9.*shta_9*(Hw1_9+Hw4_9)/3-chta_9.*chta_9*Hw3_9/3+...
(i/2)*rho_9*sh2ta_9*(Hw2_9+sin(su2_9)*Hw6_9+...
sin(su2_sh_9).*Hw5_9)/3+...
rho_9*rho_9*shta_9.*shta_9*(cos(su2_9)*Hw6_9+...
cos(su2_sh_9).*Hw5_9-Hw4_9)/3;
G21=shta_9.*shta_9*Hw1_9-Hw3_9+rho_9*(i*shta_9*chta_9*Hw2_9-...
shta_9.*shta_9*Hw3_9);
G22= (2/3)*cos(su4_9)+Hw1_9/3+...
shta_9.*shta_9*(cos(su4_9)-Hw3_9)/3+...
(i/2)*rho_9*sh2ta_9*Hw2_9/3+...
rho_9*rho_9*shta_9.*shta_9*(Hw1_9-cos(su4_9))/3;
%Lupmed section No.10
```

```
su1_10=su_10*q3;
su1_sh_10=su_10*q3_sh(m,k);
su2_10=su_10*q1;
su2_sh_10=su_10*q1_sh(m,k);
su3_10=su_10*(q1+q1_sh(m,k));
su4_10=su_10*(q3-q3_sh(m,k));
Hw1_10=cos(su2_10).*cos(su2_sh_10);
Hw2_10=sin(su3_10);
Hw3_10=sin(su2_10).*sin(su2_sh_10);
Hw4_10=sin(su1_10).*sin(su1_sh_10);
Hw5_10=cos(su2_10)-cos(su1_10);
Hw6_10=cos(su2_sh_10)-cos(su1_sh_10);
chta_10=cosh(ta_10);
shta_10=sinh(ta_10);
ch2ta_10=cosh(2*ta_10);
sh2ta_10=sinh(2*ta_10);
P11=chta_10.*chta_10.*Hw1_10+...
+(i/2)*sh2ta_10.*Hw2_10*rho_10-...
shta_10.*shta_10*Hw3_10*rho_10*rho_10;
P12=shta_10.*shta_10*(Hw1_10+Hw4_10)/3-chta_10.*chta_10*Hw3_10/3+...
(i/2)*rho_10*sh2ta_10*(Hw2_10+sin(su2_10)*Hw6_10+...
sin(su2_sh_10).*Hw5_10)/3+...
rho_10*rho_10*shta_10.*shta_10*(cos(su2_10)*Hw6_10+...
cos(su2_sh_10).*Hw5_10-Hw4_10)/3;
P21=shta_10.*shta_10*Hw1_10-Hw3_10+rho_10*(i*shta_10*chta_10*Hw2_10-...
shta_10.*shta_10*Hw3_10);
P22= (2/3)*cos(su4_10)+Hw1_10/3+...
shta_10.*shta_10*(cos(su4_10)-Hw3_10)/3+...
(i/2)*rho_10*sh2ta_10*Hw2_10/3+...
```

```
rho_10*rho_10*shta_10.*shta_10*(Hw1_10-cos(su4_10))/3;
%%%%%%%%%%%%%%%%%%%%%%%%%%%%%%%%%%%%%%%%%%%%%%%%%%%%%%%
clear Gamma_0,clear Gamma
temp11=ex3.*cosh(g);
temp22=ex3.*sh;
temp33=temp22.*f;
temp44=temp22.*d;
M11=temp11+temp33;
M12=temp44/3;
M21=temp44;
M22=temp11-temp33;
%%%%%%%%%%%%%%%%%%%%%%%%%%%%%%%%%%%%%%%%%%%%%%%%%%%%%%%
 AO1=F11;
 AO2=F21;
 BO1=S11.*AO1+S12.*AO2;
 BO2=S21.*AO1+S22.*AO2;
 CO1=T11.*BO1+T12.*BO2;
 CO2=T21.*BO1+T22.*BO2;
 DO1=O11.*CO1+O12.*CO2;
 DO2=O21.*CO1+O22.*CO2;
 EO1=V11.*DO1+V12.*DO2;
 EO2=V21.*DO1+V22.*DO2;    %5 lumped sections
 FO1=X11.*EO1+X12.*EO2;
 FO2=X21.*EO1+X22.*EO2;
 LO1=N11.*FO1+N12.*FO2;
 LO2=N21.*FO1+N22.*FO2;
 HO1=E11.*LO1+E12.*LO2;
 HO2=E21.*LO1+E22.*LO2;
 PO1=G11.*HO1+G12.*HO2;
```

```
 PO2=G21.*HO1+G22.*HO2;
 UO1=P11.*PO1+P12.*PO2;
 UO2=P21.*PO1+P22.*PO2;
 ZO1=M11.*UO1+M12.*UO2;
 ZO2=M21.*UO1+M22.*UO2;   %10 lumped sections
%%%%%%%%%%%%%%%%%%%%%%%%%%%%%%%%%%%%%%%%%%%%%%%
 Gamma_0=ZO1;
 Gamma=ZO2;
 GpG=Gamma_0+Gamma/3;
 funct=GpG;
 funct_s=fftshift(funct);
 I2 = z;
 I2g=z.*CD_sh.*funct_s;
for j = 1:2:length(size(z))
I2 = fft(I2,[],j);
I2 = ifft(I2,[],j+1);
I2g= fft(I2g,[],j);
I2g= ifft(I2g,[],j+1);
end
DI2=diag(I2);
DI2_m(m,:)=DI2';
DI2g=diag(I2g);
DI2g_m(m,:)=DI2g';
end
DI2_km(k,:,:)=DI2_m;
DI2g_km(k,:,:)=DI2g_m;
end
gp_i=ones(n,n);
zgp_i=ones(n,n,n);
```

```
gp=ones(n,n);
zgp1=ones(n,n,n);
for j=1:n
gp_i(:,:)=DI2_km(:,:,j);
gp(:,:)=DI2g_km(:,:,j);
zz=z.*gp_i;
zz3(:,:,j)=zz(:,:);
zgp=z.*gp.*CD_sh;
zgp1(:,:,j)=zgp(:,:);
end
Ip_i3=ones(n,n,n);
Igp_o3=ones(n,n,n);
Ip = ones(n,n);
Igp=ones(n,n);
for j=1:n
Ip(:,:)=zz3(:,:,j);
Igp(:,:)=zgp1(:,:,j);
for p = 1:2:length(size(z))
Ip = fft(Ip,[],p);
Ip = ifft(Ip,[],p+1);
Igp= fft(Igp,[],p);
Igp= ifft(Igp,[],p+1);
end
Ip_i3(j,:,:)=Ip(:,:);
Igp_o3(j,:,:)=Igp(:,:);
end
for j=1:n
Ip_i(j)=real(Ip_i3(j,j,j));
Ip_o(j)=A_n4*real(Igp_o3(j,j,j));%
```

```
end
sigm=sqrt(Ip_o'-I_out.*I_out);
Ima=max(I_out);
k_max=find(I_out==Ima);
I_mi=zeros(n,1);
for j=2:n-1
D_b=I_out(j)-I_out(j-1);
D_a=I_out(j+1)-I_out(j);
if((D_b<0) & (D_a>0))
I_mi(j)=I_out(j);
end
end
Imi=max(I_mi);
k_min=find(I_mi==Imi);
Q_fac=(I_out(k_max)-I_out(k_min))/(sigm(k_max)+sigm(k_min))
Qf(ntau)=Q_fac;
DTM(ntau)=Delta_tau_M2;
total_Delta_tau2=Delta_tau_M2+suu;
TDT(ntau)=total_Delta_tau2;
ss_max(ntau)=sigm(k_max);
ss_min(ntau)=sigm(k_min);
ssu(ntau)=suu;
end   %end   (nbeta1)
figure;plot(TDT(start_ntau:end),Qf(start_ntau:end),'*-')
toc
```

Appendix C

The explicit forms of the nine terms included in the expression $<\vec{E}_{out}(\acute{\omega})|\vec{E}_{out}(\omega)>$ in chapter 6 are :

$$S_1^*S_1 = \left\{e^{-i\left(\Psi_{L_1}^{CD}(\acute{\omega})+\Psi_{L_2}^{CD}(\acute{\omega})\right)}e^{i\left(\Psi_{L_1}^{CD}(\omega)+\Psi_{L_2}^{CD}(\omega)\right)}\right\}\times$$

$$<\vec{E}_{in}(\acute{\omega})|T^\dagger(\vec{\tau}_1,\acute{\omega})T^\dagger(\vec{\alpha}_1)T^\dagger(\vec{\tau}_2,\acute{\omega})T^\dagger(\vec{\alpha}_2)T(\vec{\alpha}_2)T(\vec{\tau}_2,\omega)T(\vec{\alpha}_1)T(\vec{\tau}_1,\omega)|\vec{E}_{in}(\omega)>,$$

$$S_2^*S_2 = \left\{e^{-i\left(\Psi_{L_2}^{CD}(\acute{\omega})\right)}e^{i\left(\Psi_{L_2}^{CD}(\omega)\right)}\right\}\times<\vec{e}_1{}^{(n)}(\acute{\omega})\left|T^\dagger(\vec{\tau}_2,\acute{\omega})T^\dagger(\vec{\alpha}_2)T(\vec{\alpha}_2)T(\vec{\tau}_2,\omega)\right|\vec{e}_1{}^{(n)}(\omega)>,$$

$$S_3^*S_3 =<\vec{e}_2{}^{(n)}(\acute{\omega})\left|\vec{e}_2{}^{(n)}(\omega)\right.>,$$

$$S_1^*S_2 = \left\{e^{-i\left(\Psi_{L_1}^{CD}(\acute{\omega})+\Psi_{L_2}^{CD}(\acute{\omega})\right)}e^{i\left(\Psi_{L_2}^{CD}(\omega)\right)}\right\}\times$$

$$<\vec{E}_{in}(\acute{\omega})|T^\dagger(\vec{\tau}_1,\acute{\omega})T^\dagger(\vec{\alpha}_1)T^\dagger(\vec{\tau}_2,\acute{\omega})T^\dagger(\vec{\alpha}_2)T(\vec{\alpha}_2)T(\vec{\tau}_2,\omega)\left|\vec{e}_1{}^{(n)}(\omega)\right.>,$$

$$S_2^*S_1 = \left\{e^{-i\left(\Psi_{L_2}^{CD}(\acute{\omega})\right)}e^{i\left(\Psi_{L_1}^{CD}(\omega)+\Psi_{L_2}^{CD}(\omega)\right)}\right\}\times$$

$$<\vec{e}_1{}^{(n)}(\acute{\omega})\left|T^\dagger(\vec{\tau}_2,\acute{\omega})T^\dagger(\vec{\alpha}_2)T(\vec{\alpha}_2)T(\vec{\tau}_2,\omega)T(\vec{\alpha}_1)T(\vec{\tau}_1,\omega)\right|\vec{E}_{in}(\omega)>,$$

$$S_1^*S_3 = \left\{e^{-i\left(\Psi_{L_1}^{CD}(\acute{\omega})+\Psi_{L_2}^{CD}(\acute{\omega})\right)}\right\}<\vec{E}_{in}(\acute{\omega})|T^\dagger(\vec{\tau}_1,\acute{\omega})T^\dagger(\vec{\alpha}_1)T^\dagger(\vec{\tau}_2,\acute{\omega})T^\dagger(\vec{\alpha}_2)\left|\vec{e}_2{}^{(n)}(\omega)\right.>,$$

$$S_3^*S_1 = \left\{e^{i\left(\Psi_{L_1}^{CD}(\omega)+\Psi_{L_2}^{CD}(\omega)\right)}\right\}<\vec{e}_2{}^{(n)}(\acute{\omega})\left|T(\vec{\alpha}_2)T(\vec{\tau}_2,\omega)T(\vec{\alpha}_1)T(\vec{\tau}_1,\omega)\right|\vec{E}_{in}(\omega)>,$$

$$S_2^*S_3 = \left\{e^{-i\left(\Psi_{L_2}^{CD}(\acute{\omega})\right)}\right\}<\vec{e}_1{}^{(n)}(\acute{\omega})\left|T^\dagger(\vec{\tau}_2,\acute{\omega})T^\dagger(\vec{\alpha}_2)\right|\vec{e}_2{}^{(n)}(\omega)>,$$

$$S_3^*S_2 = \left\{e^{i\left(\Psi_{L_2}^{CD}(\omega)\right)}\right\}<\vec{e}_2{}^{(n)}(\acute{\omega})\left|T(\vec{\alpha}_2)T(\vec{\tau}_2,\omega)\right|\vec{e}_1{}^{(n)}(\omega)>.$$

Appendix D

Newton's method to solve the equation

$$\Phi'_{t_k}(\tilde{s}) = \sum_{j=1}^{M} \{ \frac{2\sigma^2 |\widetilde{b_j}|^2 \tilde{s} \ \ (1-\sigma^2\lambda_j\tilde{s}/2)}{[1-\sigma^2\lambda_j\tilde{s}]^2} + \frac{\sigma^2\lambda_j}{[1-\sigma^2\lambda_j\tilde{s}]} \} - \frac{1}{\tilde{s}} - y_{th}$$

Starting with $\tilde{s} = s_0$, the roots of this equation (saddle points) are the limit of the sequence

$$\tilde{s}_{n+1} = \tilde{s}_n - \frac{\acute{\Phi}_{t_k}(\tilde{s})}{\acute{\acute{\Phi}}_{t_k}(\tilde{s})}$$

The starting point has to be in the range $-\frac{1}{max|\sigma^2\lambda_j{}^-|} < s_0 < \frac{1}{max|\sigma^2\lambda_j{}^+|}$.

The second derivative of $\Phi_{t_k}(\tilde{s})$ is given by

$$\Phi''_{t_k}(\tilde{s}) = \sum_{j=1}^{M} \{ \frac{(2\sigma^2|\widetilde{b_j}|^2)}{[1-\sigma^2\lambda_j\tilde{s}]} + \frac{(\sigma^2\lambda_j)^2}{[1-\sigma^2\lambda_j\tilde{s}]^2} + \frac{4(2\sigma^2|\widetilde{b_j}|^2)(2\sigma^2\lambda_j) \ \ [1-\sigma^2\lambda_j\tilde{s}/2]\tilde{s}}{[1-\sigma^2\lambda_j\tilde{s}]^3} \} + \frac{1}{(\tilde{s})^2}$$

The iteration is stopped when $|\tilde{s}_{n+1} - \tilde{s}_n|$ falls below 10^{-12}.

Appendix E

% Bit Error Rate Calculation Code

```
Tic
clear;
format long e;
T=100;        % Pulse width in ps
T2=T*T;
m=11;
n=32*m;
n_noise=11;   % n_noise=2*M+1,  M=(n_noise-1)/2
t_tilda=T;    % (DPSK)
%t_tilda=0;   % (OOK)
ss=0.01;      % y_th (DPSK)
%ss=0.48;     % y_th (OOK)
  ss;
gamma_th=ss/100;   % the decision threshold
h_planck= 6.626068e-34;   %Planck's constant (j.s)= m2kg / s
cLV=3*10^8;            %light velocity
pi2=pi*2;
cc=pi2*cLV*10^-3;        %nm/ps
p4=4*pi*pi;
Disp_1=17;             % D (ps/nm)
Disp_2=17;
lambda_0=1550;         % The wavelength
omega_0=cc/lambda_0;
BOT=1.2;               % Optical filter bandwidth
L_1=(10/17)*100;       % The length of the first section
```

```
L_2=(10/17)*100;        % The length of the second section
%%%%%%%%%%%%%           Noise parameters
eta_1_t=0;
eta_2_t=1;
etan_1=sqrt(eta_1_t);
etan_2=sqrt(eta_2_t);
%%%%%%%%%%%%%           BMD , PDL
dir=rand(1,3);
Delta_tau_dir_1=dir/norm(dir);
Delta_tau_1=20*norm(Delta_tau_dir_1);  %ps
%Delta_tau_1=10^-99;  %ps comparesion
dir=rand(1,3);
Delta_tau_dir_2=dir/norm(dir);
Delta_tau_2=20*norm(Delta_tau_dir_2);  %ps
%Delta_tau_2=10^-99;  %ps comparesion
dir=rand(1,3);
pdl_dB_dir_1=1*dir/norm(dir);
pdl_dB_1=(0)*norm(pdl_dB_dir_1);  %dB
%pdl_dB_1=10^-99;  %dB comparison
dir=rand(1,3);
pdl_dB_dir_2=1*dir/norm(dir);
pdl_dB_2=(1)*norm(pdl_dB_dir_2);  %dB
%pdl_dB_2=10^-99;   %dB comparison
eta_1=pdl_dB_1/(20*log10(exp(1)));
eta_2=pdl_dB_2/(20*log10(exp(1)));
dot_1=dot(Delta_tau_dir_1,pdl_dB_dir_1);
dot_2=dot(Delta_tau_dir_2,pdl_dB_dir_2);
cross_1=cross(Delta_tau_dir_1,pdl_dB_dir_1);
cross_2=cross(Delta_tau_dir_2,pdl_dB_dir_2);
```

```
exeta_1=exp(-eta_1);
exeta_2=exp(-eta_2);
exeta_1m=1-exeta_1;
exeta_1p=1+exeta_1;
exeta_2m=1-exeta_2;
exeta_2p=1+exeta_2;
eta_1_2=eta_1.*eta_1;
eta_2_2=eta_2.*eta_2;
eta2_ave=eta_1_2.*eta_2_2;
A_n4=exp(-eta2_ave);
A_n2=sqrt(A_n4);
%%%%%%%%%%%%%%        Gaussian variance   <Delta^2>
N=32;
neu_0=cLV/(lambda_0*(10^(-9)));
photon_energy=h_planck*neu_0;
n_sp=1;              % spontaneous emission parameter [1.4-4]
N_0=n_sp*photon_energy; % (amplifier_gain_1-1/amplifier_gain_1);
meu=0.72;             % dimentionless parameter =~0.6  0.8  1
B_ON=BOT*(10^12)/T;     % noise equivalent bandwidth ofoptical lowpass filter
B_RN=0.65*(10^12)/T;    % noise equivalent ofpostdetection filter
T_0=meu*((1/B_ON)+(1/B_RN))*(10^12);
% Gauss_variance=N_0/(2*T_0);
% Gauss_Variance_2=2* Gauss_variance;
sss=[];
for  s=1:3
   s
   Input_SNR=s+9;  %dB
   Input_SNR;
In_SNR_Dless=10^(Input_SNR/10);
```

```
%%%%%%%%%%%%%%%         Noise
E_b=T*10^-3;
Gauss_variance=E_b/(2*T_0*In_SNR_Dless);
Gauss_Variance_2=2* Gauss_variance;
%%%%%%%%%%%%%%          Input state of polarization
seta=1*(pi/4);
fai=1*(pi/4);
m_in=[sin(seta)*cos(fai) sin(seta)*sin(fai) cos(seta)];
m_p=[cos(seta)*cos(fai)-i*sin(fai) cos(seta)*sin(fai)+...
   i*cos(fai) -sin(seta)];
% m_p=[sin(seta/2)^2*exp(i*fai)-cos(seta/2)^2*exp(-i*fai)...
% -i*sin(seta/2)^2*exp(i*fai)-i*cos(seta/2)^2*exp(-i*fai) sin(seta)];
m_ps=conj(m_p);
aaa=56;
%%%%
 for bin=1:32
      bin
plu=bin-1;
NoP=32;
if (bin<6)
  qqq=-1;
elseif (bin<9)
  qqq=1;
elseif (bin<10 )
  qqq=-1;
elseif (bin<15)
  qqq=1;
elseif (bin<17)
  qqq=-1;
```

```
elseif (bin<18)
  qqq=1;
elseif (bin<19)
  qqq=-1;
elseif (bin<21)
  qqq=1;
elseif (bin<22)
  qqq=-1;
elseif (bin<23)
  qqq=1;
elseif (bin<24)
  qqq=-1;
elseif (bin<24)
  qqq=1;
elseif (bin<27)
  qqq=-1;
elseif (bin<29)
  qqq=1;
elseif (bin<32)
  qqq=-1;
elseif (bin<33)
  qqq=1;
end
QQ=qqq;
norma=sqrt(T/sqrt(pi));
 A_in=sqrt(2*E_b/(T*(10^-12)));
 L=(n-1)/2;
t=linspace(0,NoP*T,n);
t_k=aaa+plu*T;
```

```
%%%%%%%%%%%%        Pulse shape
%%%%    Gaussian Pulse
%       [fin,NoP]=f_in_t(t,T,D2T2,ch,2,NoP);
%       ftt=A_in*fin;/sq
%%%%    Rised COSINE
        [fin_33,fin_50,fin_67,NoP]=RZ_inputP_dpsk(t,T,NoP);
        ftt=A_in*fin_33;
        %ftt=A*fin_50;
        %ftt=A*fin_67;
        fttc=conj(ftt);
fw=fft(ftt);% Fourier-transform of the input  field
fwp=conj(fw)/n;
fw_fwp=fw.*fwp;
fttc=conj(ftt)/n;
[B1,B2]=meshgrid(fw,fwp);
z=(B1.*B2);
%%%%%%%%%%%%        L=linspace(0,NoP*T,n);
L=(n-1)/2;
Ws=2*pi/(N*T);
ww=Ws*(-L:L);%Ws*L;% wwp=-Ws*L;
[wp,w]=meshgrid(ww);
wmwp=wp-w;
%%%%%%%%%%%%        The optical filter (Fabry-Perot opticalfilter (FFP) )
wBand=B_ON;% 0.90=900 Ghz
Half_wB=wBand/2; % 0.450==450 GHz( 10^9 Hz )
H_o=1./(1+i*(w)/(pi*B_ON)); % the transfer function ofthe FFP
H_op=1./(1-i*(wp)/(pi*B_ON));
H_opc=conj(H_op);
for ll=1:n
```

```
  ll;
  H_oc(ll,ll)=H_o(ll,ll);
  H_opc(ll,ll)=H_op(ll,ll);
  H_opcc(ll,ll)=H_opc(ll,ll);
end
%%%%%%%%%%          The electrical filter  ( fifth-orderBessel filter )
 D_ll=(exp(2*pi*i*w/N)+exp(-2*pi*i*wp/N))/2;
 dfreq=(-wmwp)/(2*pi*N*T);
 Dfreq=2.43*(dfreq/(B_RN))*(D_ll);
 H_e=945./(i*Dfreq^5+15*Dfreq^4-105*i*Dfreq^3-420*Dfreq^2+...
  945*i*Dfreq+945); % the transfer function of the fifth-order
                               % Bessel function
%%%%
bet2_1=-lambda_0^2*Disp_1/(2*pi*cLV);  %(ps)^2/m
bet2_2=-lambda_0^2*Disp_2/(2*pi*cLV);
pipi=2*pi;
tab=2*pi*pi;
CD_L1=exp(-i*tab*(bet2_1*(w/pipi).*(w/pipi))*L_1);
CD_L1p=exp(i*tab*(bet2_1*(w/pipi).*(w/pipi))*L_1);
CD_L2=exp(-i*tab*(bet2_2*(w/pipi).*(w/pipi))*L_2);
CD_L2p=exp(i*tab*(bet2_2*(w/pipi).*(w/pipi))*L_2);
CD12=CD_L1.*CD_L2;
CD12p=CD_L1p.*CD_L2p;
CD_total=CD_L1.*CD_L1p.*CD_L2.*CD_L2p;
for cc=1:n
  cc;
  CD12c(cc,cc)=CD12(cc,cc);
  CD12pc(cc,cc)=CD12p(cc,cc);
end
```

```
Dtw_1=Delta_tau_1*w/2;  % PMD for the first section (w)
Dtw_2=Delta_tau_2*w/2;  % PMD for the second section (w)
A_0_1=exeta_1p*cos(Dtw_1)/2 ...
    -i*exeta_1m*sin(Dtw_1)*dot_1/2;
B_1_x=exeta_1m*cos(Dtw_1)*pdl_dB_dir_1(1)/2 ...
   -i*exeta_1p*sin(Dtw_1)*Delta_tau_dir_1(1)/2 ...
   +exeta_1m*sin(Dtw_1)*cross_1(1)/2;
B_1_y=exeta_1m*cos(Dtw_1)*pdl_dB_dir_1(2)/2 ...
   -i*exeta_1p*sin(Dtw_1)*Delta_tau_dir_1(2)/2 ...
   +exeta_1m*sin(Dtw_1)*cross_1(2)/2;
B_1_z=exeta_1m*cos(Dtw_1)*pdl_dB_dir_1(3)/2 ...
   -i*exeta_1p*sin(Dtw_1)*Delta_tau_dir_1(3)/2 ...
   +exeta_1m*sin(Dtw_1)*cross_1(3)/2;
A_0_2=exeta_2p*cos(Dtw_2)/2 ...
    -i*exeta_2m*sin(Dtw_2)*dot_2/2;

B_2_x=exeta_2m*cos(Dtw_2)*pdl_dB_dir_2(1)/2 ...
   -i*exeta_2p*sin(Dtw_2)*Delta_tau_dir_2(1)/2 ...
   +exeta_2m*sin(Dtw_2)*cross_2(1)/2;
B_2_y=exeta_2m*cos(Dtw_2)*pdl_dB_dir_2(2)/2 ...
   -i*exeta_2p*sin(Dtw_2)*Delta_tau_dir_2(2)/2 ...
   +exeta_2m*sin(Dtw_2)*cross_2(2)/2;
B_2_z=exeta_2m*cos(Dtw_2)*pdl_dB_dir_2(3)/2 ...
   -i*exeta_2p*sin(Dtw_2)*Delta_tau_dir_2(3)/2 ...
   +exeta_2m*sin(Dtw_2)*cross_2(3)/2;

Dtw_1p=Delta_tau_1*wp/2;  % PMD for the first section (wp)
Dtw_2p=Delta_tau_2*wp/2;  % PMD for the second section (wp)
A_0_1_c=exeta_1p*cos(Dtw_1p)/2 ...
```

```
    +i*exeta_1m*sin(Dtw_1p)*dot_1/2;
B_1_x_c=exeta_1m*cos(Dtw_1p)*pdl_dB_dir_1(1)/2 ...
   +i*exeta_1p*sin(Dtw_1p)*Delta_tau_dir_1(1)/2 ...
   +exeta_1m*sin(Dtw_1p)*cross_1(1)/2;
B_1_y_c=exeta_1m*cos(Dtw_1p)*pdl_dB_dir_1(2)/2 ...
  +i*exeta_1p*sin(Dtw_1p)*Delta_tau_dir_1(2)/2 ...
   +exeta_1m*sin(Dtw_1p)*cross_1(2)/2;
B_1_z_c=exeta_1m*cos(Dtw_1p)*pdl_dB_dir_1(3)/2 ...
   +i*exeta_1p*sin(Dtw_1p)*Delta_tau_dir_1(3)/2 ...
   +exeta_1m*sin(Dtw_1p)*cross_1(3)/2;
A_0_2_c=exeta_2p*cos(Dtw_2p)/2 ...
    +i*exeta_2m*sin(Dtw_2p)*dot_2/2;

B_2_x_c=exeta_2m*cos(Dtw_2p)*pdl_dB_dir_2(1)/2 ...
   +i*exeta_2p*sin(Dtw_2p)*Delta_tau_dir_2(1)/2 ...
   +exeta_2m*sin(Dtw_2p)*cross_2(1)/2;
B_2_y_c=exeta_2m*cos(Dtw_2p)*pdl_dB_dir_2(2)/2 ...
   +i*exeta_2p*sin(Dtw_2p)*Delta_tau_dir_2(2)/2 ...
   +exeta_2m*sin(Dtw_2p)*cross_2(2)/2;
B_2_z_c=exeta_2m*cos(Dtw_2p)*pdl_dB_dir_2(3)/2 ...
   +i*exeta_2p*sin(Dtw_2p)*Delta_tau_dir_2(3)/2 ...
   +exeta_2m*sin(Dtw_2p)*cross_2(3)/2;
%%%%%%%%%%%%          Calculation of term one
A_0_21=A_0_2.*A_0_1+B_2_x.*B_1_x+B_2_y.*B_1_y+B_2_z.*B_1_z;
B_21_x=A_0_2.*B_1_x+B_2_x.*A_0_1+i*(B_2_y.*B_1_z-B_2_z.*B_1_y);
B_21_y=A_0_2.*B_1_y+B_2_y.*A_0_1+i*(B_2_z.*B_1_x-B_2_x.*B_1_z);
B_21_z=A_0_2.*B_1_z+B_2_z.*A_0_1+i*(B_2_x.*B_1_y-B_2_y.*B_1_x);
A_02c_21=A_0_2_c.*A_0_21+B_2_x_c.*B_21_x+B_2_y_c.*B_21_y+B_2_z_c.*B_21_z;
B_2c_21_x=A_0_2_c.*B_21_x+B_2_x_c.*A_0_21+i*(B_2_y_c.*B_21_z-B_2_z_c.*B_21_y);
```

```
B_2c_21_y=A_0_2_c.*B_21_y+B_2_y_c.*A_0_21+i*(B_2_z_c.*B_21_x-B_2_x_c.*B_21_z);
B_2c_21_z=A_0_2_c.*B_21_z+B_2_z_c.*A_0_21+i*(B_2_x_c.*B_21_y-B_2_y_c.*B_21_x);
A_0_te1=A_0_1_c.*A_02c_21+B_1_x_c.*B_2c_21_x+B_1_y_c.*B_2c_21_y+...
   B_1_z_c.*B_2c_21_z;
B_te1_x=A_0_1_c.*B_2c_21_x+B_1_x_c.*A_02c_21+ ...
   i*(B_1_y_c.*B_2c_21_z-B_1_z_c.*B_2c_21_y);
B_te1_y=A_0_1_c.*B_2c_21_y+B_1_y_c.*A_02c_21+...
   i*(B_1_z_c.*B_2c_21_x-B_1_x_c.*B_2c_21_z);
B_te1_z=A_0_1_c.*B_2c_21_z+B_1_z_c.*A_02c_21+ ...
   i*(B_1_x_c.*B_2c_21_y-B_1_y_c.*B_2c_21_x);
A_0_term1=A_0_te1;
B_term1=B_te1_x.*m_in(1)+B_te1_y.*m_in(2)+B_te1_z.*m_in(3);
%%%%
T_term1=A_0_term1+B_term1;
H_et=H_e';
Drc=H_et*T_term1;
TT=CD12pc*H_opc*Drc*CD12c*H_oc;
g_sh=fftshift(TT);
g=g_sh;
   l=z;
g=CD_total.*H_op.*H_et.*T_term1.*H_o;%
zg=z.*g;
fg=B1.*g;
lg=zg;
for p = 1:2:length(size(z))
   l = fft(l,[],p);
   l = ifft(l,[],p+1);
   fg=fft(fg,[],p);
   fg= ifft(fg,[],p+1);
```

```
   Ig= fft(Ig,[],p);
   Ig= ifft(Ig,[],p+1);
end
I_i=real(diag(I));
f_o=real(diag(fg));
I_o=A_n2*real(diag(Ig));
%%%%
pa=(bin-1)*(m)+(m+1)/2;
I_tk_out =I_o(pa,1);
I_tk_in=I_i(pa,1);
y_ss=QQ*I_tk_out/(A_in*A_in)
%%%%%%%%%%%%        Noise
M=1*(n_noise-1)/2;
et=M/(B_ON*T_0); % this eta is vareing
T_0_less=T_0;
Ws=2*pi/T_0;
wwn=Ws*(-M:M);
[wnp,wn]=meshgrid(wwn);
wmwpn=wnp-wn;
%%%%%%%%%%%%        The optical filter (Fabry-Perot opticalfilter (FFP)
wBand=B_ON;                % 0.90=900 Ghz
Half_wB=wBand/2;            % 0.450==450 GHz( 10^9 Hz )
H_on=1./(1+i*(wn)/(pi*B_ON)); % the transfer functionof the FFP
H_opn=1./(1+i*(wnp)/(pi*B_ON));
H_opcn=conj(H_opn);
for ll=1:n_noise
   ll;
  H_ocn(ll,ll)=H_on(ll,ll);
   H_opcn(ll,ll)=H_opn(ll,ll);
```

```
  H_opccn(ll,ll)=H_opcn(ll,ll);
end
%%%%%%%%%%%%          The electrical filter  ( fifth-orderBessel filter )
D_ll=(exp(2*pi*i*wn*T/T_0)+exp(-2*pi*i*wnp*T/T_0))/2;
dfreq=(-wmwpn)/(2*pi*N*T);
Dfreq_n=2.43*(dfreq/(B_RN))*(D_ll);
H_en=945./(i*Dfreq_n^5+15*Dfreq_n^4-105*i*Dfreq_n^3-420*Dfreq_n^2+...
  945*i*Dfreq_n+945);
%%%%
bet2_1=-lambda_0^2*Disp_1/(2*pi*cLV);  %(ps)^2/m
bet2_2=-lambda_0^2*Disp_2/(2*pi*cLV);
CD_L1=exp(i*tab*((bet2_1*wn.*wn)*L_1));
CD_L1p=exp(-i*tab*((bet2_1*wnp.*wnp)*L_1));
CD_L2=exp(i*tab*((bet2_2*wn.*wn)*L_2));
CD_L2p=exp(-i*tab*((bet2_2*wnp.*wnp)*L_2));
CD1=CD_L1.*CD_L1p;
CD2=CD_L2.*CD_L2p;
CD_total=CD_L1.*CD_L2.*CD_L1p.*CD_L2p;
CD12=CD_L1.*CD_L2;
CD12p=CD_L1p.*CD_L2p;
CD_total=CD_L1.*CD_L1p.*CD_L2.*CD_L2p;
for cc=1:n_noise
   cc;
   CD_L1c(cc,cc)=CD_L1(cc,cc);
   CD_L1pc(cc,cc)=CD_L1p(cc,cc);
   CD_L2c(cc,cc)=CD_L2(cc,cc);
   CD_L2pc(cc,cc)=CD_L2p(cc,cc);
   CD12c(cc,cc)=CD12(cc,cc);
   CD12pc(cc,cc)=CD12p(cc,cc);
```

```
   CD2c(cc,cc)=CD2(cc,cc);
   CD1c(cc,cc)=CD1(cc,cc);
end
%%%%
HH=H_en.*H_ocn.*conj(H_opcn)/(2*pi);
e=exp(i*wnp.*t_tilda)+exp(-i*wn.*t_tilda);
exwnp=exp(-1*i*wnp.*(t_k));
exwn=exp(1*i*wn.*(t_k));
ee=exwnp.*exwn.*e;
f_term=ee.*HH;
%%%%
Dtwn_1=Delta_tau_1*wn/2;  % PMD for the first section  (wn)
Dtwn_2=Delta_tau_2*wn/2;  % PMD for the second section (wn)
A_0_1=exeta_1p*cos(Dtwn_1)/2 ...
    -i*exeta_1m*sin(Dtwn_1)*dot_1/2;
B_1_x=exeta_1m*cos(Dtwn_1)*pdl_dB_dir_1(1)/2 ...
   -i*exeta_1p*sin(Dtwn_1)*Delta_tau_dir_1(1)/2 ...
   +exeta_1m*sin(Dtwn_1)*cross_1(1)/2;
B_1_y=exeta_1m*cos(Dtwn_1)*pdl_dB_dir_1(2)/2 ...
   -i*exeta_1p*sin(Dtwn_1)*Delta_tau_dir_1(2)/2 ...
   +exeta_1m*sin(Dtwn_1)*cross_1(2)/2;
B_1_z=exeta_1m*cos(Dtwn_1)*pdl_dB_dir_1(3)/2 ...
   -i*exeta_1p*sin(Dtwn_1)*Delta_tau_dir_1(3)/2 ...
   +exeta_1m*sin(Dtwn_1)*cross_1(3)/2;
A_0_2=exeta_2p*cos(Dtwn_2)/2 ...
    -i*exeta_2m*sin(Dtwn_2)*dot_2/2;
B_2_x=exeta_2m*cos(Dtwn_2)*pdl_dB_dir_2(1)/2 ...
   -i*exeta_2p*sin(Dtwn_2)*Delta_tau_dir_2(1)/2 ...
   +exeta_2m*sin(Dtwn_2)*cross_2(1)/2;
```

```
B_2_y=exeta_2m*cos(Dtwn_2)*pdl_dB_dir_2(2)/2 ...
   -i*exeta_2p*sin(Dtwn_2)*Delta_tau_dir_2(2)/2 ...
   +exeta_2m*sin(Dtwn_2)*cross_2(2)/2;
B_2_z=exeta_2m*cos(Dtwn_2)*pdl_dB_dir_2(3)/2 ...
   -i*exeta_2p*sin(Dtwn_2)*Delta_tau_dir_2(3)/2 ...
   +exeta_2m*sin(Dtwn_2)*cross_2(3)/2;
%%%%
Dtwn_1p=Delta_tau_1*wnp/2;  % PMD for the first section (wnp)
Dtwn_2p=Delta_tau_2*wnp/2;  % PMD for the second section (wnp)
A_0_1_c=exeta_1p*cos(Dtwn_1p)/2 ...
    +i*exeta_1m*sin(Dtwn_1p)*dot_1/2;
B_1_x_c=exeta_1m*cos(Dtwn_1p)*pdl_dB_dir_1(1)/2 ...
   +i*exeta_1p*sin(Dtwn_1p)*Delta_tau_dir_1(1)/2 ...
   +exeta_1m*sin(Dtwn_1p)*cross_1(1)/2;
B_1_y_c=exeta_1m*cos(Dtwn_1p)*pdl_dB_dir_1(2)/2 ...
  +i*exeta_1p*sin(Dtwn_1p)*Delta_tau_dir_1(2)/2 ...
   +exeta_1m*sin(Dtwn_1p)*cross_1(2)/2;
B_1_z_c=exeta_1m*cos(Dtwn_1p)*pdl_dB_dir_1(3)/2 ...
   +i*exeta_1p*sin(Dtwn_1p)*Delta_tau_dir_1(3)/2 ...
   +exeta_1m*sin(Dtwn_1p)*cross_1(3)/2;
A_0_2_c=exeta_2p*cos(Dtwn_2p)/2 ...
    +i*exeta_2m*sin(Dtwn_2p)*dot_2/2;
B_2_x_c=exeta_2m*cos(Dtwn_2p)*pdl_dB_dir_2(1)/2 ...
   +i*exeta_2p*sin(Dtwn_2p)*Delta_tau_dir_2(1)/2 ...
   +exeta_2m*sin(Dtwn_2p)*cross_2(1)/2;
B_2_y_c=exeta_2m*cos(Dtwn_2p)*pdl_dB_dir_2(2)/2 ...
   +i*exeta_2p*sin(Dtwn_2p)*Delta_tau_dir_2(2)/2 ...
   +exeta_2m*sin(Dtwn_2p)*cross_2(2)/2;
B_2_z_c=exeta_2m*cos(Dtwn_2p)*pdl_dB_dir_2(3)/2 ...
```

```
    +i*exeta_2p*sin(Dtwn_2p)*Delta_tau_dir_2(3)/2 ...
    +exeta_2m*sin(Dtwn_2p)*cross_2(3)/2;
%%%%%%%%%%%%        Calculation of Q matrix
%%%%%%%%%%%%        Term 9
A_0_2=A_0_2;
B_2_x=B_2_x;
B_2_y=B_2_y;
B_2_z=B_2_z;
%%%%%%%%%%%%        Term 8
A_0_2_c=A_0_2_c;
B_2_x_c=B_2_x_c;
B_2_y_c=B_2_y_c;
B_2_z_c=B_2_z_c;
%%%%%%%%%%%%        Term 2
A_02=(A_0_2_c.*A_0_2+B_2_x_c.*B_2_x+B_2_y_c.*B_2_y+B_2_z_c.*B_2_z);
B_x2=(A_0_2_c.*B_2_x+B_2_x_c.*A_0_2+i*(B_2_y_c.*B_2_z-B_2_z_c.*B_2_y));
B_y2=(A_0_2_c.*B_2_y+B_2_y_c.*A_0_2+i*(B_2_z_c.*B_2_x-B_2_x_c.*B_2_z));
B_z2=(A_0_2_c.*B_2_z+B_2_z_c.*A_0_2+i*(B_2_x_c.*B_2_y-B_2_y_c.*B_2_x));
%%%%
T_11=A_02+B_x2.*m_in(1)+B_y2.*m_in(2)+B_z2.*m_in(3);  %q11
T_12=B_x2.*m_ps(1)+B_y2.*m_ps(2)+B_z2.*m_ps(3);       %q12
T_21=B_x2.*m_p(1)+B_y2.*m_p(2)+B_z2.*m_p(3);          %q21
T_22=A_02-(B_x2.*m_in(1)+B_y2.*m_in(2)+B_z2.*m_in(3));%q22
T_13=A_0_2_c+B_2_x_c.*m_in(1)+B_2_y_c.*m_in(2)+B_2_z_c.*m_in(3);%q13
T_14=B_2_x_c.*m_ps(1)+B_2_y_c.*m_ps(2)+B_2_z_c.*m_ps(3);        %q14
T_23=B_2_x_c.*m_p(1)+B_2_y_c.*m_p(2)+B_2_z_c.*m_p(3);           %q23
T_24=A_0_2_c-(B_2_x_c.*m_in(1)+B_2_y_c.*m_in(2)+B_2_z_c.*m_in(3));%q24
T_31=A_0_2+B_2_x.*m_in(1)+B_2_y.*m_in(2)+B_2_z.*m_in(3);  %q31
T_32=B_2_x.*m_ps(1)+B_2_y.*m_ps(2)+B_2_z.*m_ps(3);        %q32
```

```
T_41=B_2_x.*m_p(1)+B_2_y.*m_p(2)+B_2_z.*m_p(3);         %q41
T_42=A_0_2-(B_2_x.*m_in(1)+B_2_y.*m_in(2)+B_2_z.*m_in(3));%q42
%%%%
 f_CD=f_term.*CD2c;
 q_11=etan_1*eta_2*f_CD.*T_11/2;%f_CD.*T_11/2;%
 q_12=etan_1*eta_2*f_CD.*T_12/2;%f_CD.*T_12/2;%
 q_21=etan_1*eta_2*f_CD.*T_21/2;%f_CD.*T_21/2;%
 q_22=etan_1*eta_2*f_CD.*T_22/2;%f_CD.*T_22/2;%
 f_CD_fp= f_term.*(CD_L2pc);
 q_13=etan_1*eta_2*f_CD_fp.*T_13/2;%f_CD_fp.*T_13/2;%
 q_14=etan_1*eta_2*f_CD_fp.*T_14/2;%f_CD_fp.*T_14/2;%
 q_23=etan_1*eta_2*f_CD_fp.*T_23/2;%f_CD_fp.*T_23/2;%
 q_24=etan_1*eta_2*f_CD_fp.*T_24/2;%f_CD_fp.*T_24/2;%
 f_CD_f =f_term.*CD_L2c;
 q_31=etan_1*eta_1*f_CD_f.*T_31/2;%f_CD_f.*T_31/2;%
 q_32=etan_1*eta_1*f_CD_f.*T_32/2;%f_CD_f.*T_32/2;%
 q_41=etan_1*eta_1*f_CD_f.*T_41/2;%f_CD_f.*T_41/2;%
 q_42=etan_1*eta_1*f_CD_f.*T_42/2;%f_CD_f.*T_42/2;%
 %%%%%%%%%%%%%%%%        Term3
 q_33=etan_2*etan_2*(f_term/2);%(f_term/2);%
 q_34=0;
 q_43=0;
 q_44=etan_2*etan_2*(f_term/2);%(f_term/2);%
  eee=0;
  QQ=[];
 for k=1:n_noise
    QQ1=[];QQ2=[];QQ3=[];QQ4=[];QQ5=[];QQ6=[];QQ7=[];QQ8=[];QQ9=[];
    for j=1:n_noise
       QQ1=[QQ1 q_11(k,j) q_12(k,j) q_13(k,j) q_14(k,j) eee eee eee eee eee];
```

```
      QQ2=[QQ2 q_21(k,j) q_22(k,j) q_23(k,j) q_24(k,j) eee eee eee eee eee];
      QQ3=[QQ3 q_31(k,j) q_32(k,j) q_33(k,j) q_34 eee eee eee eee eee];
      QQ4=[QQ4 q_41(k,j) q_42(k,j) q_43 q_44(k,j) eee eee eee eee eee];
      QQ5=[QQ5 q_11(k,j) q_12(k,j) q_13(k,j) q_14(k,j) eee eee eee eee eee];
      QQ6=[QQ6 q_21(k,j) q_22(k,j) q_23(k,j) q_24(k,j) eee eee eee eee eee];
      QQ7=[QQ7 q_31(k,j) q_32(k,j) q_33(k,j) q_34 eee eee eee eee eee];
      QQ8=[QQ8 q_41(k,j) q_42(k,j) q_43 q_44(k,j) eee eee eee eee eee];
      QQ9=[QQ9 q_11(k,j) q_12(k,j) q_13(k,j) q_14(k,j) eee eee eee eee eee];
    end
    QQ=[QQ; QQ1; QQ2; QQ3; QQ4; QQ5; QQ6; QQ7; QQ8; QQ9];
  end
%%%%%%%%%%%%%%      The Eigen values and eigenvectors
 [V,D]=eig(QQ); % the eigen values D and the eigenvectors V
          %of the Q matrix (the size of Q is 4(n)*4(n))
 D_r=real(D);
for jj=1:4*n_noise
   jj;
   DD(jj)=D(jj,jj);
end
DD_r=real(DD);
jeff_p=max(DD_r);
jeff_m=abs(min(DD_r));
%%%%%%%%%%%%%%      Calculation for b matrix
%%%%%%%%%%%%%%      Term 5
A_0_21=A_0_2.*A_0_1+B_2_x.*B_1_x+B_2_y.*B_1_y+B_2_z.*B_1_z;
B_21_x=A_0_2.*B_1_x+B_2_x.*A_0_1+i*(B_2_y.*B_1_z-B_2_z.*B_1_y);
B_21_y=A_0_2.*B_1_y+B_2_y.*A_0_1+i*(B_2_z.*B_1_x-B_2_x.*B_1_z);
B_21_z=A_0_2.*B_1_z+B_2_z.*A_0_1+i*(B_2_x.*B_1_y-B_2_y.*B_1_x);
A_02c_21=A_0_2_c.*A_0_21+B_2_x_c.*B_21_x+B_2_y_c.*B_21_y+B_2_z_c.*B_21_z;
```

```
B_2c_21_x=A_0_2_c.*B_21_x+B_2_x_c.*A_0_21+i*(B_2_y_c.*B_21_z-B_2_z_c.*B_21_y);
B_2c_21_y=A_0_2_c.*B_21_y+B_2_y_c.*A_0_21+i*(B_2_z_c.*B_21_x-B_2_x_c.*B_21_z);
B_2c_21_z=A_0_2_c.*B_21_z+B_2_z_c.*A_0_21+i*(B_2_x_c.*B_21_y-B_2_y_c.*B_21_x);
Tb1_0=A_02c_21;
Tb1_x=B_2c_21_x;
Tb1_y=B_2c_21_y;
Tb1_z=B_2c_21_z;
Tb3_0=A_0_21;
Tb3_x=B_21_x;
Tb3_y=B_21_y;
Tb3_z=B_21_z;
bra_b1=Tb1_0+Tb1_x.*m_in(1)+Tb1_y.*m_in(2)+Tb1_z.*m_in(3);
bra_b2=0+Tb1_x.*m_p(1)+Tb1_y.*m_p(2)+Tb1_z.*m_p(3);
bra_b3=Tb3_0+Tb3_x.*m_in(1)+Tb3_y.*m_in(2)+Tb3_z.*m_in(3);
bra_b4=0+Tb3_x.*m_p(1)+Tb3_y.*m_p(2)+Tb3_z.*m_p(3);
bb_1=CD_L1c.*CD_L2c.*CD_L2pc.*f_term.*bra_b1;
[bbb1,BB1]=meshgrid(bb_1,B1);
bbbb_1=etan_1*(bbb1.*BB1); %(bbb1.*BB1); %
bb_2=CD_L1c.*CD_L2c.*CD_L2pc.*f_term.*bra_b2;
[bbb2,BB2]=meshgrid(bb_2,B1);
bbbb_2=etan_1*(bbb2.*BB2);%(bbb2.*BB2);%
bb_3=CD_L1c.*CD_L2c.*f_term.*bra_b3;
[bbb3,BB3]=meshgrid(bb_3,B1);
bbbb_3=etan_2*(bbb3.*BB3);%(bbb3.*BB3);%
bb_4=CD_L1c.*CD_L2c.*f_term.*bra_b4;
[bbb4,BB4]=meshgrid(bb_4,B1);
bbbb_4=etan_2*(bbb4.*BB4);%(bbb4.*BB4);%
b_1_int=trapz(bbbb_1,2)/2;
b_2_int=trapz(bbbb_2,2)/2;
```

```
b_3_int=trapz(bbbb_3,2)/2;
b_4_int=trapz(bbbb_4,2)/2;
%%%%
 PP=[];
 for k=1:n
    PP1=[];PP2=[];PP3=[];PP4=[];
    for j=1:1
       PP1=[PP1;b_1_int(k,j)];
       PP2=[PP2;b_2_int(k,j)];
       PP3=[PP3;b_3_int(k,j)];
       PP4=[PP4;b_4_int(k,j)];
    end
    PP=[PP; PP1; PP2; PP3; PP4];
 end
    [Vv,PPp]=meshgrid(V,PP);
    b_tilda=Vv.*PPp;       % |b_tilda>=U*|b>
    mod_b_tilda_2=norm(b_tilda).^2;
 mod_b_tilda_2=real(b_tilda).^2+imag(b_tilda).^2;
%%%%%%%%%%%%        Mean, Variance
sum_lam=sum(DD_r);    % The mean
mean_t=Gauss_Variance_2*(sum_lam);
sum_lam_p=sum(mod_b_tilda_2)+Gauss_variance*sum(DD_r.^2);
varia=2*Gauss_Variance_2*sum_lam_p;  %Thevariance
%%%%%%%%%%%%        S_0_p    S_0_m
 s_0_m=-0.99/abs(min(DD_r))  % S_0 wnith negative sing
 s_0_p=+0.99/max(DD_r)       % S_0 wnith positive sing
%%%%%%%%%%%%        Calculation of zee
 vk=Gauss_Variance_2*sum(mod_b_tilda_2);
 zee=gamma_th-y_ss;
```

```
%%%%%%%%%%%%         Saddle point minus
 for kj=1:380
    kj;
   old_s_0_m=s_0_m;
  for mul=1:4*n_noise
      mul;
      beta(1,mul)=Gauss_Variance_2*DD_r(1,mul);
gama(1,mul)=beta(1,mul)/(1-beta(1,mul)*s_0_m);
xai(1,mul)=Gauss_Variance_2.*mod_b_tilda_2(mul,1)./...
         (1-beta(1,mul)*s_0_m);
  phai_1_s0_m(mul)=xai(1,mul).*s_0_m.*s_0_m;
  phai_2_s0_m(mul)=log(1./(1-beta(1,mul).*s_0_m));
  phai_3_s0_m(mul)=2*xai(1,mul).*s_0_m;
  phai_4_s0_m(mul)=gama(1,mul);
  phai_5_s0_m(mul)=xai(1,mul).*gama(1,mul).*s_0_m.*s_0_m;
  phai_6_s0_m(mul)=2*xai(1,mul);
  phai_7_s0_m(mul)=4*xai(1,mul).*gama(1,mul).*s_0_m;
  phai_8_s0_m(mul)=gama(1,mul).^2;
  phai_9_s0_m(mul)=2*xai(1,mul).*gama(1,mul).^2.*s_0_m.*s_0_m;
  end  % mul
  phai_m=sum(phai_1_s0_m)-sum(phai_2_s0_m)-log(s_0_m)-s_0_m*zee;
  phaip_m=sum(phai_3_s0_m)+sum(phai_4_s0_m)+sum(phai_5_s0_m)-1/s_0_m-zee
  phaipp_m=sum(phai_6_s0_m)+sum(phai_7_s0_m)+...
  sum(phai_8_s0_m)-sum(phai_9_s0_m)+1/s_0_m.^2;
  tata=phaip_m/phaipp_m;
  s_0_m=s_0_m-(tata);
  new_s_0_m=s_0_m
  if (abs(new_s_0_m-old_s_0_m)<1e-10)
       break;
```

```
  end
 end
 u_0_m=new_s_0_m;
%%%%%%%%%%%%        Saddle point pluse
 for kjp=1:380
   kjp;
  old_s_0_p=s_0_p;
 for mul=1:4*n_noise
    mul;
    beta(1,mul)=Gauss_Variance_2*DD_r(1,mul);
   gama(1,mul)=beta(1,mul)/(1-beta(1,mul)*s_0_p);
   xai(1,mul)=Gauss_Variance_2.*mod_b_tilda_2(mul,1)./...
       (1-beta(1,mul)*s_0_p);
   phai_1_s0_p(mul)=xai(1,mul).*s_0_p.*s_0_p;
   phai_2_s0_p(mul)=log(1./(1-beta(1,mul).*s_0_p));
   phai_3_s0_p(mul)=2*xai(1,mul).*s_0_p;
   phai_4_s0_p(mul)=gama(1,mul);
   phai_5_s0_p(mul)=xai(1,mul).*gama(1,mul).*s_0_p.*s_0_p;
   phai_6_s0_p(mul)=2*xai(1,mul);
   phai_7_s0_p(mul)=4*xai(1,mul).*gama(1,mul).*s_0_p;
   phai_8_s0_p(mul)=gama(1,mul).^2;
   phai_9_s0_p(mul)=2*xai(1,mul).*gama(1,mul).^2.*s_0_p.*s_0_p;
   end  % mul
   phai_p=sum(phai_1_s0_p)-sum(phai_2_s0_p)-log(s_0_p)-s_0_p*zee;
   phaip_p=sum(phai_3_s0_p)+sum(phai_4_s0_p)+sum(phai_5_s0_p)-1/s_0_p-zee
   phaipp_p=sum(phai_6_s0_p)+sum(phai_7_s0_p)+sum(phai_8_s0_p)-sum(phai_9_s0_p)+...
     1/s_0_p.^2;
   tata=phaip_p/phaipp_p
   s_0_p=s_0_p-(tata)
```

```
  new_s_0_p=s_0_p;
  if (abs(new_s_0_p-old_s_0_p)<1e-12)
     break;
  end
end
u_0_p=new_s_0_p;
%%%%%%%%%%%       Calculation of kk % minus
for mulll=1:2*n_noise
    mulll;
   gama_um(1,mulll)=beta(1,mulll)/(1-beta(1,mulll)*u_0_m);
   xai_um(1,mulll)=Gauss_Variance_2.*mod_b_tilda_2(mulll,1)./...
       (1-beta(1,mulll).*u_0_m);
   phai_1_m(mulll)=xai_um(1,mulll).*u_0_m.*u_0_m;
   phai_2_m(mulll)=log10(1-beta(1,mulll).*u_0_m);
   phai_3_m(mulll)=2*xai_um(1,mulll).*u_0_m;
   phai_4_m(mulll)=gama_um(1,mulll);
   phai_5_m(mulll)=xai_um(1,mulll).*gama_um(1,mulll).*u_0_m.*u_0_m;
  phai_6_m(mulll)=2*xai_um(1,mulll);
  phai_7_m(mulll)=4*xai_um(1,mulll).*gama_um(1,mulll).*u_0_m;
  phai_8_m(mulll)=gama_um(1,mulll).^2;
  phai_9_m(mulll)=2*xai_um(1,mulll).*gama_um(1,mulll).^2.*u_0_m.*u_0_m;
  phai_10_m(mulll)=6*xai_um(1,mulll).*gama_um(1,mulll);
  phai_11_m(mulll)=4*xai_um(1,mulll).*gama_um(1,mulll).^2.*u_0_m;
  phai_12_m(mulll)=2*gama_um(1,mulll).^3;

phai_13_m(mulll)=6*xai_um(1,mulll).*gama_um(1,mulll).^3.*u_0_m.*u_0_m;
end  % mulll
phai_u_m=sum(phai_1_m)-sum(phai_2_m)-log10(u_0_m)-u_0_m*zee
phaip_u_m=sum(phai_3_m)+sum(phai_4_m)+sum(phai_5_m)-1/u_0_m-zee;
```

```
phaipp_u_m=sum(phai_6_m)+sum(phai_7_m)+sum(phai_8_m)-sum(phai_9_m)+1/(u_0_m.^2);

phaippp_u_m=sum(phai_10_m)+sum(phai_11_m)+sum(phai_12_m)-
sum(phai_13_m)+2/u_0_m.^3;

k_m=0;

%%%%%%%%%%%%        Calculation of kk %  pluse

   for mulll=1:4*n_noise

     mulll;

       gama_up(1,mulll)=beta(1,mulll)/(1-beta(1,mulll)*u_0_p);

      xai_up(1,mulll)=Gauss_Variance_2.*mod_b_tilda_2(mulll,1)./...

        (1-beta(1,mulll)*u_0_p);

phai_1_p(mulll)=xai_up(1,mulll).*u_0_p.*u_0_p;

phai_2_p(mulll)=log10(1-beta(1,mulll).*u_0_p);

phai_3_p(mulll)=2*xai_up(1,mulll).*u_0_p;

phai_4_p(mulll)=gama_up(1,mulll);

phai_5_p(mulll)=xai_up(1,mulll).*gama_up(1,mulll).*u_0_p.*u_0_p;

phai_6_p(mulll)=2*xai_up(1,mulll);

phai_7_p(mulll)=4*xai_up(1,mulll).*gama_up(1,mulll).*u_0_p;

phai_8_p(mulll)=gama_up(1,mulll).^2;

phai_9_p(mulll)=2*xai_up(1,mulll).*gama_up(1,mulll).^2.*u_0_p.*u_0_p;

phai_10_p(mulll)=6*xai_up(1,mulll).*gama_up(1,mulll);

phai_11_p(mulll)=12*xai_up(1,mulll).*gama_up(1,mulll).^2.*u_0_p;


phai_12_p(mulll)=2*gama_up(1,mulll).^3;

phai_13_p(mulll)=6*xai_up(1,mulll).*gama_up(1,mulll).^3.*u_0_p.*u_0_p;

  end  % mulll

phai_u_p=sum(phai_1_p)-sum(phai_2_p)-log10(u_0_p)-u_0_p*zee

phaip_u_p=sum(phai_3_p)+sum(phai_4_p)+sum(phai_5_p)-1/u_0_p-zee;

phaipp_u_p=sum(phai_6_p)+sum(phai_7_p)+sum(phai_8_p)-sum(phai_9_p)+1/u_0_p.^2;
```

```
phaippp_u_p=sum(phai_10_p)+sum(phai_11_p)+sum(phai_12_p)-
sum(phai_13_p)+2/u_0_p.^3;

k_p=0;

%%%%%%%%%%%%%%%          f(0)

 f_0_p=real(exp(phai_u_p));

 f_0_m=real(exp(phai_u_m));

hav=5;

delta_new_m=1/((2^(hav-1))*(sqrt(2*phaipp_u_m)));

delta_new_p=1/((2^(hav-1))*(sqrt(2*phaipp_u_p)));

%%%%%%%%%%%%%%%         f(n delta new +)

   for fnn=1:1000

               fnn;

ndelta_new_m(fnn)=(fnn)*delta_new_m;

kus_m(fnn)=1-(i*k_m*ndelta_new_m(fnn));

par_m(fnn)=u_0_m+k_m*(ndelta_new_m(fnn)^2)/2+i*ndelta_new_m(fnn);

   for ph=1:4*n_noise

       ph;

brac_2_m_nv(1,ph)=1-Gauss_Variance_2*DD_r(1,ph)*par_m(fnn);

phai_1_m_nv(1,ph)=Gauss_Variance_2.*mod_b_tilda_2(ph,1).*...

par_m(fnn)*par_m(fnn)./brac_2_m_nv(1,ph);

phai_2_m_nv(1,ph)=log(brac_2_m_nv(1,ph));

 end  % ph

phai_m_nv(fnn)=sum(phai_1_m_nv)-sum(phai_2_m_nv)-...

log(ndelta_new_m(fnn))-ndelta_new_m(fnn)*zee;

f_m(fnn)=real(kus_m(fnn)*exp( phai_m_nv(fnn)));

  end  %fnn

    f_mnv=sum(f_m(fnn)) ;

    PP_m(bin)= delta_new_m*(f_0_m/2+f_mnv)/pi ;  %the propapility for u0+

    PP_m_new= PP_m
```

```
P_0_0=PP_m_new;
%%%%%%%%%%%%      f(n delta new +)
 for   fnn=1:1000
     fnn ;
     ndelta_new_p(fnn)=(fnn)*delta_new_p;
   kus_p(fnn)=1-(i*k_p*ndelta_new_p(fnn));
   par_p(fnn)=u_0_p+k_p*(ndelta_new_p(fnn)^2)/2+i*ndelta_new_p(fnn);
   for ph=1:4*n_noise
     ph;
 brac_2_p_nv(1,ph)=1-Gauss_Variance_2*DD_r(1,ph)*par_p(fnn);
 phai_1_p_nv(1,ph)=Gauss_Variance_2.*mod_b_tilda_2(ph,1).*...
 par_p(fnn)*par_p(fnn)./brac_2_p_nv(1,ph);
 phai_2_p_nv(1,ph)=log(brac_2_p_nv(1,ph));
  end  % ph
 phai_p_nv(fnn)=sum(phai_1_p_nv)-sum(phai_2_p_nv)-...
 log(ndelta_new_p(fnn))-ndelta_new_p(fnn)*zee;
 f_p(fnn)=real(kus_p(fnn)*exp( phai_p_nv(fnn)));
  end  %fnn
 f_pnv=sum(f_p(fnn))
 PP_p(bin)= delta_new_p*(f_0_p/2+f_pnv)/pi ;  %the propapility for u0+
 PP_p_new= PP_p
 P_0_0=PP_p_new;
end  %bin
P_1=-1*(1*PP_m_new(6)+1*PP_m_new(7)+1*PP_m_new(8)+1*PP_m_new(10)+...
1*PP_m_new(11)+1*PP_m_new(12)+1*PP_m_new(13)+1*PP_m_new(14)+...
  1*PP_m_new(17)+1*PP_m_new(19)+1*PP_m_new(20)+1*PP_m_new(22)+...
  1*PP_m_new(24)+1*PP_m_new(27)+1*PP_m_new(28)+1*PP_m_new(32))/16;
P_0=(1*PP_p_new(1)+1*PP_p_new(2)+1*PP_p_new(3)+1*PP_p_new(4)+...
 1*PP_p_new(5)+1*PP_p_new(9)+1*PP_p_new(15)+1*PP_p_new(16)+...
```

```
    1*PP_p_new(18)+1*PP_p_new(21)+1*PP_p_new(23)+1*PP_p_new(25)+...
    1*PP_p_new(26)+1*PP_p_new(29)+1*PP_p_new(30)+1*PP_p_new(31))/16;
P_ber=(P_0+P_1)/2
sss=[sss Input_SNR];
P_SNR(s)=P_ber;
mmm=log10(P_SNR);
end %Input_SNR
figure;plot(sss,mmm,'-o')
toc
```

Input pulse

```
function [fin_33,fin_50,fin_67,NoP]=RZ_inputP(t,T,NoP)
%dum2=zeros(1,length(t));
for jj=1:NoP;
  for kk=1:length(t)
  if(t(kk)>-jj*T & t(kk)<-(jj-1)*T)
    fm(kk)=sin(pi*(1+sin(pi*(t(kk)+(2*jj-1)*T/2)/T))/2);
    fm_2(kk)=sin(pi*(1+cos(2*pi*(t(kk)+(2*jj-1)*T/2)/T))/4);
    fm_3(kk)=sin(pi*cos(pi*(t(kk)+(2*jj-1)*T/2)/T)/2);
  else
    fm(kk)=0;
    fm_2(kk)=0;
    fm_3(kk)=0;
  end
  if(t(kk)>(jj-1)*T & t(kk)<jj*T)
    fp(kk)=sin(pi*(1+sin(pi*(t(kk)-(2*jj-1)*T/2)/T))/2);
    fp_2(kk)=sin(pi*(1+cos(2*pi*(t(kk)-(2*jj-1)*T/2)/T))/4);
    fp_3(kk)=sin(pi*cos(pi*(t(kk)-(2*jj-1)*T/2)/T)/2);
  else
    fp(kk)=0;
    fp_2(kk)=0;
    fp_3(kk)=0;
  end
  end
  %fm=exp(-(t+(2*jj-1)*T/2).^Sup_Gau*dum1);
  %fp=exp(-(t-(2*jj-1)*T/2).^Sup_Gau*dum1);
  dum2=fm+fp;%(:,jj);dum2+
  dum2_2=fm_2+fp_2;
```

```
  dum2_3=fm_3+fp_3;
  dum3(jj,:)=dum2(:);
  dum3_2(jj,:)=dum2_2(:);
  dum3_3(jj,:)=dum2_3(:);
end
if(NoP >1)
  fin=sum(dum3);
  fin_2=sum(dum3_2);
  fin_3=sum(dum3_3);
else
  fin=dum2;
  fin_2=dum2_2;
  fin_3=dum2_3;
end
fin_33=fin;
fin_50=fin_2;
fin_67=fin_3;
```

Bibliography

1- C. D. Poole, and J. A. Nagel, "Polarization Effects in Lightwave Systems," in Optical Fiber Telecommunications III A (I. P. Kaminow and T. Li, eds),San Diego, CA, Academic Press, 1997, pp. 114-161.

2- C. P. Agrawal. Fiber-Optic Communication Systems. John Wiley& Sons, Inc., Rochester, NY, 3rd edition, 2002.

3- G. P. Agrawal, Fiber Optic Communication Systems, Second edition, sections 1.3 and 1.4, John Willey & Sons, Inc., New York, 1997.

4- C. D. Poole, and R. E. Wagner, "Phenomenological Approach to Polarization Dispersion in Long Single-Mode Fibers," Electronics Letters, Vol. 22, No. 19, Sept., pp. 1029-1030, 1986.

5- H. Bulow and Henning, "System Outage Probability Due to First and Second-Order PMD,"IEEE Photonics Technology Letters, Vol. 10, No. 5, pp. 696-698, May 1998.

6- B. Huttner, C. Geiser and N. Gisin, "Polarization-Induced Distortion in Optical Fiber Networks with Polarization-Mode Dispersion and Polarization-Dependent Losses," IEEE Journal of Selected Topics in Quantum Electronics, Vol. 6, No. 2, pp. 317-329, 2000.

7- J. Chameron, PhD thesis, Physics Department, University of New Brunswick, 2000.

8- N. Gisin, "Statistics of Polarization Dependent Losses," Optics Communications, Vol. 114, pp. 399-405, February 1995.

9- N. Gisin and B. Huttner, "Combined Effects of Polarization Mode Dispersion and Polarization Depended Loss in Optical Fibers," Optics Communication, Vol. 142, pp. 119-125, 1997.

10-N. Gisin and J. P. Pellaux, "Polarization Mode dispersion: Time versus Frequency Domains," Optics Communications, vol. 89, pp. 316-323, 1992.

11-A. Galtarossa and L. Palmieri, "Relationship Between Pulse Broadening due to Polarization Mode Dispersion and Differential Group Delay in Long Single Mode Fibers," Electronics Letters, Vol. 34, pp. 492-493, 1998.

12-L. Chen, J. Cameron, X. Bao, "Statistics of Polarization Mode Dispersion in Presence of the Polarization Dependent Loss in Single Mode Fibers," Optics Communications, Vol. 169, pp. 69-73, 1999.

13-L. Chen and X. Bao, "Polarization-Dependent Loss Induced Pulse Narrowing in Birefringent Optical Fiber with Finite Differential Group Delay," Journal of ligthwave Technology, Vol. 18, No. 5, pp. 665-667, 2000.

14-B. Huttner and N. Gisin, "Anomalous Pulse Spreading in Birefringent Optical Fibers with Polarization-Dependent Loss," Optics Letters, Vol. 22, No. 8, pp. 504-506, April 1997.

15-J. P. Elbers, C. Glingener, M. Duser and E. Voges, "Modeling of Polarization Mode Dispersion in Single mode Fibers," Electronics Letters, Vol. 33, No. 22, pp. 1004-1005, October 1997.

16-J. P. Gordon and H. Kogelnik, "PMD Fundamentals: Polarization Mode Dispersion in Optical Fibers," Proc. Natl. Acad. Sci. USA, Vol. 97, No. 9, pp. 4541-4550, 2000.

17- C. D. Poole, R. W. Tkach, A. R. Chraplyvy, and D. A. Fishman, "Fading in Lightwave Systems Due to Polarization Mode Dispersion," IEEE Photonic Technology Letters, Vol. 3, pp. 68-70, 1991.
18-E. Collett, "Polarized Light in Fiber Optics," Chapter 16, The Polawave Group, Lincroft, New Jersey, USA, pp.518-519,2003.
19- D. Penninckx, "Jones Matrix of Polarization Mode Dispersion," Optics Letters, Vol. 24, No. 13, pp. 875-877, July 1999.
20-H. Kogelnik, R.M. Jopson and L. E. Nelson, "Polarization-Mode Dispertion," Chapter 15, Optical Fiber Telecommunications, Volume IV B, edited by I. P. Kaminow and T. Li, Academic Press, San Diego, CA, 2002.
21- H. Dong, P. Shum, M. Yan, G. Ning, Y. Gong, and C. Wu, "Generalized frequency dependence of output Stokes parameters in an optical fiber system with PMD and DL/PDG," Optics Express, Vol. 13, pp. 8875-8881, 2005.
22-G. J. Foschini and C. D. Poole, "Statistical Theory of Polarization Dispersion in Single Mode Fibers," IEEE Journal of lightwave Technology, Vol. 9, pp. 1439-1156, 1991.
23-A. Galtarossa et al., "In-Field Comparison among Polarization Mode Dispersion Measurement Techniques," Journal of lightwave Technology, Vol. 14,Jan 1996.
24-H. Sunnerud, M. Karlsson, C. Xie, and P. A. Andrekson, "Polarization-Mode Dispersion in High-Speed Fiber-Optic Transmission Systems," Journal of Lightwave Technology, Vol. 20, No. 12, pp. 2204-2219, Dec. 2002.
25-E. Forestieri, and G. Prati, "Exact Analytical Evaluation of Second-Order PMD Impact on the Outage Probability for a Compensated System," Journal of Lightwave Technology, Vol. 22, No. 4, pp. 988-996, April 2004.
26-G. Biondini, W. L. Kath, and C. R. Menyuk, "Importance Sampling for Polarization-Mode Dispersion: Techniques and Applications," Journal of Lightwave Technology, Vol. 22, No. 4, pp. 1201-1215, April 2004.
27-C. Francia, D. Penninckx, F. Bruyere, and M. W. Chbat, "PMD Second-order Effects on Pulse Propagation in Single-mode Fibers," IEEE Photon. Technol. Lett. , Vol. 10, pp. 1739-1741, Dec. 1998.
28-G. J. Foschini, L. E. Nelson, R. M. Jopson, and H. Kogelnik, "Probability Densities of Second-Order Polarization Mode Dispersion Including Polarization Dependent Chromatic Fiber Dispersion," IEEE Photonics Technology Letters, Vol. 12, No. 3, pp. 293-295, March 2000.
29-C. Vassallo, "PMD pulse deformation," *Elec. Lett.*, vol.31, No.18, pp.1597-1598, Aug 1995.
30-A. Eyal, W. K. ZMarshall, M. Tur and A. Yariv, "Representation of Second-order Polarization Mode Dispersion," Electronics Letters, Vol. 35, No. 19, pp. 1658-1659, Sep. 1999.
31-Fred Heisman, "Polarization Mode Dispersion: Fundamentals and Impact on Optical Communication Systems," Bell Labs, Lucent Technologies, 101 Crawfords Corner Road, Holmdel, NJ 07733, U.S.A.
32-B. Nyman, "Automated System for Measuring Polarization-Dependent Loss," in Optical Fiber Communication Conference, OFC, Tech. Dig., ThK6, 1994.

33-B. Heffiner, "Deterministic and Analytically Complete Measurement of Polarization Dependent Transmission through Optical Devices," IEEE Photon. Technol. Lett., Vol. 4, pp. 451-453, 1992.
34-E. Lichtman, "Limitations Imposed by Polarization-dependent Gain and Loss on All-optical Ultralong Communication Systems," Journal of Lightwave Technology, Vol. 13, pp. 906-913, May 1995.
35-M. Shtaif and O. Rosenberg, "Polarization-dependent Loss as a waveform-distoring Mechanism and Effect on Fiber-Optic Systems," Journal of Lightwave Technology, Vol. 23, No. 2, pp. 923-929, 2005.
36- C. Xie, "Polarization Dependent Loss Induced Outage Probabilities in Optical Communication Systems," IEEE Photonics Technology Letters, Vol. 20, No. 13, pp. 1091-1093, 2008.
37-A. Amari, N. Gisin, B. Perny, H. Zbinden, and C. Zimmer, "Statistical Prediction and Experimental Verification of Concatenations of Fiber Optic Components with Polarization Dependent Loss," J. Ligthwave Technol., Vol. 16, No. 3, pp. 332-339(1998).
38-L. Chen, S. Hadjifaradji, D. Waddy, and X. Bao, "Effect of Local PMD and PDL Directional Correlation on The Principle State of Polarization Vector Autocorrelation," Optics Express, Vol. 11, No. 23, pp. 3141-3146, 2003.
39-B. Huffner, C. De Barros, B. Gisin and N. Gisin, "Polarization-Induced Pulse Spreading in Birefringent Optical Fibers with Zero Differential Group Delay," Opt. Lett., Vol. 24, pp. 370-372, June 1999.
40-W. Shieh, "Principal States of Polarization for An Optical Pulse," IEEE Photonic Technology Letters, Vol. 11, No. 6, pp. 677-679, Jun. 1999.
41-P. Lu, L. Chen, and X. Bao, "Principle States of Polarization for An optical Pulse in Presence of Polarization Mode Dispersion and Polarization Dependent Loss," In Proc. 2oo Int. Conf. Applicat. Photon. Technol. (ICAPT'2000), QC, Canada, June 12-16, 2000.
42- L. Chen, O. Chen, S. Hadjifaradji, and X. Bao, "Polarization-Mode Dispersion Measurement in a System with Polarization-Dependent Loss or Gain," IEEE Photonics Technology Letters, Vol. 16, No. 10, pp. 206-208,Jan. 2004.
43-G. J. Foschini, L. E. Nelson, R. M. Jopson, and H. Kogelnik, "Probability Densities of Second-Order Polarization Mode Dispersion Including Polarization Dependent Chromatic Fiber Dispersion," IEEE Photonics Technology Letters, Vol. 12, No. 3, pp. 293-295, March 2000.
44-R. C. Jones, "A new Calculus for the Treatment of Optical Systems," J. Opt. Soc. Amer., Vol. 31, pp. 488-493, July 1941.
45-I. P. Kaminow, T. Li and A. E. Willner, Optical Fiber Telecommunications V A: Components and Systems, section 15.2, Academic Press, 2008.
46-B. L. Heffner, "Automated Measurement of Polarization Mode Dispersion Using Jones Matrix Eigenanalysis," IEEE Photonics Technology Letters, Vol. 4, pp. 1066-1069, Sep. 1992.
47-Special Issue on Optical Multi-access Networks, IEEE Network Mag., Vol. 3, Mar. 1989.
48-M. Born and E. Wolf, "Principles of Optics," Seventh Edition, Cambridge University Press, NY, 1999.

49-X. Jiang and R. Wang, "Reverse Dispersion Fiber with Depressed Core-index Profile for Dispersion-managed Fiber Pairs," Optics Communications, Vol. 255, No. 4-6, pp. 230-234,Nov. 2005.

50-M. Morimoto, I. Kobayashi, H. Hiramatsu, K. Mukasa, R. Sugizaki, Y. Suzuki and Y. Kamikura, "Development of Dispersion Compensation Cable Using Reverse dispersion Fiber," Fifth Asia-Pacific Conference and Fourth Optoelectronics and communication conference, Vol. 2,pp. 1590-1593, 1999.

51-I. Shake, H. Takara, "Averaged Q-Factor Method Using Amplitude Histogram Evaluation for Transparent Monitoring of Optical Signal-to-Noise Ratio Degradation in Optical Transmission System," Journal of Lightwave Technology, Vol. 20, No. 8, Aug. 2002.

52-S. Okamoto and K.-1 Sato, "Inter-network Interface for Photonic Transport Networks and SDH Transport Networks," in Procl. IEEE Global Telecommunications Conf. (GLOBECOM'97), Vol. 2, 1997, pp. 850-855.

53-S. K. Shin, C.-H. Lee, and T. C. Chung, "A Novel Frequency and Power Monitoring Method for WDM Optical Network," in Proc. Optical Fiber Communication Conf. (OFC'98), 1998, pp. 168-170.

54-N. S. B. Bergano, F. W. Kerfoot, and C. R. Davidson, "Margin Measurements in Optical Amplifier Systems," IEEE Photonics Technology Letters, Vol. 3, pp. 304-306, May 1993.

55-R. Wiesman , O. Bleck, and H. Heppner, "Cost Effective Performance Monitoring in WDM Systems," in Proc. Optical Fiber Communication Conf. (OFC2000), Vol. 2, 2000, pp. 171-173.

56-M. C. Jeruchim, "Techniques for Estimating the Bit Error Rate in the Simulation of Digital Communication Systems," IEEE Journal on Selected Areas in Communications, Vol. SAC-2, No. 1, PP. 153-170, 1984.

57-D. Remondo, R. Srinivasan, V. F. Nicola, W. C. Van Etten, and H. E. P. Tattje, "Adaptive Importance Sampling for Performance Evaluation and Parameter Optimization of Communication Systems," IEEE Transactions on Communications, Vol. 48, No. 4, pp. 557-565, 2000.

58-A. Lowery, O. Lenzmann, I. Koltchanov, R. Moosburger, R. Freund, A. Richter, S. Georgi, D. Breuer, and H. ZHamster, "Mulitple Signal Representation Simulation of Photonic Devices Systems and Networks," IEEE Journal of Selected Topics in Quantum ectroincs, Vol. 6, No. 2, pp. 282-296, 2000.

59-F. Matera and M. Settembre, "Role of Q-factor and of Time Jitter in the performance Evaluation of Optically Amplified Transmission Systems," IEEE Journal of Selected Topics in Quantum Electronics, Vol. 6, pp. 308-316, 2000.

60-D. Marcuse, "Derivation of analytical Expressions for the Bit-error Probability in Lightwave Systems with Optical Amplifiers," Journal of Lightwave Technology, Vol. 8, No. 12, pp. 1816-1823, Dec. 1990.

61-F. Ruhl and R. Ayre, "Explicit Expressions for the Receiver Sensitivity Terms," IEEE Photonic Technology Letters, Vol. 5, pp. 358-361, Mar. 1993.

62-C. Anderson and J. Lyle, "Technique for Evaluating System Performance Using Q in Numerical Simulations Exhibiting Intersymbol Interference," Electronic Letters, Vol. 30, pp. 71-72, Jan. 1994.

63-E. Laedke, N. Goder, T. Schaefer, K. Spatschek, and S. Turitsyn, "Improvement of Optical Fiber Systems Performance by Optimization of Reciever Filter Bandwidth and Use of Numerical Methods to Evaluate Q-factor," Electronic Letters, Vol. 35, pp. 2131-2133, Nov. 1999.
64-G. P. Agrawal, Nonlinear Fiber Optics. New Yourk: Academic, 1995.
65-M. Rasztovits-Wiech, K. Studer, and W. R. Leeb, "Bit Error Probability Estimation Algorithm for Signal Supervision in All-Optical Networks," Electron. Lett. , Vol. 35, pp. 1754-1755, 1999.
66-R. E. Collins, Field Theory of Guided Waves, 2nd Edition, IEEE Press, New York, 1991.
67-M. Shah Alam, Kunimasa Saitoh, and Masanori Koshiba, "High Group Birefringence in Air-core Photonic Bandgap Fibers," Optics Letters, Vol. 30, No. 8, pp. 824-826, April 2005.
68-Daniel A. Nolan, Xin Chen, and Ming-Jun Li, "Fibers with Low Polarization-Mode Dispersion," J. of Lightwave Technology, Vol. 22, No. 4, pp. 1066-1077, April 2004.
69-C. Xie, and L. Moller, "The Accuracy Assessment of Different Polarization Mode Dispersion Models," Optical Fiber Technology, Vol.12, No. 6, pp. 101-109, April2006.
70-F. Curti, B. Daino, G. DeMarchis, and F. Matera, "Statistical Treatment of The Evolution of the Principal States of Polarization in Single-Mode Fibers," IEEE Journal of lightwave Technology, LT-8, pp. 1162-1166, 1990.
71-P. Lu, L. Chen, and X. Bao, "A new Waveplate Model of Characterizing the System Impact Due to PMD," in Proc. SPIE : Photonics North's, 2002, Vol. 4833.
72-B. W. Hakki, "Polarization Mode Dispersion in a Single Mode Fiber," J. Lightwave Technology, Vol. 14, No. 10, pp. 2202-2208, Oct. 1996.
73-M. Karlsson, "Probability Density Functions of the Differential Group Delay in Optical Fiber Communication Systems," Journal of Lightwave Technology, Vol. 19, No. 3, pp.324-331, March 2001.
74-M. Karlsson and J. Brentel, "Autocorrelation Function of the Polarization-mode Dispersion Vector," Optics Letters, Vol. 24, No. 14, pp. 939-941, July 1999.
75-P. Lu, L. Chen, and X. Bao, "Statistical Distribution of Polarization-dependent Loss in the Presence of Polarization-mode Dispersion in Single-mode Fibers," IEEE Photonic Technology Letters, Vol. 13, pp. 451-453, May 2001.
76-N. Gisin, B. Huttner, "Influence of Polarization Dependent Loss On Birfringent Optical Fibre Networks," *in Proc OFC',* Baltimore,USA, 2000.
77-C. Antonelli, and A. Mecozzi, "Non-Maxwellian Probability Density Function of Fibers with Lumped Polarization Mode Dispersion Elements," *Opt. Lett.*, vol. 29, No. 10, pp. 1057-1059, 2004.
78-L. F. B. Ribeiro, J. R. F. Da Rocha, and O. L. Pinto, "Performance Evaluation of EDFA Preamplified Receivers Taking into Account Intersymbol Interference," J. Lightwave Technol. , Vol. 13, pp. 225-232, 1995.
79-J. Zhang, M. Yao, X. Chen, L. Xu, M. Chen, and Y. Gao, "Bit Error Rate Analysis of OTDM System Based on Moment Generation Function," Journal of Lightwave Technology, Vol. 18, No. 11, pp. 1513-1518, 2000.

80-R. M Mu, T. Yu, V. S. Grigoryan, and C. R. Menyuk, "Dynamics of the Chirped Return-to-Zero Modulation," Journal of Lightwave Technology, Vol. 20, No. 1, pp. 47-57, 2002.
81-P. P. Smyth, R. Wyatt, A. Fidler, P. Eardley, A. Sayles, and S. Craig-Ryan, "152 Photons per Bit Detection at 622 Mbit/s to 2.5 Gbit/s Using an Erbium Fiber Preamplifier," Electron. Lett., Vol. 26, pp. 1904-1605, 1990.
82-R. C. Steele and G. R. Walker, "High Sensitivity FSK Signal Detection with an Erbium Doped Fiber Preamplifier and Fabry-Perot Etalon Demodulation," IEEE Photonic. Technology Letters, Vol. 2, pp. 753-754, 1990.
83-O. K. Tonguz and L. G. Kazovsky, "Theory of Direct-Detection Lightwave Receivers Using Optical Amplifiers,." Journal of Lightwave Technology, Vol. 9, No. 2, pp. 174-181, Feb. 1991.
84-P. C. Becker, N. A. Olsson, J. R. Simpson: Erbium-Doped Fiber Amplifiers, Fundamentals and Technology, Academic Press, San Diego, 1999.
85- I. Jacobs, "Effect of Optical Amplifier Bandwidth on Receiver Sensitivity," IEEE Trans. On Commun., Vol. 38, No. 10, pp 1863-1864, Oct. 1990.
86- N. Khrais, A. Elrefaie, R. Wagner, and S. Ahmed, "Performance of Cascade misaligned Optical (De)multiplexers in Multiwavelength Optical Networks, IEEE Photonic Technology Letters, Vol. 8, pp. 1073-1075, Aug. 1996.
87- R. Fyath and J. O'Reilly, "Performance of Optically Preamplified Directdetection Receivers in the Presence of Laser Chirp- Part1: Ideal Travelling-wave Amplifier," IEE Proc. Optoelectron. J, Vol. 136, pp. 249-255, Oct. 1989.
88-M. Kuznetsov, N. Froberg, S. Henion, and K. Rauschenbach, "Power Penalty for Optical Signals Due to Dispersion Slope in WDM Filter Cascades," IEEE Photonics Technology Letters, Vol. 11, pp. 1411-1413, Nov. 1999.
89-I. T. Lima, A. O. Lima, Y. Sun, H. Jiao, J. Zweck, C. R. Menyuk, and G. M. Carter, "A receiver Model for Optical Fiber Communication Systems With Arbitrarily Polarized Noise," Journal of Lightwave Technology, Vol. 23, pp. 1478-1490, 2005.
90- Z. Zhang, L. Chen, X. Bao, "Accurate BER Evaluation for Lumped DPSK and OOK Systems with PMD and PDL," Optics Express, Vol. 15, No. 15, pp.9418-9433, July 2007.
91-E. Forestiri, "Evaluating the Error Probability in Lightwave Systems with Chromatic Dispersion, Arbitrary Pulse Shape and Pre—and Postdetection Filtering,", J. Lightwave Technology, Vol. 18, No. 11, PP.1493-1503(2000).
92-J. Wang and J. M. Kahn, "Impact of chromatic and polarization-mode dispersion on DPSK systems using Interferometric Demodulation and Direct Detection," Journal of Lightwave Technology, Vol. 22, No. 2, pp. 362-371, 2004.
93- L. Chen, S. Hadjifaradji and X. Bao, "Analytic Optical Eye Digram Evaluation in the presence of Polarization Mode Dispersion, Ploarization dependent Loss, Chromatic Dispersion in Dynamic Single Mode Fiber Communication Networks" J. Opt. Sec. Am, B 21, No. 10, pp. 1860-1865, 2004.

94-S. W. Golomb, Shift Register Sequences, San Francisco, CA: Holden-Day, 1967.
95-L. Chen, Z. Zhang, and X. Bao, "Combined PMD-PDL Effects on BERs in Aimplified Optical Systems: an Analytical Approach," Opt. Express, Vol. 15, pp. 2106-2119, 2007.
96-H. Haunstein, W. Sauer-Greff, A. Dittrich, K. Sticht and R. Urbansky, "Principles for Electronic Equalization of Polarization-Mode Dispersion," JournaL OF Lightwave Technology, Vol. 22, No. 4, pp.1169-1182, 2004.
97-P. Humbletand M. Azizoglu, "On the Bit Error Rate Of Lightwave Systems with Optical Amplifiers," J. Lightwave Tech., Vol. 9, No. 11, PP.1576-1582 (1991).
98-N. Young Kim, D. Lee, H. Yoon, J. Park and N. Park, "Limitation of PMD compensation due to polarization-dependent loss in high-speed optical transmission links," IEEE Photonics Technology Letters,Vol. 14, No. 1, PP.104-106(2000).
99-H. Haunstein and H. Kallert, "Influence of PMD on the Performance of Optical Transmission Systems in the Presence of PDL," Proc. OFC, Paper WTA (2001).
100- J. Cameron, L. Chen, and X. Bao, "Limitation of first order PMD compensation techniques in the presence of chromatic dispersion," opt. Comm., Vol. 171, No. 1-3, PP.15-21 (1999).
101- F. Bruyere and O. Audouin, "Penalties in long-haul Optical Amplifier Systems Due to Polarization Dependent Loss and Gain," IEEE Photonics Technology Letters, Vol. 6, No. 5,pp.654-656, May 1994.
102- L. Chen and X. Bao, "Polarization-Dependent Loss-Induced Pulse Narrowing in Birefringent Optical Fibers with Finite Differential Group Delay," Journal of Lightwave Technology, Vol. 18,No. 5, pp. 665-667, May 2000.
103- P. Winzer and A. Kalmar, "Sensitivity Enhancement of Optical Receivers by Impulsive Coding," J. Ligthwave Tech., Vol. 17, No. 2, PP.171-177(1999).
104- E. Lichtman, "Limitations Imposed by Polarization-dependent Gain and Loss on All-optical Ultralong Communication Systems," Journal of Lightwave Technology, Vol. 13, pp. 906-913, May 1995.
105- T. Okoshi, "Recent Advances in Coherent Optical fiber Communication Systems,"J. Lightwave Tech., Vol. 17, No. 2, PP.171-177(1987).
106- K. Wansey, A. Dandridge and A. Tveten, "Dependence of visibility on input polarization in interferometric fiber-optic sensors," Opt. Lett., Vol. 13, No.4,PP. 288- (1988).
107- F. Bruyere and O. Audouin, "Measurement of OSNR in the Presence of Partially Polarized ASE," IEEE Photonics Technology Letters, Vol. 17, No. 2, PP.435-437(2005).
108- P. J. Winzer, M. Pfennigbauer, M. Strasser, and W. R. Leeb, "Optimum Filter Bandwidth for Optically Preamplifier NRZ Receivers," Journal of Lightwave Technology, Vol. 19, No. 9, pp. 1263-1273, Sep. 2001.
109- L. Boivin, M. Nuss, J. Shah, D. Miller and H. Haus, "Receiver Sensitivity Improvement by Impulsive Coding," IEEE Photon. Technol. Lett., Vol. 9, no. 5,PP. 684-686 (1997).